

For Reference

NOT TO BE TAKEN FROM THIS ROOM

Ex LIBRIS
UNIVERSITATIS
ALBERTAEASIS



THE UNIVERSITY OF ALBERTA

RELEASE FORM

NAME OF AUTHOR C.M. Matthews

TITLE OF THESIS


Designing Floor Systems for Dynamic Response

DEGREE FOR WHICH THESIS WAS PRESENTED Master of Science

YEAR THIS DEGREE GRANTED Fall 1982

Permission is hereby granted to THE UNIVERSITY OF ALBERTA LIBRARY to reproduce single copies of this thesis and to lend or sell such copies for private, scholarly or scientific research purposes only.

The author reserves other publication rights, and neither the thesis nor extensive extracts from it may be printed or otherwise reproduced without the author's written permission.



THE UNIVERSITY OF ALBERTA

Designing Floor Systems for Dynamic Response

by

C.M. Matthews



A THESIS

SUBMITTED TO THE FACULTY OF GRADUATE STUDIES AND RESEARCH
IN PARTIAL FULFILMENT OF THE REQUIREMENTS FOR THE DEGREE

OF Master of Science

IN

Civil Engineering

Department of Civil Engineering

EDMONTON, ALBERTA

Fall 1982

THE UNIVERSITY OF ALBERTA
FACULTY OF GRADUATE STUDIES AND RESEARCH

The undersigned certify that they have read, and recommend to the Faculty of Graduate Studies and Research, for acceptance, a thesis entitled Designing Floor Systems for Dynamic Response submitted by C.M. Matthews in partial fulfilment of the requirements for the degree of Master of Science.

To the memory of my father,
A. Clifford Matthews

Abstract

The dynamic characteristics of a stub girder floor system and an open web steel joist dance floor are investigated through extensive experimental programs. The dynamic parameters derived for each floor system through a frequency domain analysis included the natural frequencies of vibration, the associated mode shapes and modal damping ratios and the peak accelerations generated by heel drop impacts on the floors. In the dance floor study, the prominent frequencies of several dances and various parameters reflecting the forced response of the floor system during those dances are also determined. The experimental results are subsequently used to evaluate the applicability of current dynamic design procedures to the two floor systems.

The stub girder floor system had a complex dynamic response characterized by prominent natural frequencies at 5.4, 6.2, 6.6, 7.2, 11.3, 11.6, and 12.2 Hz. The associated mode shapes fell into two distinct categories, with the first modal group (5.4, 6.2, 6.6, and 7.2 Hz) characterized by a one-half sine wave pattern parallel to the stub girders. The remaining frequencies were associated with a full sine wave shape parallel to the stub girders. Differences in the modal patterns perpendicular to the stub girders appear to be responsible for the variation in modal frequencies within the individual groups. The experimental results suggested that the stub girder floor system is more

than satisfactory for quiet occupancy usage.

A comparison of experimental and theoretical results showed that a reasonable design stage evaluation of the stub girder floor system could be made using current dynamic design procedures in the manners suggested.

The results of the heel impact study on the open web steel joist dance floor show the response was dominated by the fundamental frequency of 5.0 Hz with less prominent natural frequencies at 6.8, 7.2, 9.4, and 9.8 Hz. The entire sunken area containing the dance floor participated as the vibrating panel of the fundamental mode with a typical one-half sine wave shape in both directions. An evaluation of the floor response to heel drop impacts suggested the floor system would be adequate for use as a quiet occupancy (ie: dining). However, since the vibrations generated during dancing were bothersome to patrons seated in the dining areas adjacent to the dance floor, the floor system was inadequate for the combined dining-dancing occupancy. The annoying vibrations were the result of a forced response at well below the fundamental floor frequency and they were attributed to an inadequate floor stiffness.

The results of the dance vibration study were used in the development of a procedure to evaluate the dynamic response of dance floors at the design stage. Additional studies on other dance floors are recommended to verify the procedure.

Acknowledgements

It is with great pleasure that I finally get to express my sincere gratitude to my supervisors, Dr. C. James Montgomery and Dr. Dave W. Murray, for their invaluable assistance in completing this thesis. I am heavily indebted to both of them for their guidance and intellectual aid throughout the duration of my study.

Thanks are also expressed to Dr. H. J. Rainer for his advice and assistance during the experimental phase of the study, and to Dr. R. E. Rink for his tremendous help in data reduction aspects.

I would also like to thank Tom Casey for his expert advice and assistance in computer related areas, the secretaries of the department, especially Eleanor Kangas who did many favors for me, and finally my wife Dawn, for her undying patience and for typing the original manuscript.

Table of Contents

Chapter	Page
1. Introduction	1
1.1 Introductory Remarks	1
1.2 Historical Review	2
1.3 Purpose and Scope	8
2. Theoretical Evaluation of Vibrating Floor Systems	10
2.1 Introduction	10
2.2 Acceptable Vibration Limits	10
2.3 System Modelling and Theoretical Formulation	13
2.3.1 Fundamental Frequency	13
2.3.2 Initial Peak Accelerations	16
2.3.3 Damping	23
2.4 Remedial Measures to Correct Floor Vibration Problems	24
3. Data Acquisition and Reduction	31
3.1 Introduction	31
3.2 Data Acquisition	31
3.3 Analog to Digital Conversion	34
3.4 Data Preprocessing	36
3.5 Frequency Analysis	37
3.5.1 Introduction	37
3.5.2 Fourier Analysis	38
3.6 Analysis of Transient Events	41
3.6.1 General	41
3.6.2 Analysis	42
3.7 Analysis of Continuous Signals	45

3.7.1	General	45
3.7.2	Analysis	45
3.8	Determination of Dynamic Characteristics	47
3.8.1	Natural Frequencies	47
3.8.2	Mode Shapes	48
3.8.3	Modal Damping Ratios	52
3.9	Filtered Acceleration-Time Signals	53
3.9.1	Introduction	53
3.9.2	Analog Filter System	54
3.9.3	Digital Filter	54
4.	Dynamic Characteristics of a Stub Girder Floor System	73
4.1	Introduction	73
4.2	Description of Floor System	73
4.3	Test Procedures	75
4.4	Experimental Results and Discussion	77
4.4.1	Natural Frequencies of Vibration	77
4.4.1.1	Discussion of Natural Frequencies ...	78
4.4.2	Mode Shapes	80
4.4.2.1	Discussion of Mode Shapes	84
4.4.2.2	The Effects of Spectral Interference	87
4.4.3	Modal Damping Values	91
4.4.4	Peak Accelerations	94
4.5	Theoretical Evaluation of the Stub Girder Floor System	96
4.5.1	Fundamental Frequency	96
4.5.2	Peak Acceleration	98
4.5.3	Evaluation	99

5. Dynamic Characteristics of an Open Web Steel Joist Dance Floor	125
5.1 Introduction	125
5.2 Description of Floor System	126
5.3 Heel Impact Tests	127
5.3.1 Test procedures	127
5.3.2 Heel Impact Test Results and Discussion	129
5.3.2.1 Natural Frequencies	129
5.3.2.2 Mode Shapes	131
5.3.2.3 Modal Damping Ratios	132
5.3.2.4 Peak Acceleration	134
5.4 Theoretical Evaluation of the Floor System	135
5.4.1 Fundamental Frequency	135
5.4.2 Peak Acceleration	136
5.4.3 Evaluation	137
5.5 Dance Vibration Study	137
5.5.1 Test Procedures	137
5.5.2 Dance Test Results and Discussion	138
5.5.2.1 Results	138
5.5.2.2 Discussion	141
5.6 Design Proposal for Dance Floors	143
5.6.1 Introduction	143
5.6.2 Analytical Development	144
5.6.2.1 Model of Floor System	144
5.6.2.2 Theoretical Derivation	144
5.6.2.3 Design Parameters	146
5.6.2.4 Summary of Recommended Design Procedures	148

5.6.2.5 Design Example	149
6. Summary and Conclusions	164
REFERENCES	169
APPENDIX A	174
APPENDIX B	194
APPENDIX C	216
APPENDIX D	234
APPENDIX E	242

List of Tables

Table	Page
4.1 Natural Frequencies of the Stub Girder Floor System	101
4.2 Modal Damping Ratios Derived by One-half Power Bandwidth Method	101
4.3 Damping Ratios Derived from Decay Curves	102
4.4 Peak Accelerations of the Stub Girder Floor System	103
4.5 Results of Frequency Calculations	104
4.6 Theoretical Peak Accelerations of the Stub Girder Floor System	104
5.1 Natural Frequencies of the OWSJ Floor System	151
5.2 Modal Damping Ratios of the OWSJ Dance Floor	151
5.3 Summary of Dance Test Results	152
5.4 Proposed Dance Floor Acceleration Level Evaluations	154
5.5 Theoretical Peak Accelerations of the OWSJ Dance Floor	154

List of Figures

Figure	Page
2.1 Annoyance Threshold Chart	27
2.2 Definition of Effective Floor Width	28
2.3 Assumed Configuration of Vibrating Panel	29
2.4 Force vs. Time Curve for Heel Drop Impact	30
3.1 Processing and Analysis Steps	56
3.2 Typical Instrumentation Setup	57
3.3 Aliasing Phenomenon	58
3.4 (a) Voltage Offset in a Digital Record, (b) Corrected Trace	59
3.5 Illustration of the DFT Pair	60
3.6 (a) A Typical Sequence of Transient Events, (b) A Single Transient Event	61
3.7 A Typical Magnitude Spectrum	62
3.8 A Typical Phase Spectrum	62
3.9 (a) Typical Portion of a Continuous Dance Record, (b) Modified Dance Record	63
3.10 Scaling Envelope for Continuous Dance Records	64
3.11 Floor Layout and Accelerometer Locations to Determine Mode Shapes	65
3.12 Magnitude Spectra Associated With Six Test Positions	66
3.13 Relative Phase Spectra for A2-A6 and A3-A5	68
3.14 Mode Shapes along Line of Accelerometers	69
3.15 (a) Damping Ratios by the One-half Power Bandwidth Method, (b) Damping Ratios by the Exponential Decay Method	70
3.16 (a) Typical Unfiltered Analog Signal,	

Figure	Page
(b) Corresponding Signal Filtered by Analog Filter System	71
3.17 (a) Typical Unfiltered Digital Signal, (b) Corresponding Signal Filtered with FIR Filter	72
4.1 Illustration of Stub Girders in the Nova Building	105
4.2 General Floor Plan of the Nova Building	106
4.3 Illustrations of Completed and Uncompleted Composite Slab Floor	107
4.4 Typical Cross-section of Floor at Stub Girder Position	108
4.5 Detail of Test Area indicating Accelerometer Positions	109
4.6 Representative Magnitude Spectra	110
4.7 Relative Modal Amplitudes along Lines 3, 5, and 7 (a) Mode 1, (b) Mode 2	111
4.8 Relative Modal Amplitudes along Lines 3, 5, and 7 (a) Mode 3, (b) Mode 4	112
4.9 Relative Modal Amplitudes along Line D (a) Mode 1, (b) Mode 2	113
4.10 Relative Modal Amplitudes along Line D (a) Mode 3, (b) Mode 4	114
4.11 Three Dimensional View of Mode 2 over Test Area	115
4.12 Three Dimensional View of Mode 3 over Test Area	116
4.13 Relative Modal Amplitudes along Lines 3, 5, and 7 (a) Mode 5, (b) Mode 6	117
4.14 Relative Amplitude of Mode 7 along Lines 3, 5, and 7	118
4.15 Relative Amplitude of Mode 5 along Line D	119
4.16 Magnitude Spectra From Manufactured Traces (a) 20 Hz Component,	

Figure	Page
(b) 20 and 21 Hz Components, (c) 20 and 20.5 Hz Components, (d) 20 and 20.5 Hz Components with 2:1 Amplitude Ratio	120
4.17 Magnitude Spectra from Test Positions (a) Position 3D, (b) Position 7D	122
4.18 (a) Trace Indicating Beating Phenomenon, (b) Envelope used to Determine Damping Ratio	123
4.19 Typical Event Indicating Peak Acceleration	124
5.1 Structural Layout of Dance Floor and Surrounding Area	155
5.2 Detail Planview of Sunken Dance Floor Area	156
5.3 Typical Magnitude Spectra (a) Response at Midspan of Joists, (b) Response Over Supporting Beam	157
5.4 Vibration Patterns of Mode 1 (a) Along Line C, (b) Along Line E, (c) Along Line 6	158
5.5 Peak Acceleration at Position E6	160
5.6 Typical Magnitude Spectra (a) Waltz, (b) Polka, (c) Rock and Roll	161
5.7 Average and Maximum Peak Acceleration of a Typical Dance Record	162
5.8 Model of Dance Floor for Design Proposal	163

List of Symbols

A_o	=	peak acceleration response of a floor system
$A(f)$	=	approximation to desired frequency response of a filter
$A_d(f)$	=	desired frequency domain response of a filter
A_m	=	amplitude of modal response curve after m cycles of vibration
a_k	=	real part of complex frequency component
b	=	vibrating panel width perpendicular to the joists
b_k	=	imaginary part of complex frequency component
D_n	=	dynamic magnification factor for n^{th} mode of vibration
D_x	=	flexural stiffness of vibrating panel perpendicular to joists
D_y	=	flexural stiffness of vibrating panel parallel to joists
E_s	=	modulus of elasticity of steel
F_l	=	inertial force of an elemental area $dx dy$ of a vibrating panel
f	=	frequency of a system
$f_1 \& f_2$	=	frequency limits defining bandwidth of filter
f_f	=	floor system fundamental frequency
f_g	=	fundamental frequency of girders supporting of T-beams
f_j	=	fundamental frequency of T-beam
f_n	=	frequency of mode n
f_s	=	sampling frequency of analog signals

$G(f_k)$	= complex frequency component at discrete frequency f_k where k is any integer
$ G(f_k) $	= magnitude of complex frequency component
$g(t_n)$	= discrete time function with each sample corresponding to a time t_n where n is any positive integer
$H(z)$	= finite impulse response transfer function
$h(t)$	= discrete transfer function in time domain
I	= force impulse
I_t	= transformed moment of inertia of T-beam
j	= $\sqrt{-1}$
K	= kinetic energy of flexural system
L	= length of joists or beams
M_E	= equivalent modal mass of vibrating panel
M_n	= generalized mass for mode shape n of T-beam
\bar{m}	= mass per unit length of T-beam
$\bar{\bar{m}}$	= mass per unit area of vibrating panel
N	= total number of samples in time function $g(t)$
n	= modular ratio
$P_n(t)$	= generalized loading for mode shape n of T-beam
P_o	= effective dance load
$R(f)$	= frequency domain representation of filtered signal
$r(t)$	= filtered signal in time domain
s	= spacing of floor joists or beams
T	= period of time function
t_e	= effective thickness of concrete slab
V	= potential energy of flexural system

$v(t)$	=	time dependent displacement response of a single degree of freedom system
$v(x,t)$	=	displacement response of T-beam
$v(x,y,t)$	=	time dependent displacement of vibrating panel
$\dot{v}(0)$	=	initial velocity
\ddot{v}_{\max}	=	maximum acceleration response of a single degree of freedom system
W_a	=	average weight of concrete per unit area of floor panel
$w(t)$	=	coefficient of window function
$Y_n(t)$	=	generalized displacement of T-beam in mode n
\bar{y}	=	distance to neutral axis of composite T-beam
Z_0	=	generalized coordinate
$Z(t)$	=	a function of time
β_n	=	frequency ratio of n^{th} mode
Δf	=	spacing of discrete frequency components
Δf_p	=	width of a spectral peak at 0.707 times its magnitude
Δt	=	time between discrete samples of a record
$\Delta \dot{v}$	=	change in velocity of a system
ω	=	undamped natural frequency of a system in radians per second
ω_D	=	damped natural frequency of a system in radians per second
ω_n	=	natural frequencies of T-beams in radians per second
$\bar{\omega}$	=	frequency of harmonic loads
$\phi_n(x)$	=	mode shapes of T-beams
$\psi(x)$	=	assumed shape function of T-beam

- $\psi(x,y)$ = assumed shape function of vibrating panel
- θ = phase angle by which the T-beam response lags the applied load
- θ_k = phase angle of complex frequency component
- ξ = percentage of critical damping
- ξ_n = damping ratio of mode n

1. Introduction

1.1 Introductory Remarks

In recent years, an increasing number of long span floor systems have exhibited annoying vibrations in response to the dynamic forces generated by the human occupants. Consequently, structural dynamics has become an important consideration in the design of these floors.

Advances in technology and material production are responsible for the modern day trend toward large column-free floor spaces. High-strength steel, lightweight concrete, suspended ceilings, and composite construction are all factors which have made the construction of such floor systems possible. Since the numerous advantages of large open floor areas ensure this form of construction will continue, long span floors must be designed such that any vibration occurs outside the range of human perception and the need for a dynamic approach to floor design is thus apparent.

Transient floor vibration is a distinct phenomenon which generally is not influenced by strength. Even in the worst cases, the vibration caused by human occupancy generally produces stress levels well below design values. The acceptability of a floor with respect to vibration depends on the dynamic characteristics of the floor, the type of excitation, and the level of acceptable vibrations.

These three factors interact in establishing reasonable design criteria for all types of floor systems.

This study investigates the dynamic characteristics of the relatively new "stub girder floor system" and those of a steel joist-concrete slab floor. The experimental results are subsequently used to evaluate the applicability of current design procedures to the two floor systems.

1.2 Historical Review

Research dealing with floor vibrations has increased greatly in quantity and scope during the past two decades. Concentrated efforts in the field began in 1959 under the direction of Dr. K. Lenzen at the University of Kansas. This research was sponsored by the Steel Joist Institute of America.

In the first phase of the study, Lenzen and Keller (1) developed the "T-beam analogy" for calculating the natural frequencies of steel joist-concrete slab floor systems. The relatively simple method is described in Chapter 2. In the same study the authors collected and reviewed the information available on human sensitivity to vibration. A set of curves presented by Reiher and Meister (2), which related human response to the amplitude and frequency of steady state vibration, was modified to evaluate the transient (short term) vibrations generated by the human occupants on a floor system.

To examine the accuracy of the proposed T-beam analogy, Lenzen and Keller (3) conducted vibration tests on forty steel joist-concrete slab floor systems. They found that the method predicted the natural frequencies of the floors with reasonable accuracy.

Keller (4) conducted the second phase of the original study on human sensitivity to vibration of steel joist-concrete slab floors. By using a laboratory test floor and a selected group of subjects, he examined human response to steady state and transient vibrations. His results substantiated the set of curves postulated by Lenzen and Keller (1) for evaluating the transient response of floors.

The scope of the original investigation was extended by Wiley (5) to cover the vibration of rectangular, anisotropic plates. He also demonstrated that the T-beam analogy was a good first approximation for calculating the natural frequencies of steel joist floor systems.

Because the vibrational acceptability of steel joist floors was largely influenced by damping, additional studies were undertaken to investigate the possibility of eliminating undesirable transient vibrations of a floor through an artificial increase in damping. Barr and Lyons (6,7) proposed and tested several types of vibration absorbers or dampers with the objective of being able to correct unsatisfactory floor response without costly structural changes. Of all the methods considered, only mass damping units were found to be effective in

substantially increasing the damping of a floor system.

The mass damping units consisted of a weight attached to the bottom chords of the floor joists by springs and a damping mechanism. The damping units were designed to have a frequency approximately 0.5 Hz lower than the fundamental floor frequency and upon installation they were tuned to operate out of phase with the floor system. The out of phase motion and damping of the units resulted in a significant reduction of the floor vibration after very few cycles.

In 1962, Lenzen (8) presented a complete summary of the preceding studies on the vibration of steel joist-concrete slab floors.

In 1965, a second set of vibration studies began at the University of Kansas in an attempt to provide answers to some of the questions which arose from the previous studies.

An investigation by Meyer (9) examined the applicability of the T-beam analogy to steel beam-concrete slab floor systems in steel framed buildings. Through analytical and experimental work, he found that the method could be used to closely approximate the frequency of such floors, but that considerable errors occurred when the method was used to predict the initial vibratory amplitude.

In another study, Ohmart (10) addressed the problem of accurately computing the dynamic displacement response of a steel-beam concrete slab floor at the design stage. He approximated individual floor bays by an eccentrically

stiffened, simply supported, rectangular plate and then derived the impulse response of the system. Ohmart also obtained the force versus time relationship for the human excitation of a floor system. This excitation function, commonly referred to as the heel drop impact, has subsequently been used as the standard in evaluating floor performance both experimentally and analytically. The heel drop impact and the associated force-time relationship are described in Chapter 2.

Lenzen and Murray (11) drew from all of the previous research work in an attempt to develop a qualitative design procedure concerning floor vibrations. They also conducted vibration tests on twenty different floor systems to study the effect of as many variables as possible. The comparison of data associated with the various types of floor construction failed to indicate any significant differences in the vibrational characteristics of the floors. They concluded the results of the study were insufficient to establish a dynamic design criteria applicable to the majority of floor systems.

In 1968, Lenzen and Dorsett (12) directed a large scale laboratory investigation aimed at accurately outlining the effects of various structural parameters on the vibrational characteristics of floor systems. The study was the first to direct full attention to the concept of an effective floor area participating in an impact induced vibration. An empirical formula for determining the size of effective

floor areas was presented in the report.

While the above laboratory investigations were underway, Sokolowski, Lenzen, and Dorsett (13) developed a more precise analytical theory for predicting the response of steel joist-concrete slab floor systems. They generalized the floor system as an orthotropic plate and solved the associated deflection and natural frequency problems from the classical force-equilibrium viewpoint. In addition, the authors developed a simplified model which allowed the floor system to be considered as an effective number of joists or T-beams. They presented theoretical formulas for calculating the width of the effective floor area and the number of "fully effective" joists. The analytical procedures were then checked against the results of the laboratory study. Moderow (14) further substantiated their work through experimental field studies.

The important conclusions and design procedures derived from the University of Kansas research were condensed by Galambos (15) into a brief report for the use of the structural design profession.

Allen and Rainer (16) developed annoyance criteria for walking induced vibrations of long span floors which have been adopted by the Canadian Standards Association (CSA) and presented in the CSA Standard S16.1-M78 (17). The suggested criteria, which are applicable to quiet occupancies, represented an extension of the criteria presented by Lenzen and his co-workers. Allen and Rainer also formulated a

complete method for predicting the vibrational performance of a floor system through design calculations and subsequently experimentally verified those procedures. These design criteria are described in detail in Chapter 2.

Wilson and Heidebrecht (18) summarized much of the previous work on the vibration of long span floors and presented a state-of-the-art report which also included the results of some experimental work. They critically reviewed the various means of theoretically evaluating floor performance through several design examples and itemized remedial measures for floors exhibiting annoying vibrations.

In a recent publication, Rainer (19) described an in-depth dynamic study of a steel joist-concrete slab floor system. By means of a frequency domain analysis, he identified several natural frequencies of vibration and the associated mode shapes and critical damping ratios. This study was one of the first to consider several modes of vibration, which represents the start of a new era in the dynamic analysis of floor systems.

Several other recent papers on the subject of floor vibrations have been included in the list of references (20,21,22,23).

1.3 Purpose and Scope

The purpose of this study was to experimentally determine and evaluate the dynamic characteristics of the stub girder floor system. The composite floor system derives its name from the built-up girders called "stub girders" which act as the principal framing members. Secondary members, comprised of standard wide flange sections, are arranged in a cantilever system spanning in the transverse direction. The structural system was developed to allow mechanical and electrical ductwork to be incorporated within the framework of the floor. The investigation described herein is believed to represent the first detailed dynamic study of the novel floor system. Some consideration has also been given to the applicability of current design procedures to the system.

The lack of proper dynamic design criteria for dance floors prompted an investigation into the dynamic response of a steel joist-concrete slab dance floor. Separate experimental investigations were undertaken to determine the dynamic characteristics of the floor system (ie: natural frequencies, mode shapes, and modal damping ratios, etc.) and to monitor the forced response of the floor during dances.

The results of the latter investigation were used in the development of a procedure for evaluating the dynamic response of dance floors at the design stage.

In addition to presenting the results of the above studies, the current analytical evaluation procedures are discussed in detail. The important aspects of the data acquisition and reduction stages of the studies are also discussed.

2. Theoretical Evaluation of Vibrating Floor Systems

2.1 Introduction

Because of the increasing number of long span floor systems exhibiting bothersome vibrations in response to normal human activity, researchers have developed design procedures and criteria to evaluate the dynamic response of such floors at the design stage. This chapter is devoted to a discussion of the floor vibration criteria presently used in Canada in the dynamic design of floor systems.

In addition to a discussion on acceptable levels of floor vibration, the chapter includes a detailed presentation of the analytical methods used to determine the dynamic characteristics of floor systems and an itemized list of corrective measures for floors with annoying vibrations.

2.2 Acceptable Vibration Limits

All floor systems vibrate in response to the dynamic loads generated by human occupancy. When the floor design is satisfactory, the vibration amplitudes are below the threshold of annoyance for the occupants. To achieve such a design, a knowledge of human sensitivity to vibration is required.

Studies (2,24) have shown that human sensitivity to any movement or vibration depends on the frequency, amplitude,

and duration of the vibration. For quiet occupancies such as office buildings, transient vibrations caused by the human occupants that last more than five cycles are the main source of concern. A number of recent studies (4,25,26) have been carried out to determine human sensitivity to such vibration. The results have generally been expressed in a set of curves which relate level of perceptibility or degree of annoyance to: (a) the fundamental natural frequency, (b) the damping characteristics, and (c) the maximum displacement or acceleration response of the floor produced by a specific aperiodic excitation force. Acceleration has been chosen as the parameter to measure the magnitude of floor vibrations in this study since it is most convenient for both experimental and analytical work.

The standard heel drop is the force impact commonly used to excite the floor in actual vibration tests to measure floor response. For this test, a man weighing approximately 77 kg, wearing hard soled shoes, supports his weight on the balls of his feet with his heels raised approximately 65 mm from the floor surface. The man then suddenly relaxes, transferring his full body weight to his heels, resulting in an impact on the floor. This type of impact varies somewhat from person to person but tests (18) have shown that a single individual produces impacts which are quite consistent.

Although this test provides a correlation between certain dynamic floor properties and acceptability of a

floor under human occupancy, it does not directly simulate any specific servicability condition. However, the heel drop test is used because it is simple, can be used to develop reasonable guidelines, and can be used in the experimental evaluation of a floor system.

A set of annoyance threshold curves for the heel impact test are shown in Fig. 2.1. These annoyance thresholds, commonly used in floor vibration studies in Canada (17), apply to quiet occupancies such as an office building or home where the majority of floor vibrations are caused by the walking impacts of inhabitants. The annoyance thresholds are expressed as a function of frequency, initial peak acceleration, and damping. Of the many parameters available to establish acceptable vibration levels, these measures have been found to best reflect human perception of floor vibrations.

Human activities on some floor systems, such as dance hall and school gymnasium floors, result in vibrations which last longer than twelve cycles and therefore are perceived as steady state. At the present time, annoyance threshold curves similar to those referred to above for quiet occupancies, have not been developed for steady state floor vibrations. The applicability of curves such as those presented by Reiher and Meister (2) for steady state vibrations, to such floors has not been investigated and is therefore uncertain. The only guideline given in the CSA standard (17) for floors subjected to repetitive activities

is a recommendation to produce a floor design which results in a fundamental frequency greater than 10 Hertz (1 Hz = 1 cycle/sec). The difficulty of designing a floor to economically meet this requirement indicates the need for better design criteria.

2.3 System Modelling and Theoretical Formulation

A prime responsibility of a design engineer is to ensure that a floor system is serviceable under dynamic loads generated by human occupancy. In order to determine whether or not a floor is acceptable using the guidelines presented in the previous section, a designer must have a mathematical model which can be used to evaluate the fundamental frequency, the acceleration response, and the damping of the proposed floor system. This analytical model must accurately represent the behavior of the actual floor system.

2.3.1 Fundamental Frequency

Several analytical models have been considered in past research work to determine the fundamental frequency of floor systems. Although reasonable results were obtained from most of the models considered, the analysis involved was too complicated and time consuming for design practice. However, the relatively simple T-beam analogy, proposed by Lenzen (1), has been used with success for some time in

predicting the fundamental frequencies of several floor types. The T-beam concept for steel joist-concrete slab floors and floors composed of a concrete slab supported on steel beams has been developed using the following simplifying assumptions:

- 1) The floor system is broken up into a series of simply supported T-beams, with each steel joist or beam acting compositely with a width of concrete floor (s) equal to the distance between joists.
- 2) Reinforcing steel and metal decking are ignored for considerations other than weight.
- 3) The effective thickness of the concrete flange (t_e) is determined from the average weight of concrete including any that is contained in the ribs of the corrugated formwork.
- 4) The individual T-beams are assumed to have free sides.

Although floor systems vibrate in several modes, the fundamental mode has, in general, the most important influence on the majority of floors which exhibit troublesome vibrations. The fundamental frequency of the assumed T-beam is calculated using the theoretical formula for determining the fundamental frequency of a simply supported uniform beam. This natural frequency expression is (27)

$$f_j = 1570 \sqrt{\frac{E_s I_t}{m L^4}} \quad (2.1)$$

in which f_j = fundamental frequency of assumed T-beam
in Hertz (1 Hz = 1 cycle/sec)
 E_s = modulus of elasticity for steel
(200000 MPa)
 I_t = transformed moment of inertia of T-beam
assuming full composite action (mm^4)
 \bar{m} = mass per unit length of T-beam (kg/m)
 L = length of T-beam (mm)

The technique can be extended to floors where the steel joists or beams are supported at their ends by non-rigid steel girders. This is accomplished by assuming that the steel girders act as spring supports for the joists or beams. With the further assumption that the spring constant is the same at each end, the desired system frequency is calculated by Dunkerly's formula (28) as

$$\frac{1}{f_f^2} = \frac{1}{f_j^2} + \frac{1}{f_g^2} \quad (2.2)$$

in which f_f = the fundamental frequency of the floor
in Hertz
 f_j = frequency of joists or beams as
determined using Eqn. 2.1
 f_g = frequency of supporting girders loaded
with the floor weight they support and
their own self weight but neglecting any
contribution of the slab to the
stiffness, unless the girders are
designed to behave compositely.

The floor system frequency calculated from Eqn. 2.2 is always lower than the individual component frequencies f_j and f_g .

2.3.2 Initial Peak Accelerations

In determining the initial peak acceleration of a floor system subjected to a heel impact, the floor is assumed to oscillate in its fundamental mode. A large floor area normally consists of several vibrating panels each with a length equal to the distance between joist supports and a width which depends on the stiffness properties of the floor perpendicular to the joists. The adjacent panels move in opposite directions thus forming nodal lines or lines of zero displacement. Figure 2.2 illustrates the effective width of floor participating in an impact induced vibration. The concept of an "effective floor width" was first used by Lenzen and Dorsett (12) to determine the peak displacement response of a floor to the heel drop impact.

More recently, Allen and Rainer (16) have formulated the peak acceleration response of an individual panel bounded by nodal lines to correspond to that of a simple oscillator. They assume that the width (b) of the effective floor (see Fig. 2.2) is equal to $60t_e$, where t_e is the effective thickness of the concrete slab. As mentioned previously, in the case of ribbed decking the effective slab thickness is calculated on the basis of the average weight of concrete including the ribs.

A more detailed method for calculating the effective width of the vibrating panel was derived by Sokolowski (13). The method takes into consideration the stiffness of the floor both along and perpendicular to the steel joists or beams. The effective width (b) can be determined by the expression

$$b = \frac{3\sqrt{2}\epsilon L}{2} \quad (2.3)$$

in which b = width of the effective floor
perpendicular to the joists

L = length of the joists

$\epsilon = (D_x/D_y)^{1/4}$

and D_x = flexural stiffness perpendicular to the
joists (slab only)

D_y = flexural stiffness parallel to the
joists (composite section)

The flexural rigidities in the two directions are given by

$$D_x = \frac{E_s t_e^3}{12n} \quad (2.4)$$

and

$$D_y = \frac{E_s I_t}{s} \quad (2.5)$$

in which E_s = modulus of elasticity for steel

n = modular ratio

I_t = moment of inertia of assumed T-beam

s = spacing of the joists or beams

The above method is recommended for calculating the effective

floor width instead of the $60t_e$ approximation because of improved accuracy and because little additional effort is required.

With the effective floor width determined by one of the above methods, the mass of the equivalent simple oscillator can be closely approximated by assuming that the vibrating panel forms a typical one-half sine wave shape in both directions. The time dependent displacement of the panel $v(x,y,t)$ is given by (see Fig. 2.3)

$$v(x,y,t) = \psi(x,y)Z(t) \quad (2.6)$$

in which $\psi(x,y) = \sin\frac{\pi x}{L} \sin\frac{\pi y}{b}$
 = the assumed shape in the fundamental
 mode of vibration

$Z(t)$ = a function of time only.

The inertial force (dF_I) generated during vibrations in an elemental area of the panel with dimensions dx by dy is equal to

$$dF_I = \psi(x,y) \ddot{Z}(t) \bar{m} dx dy \quad (2.7)$$

where \bar{m} is the mass per unit area and a dot above a symbol represents one differentiation with respect to time. The equivalent modal mass of the entire panel (M_E) can therefore be obtained by integrating the elemental inertial forces over the area and dividing the results by $Z(t)$. The resulting expression is

$$M_E = \int_y \int_x \psi(x,y) \bar{m} dx dy \quad (2.8)$$

which upon substitution for $\psi(x,y)$ and integrating between the limits of x equal to zero and L and y equal to zero and b gives

$$M_E = \frac{4}{\pi^2} b L \bar{m} \quad (2.9)$$

Equation 2.9 can be approximated by the expression

$$M_E = 0.4 b L \bar{m} \quad (2.10)$$

In evaluating the equivalent modal mass, the mass per unit area is determined by averaging over the panel area the mass of the concrete slab, the steel joists, the ceiling panels, the flooring, and the ductwork included within the effective floor area.

To determine the acceleration response of a floor panel subjected to a heel impact, the force-time relationship of the heel impact must be known. The force versus time curve resulting from the heel drop test as obtained by researchers at the University of Kansas (10) is shown in Fig. 2.4. The actual response curve can be approximated by the triangle shown, which has the same enclosed area.

In this study, an attempt was made to examine the validity of the above force versus time curve by constructing a beam fitted with a load cell. The load cell acted as a simple support at one end of the beam while the other end had a roller-like support. Heel drop impacts were

delivered directly over the load cell and the resulting signals were recorded and then subsequently converted into plots of the loading function. A typical force versus time curve is presented in Appendix D along with some pictures of the test setup (see Figs. D.1 and D.2).

Although several tests were conducted with various subjects of different weights wearing a variety of shoe types, the peak value of the measured force was always significantly below that obtained at the University of Kansas. In general, the enclosed area of the loading function was also 15-20% less. However, the University of Kansas curve (see Fig. 2.4) will be used in the derivations in the remainder of this chapter in order to maintain a direct relationship with current design specifications.

If the fundamental frequency of a floor system is below ten Hertz, the heel drop impact can be considered as an impulse I , equal to the area under the force-time curve which is 67 Newton-seconds. The response of the floor system is found by first calculating the change in velocity of the floor ($\Delta \dot{v}$) from the impulse momentum relationship (29) using the expression

$$\Delta \dot{v} = \frac{I}{M_E} \quad (2.11)$$

Then the dynamic response is calculated using the expression for the displacement response of a single degree of freedom (SDF) system to an initial velocity. This expression is given by

$$v(t) = e^{-\xi\omega t} \frac{\dot{v}(0)}{\omega_D} \sin \omega_D t \quad (2.12)$$

in which

ξ = percentage of critical damping

ω = undamped natural frequency of the floor panel

ω_D = damped natural frequency of the floor panel

$\dot{v}(0)$ = initial velocity

Under the assumption that the floor is initially at rest, the initial velocity is equal to the change in velocity of the floor derived above, and the response is

$$v(t) = e^{-\xi\omega t} \frac{I}{M_E \omega_D} \sin \omega_D t \quad (2.13)$$

If Eqn. 2.13 is differentiated twice with respect to time, the acceleration response can be determined from the expression

$$\ddot{v}(t) = e^{-\xi\omega t} \frac{I}{M_E} \left[\left\{ \omega_D - \frac{(\xi\omega)^2}{\omega_D} \right\} \sin \omega_D t + 2\xi\omega \cos \omega_D t \right] \quad (2.14)$$

Equation 2.14 can be used to estimate the maximum acceleration response by assuming low damping values, an assumption valid for floor vibrations where ξ is typically below 15 percent for the fundamental mode, and by assuming that the maximum response occurs at $\omega_D t = \pi/2$. Since for low damping ω_D is approximately equal to ω , which is in turn equal to $2\pi f$ (where f is the frequency in Hertz), the maximum acceleration response is given approximately by the expression

$$\ddot{v}_{\max} = \frac{0.9 (2\pi f) I}{M_E} \quad (2.15)$$

By substituting Eqn. 2.10 into Eqn. 2.15 and assuming I is equal to 67 Newton-seconds, the expression in terms of percent gravity (%g) for the maximum acceleration response (A_o) of a floor panel subjected to a heel drop impact is

$$A_o = \frac{9655 f}{bL\bar{m}} \quad (2.16)$$

In this equation

f = the fundamental frequency of the floor system in Hertz

b = effective floor width perpendicular to the joists (m)

L = length of floor joists (m)

\bar{m} = the floor mass per unit area (kg/m²)

The equations for calculating A_o in the CSA standard (17) can be obtained from Eqn. 2.16 by letting the effective floor width be equal to $60t_e$ and by incorporating the mass of all floor components into an equivalent thickness of concrete slab. The CSA equations assume that the mass of additional floor components (ie: floor covering, ductwork, etc.) is equal to an additional 25 mm thickness of concrete.

2.3.3 Damping

The final structural parameter required for an evaluation of the dynamic properties of a floor system is the damping ratio. The important influence of damping on floor vibrations is clearly shown on the annoyance threshold chart in Fig. 2.1 by the large increase in allowable initial peak accelerations for relatively small increases in the critical damping ratio. Unfortunately, damping is one parameter which cannot be calculated, and is difficult to estimate, at the design stage. Therefore, an estimate based on past experience with similar floors must be used.

Some guidelines are given in the CSA standard (17) for estimating damping values of a floor at various construction stages and for different types of occupancies. These are rather vague, however, and a slightly incorrect estimate can greatly affect the acceptability of a floor as determined by the annoyance thresholds of Fig. 2.1. There are several papers (8,16,18,30) which present damping values, found experimentally, for various floor systems and therefore, a better approximation can sometimes be made by finding a published value for a floor of similar construction and usage as the one in question.

2.4 Remedial Measures to Correct Floor Vibration Problems

If a vibration problem exists after construction of a floor, remedial measures must be taken to correct the condition. These measures may include the following:

- 1) The stiffness of a floor may be increased by adding cover plates to the bottom chords of existing joists or by adding new joists to the floor system. In addition to increasing the strength of a floor, these alterations result in a higher floor frequency and decreased amplitudes of vibration and are therefore beneficial for floor systems where repetitive activities are creating vibration problems.
- 2) An increase in the thickness of the concrete slab tends to reduce the initial peak acceleration (refer to Eqn. 2.16), to lower the natural frequency because of increased mass, and to increase the damping of a floor system. Although this modification is very useful for lowering human perception of floor vibrations, the extra loading sometimes prohibits its use.
- 3) Placing concrete on the lower chords of the floor joists tends to increase the damping of a completed floor by about 2%.
- 4) Placing carpets on bare floors reduces the force of walking impacts and slightly increases the damping of those floors.

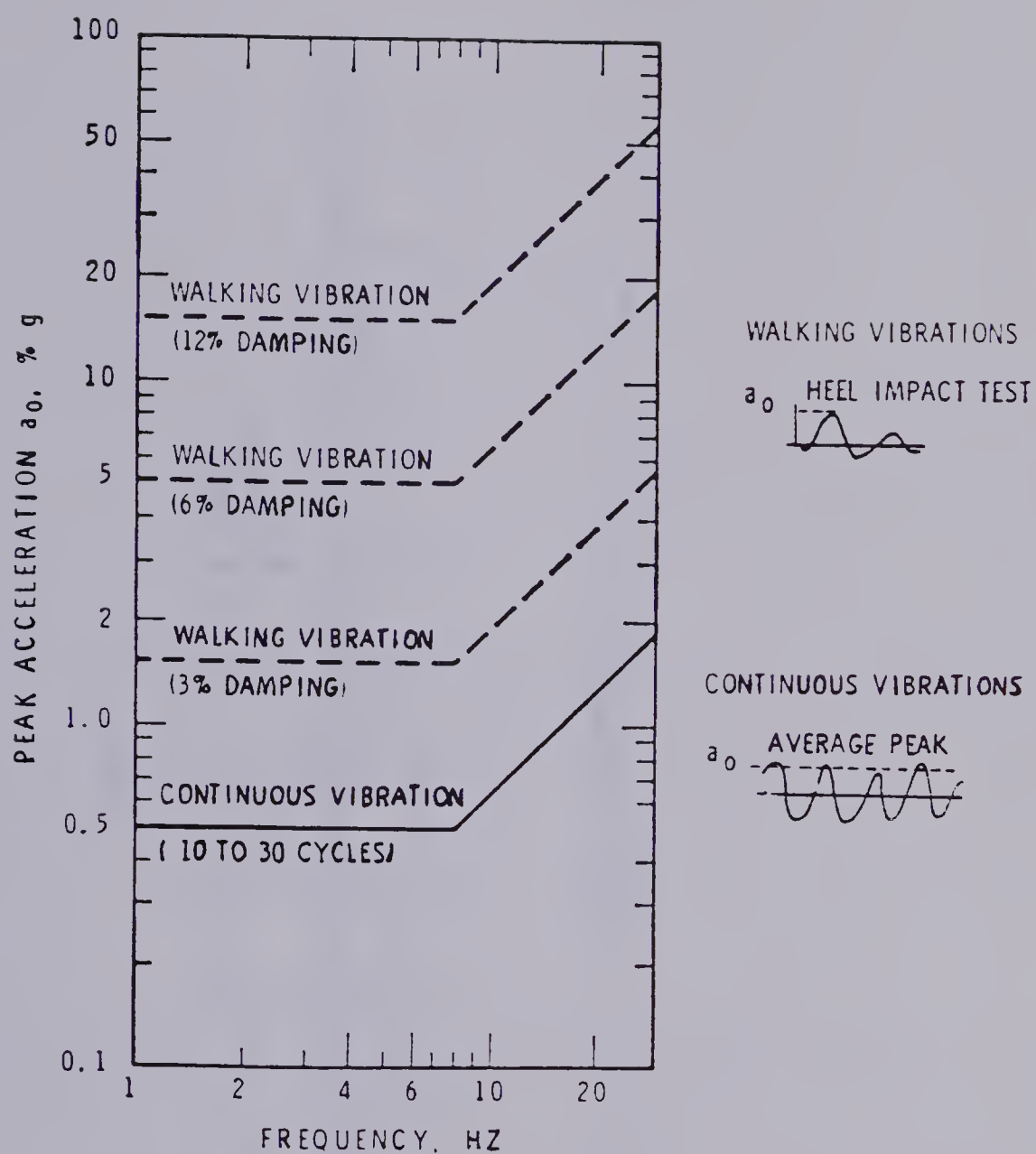
- 5) The addition of partitions, either above or below a problem floor, is very effective in increasing the damping of the floor system. Even light, low partitions can increase damping by 10% of critical. If properly oriented, the partitions can also significantly reduce the amplitudes of vibration of the floor.
- 6) Dynamic damping units or damper posts can be installed to increase the damping of a troublesome floor system (22). The mass damping units (also called vibration absorbers), which must be designed specifically for a particular floor, are usually quite successful in correcting bothersome floor vibrations although the units are expensive and not always practical. They should only be installed on the recommendation of a vibration consultant and should not be employed for floor systems subjected to repetitive activities.

Appendix D contains the results of a series of tests conducted with a plywood mass damping unit which can be used to increase the damping of a floor system in some instances..

Damping posts may be installed above or below a troublesome floor and are generally quite effective in correcting floor vibration problems. However, the disruption of open floor areas often makes the use of damping posts undesirable.

- 7) Although usually not desirable, a change in the occupancy of a floor is a measure which is sometimes necessary if other corrective measures are not feasible. In some instances, floor vibrations can be made less noticeable by rearranging furniture and walking routes.

Each of the above measures alters the vibration properties of a floor in a different manner. The type of vibration (whether continuous or transient) as well as the vibration source must be considered in determining which measure to use in correcting the problem. In most cases, the alterations required to correct a serious floor vibration problem are very expensive, indicating the need for a thorough evaluation of the problem before proceeding with repairs.



Annoyance Thresholds for Floor Vibrations Due to Footstep
(Residential, School, Office Occupancies)

Figure 2.1 Annoyance Threshold Chart

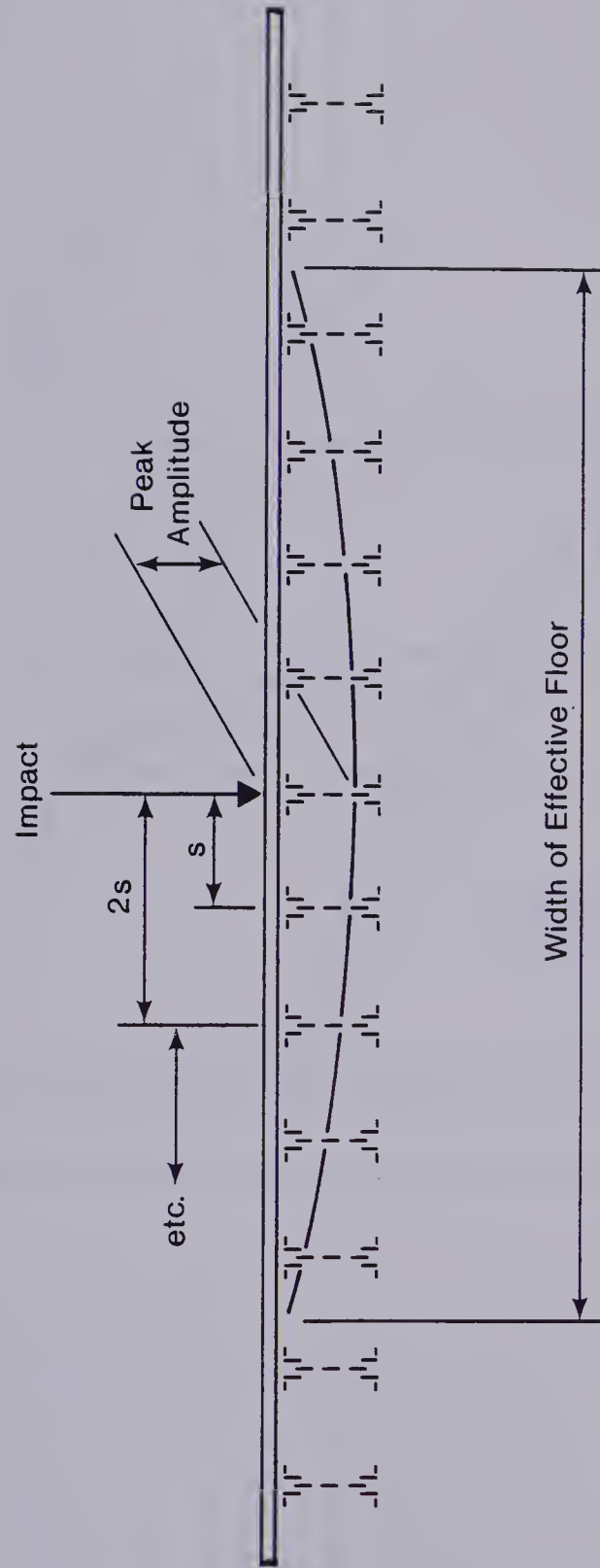


Figure 2.2 Definition of Effective Floor Width

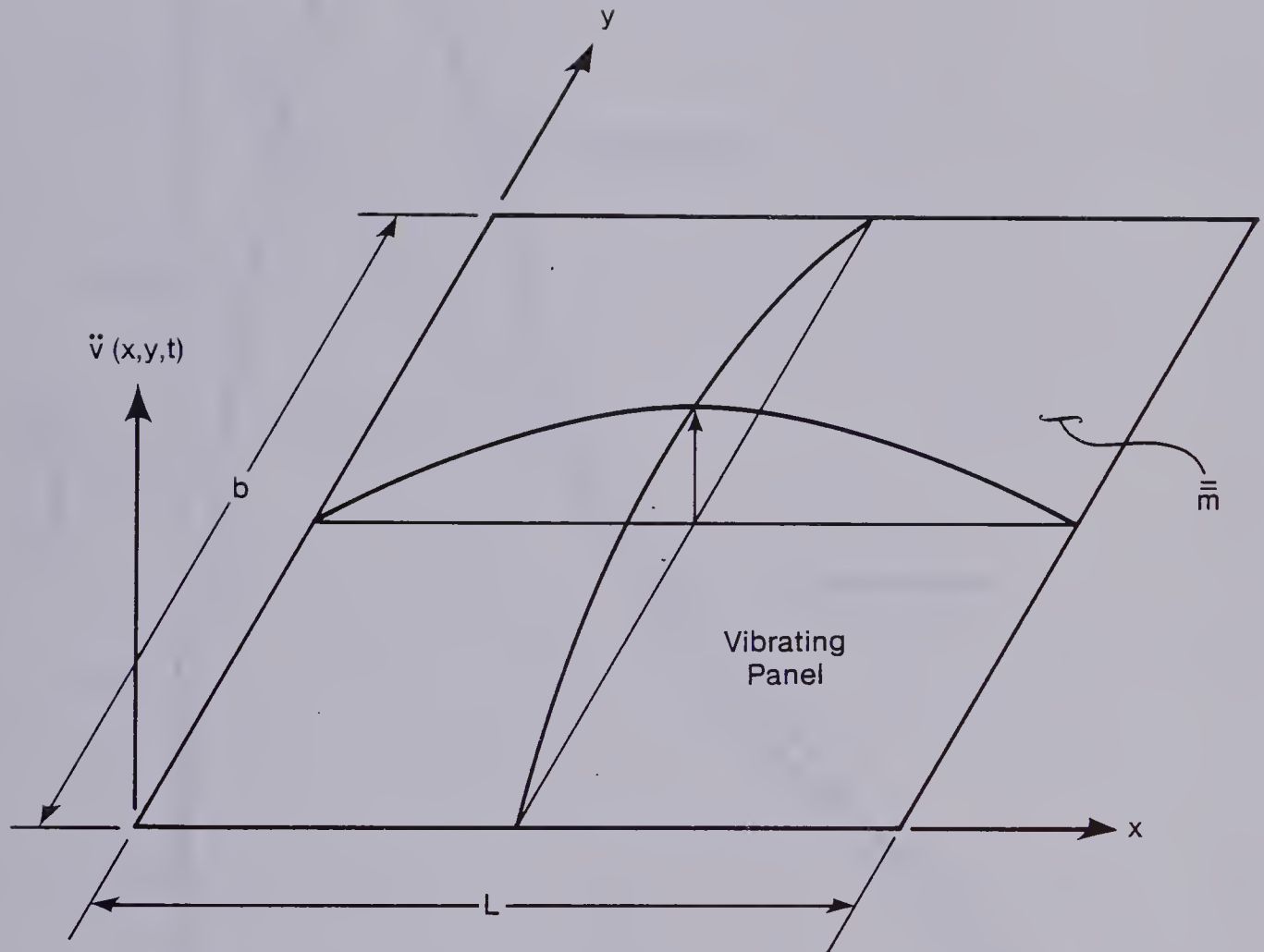


Figure 2.3 Assumed Configuration of Vibrating Panel

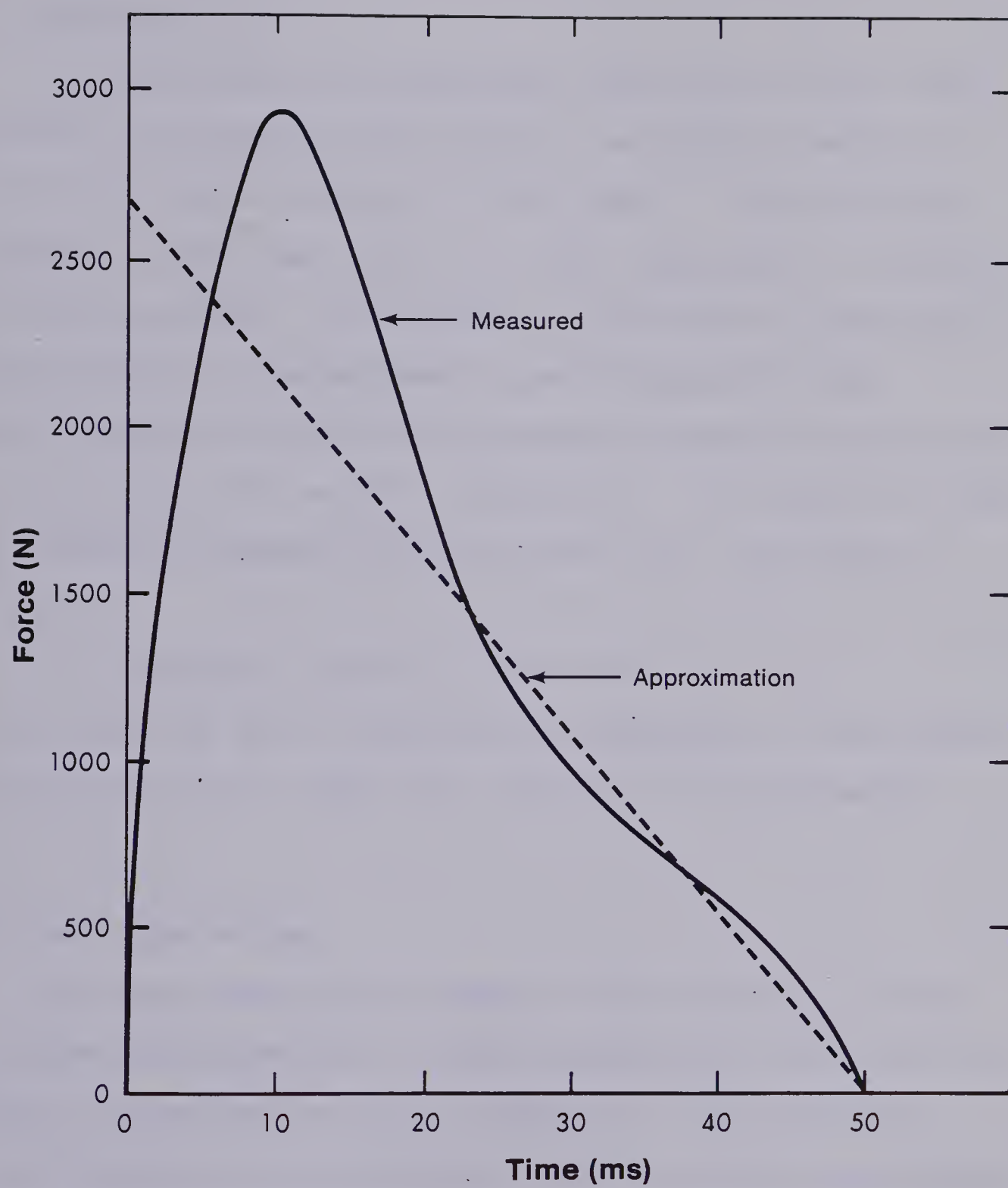


Figure 2.4 Force vs. Time Curve for Heel Drop Impact

3. Data Acquisition and Reduction

3.1 Introduction

To determine the vibrational properties of the floor systems considered in this study, the dynamic response of the floors was monitored in field tests. Vibration data recorded during the field trips were subsequently analyzed in the laboratory. This chapter is devoted to a detailed presentation of the equipment used in acquiring the experimental data and the procedures followed in processing and analyzing the recorded information. The steps involved in processing and analyzing the data are illustrated in Fig. 3.1.

In subsequent chapters, the results of the investigations and an engineering assessment of the dynamic characteristics of the floor systems will be presented.

3.2 Data Acquisition

The data acquisition stage of the vibration studies included the conversion of floor vibrations into electrical signals using acceleration transducers, the subsequent conditioning of the electrical signals, and the recording of the conditioned signals on a FM tape recorder. To ensure that reliable data were obtained, the equipment used was selected from the wide range of equipment available, after giving careful consideration to the nature of the dynamic

loadings and the probable dynamic characteristics of the floor systems involved.

Bruel and Kjaer type 8306 and 4370 accelerometers (31) were used in the studies to monitor the floor motion. These highly sensitive, piezoelectric accelerometers give excellent results in the lower frequency range and for relatively small accelerations, which are typical of floor vibrations. Bruel and Kjaer type 2804 power supplies were used to power the accelerometer pre-amplifiers built into the type 8306 accelerometers.

Special purpose cables were used to connect the accelerometers to in-line voltage amplifiers or signal conditioners. They helped to prevent the induction of "noise" or electrical interference into the signals.

Bruel and Kjaer type 2635 portable charge amplifiers, or Bruel and Kjaer type 2615 micro-phone pre-amplifiers in conjunction with a custom made amplifier-filter system, were used to condition the accelerometer signals. The equipment served to amplify the signals and to eliminate unwanted high frequency components by filtering. This prevented distortion of the signal components and resulted in realistic calibration levels, greatly improving the signal to noise ratio of the recorded data. Although in one study some were filtered at 50 Hz, in general the signals were low-pass filtered at 100 Hz.

After conditioning, filtering, and amplification, all accelerometer signals were recorded on Bruel and Kjaer

type 7003 portable FM tape recorders. The four channel capacity of the type 7003 recorder allowed four accelerometer signals to be recorded simultaneously, preserving time and phase relationships between the various signals.

In one floor study, seven accelerometers tracked the floor motion thus requiring the use of two tape recorders. An accelerometer common to both recorders was used to relate the phase of the signals recorded on the separate machines.

Initially an oscilloscope was used to view the accelerometer signals to determine the necessary adjustments of the processing and recording equipment. Miscellaneous equipment such as power supplies for the recorders, voltmeters, filters, and a DC power supply was also used in the vibration studies.

Prior to the individual floor studies, a calibration signal was recorded on each of the tape recorders involved. The calibration signals were obtained by monitoring the prescribed acceleration of an Unholtz-Dickie shaker table with the test equipment. By comparing the known input to the recorded output, the accuracy of the data acquisition and signal processing equipment could be established.

The intent of the preceding discussion was to provide a general description of the equipment involved in the data acquisition stage of the vibration studies. The instrumentation varied slightly for the floor systems considered, as did the scope of the individual

investigations. However, the general approach for each floor system was the same. Further insight into vibration monitoring equipment and data acquisition procedures is provided in related publications (28,31,32,33,34). A photograph of a typical instrumentation setup is shown in Fig. 3.2.

3.3 Analog to Digital Conversion

In this study, accelerometer records were stored on FM tape as continuous or "analog" signals. To process these signals using the digital computer facilities at the University of Alberta, an analog to digital (A/D) conversion was necessary. In this conversion process or "digitization" the analog signals were sampled at discrete times.

A proper sampling rate was necessary to obtain an accurate digital representation of the analog signals. Shannon's Sampling Theorem (28) states that to properly define an analog signal in digital form, the sampling rate must be at least as high as twice the highest frequency component in the signal. If higher frequency components are present in the signal, "aliasing" will occur. As illustrated in Fig 3.3, aliasing is the misinterpretation of frequency components above one-half the sampling rate, as lower frequency components. The frequency component in Fig. 3.3a is properly defined by the chosen sampling rate (indicated by *'s), while the component in Fig. 3.3b is

misinterpreted as being at the same frequency.

To ensure the requirements of the sampling theorem were met, the recorded signals were lowpass filtered prior to digitization. Krohn-Hite model 3342 filters were employed to eliminate frequency components above one-third of the selected sampling rates. Although some of the records from one floor study were digitized at 250 points/second, the majority of the signals were sampled at 500 points/second. The recorded accelerometer signals were digitized simultaneously to preserve phase relationships.

The system used to perform the A/D conversion consisted of a Redcor model 720, ten channel multi-plexer, 12 bit A/D convertor interfaced with a Digital PDP 11/20 computer. This equipment converted the voltage signals from the FM recorders into binary units which were stored in the computer for writing on magnetic tape. A Wang nine track tape unit, also interfaced with the PDP 11/20 computer, provided a word transfer to and from the magnetic tape.

Through the sophisticated conversion system, the analog signals were sampled at the high rates with precision. The errors introduced into the digital signals through the conversion process were of a magnitude similar to the electrical interference or "noise" contained in the original signals (35). Consequently, the final results were not adversely affected by the digitization errors.

3.4 Data Preprocessing

Following the digitization process, the stored accelerometer records were entered into the digital computer. The stored information was converted from binary form to digital representations of the originally recorded voltage signals. In preparation for the frequency analysis described in the next section, the discrete voltage signals were modified by appropriate conversion factors to give acceleration-time records. The accelerations were expressed in percent gravity ($1\text{ g} = 9.81\text{ m/s}$). A listing of the computer program used to perform the above operations is included in Appendix E.

Standard trend removal techniques (36) were employed to remove erroneous trends contained in the experimental data. The most common error, shown in Fig 3.4a, was a constant voltage offset caused by the DC level adjustment on the anti-aliasing filters. A corrected version of the accelerometer trace is shown in Fig 3.4b.

Two types of acceleration-time records were measured. The first type consisted of short duration or transient events, which start and end with zero amplitude. These events were produced by heel drop impacts on the test floors. The second type consisted of continuous acceleration-time signals which lasted several minutes. These signals were produced by people dancing on one of the floor systems studied. Because the two signal types are not the same, different modifications were required to prepare

each type for frequency analysis. These additional pre-processing steps are presented in detail in subsequent sections dealing with the analysis of the different signals.

3.5 Frequency Analysis

3.5.1 Introduction

The objective of frequency analysis is to classify signals according to their frequency content. "Fourier analysis" or "spectral analysis" are the terms commonly used to describe this process.

Frequency analysis was used in this study to transform the digital accelerometer signals from the time domain to corresponding functions in the frequency domain. The frequency domain representations were then used in determining the dynamic characteristics of the floor systems.

Only the fundamental concepts of frequency analysis, with special attention devoted to the application of this theory to the experimental floor vibration data, are presented herein. Rigorous mathematical derivations and proofs can be found in related publications (33,37,38,39).

3.5.2 Fourier Analysis

A mathematical theorem, first presented by Fourier, states that any function may be expressed as the summation of an infinite number of sine and cosine curves. Each of the curves corresponds to a single frequency component with an associated amplitude and initial phase angle. Since Fourier analysis presents a unique method for expressing any function in terms of its frequency components, it is the mathematical basis for frequency analysis.

In this study, the digital accelerometer records were processed on the digital computer by using the Discrete Fourier Transform (DFT). The DFT is a pair of equations which convert a discrete time domain function to a frequency domain representation and vice-versa. Therefore, the two equations are commonly referred to as a "forward" transform and an "inverse" transform. The forward transform is defined mathematically as

$$G(f_k) = \frac{1}{N} \sum_{n=0}^{N-1} g(t_n) e^{-j\frac{2\pi nk}{N}} \quad (3.1)$$

and the inverse transform as

$$g(t_n) = \sum_{k=0}^{N-1} G(f_k) e^{j\frac{2\pi nk}{N}} \quad (3.2)$$

in which $G(f_k)$ = complex frequency component at the discrete frequency f_k where k is any integer including zero and negative integers.

$g(t_n)$ = a discrete time function with each

sample corresponding to a time t_n
 where n is any positive integer
 including zero.

N = the total number of samples in the time
 function $g(t)$.

$$j = \sqrt{-1}$$

The DFT pair is illustrated in Fig. 3.5.

The DFT applies to functions which are sampled in both the time and the frequency domains. Because they are sampled, both the time signal $g(t)$ and the frequency spectrum $G(f)$ are implicitly periodic as well as discrete. Each period of the time record has a length

$$T = N\Delta t \quad (3.3)$$

where Δt is the time between samples. The frequency spectrum has a period equal to the sampling frequency f_s which is equal to the reciprocal of the interval Δt in the time domain. The spacing of the discrete frequency components $G(f_k)$ is denoted as Δf and is calculated as

$$\Delta f = \frac{1}{T} = \frac{f_s}{N} \quad (3.4)$$

Equation 3.4 also indicates that each period of the frequency spectrum contains $N\Delta f$ discrete values. However, it is only necessary to compute the components $G(f_k)$ for $0 \leq k \leq N/2-1$ since the the remaining components can then be obtained from symmetry.

The summation of Eqn. 3.1 extracts from the time signal $g(t)$ the components at each frequency f_k (33) to form the series of complex values $G(f_k)$. These complex frequency components can be expressed in terms of real and imaginary parts as

$$G(f_k) = a_k + jb_k \quad (3.5)$$

in which a = real part of frequency component
 b = imaginary part of frequency component.

Alternatively, the components can be written in terms of their amplitude or magnitude $|G(f_k)|$ and phase angle θ_k according to the expression

$$G(f_k) = |G(f_k)|e^{j\theta_k} \quad (3.6)$$

in which the amplitude and phase are calculated as

$$|G(f_k)| = \sqrt{a_k^2 + b_k^2} \quad (3.7)$$

and

$$\theta_k = \tan^{-1} \left(\frac{b_k}{a_k} \right) \quad (3.8)$$

Discrete Fourier Transforms were evaluated on the computer using a Fast Fourier Transform (FFT) algorithm. The results of the FFT analysis are exactly the same as the DFT analysis although a greatly reduced number of arithmetic operations are required to evaluate the summations of the transforms. Maximum efficiency using the FFT algorithm is obtained by constraining the number of time samples in a

record to an integer power of two. In the floor studies, the record lengths were selected to consist of N equal to 4096 samples corresponding to 2^{12} points.

In accordance with Eqn. 3.3, the selected number of samples results in record lengths of 8.192 and 16.384 seconds for the signals digitized at 500 points/sec and 250 points/sec, respectively. Equation 3.4 implies spacings of 0.122 Hz and 0.061 Hz between the discrete components in frequency spectra associated with the two record lengths.

3.6 Analysis of Transient Events

3.6.1 General

For the transient accelerometer traces, obtained from heel impacts on the test floors, additional pre-processing was necessary prior to the frequency analysis using the FFT. This section describes the pre-processing and subsequent analysis of those signals.

The results from the frequency analysis of the transient accelerometer records were expressed graphically in the form of magnitude and phase spectra. The magnitude spectra were required in determining the natural frequencies, mode shapes, and modal damping ratios of the floor systems. The relative phase spectra, associated with selected pairs of accelerometer records, were beneficial in determining the shapes the floors assumed when vibrating in

their various modes.

3.6.2 Analysis

In each floor study, the test program included several accelerometer placements with heel impacts at various locations. For each accelerometer placement and individual impact location, five heel drops were delivered in succession, with the floor response being allowed to damp out between impacts. Figure 3.6a shows a typical sequence of transient events associated with four consecutive heel drops on a test floor.

For frequency analysis with the FFT, the continuous digital signals were divided into segments, each segment containing the response resulting from a single heel impact. The frequency content of the individual events was unaffected because the continuous signals were sectioned at points of zero amplitude prior to the start and following the end of each event. A typical segment of the continuous signal is shown in Fig. 3.6b.

The individual events ranged in length from three to six seconds, depending on the floor type and the accelerometer position. Because of the sampling rate used in the A/D conversion process described previously, the records contained between 1500 and 3000 points. Therefore, to process the signals using the FFT algorithm with the selected N value, it was necessary to add zeroes to the ends of each event.

The addition of zeroes to the records did not influence their frequency composition, since both the altered and unaltered sequences had the same DFT (40). However, the additional zeroes resulted in a closer spacing of the discrete components within the corresponding frequency spectra and consequently provided better approximations to continuous spectra (refer to Eqn. 3.4).

The results of the forward transform analysis (Eqn. 3.1) of each event were expressed graphically in the form of a magnitude spectrum which is a plot of $|G(f_k)|$ (calculated according to Eqn. 3.7) versus frequency. Figure 3.7 shows a typical magnitude spectrum. In the figure, the points comprising the discrete frequency components have been joined with straight lines to form an envelope approximating the ideal continuous function associated with the original signal (ie: $\Delta f \rightarrow 0$)

Within a single spectrum, the magnitudes of the various peaks reflect the relative contributions of the corresponding frequency components to the measured response. Therefore, by comparing the magnitudes of the spectral peaks, the relative response of the floor at each frequency could be determined. Furthermore, since the same sampling rate, record length, and analysis procedures were employed for all of the transient events of each study, the spectral magnitudes associated with one event could also be compared to the magnitudes associated with other events. In this manner, the relative response of the floor at the various

accelerometer positions could be determined for each frequency.

Although frequency components up to 250 Hz were theoretically valid from the analysis, only those below 25 Hz were included in the results described herein. An examination of the complete spectra (ie: up to 250 Hz) revealed that the response was totally dominated by frequencies below 25 Hz in all cases, and therefore it was unnecessary to include the higher frequency components in the presentation of results.

In the vibration studies, the floor response to each heel impact was monitored simultaneously at several positions. The resulting acceleration records were considered in pairs in the subsequent derivation of relative phase spectra. These spectra were used to determine the relative direction of the floor motion at the two corresponding accelerometer positions for each natural frequency of vibration. This information was useful in determining the mode shapes of the test floors.

To obtain a relative phase spectrum from the forward transform results of two transient events, the phase spectrum of each event was first calculated using Eqn. 3.8. The relative phase spectrum was then computed as the difference in phase between the two spectra at each discrete frequency.

As illustrated in Fig. 3.8, a relative phase of zero at a particular frequency implies that both accelerometers were

moving in the same direction in the mode corresponding to that frequency. In contrast, a value near ± 180 degrees indicates they were moving in opposite directions.

3.7 Analysis of Continuous Signals

3.7.1 General

The continuous accelerometer records, measured during an evening dance at one of the test sites, were of long duration, typically about four minutes. The additional pre-processing of the traces and their subsequent analysis with the FFT are described in this section. The results of the frequency analysis are presented in terms of magnitude spectra.

3.7.2 Analysis

As mentioned previously, computer analysis with the FFT algorithm required the sampling of relatively short segments of the continuous digital signals. Therefore, the acceleration records corresponding to an individual dance were scanned and the sections containing the maximum response and those indicating significant changes in the response were selected for analysis. Figure 3.9a shows a typical section of the continuous floor response monitored during the dance. A comparison of Figs. 3.9a and 3.6 reveals that the dance records are quite different from the

transient events obtained in the heel impact tests.

Because of the continuous nature of the dance records, the sectioning of the selected segments left sharp transitions at their ends. The abrupt transitions could have resulted in a severe distortion of the spectra obtained through an FFT analysis of the segments (40,41). Accordingly, the discrete values at each end of the segments were modified to remove the discontinuities.

Smooth transition zones at the start and end of each time sequence were obtained by multiplying the discrete values within the first and last one-half second intervals by specified scaling factors. The discrete scaling factors were derived from various cosine curves to provide the envelope illustrated in Fig. 3.10. A segment of a typical dance record corrected by this procedure is shown in Fig. 3.9b. By using this procedure to correct each segment prior to FFT analysis, the end effects were reduced considerably thus significantly improving the accuracy of the spectral computations.

The various segments of the dance records selected for analysis were about twelve seconds long. Therefore, the records contained approximately 3000 points because of the 250 points/sec digitizing rate used. As with the transient events, zeroes were added to each end of the segments to extend their lengths to the number of points specified for analysis using the FFT algorithm. The altered sequences were subsequently analyzed and the corresponding

magnitude spectra plotted.

A complete listing of the computer programs used to process both the transient and continuous signals in the manners described are included in Appendix E.

3.8 Determination of Dynamic Characteristics

3.8.1 Natural Frequencies

In each floor study, the individual heel impacts generated a transient response which was the combination of several modes of vibration. The frequency analysis described previously was used to determine the natural frequencies of the floor systems by decomposing the recorded events into individual modal contributions.

In the magnitude spectrum derived from each transient event, the magnitudes of the various modal contributions were represented by peaks at the frequencies of the modes. Therefore, the natural frequencies of the floor systems were identified by the spectral peaks which appeared prominently throughout the respective results of each study.

Figure 3.7, referred to previously when discussing magnitude spectra, shows prominent spectral peaks at frequencies of 5.4, 6.2, 6.6, and 7.2 Hz. Those peaks correspond to the natural frequencies associated with various modes of vibration of the floor system.

3.8.2 Mode Shapes

To provide a clear understanding of the procedures used in determining mode shapes from the results of the FFT analysis, the method will be illustrated by an example. In one study, the floor response was monitored simultaneously at six positions along a line as illustrated in Fig. 3.11. Sequential heel drops were delivered midway between the accelerometers at positions A2 and A3, resulting in a series of transient acceleration records which were subsequently digitized and analyzed as described previously. The events corresponding to a single impact provided the six magnitude spectra shown in Fig. 3.12.

The spectra indicate two prominent natural frequencies, the first at 6.6 Hz and the second at 12.2 Hz, which can be associated with two distinct mode shapes along the line of accelerometers. The various steps in determining those mode shapes were as follows:

- 1) The first step was to obtain the relative magnitude of the peaks in each spectrum corresponding to the two natural frequencies. The spectral magnitudes are used to represent the relative modal displacements of the floor surface at the accelerometer positions. The bracketed numbers in the spectra of Fig. 3.12 designate the values used in this example.

The relative magnitude of the spectral peaks associated with a single mode also provided phase

information by indicating the presence and locations of nodal points. For example, in the magnitude spectrum of A4, the absence of a prominent peak at 12.2 Hz indicates the accelerometer was located near a nodal point of that mode. Therefore, the accelerometers on either side of A4 probably move in opposite directions in the mode associated with 12.2 Hz. This will be confirmed in the following step.

- 2) The next step was the examination of relative phase spectra to establish the relative direction of travel of the accelerometers at each natural frequency.

The relative phase spectra for accelerometers A3-A5 and A2-A6 are shown in Fig. 3.13. Although fifteen such spectra were possible from the results of the six accelerometers, the two that are presented provide enough information to correctly plot the desired mode shapes. Both spectra indicate that the accelerometers were moving in phase at 6.6 Hz and out of phase at 12.2 Hz. This confirms that a nodal point forms between A3 and A5 in the second mode.

- 3) Having determined the relative modal displacement and phase at each accelerometer position, the final step was to plot the values and draw the modal configurations. Assuming the normal position of

the floor surface as a base line, the relative modal amplitudes were plotted at the appropriate accelerometer positions, taking into account phase relationships. The mode shapes were then identified by joining the discrete points with a smooth curve.

Figure 3.14 illustrates the mode shapes associated with the natural frequencies of 6.6 and 12.2 Hz obtained by following the above procedures.

In the floor studies, spectra were calculated for up to five separate events from a single accelerometer location (ie: five heel impacts) and then averaged to obtain the relative magnitudes used in plotting the mode shape associated with each natural frequency.

Although the method described above appears relatively straightforward, difficulties were experienced in its application to some of the experimental results. In several magnitude spectra, the peaks corresponding to closely spaced natural frequencies were poorly defined and judgement was used to determine the relative amplitudes used in plotting the mode shapes. In addition, the information provided by relative phase spectra for closely spaced modes was not always reliable. However, these difficulties were overcome by giving careful consideration to all of the available results and to the modal patterns which would logically form.

To justify the validity of the mode shapes derived by this method, the factors which influenced the spectral magnitudes must be examined since they were used to represent the relative modal displacements of the floor surfaces.

Considering the spectrum associated with a particular test position, the magnitude of the individual spikes was governed by the initial amplitude of the corresponding uncoupled transient response and by the modal damping ratio which regulated the length of time the mode contributed to the total response. However, on a comparative basis, an insignificant variation in the modal damping ratios limited their influence in this respect. The limited influence of the modal damping ratios also applied to a comparison of spectra from different test positions since the individual values were relatively constant over a given floor system. Therefore, the variations in magnitude within a single spectrum reflect the relative amplitude of the response associated with each mode, and the variation in magnitude of a particular frequency component from one position to another, reflects the difference in the amplitude of the modal response at those locations. Since the spectral magnitudes are indirectly related to the amplitudes of modal response at the various test positions, their use in plotting mode shapes appears to be valid.

3.8.3 Modal Damping Ratios

Critical damping ratios for the various modes of vibration of the test floors were determined by two methods. In the first method, referred to as the one-half power bandwidth method, the modal damping ratios were derived from the widths of the corresponding spectral peaks. The second method relates the amplitude decay of a transient event to a critical damping ratio.

The modal damping values obtained by the one-half power bandwidth method were calculated using the expression (29)

$$\xi_n = \frac{\Delta f_p}{2f_n} \quad (3.9)$$

in which Δf_p is the width of a spectrum peak of a particular mode at 0.707 times its height, and f_n is the modal frequency. Figure 3.15a provides an illustration of the procedure.

To determine damping ratios using the decay method, it was necessary to obtain filtered acceleration-time signals corresponding to the desired mode of vibration. The formula which relates the critical damping ratio to the filtered decay curve for a particular mode of vibration is (29)

$$\xi = \frac{1}{2\pi m} \ln \frac{A_o}{A_m} \quad (3.10)$$

in which A_o is the initial peak acceleration and A_m is the amplitude of the response curve after m cycles of vibration. The use of Eqn. 3.10 in floor vibration studies is valid since floor systems generally have low damping values. This

method of determining damping ratios is illustrated in Fig. 3.15b.

The filtering procedures used in this study are described in the following section.

3.9 Filtered Acceleration-Time Signals

3.9.1 Introduction

Filtered acceleration-time signals were required for two purposes in this study. First, filtered acceleration-time traces were used to determine the peak modal accelerations resulting from heel impact tests. These peak accelerations were used to assess the vibration acceptability of the floor systems as described in Chapter 2. Second, filtered traces were used to determine critical damping ratios as described in the previous section.

Both analog and digital filters were used in the study to separate the acceleration records into the various modal contributions. The following sections include a brief description of the two filter types, their use, and the results provided by each. A more complete discussion on the filters, their characteristics, and the advantages and disadvantages of each is presented in Appendix A.

3.9.2 Analog Filter System

The analog filter used in the study was a Krohn-Hite model 3342, two channel, multi-purpose filter. Hardcopies of filtered voltage-time signals were obtained directly from the taped records acquired in the various tests by using the filter in conjunction with a Gould model 222 chart recorder and the Bruel and Kjaer type 7003 FM recorder. However, the analog system could only be employed after the digital frequency analysis had taken place to establish the filter ranges required to separate the recorded response into individual modal contributions. Figure 3.16 shows a typical unfiltered transient event and the corresponding filtered signal obtained from the above system.

Filter limitations (see Appendix A) prevented the accurate separation of individual modal contributions where the floor response was characterized by natural frequencies spaced less than 3 Hz apart. In those instances, the subsequent analysis of transient events was restricted to the response associated with a combination of modes of nearly the same frequency.

3.9.3 Digital Filter

The digitized accelerometer records were filtered on the computer using a finite impulse response (FIR) digital filter which was designed specifically for this study. Details of the mathematical concepts and design procedures used to obtain the FIR filter are presented in Appendix A.

The FIR filter is a frequency domain filter which was implemented after the forward transform (Eqn. 3.1) of the digital accelerometer records had been determined (see Appendix A). Following the elimination of undesired frequency components by the filter, the inverse Fourier transform (Eqn. 3.2) of the individual signals was evaluated. The resulting time signals represented the filtered response of the floors since only the frequency components within the prescribed filter range were included. An unfiltered digital signal and a corresponding filtered version obtained with the FIR filter are shown in Fig. 3.17.

The FIR filter was better adapted to the separation of closely spaced modal contributions than the analog filter described in the previous section (see Appendix A). The accuracy of the filtered results was also significantly improved. However, the FIR filter also had limitations and a spacing of at least 2 Hz between modes was necessary to separate the individual modal responses.

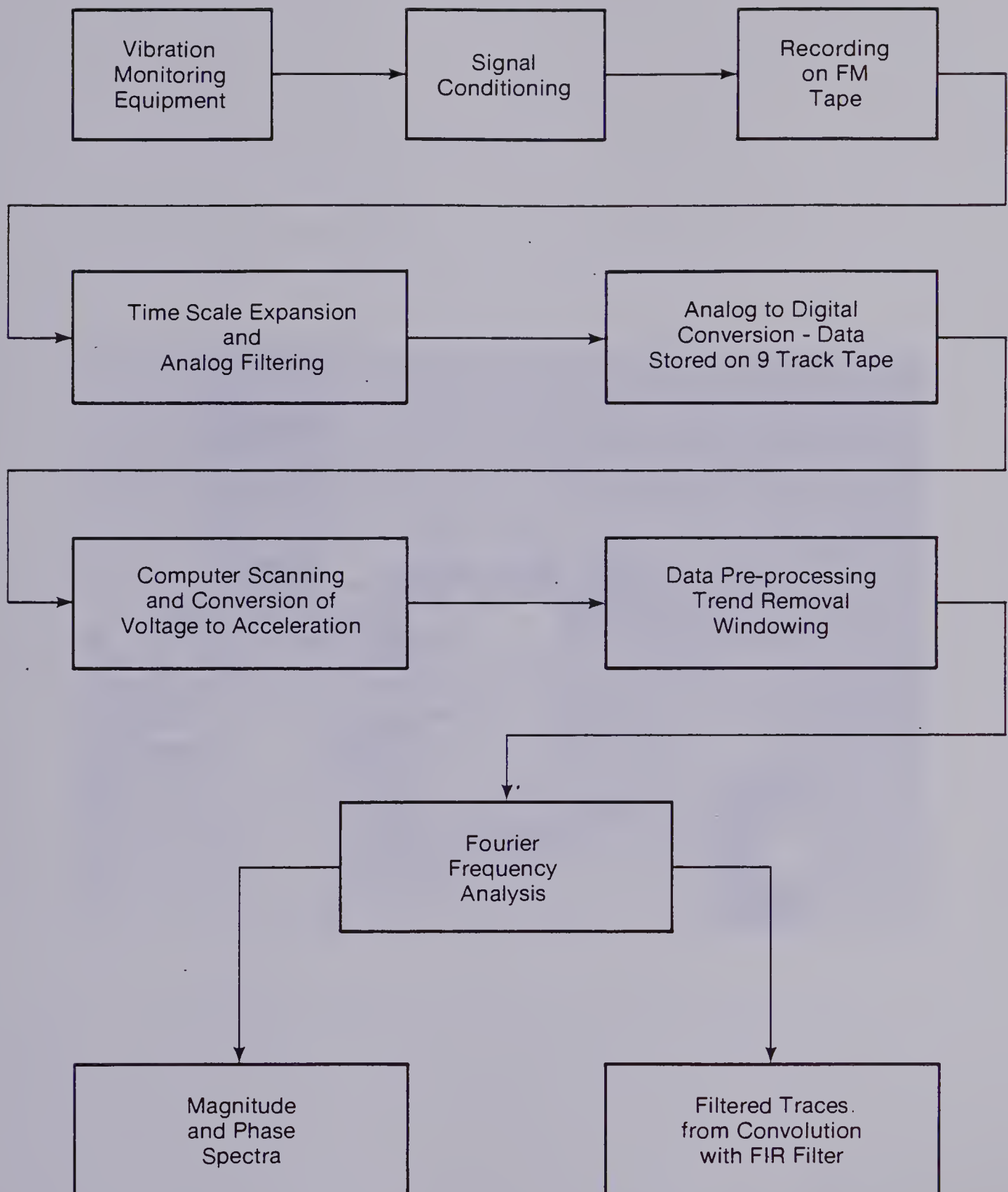
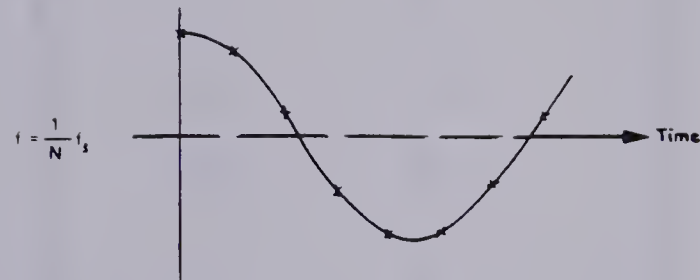


Figure 3.1 Processing and Analysis Steps

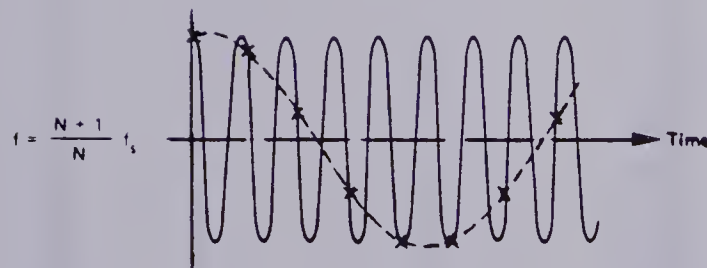


Figure 3.2 Typical Instrumentation Setup



Frequency component at $(1/N)f_s$

(a)



Frequency component at $[(N+1)/N]f_s$ interpreted as $(1/N)f_s$

(b)

Figure 3.3 Aliasing Phenomenon

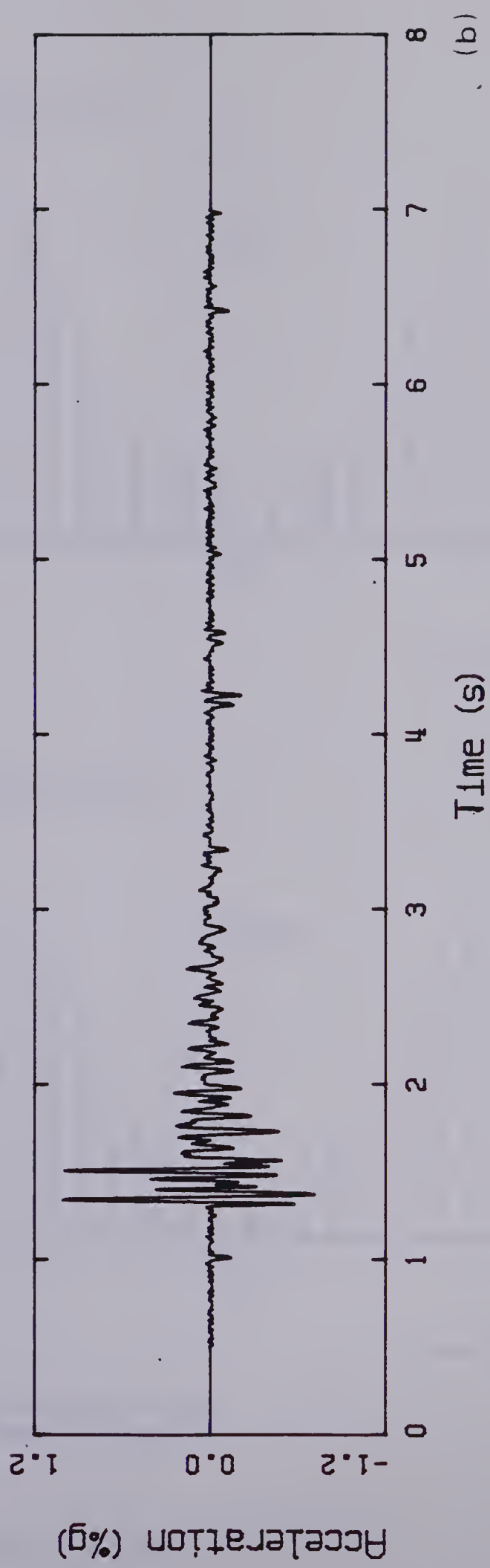
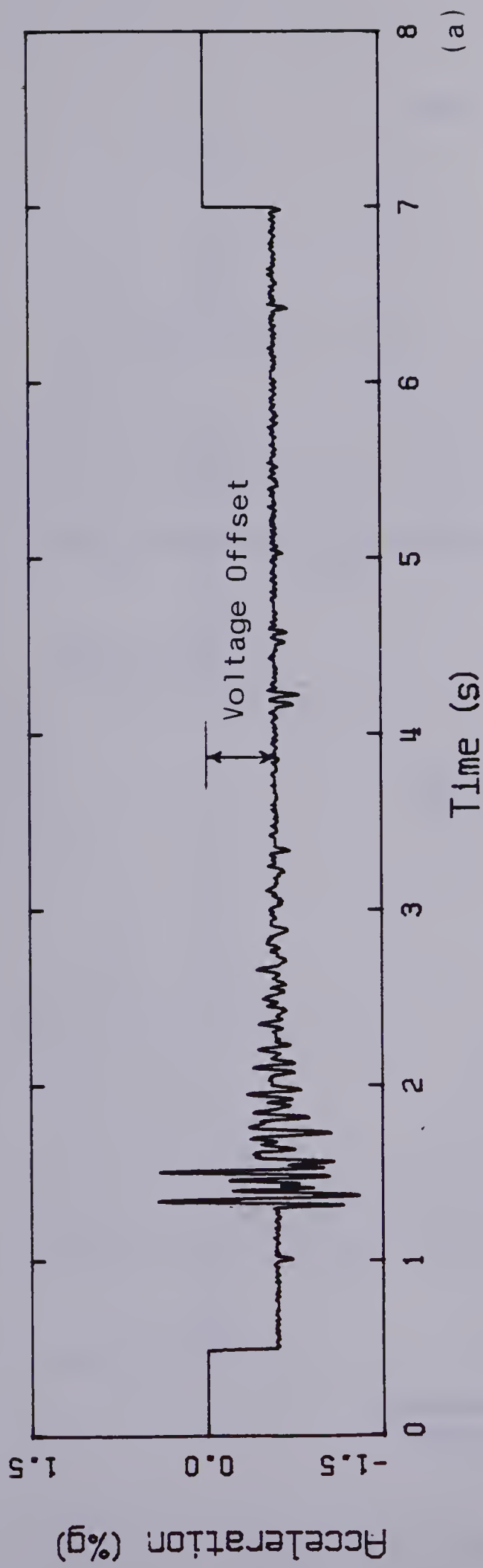


Figure 3.4 (a) Voltage Offset in a Digital Record, (b) Corrected Trace

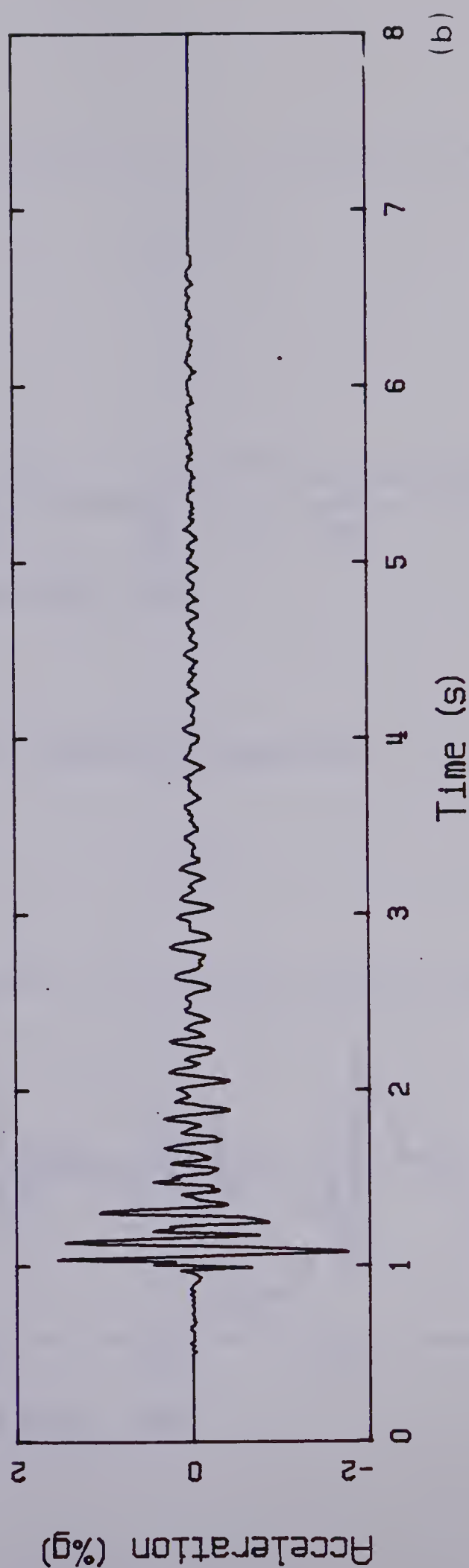
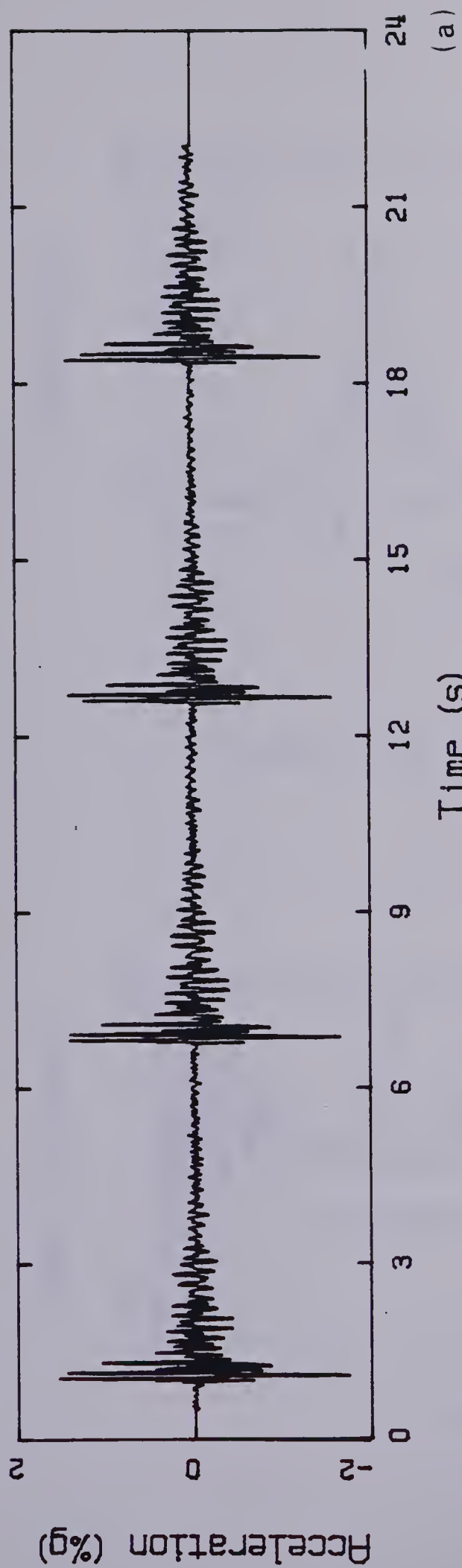


Figure 3.6 (a) A Typical Sequence of Transient Events, (b) A Single Transient Event

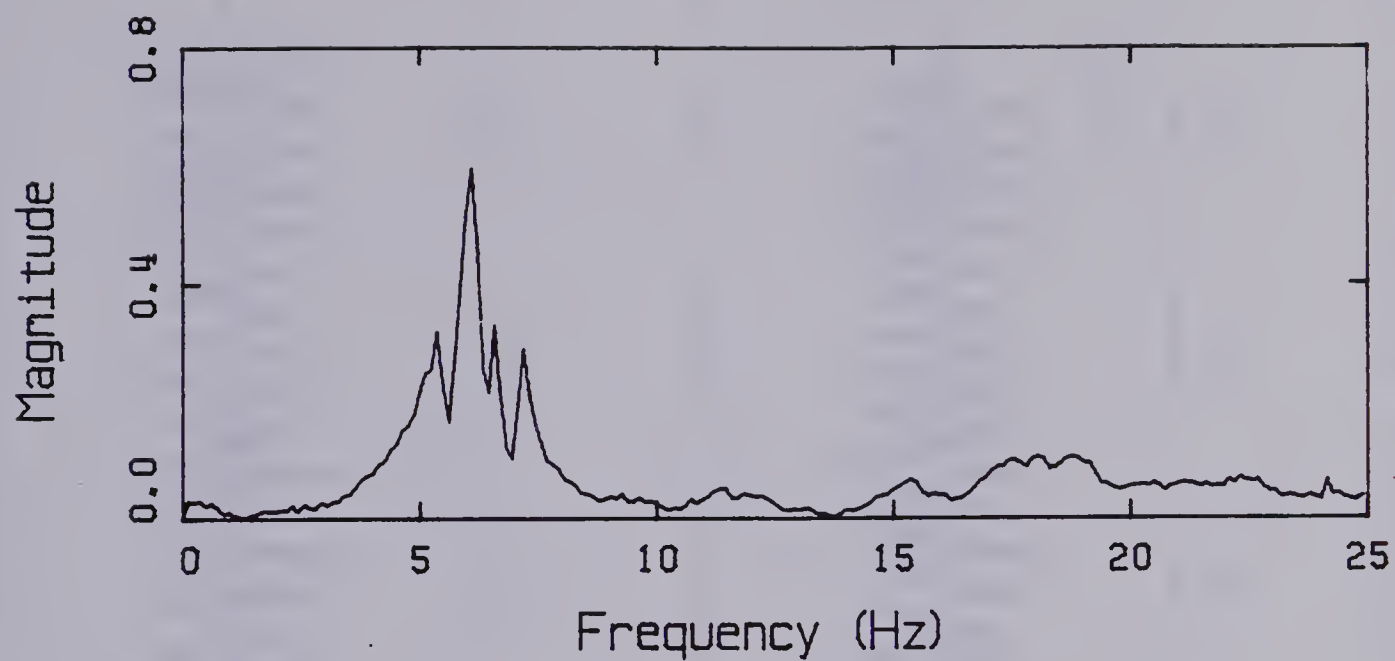


Figure 3.7 A Typical Magnitude Spectrum

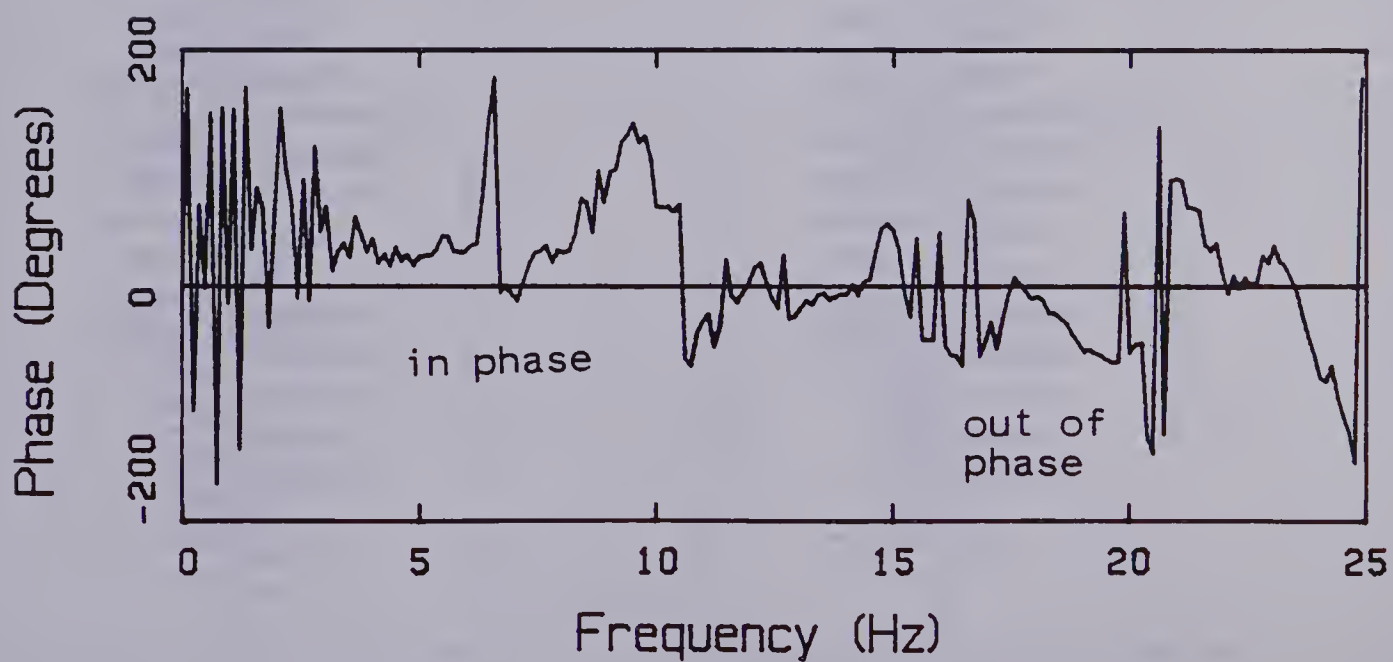


Figure 3.8 A Typical Phase Spectrum

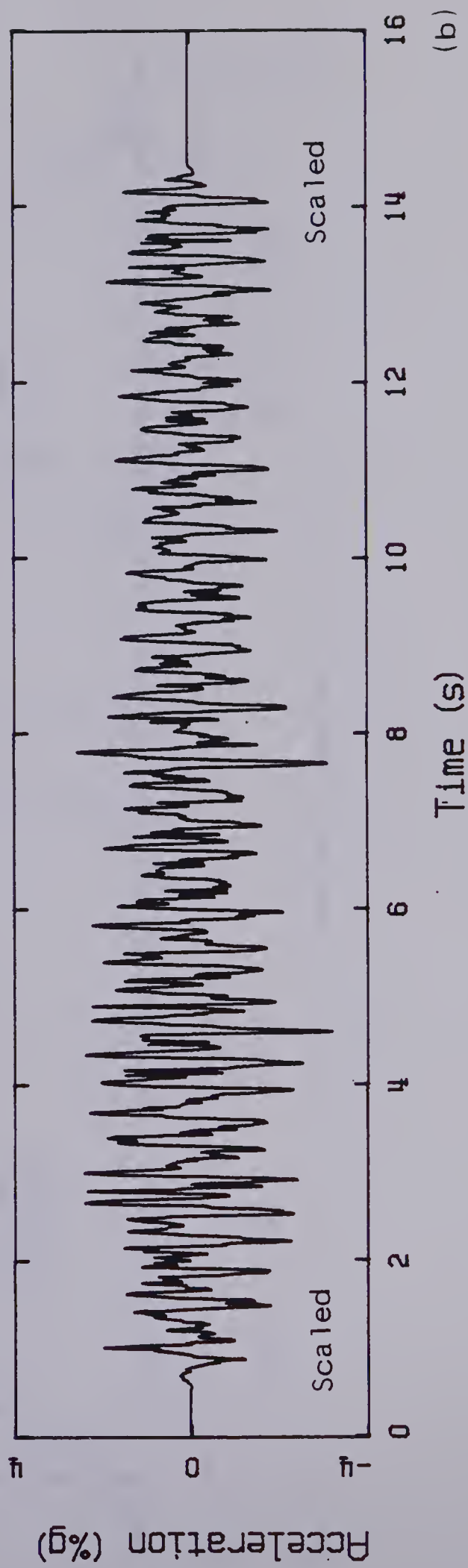
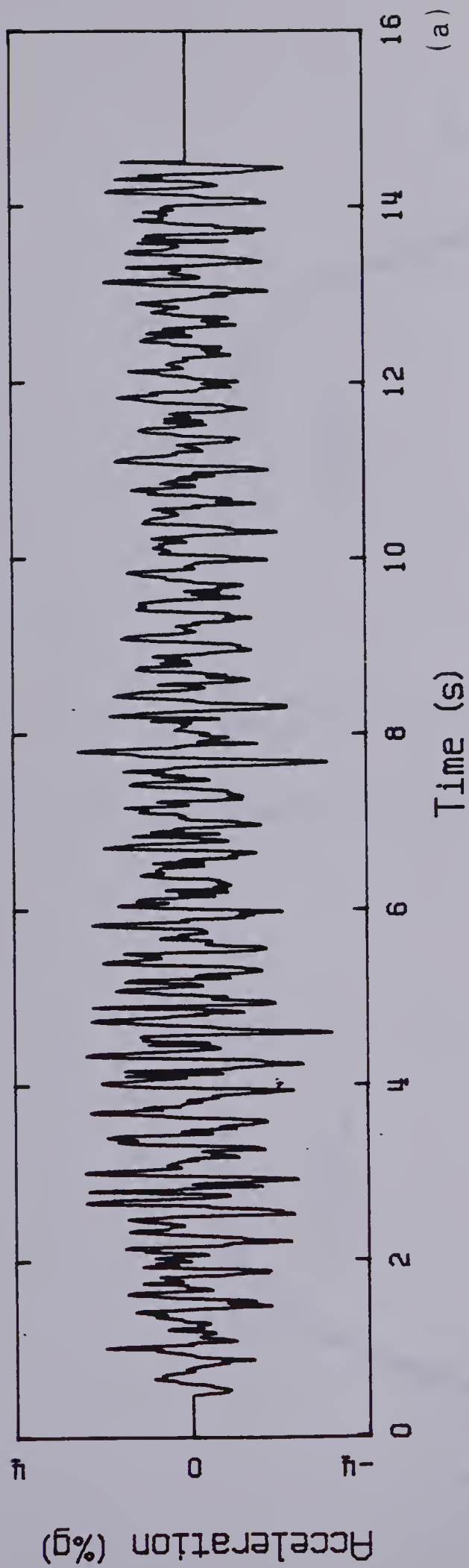


Figure 3.9 (a) Typical Portion of a Continuous Dance Record, (b) Modified Dance Record

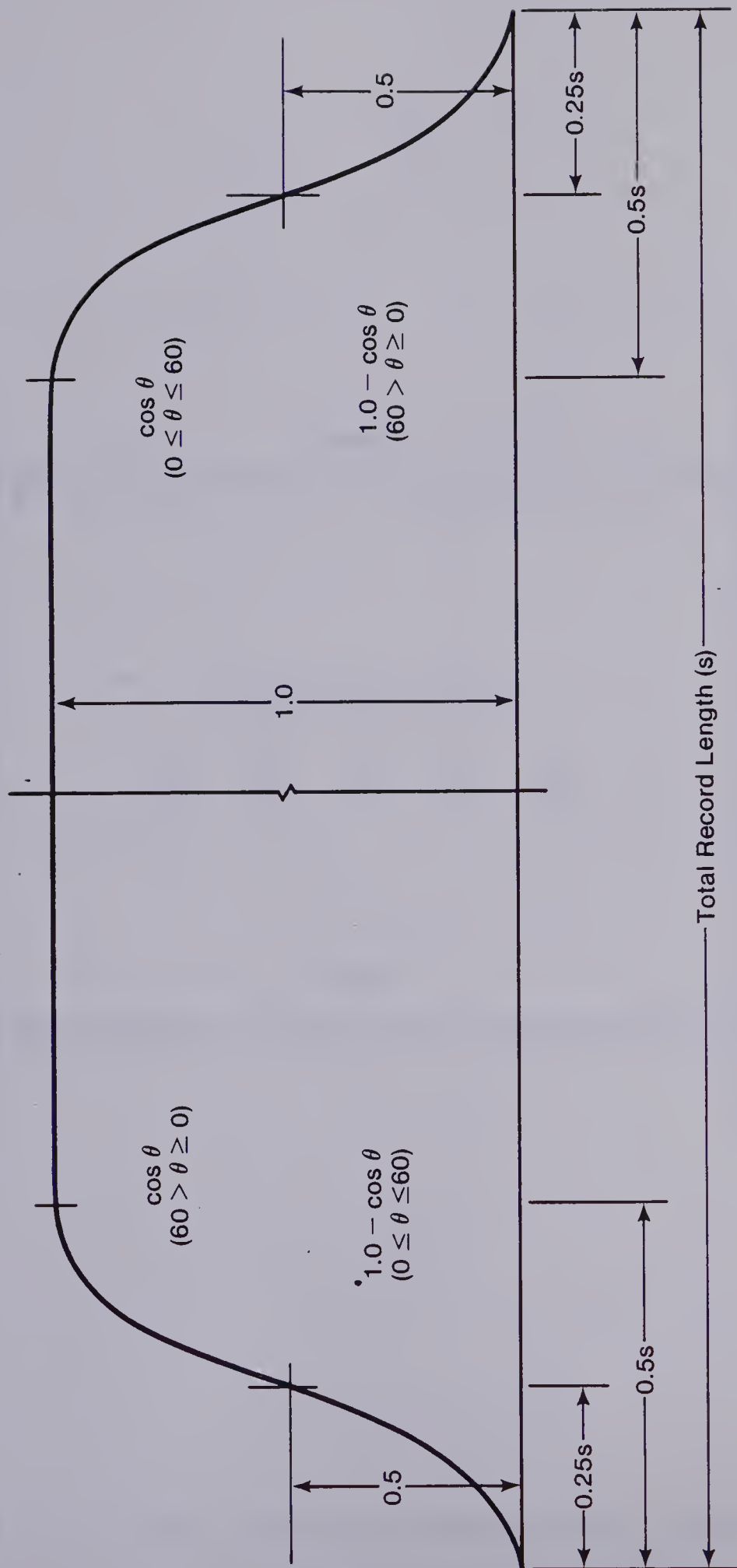


Figure 3.10 Scaling Envelope for Continuous Dance Records

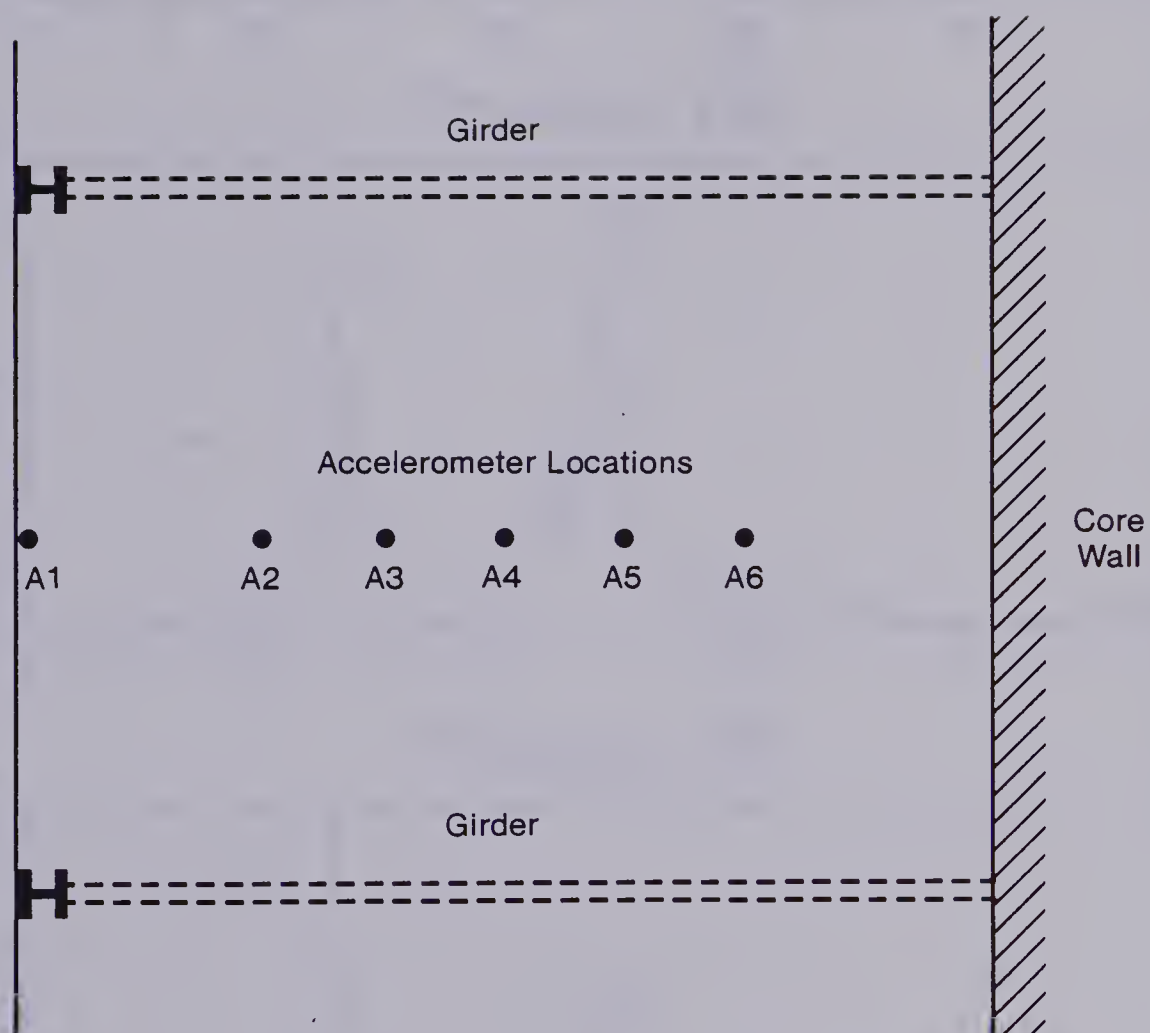


Figure 3.11 Floor Layout and Accelerometer Locations to Determine Mode Shapes

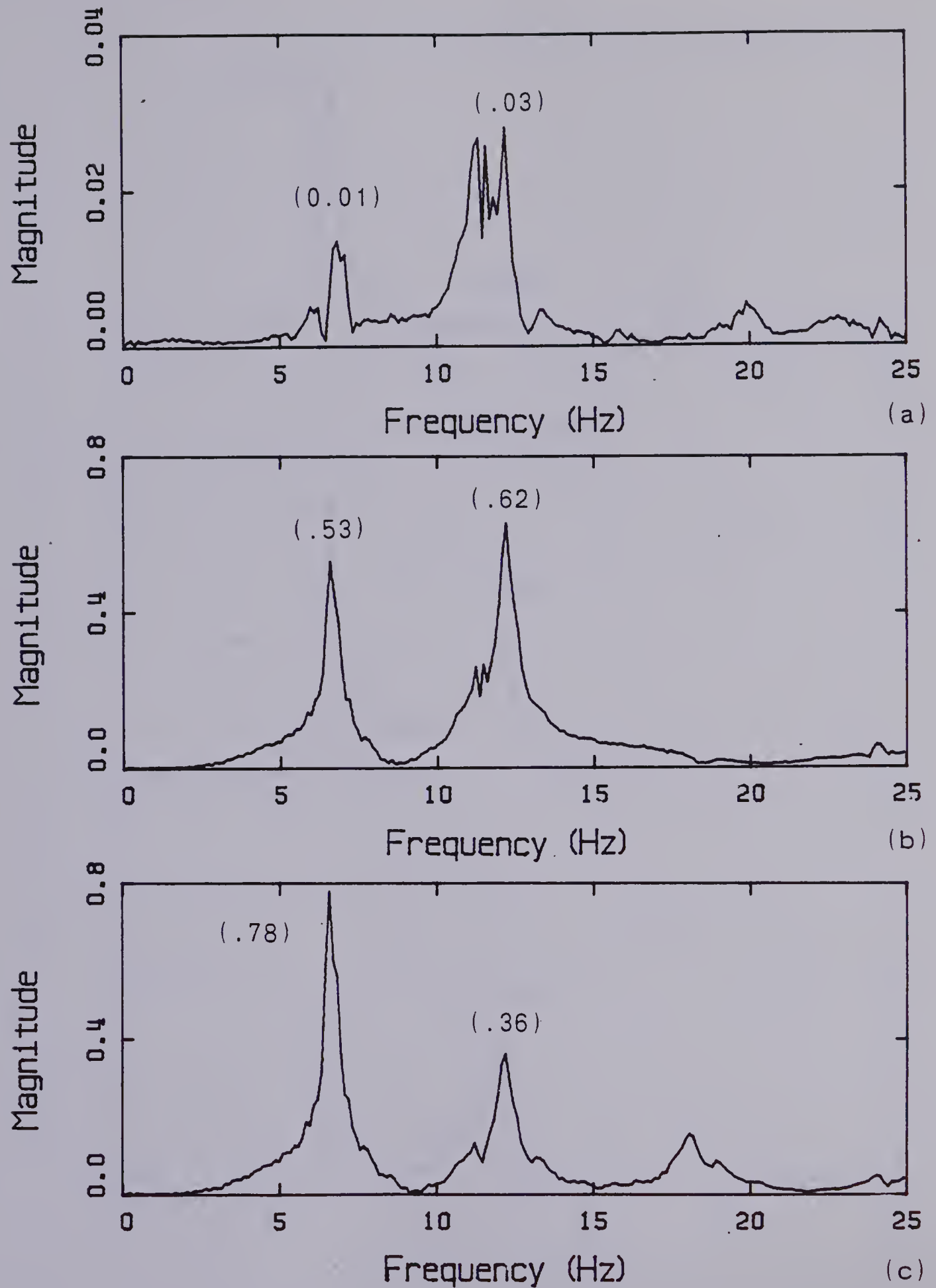


Figure 3.12 Magnitude Spectra Associated With Six Test Positions

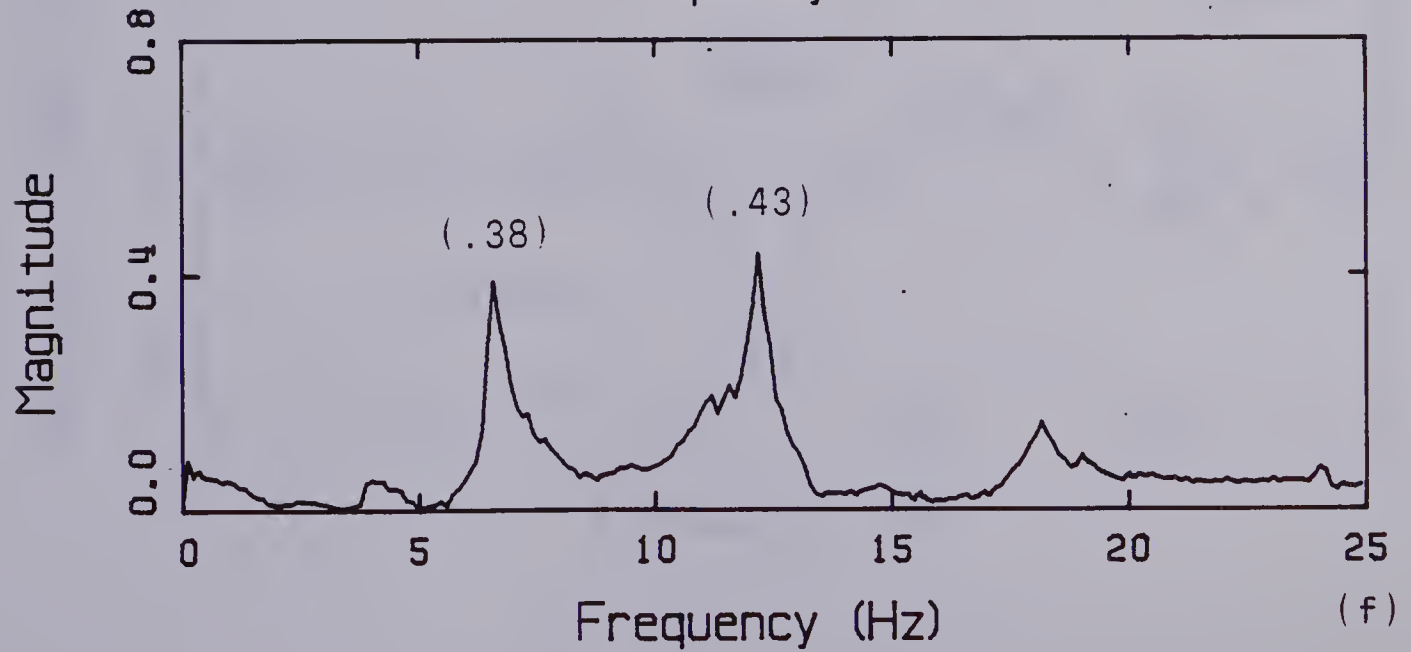
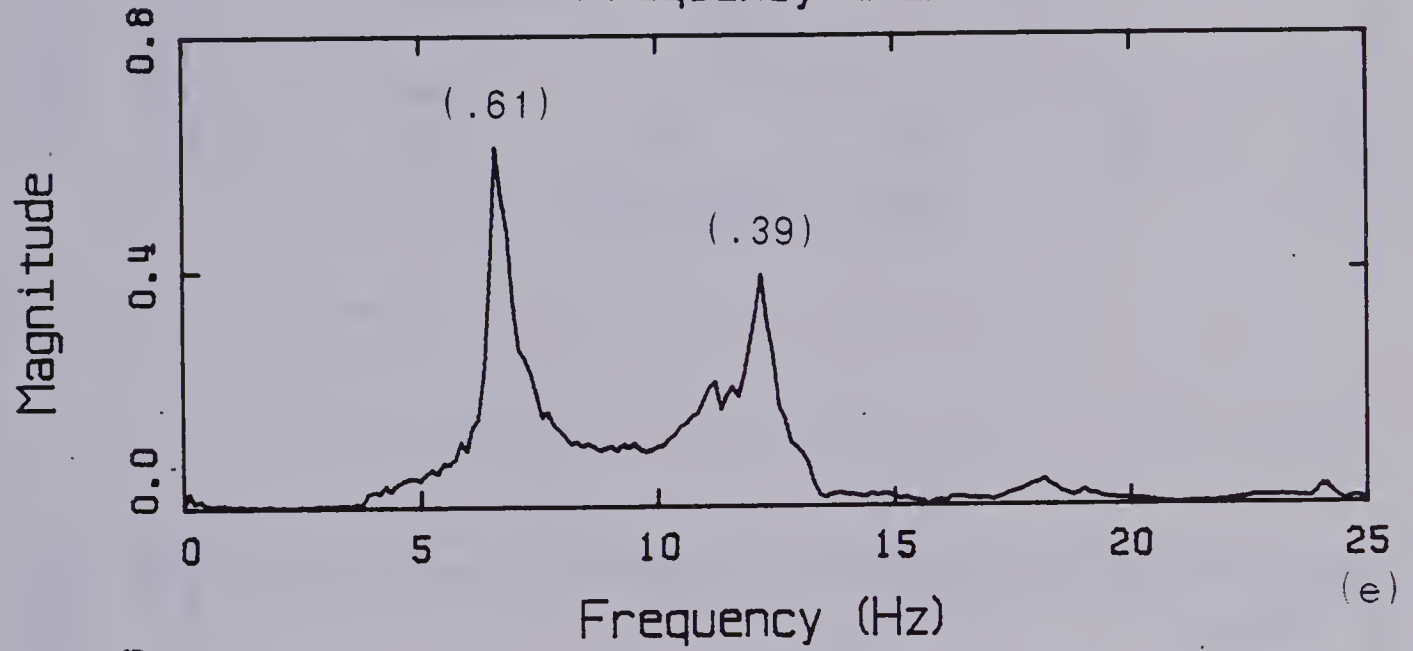
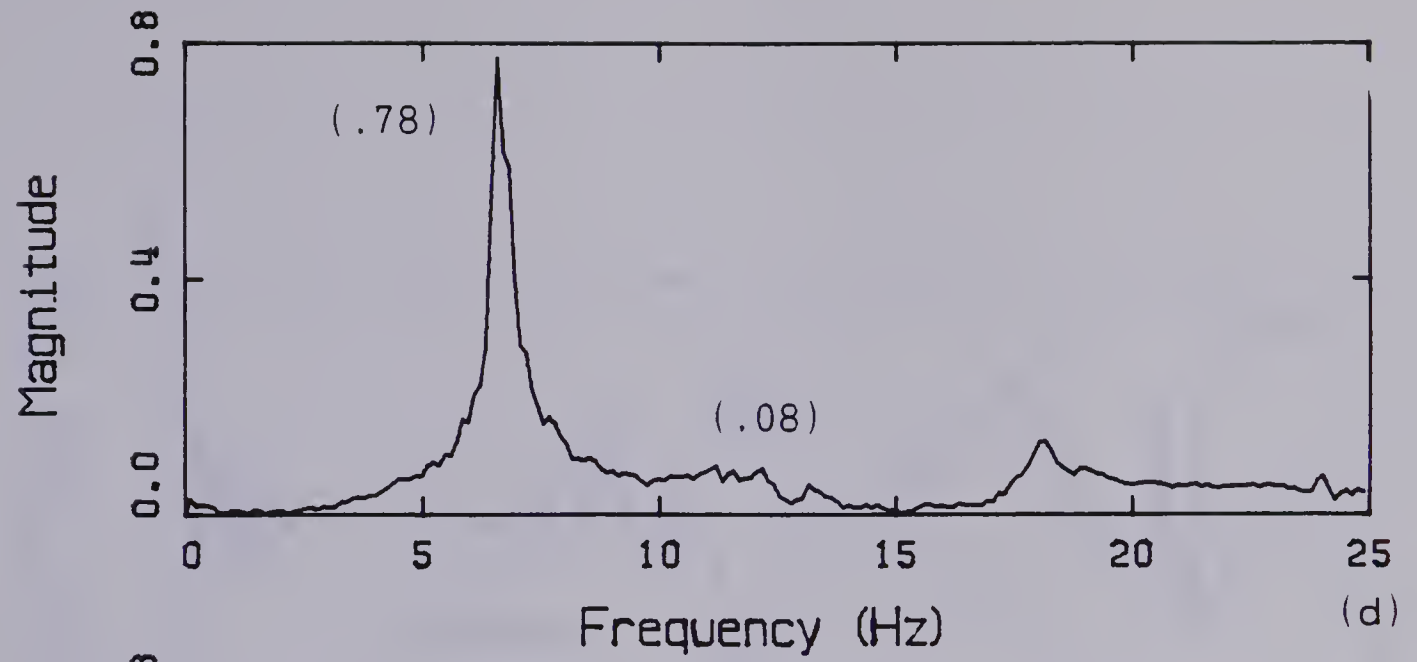


Figure 3.12 Continued

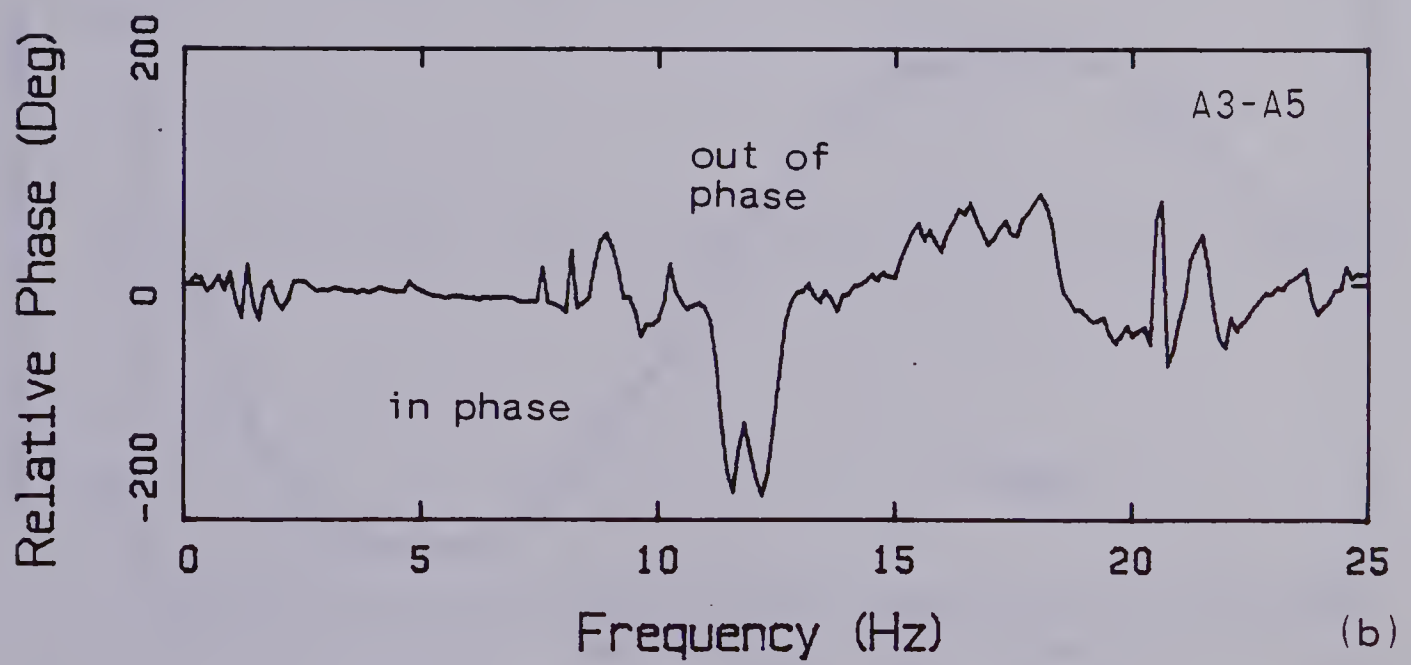
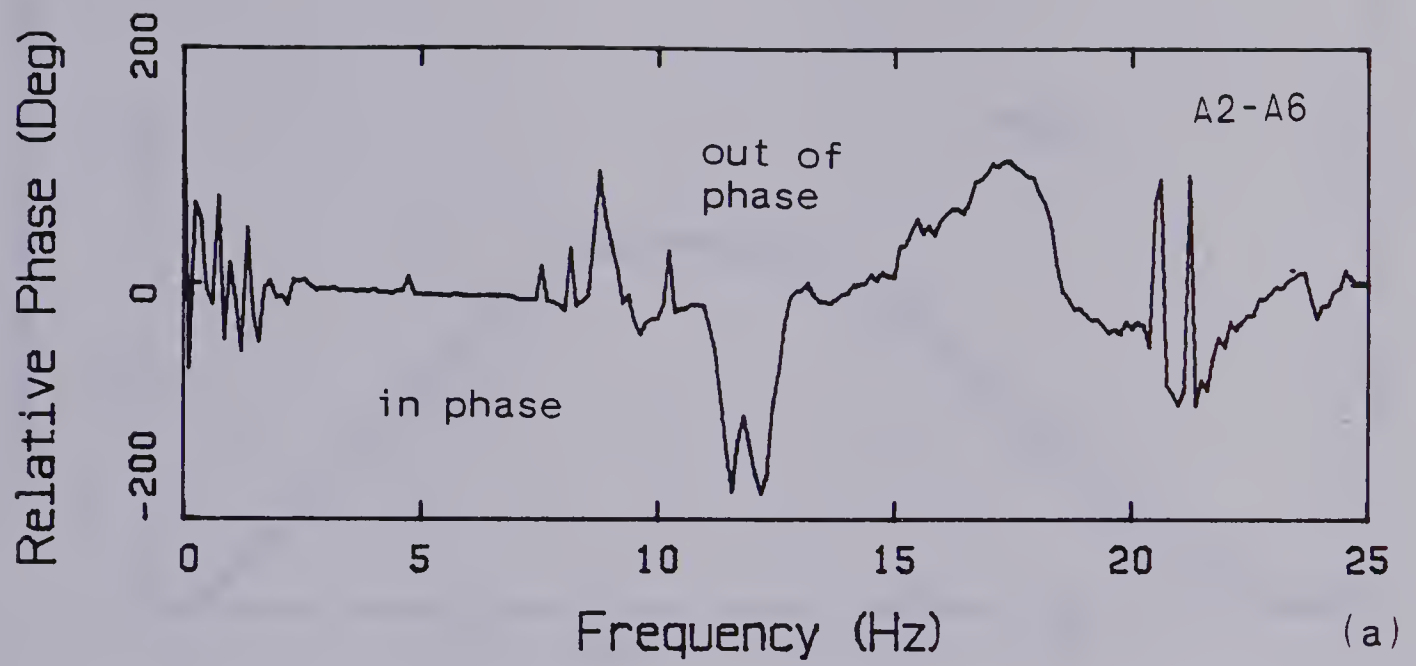


Figure 3.13 Relative Phase Spectra for A2-A6 and A3-A5

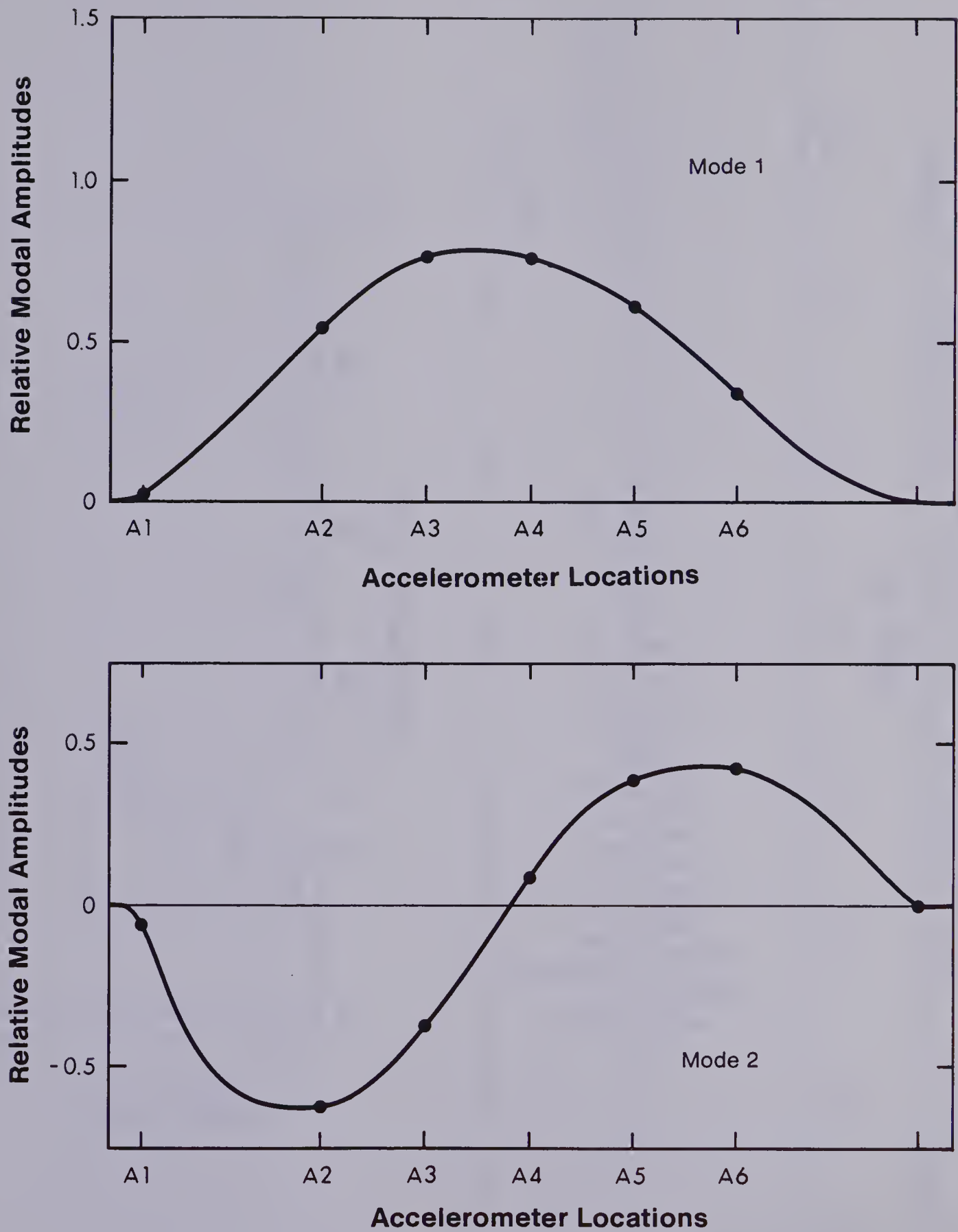


Figure 3.14 Mode Shapes along Line of Accelerometers

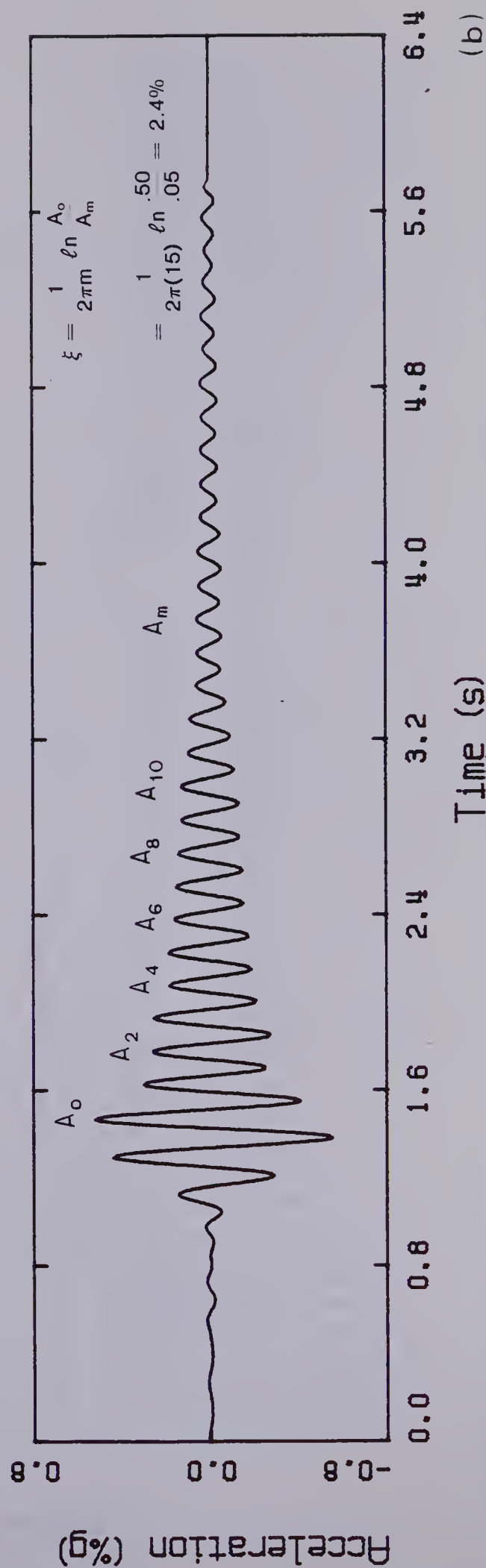
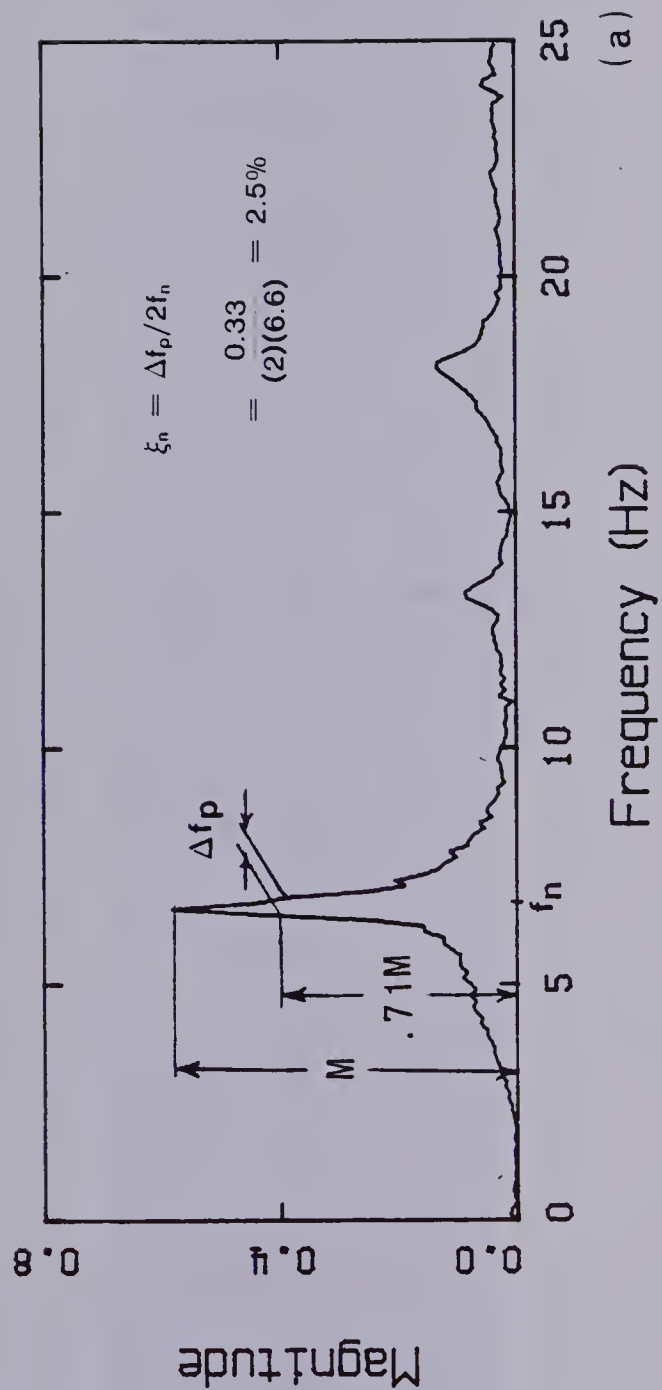


Figure 3.15 (a) Damping Ratios by the One-half Power Bandwidth Method,
 (b) Damping Ratios by the Exponential Decay Method

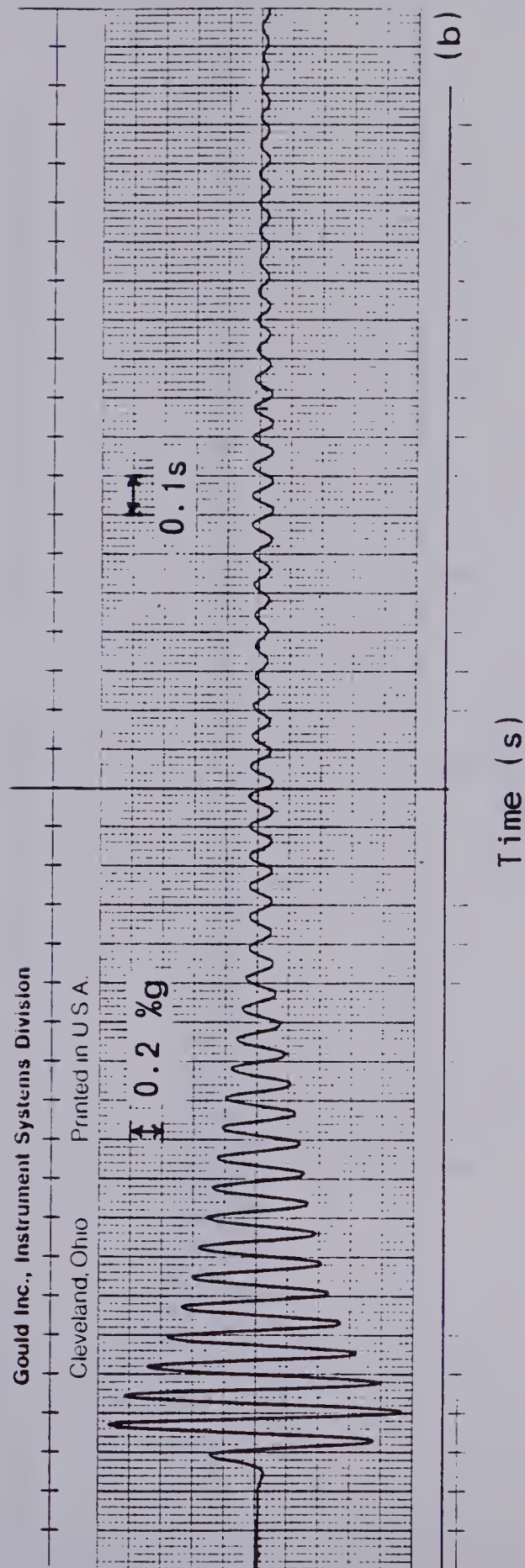
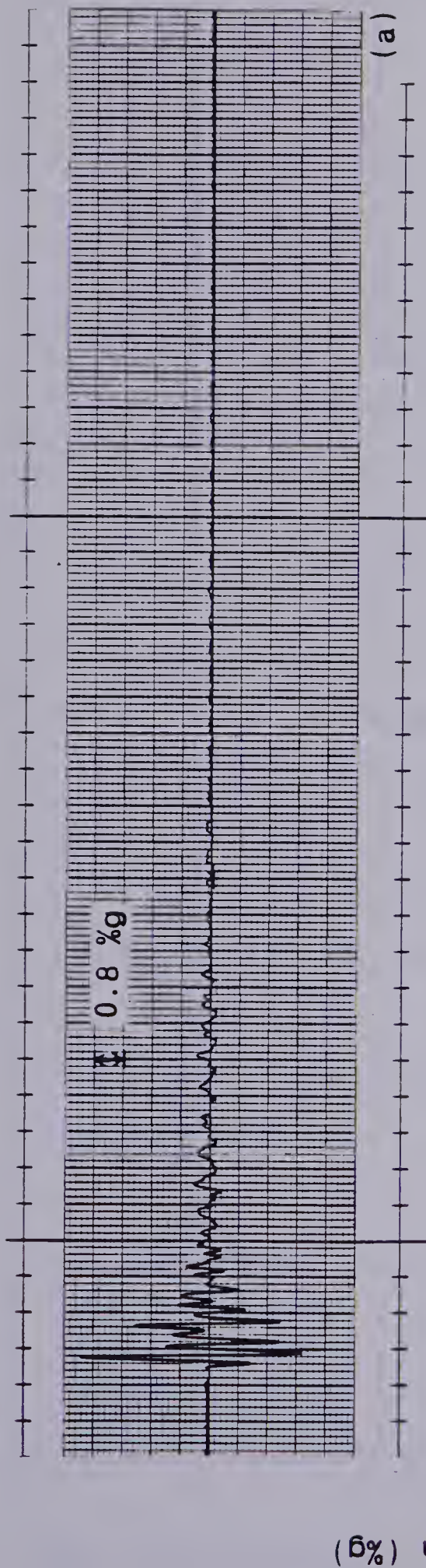


Figure 3.16 (a) Typical Unfiltered Analog Signal, (b) Corresponding Signal Filtered by Analog Filter System

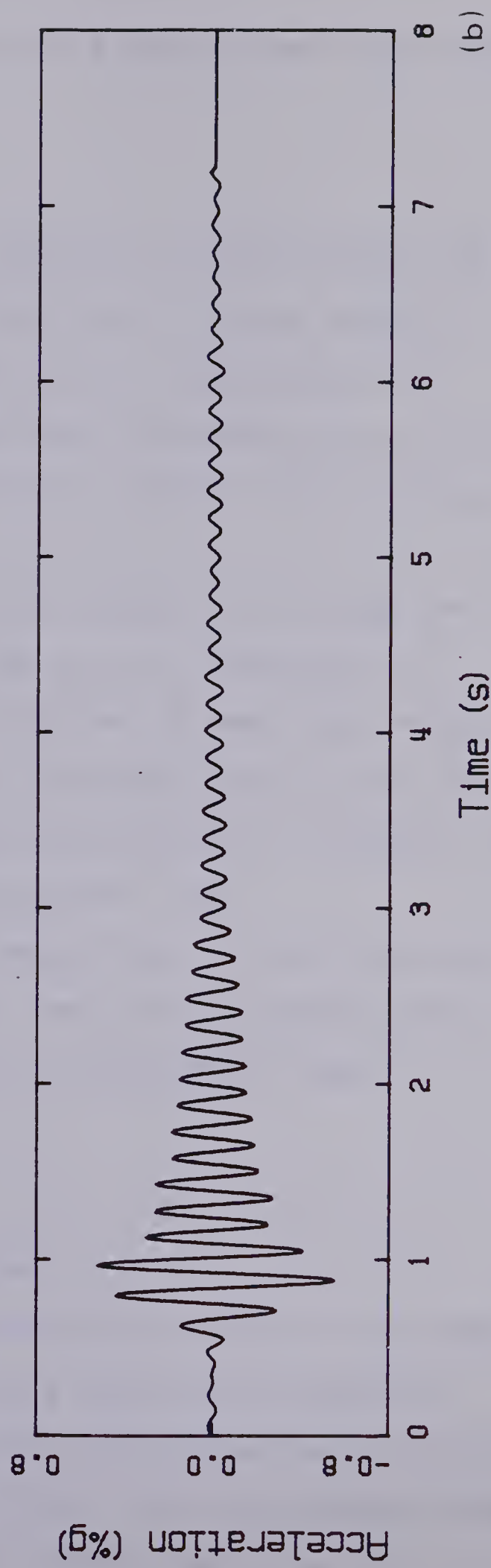
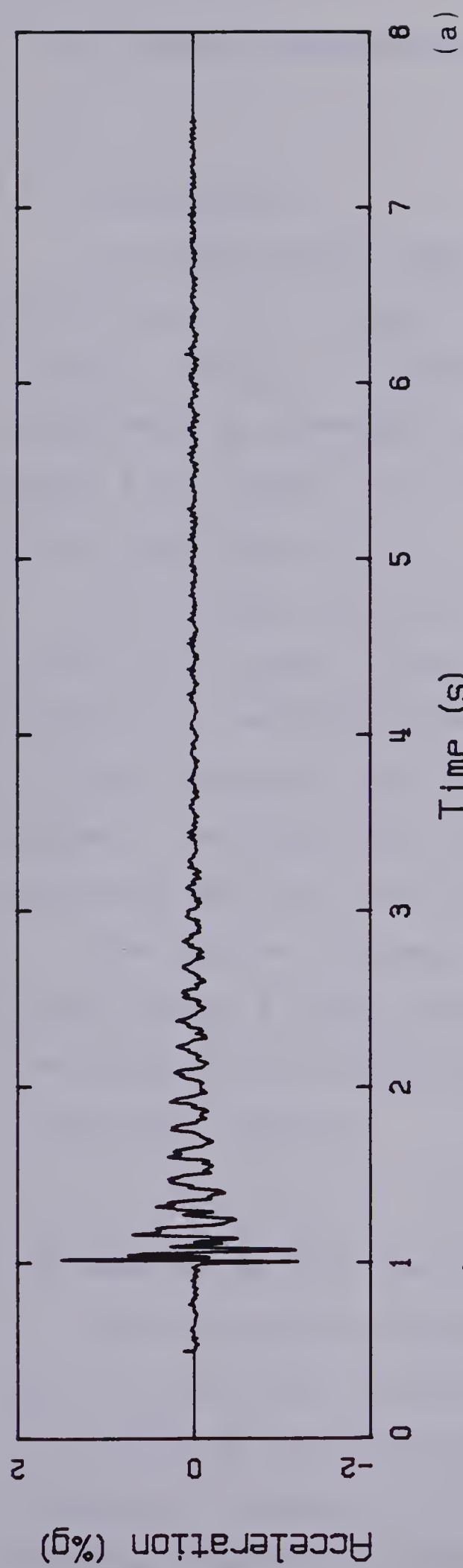


Figure 3.17 (a) Typical Unfiltered Digital Signal, (b) Corresponding Signal Filtered with FIR Filter

4. Dynamic Characteristics of a Stub Girder Floor System

4.1 Introduction

The stub girder floor system has recently been used for the first time in Canada in the Nova building located in Calgary, Alberta. A comprehensive investigation was undertaken to determine the dynamic characteristics of the novel floor system. This chapter contains the findings of that investigation.

The dynamic characteristics determined through the experimental study include the natural frequencies of vibration, the acceleration response to heel drop impacts, the modal damping ratios, and the mode shapes of the floor system. The theoretical analysis presented in Chapter 2 has also been applied to the stub girder floor.

The chapter includes a description of the stub girder floor system, a discussion of the test procedures used in the study, and a presentation of experimental and theoretical results.

4.2 Description of Floor System

The stub girder floor system was originally developed by J.P. Colaco (42) to provide a simple and economical integration of mechanical and electrical ductwork within the structural framework of the floor. This was accomplished by using built-up girders called "stub girders" as the

principal framing members of the floor system. The stub girders used in the Nova building are illustrated in Fig. 4.1.

The stub girders are composed of a wide flange section with intermittent beam segments or "stubs" shop-welded to the top flange. A series of transverse beams, arranged in a cantilever system, occupy the spaces between the stubs. The cantilever system consists of beams with overhangs, or cantilever beams as they are referred to in the remainder of this study, which span across the stub girders in alternate floor bays. Smaller beams, referred to as link beams, are then simply supported from the overhanging segments of the adjacent cantilever beams. The arrangement can be seen in Fig. 4.1. Shear studs attached to the top flange of all the beams and stubs, provide composite action with the concrete floor slab.

The plan of the floor tested, the sixth floor of the Nova building, is shown in Fig. 4.2. The composite floor slab consisted of a 84 mm concrete topping on 76 mm deformed metal deck spanning perpendicular to the cantilever beam system. Semi-lightweight concrete with a compressive strength of 30 MPa was used in casting the floor slabs. A top view of the floor system illustrating the metal decking, the slab reinforcement, and the shear studs is shown in Fig. 4.3a, while a typical section of the completed floor is shown in Fig. 4.3b. The test area, identified by shading in Fig. 4.2, consisted of W460 x 61 cantilever beams and

W200 x 27 link beams spaced at 3.225 meters. The cantilever beams were supported by W310 x 107 stub girders spaced at 9.0 meters and spanning 12.5 meters from the exterior columns to the core wall. The length of overhang of the cantilever beams was typically 2.135 meters. Short W460 x 61 beam segments comprise the stubs which occupied the spaces between the cantilever beams along the stub girder. Figure 4.4 shows a typical cross-section of the floor parallel to the stub girders.

When the tests were conducted the building had its concrete core wall completed to the 29th level, the steel skeleton erected to the 24th level, and the composite steel floors poured to the 18th level. The underside of the test floor had been sprayed with fireproofing, but no partitions, ductwork, ceilings, or other attachments were in place. All construction material was cleared from the test area prior to testing.

4.3 Test Procedures

The dynamic characteristics of the stub girder floor system were determined through an extensive experimental investigation. The vibration tests were restricted to the two floor bays indicated in Fig 4.2 since the area provided a complete representation of the stub girder system.

To fully investigate the dynamic response within the test area, the experimental program consisted of four

different sets of accelerometer placements. The test area is shown in detail in Fig. 4.5 along with the accelerometer positions in each test series. In the remainder of this chapter, the accelerometer positions will be referred to by a number-letter designation corresponding to the grid shown in the figure.

In the first three series of tests, accelerometers were placed to determine the dynamic response of the floor parallel to the stub girders. Six accelerometers were placed at positions A to F along lines 5, 7, and 3 for test series 1, 2 and 3, respectively. An accelerometer left at position 6B for each of those tests was common to both of the tape recorders used in the study. The fourth test series was designed to determine the vibrational properties of the floor system perpendicular to the stub girders. For that series, the seven accelerometers were placed along line D, occupying positions 2D to 8D.

The heel drop impact described in Chapter 2 was used to excite the floor. For consistency, all impacts were delivered by the same experimenter.

In each test series the floor was impacted at three or more locations. The impact locations were selected to excite the different modes of vibration to varying degrees. To relate the vibrational characteristics monitored along the individual lines, the floor was impacted at points 3D, 5D, and 7D in all of the test series. Impacts were also delivered between points B and C of lines 5, 7, and 3 for

test series 1, 2, and 3, respectively.

To allow the calculation of average results, the response to five heel drops was recorded for each impact location. Sufficient time was allowed between impacts for the floor to return to a state of rest.

4.4 Experimental Results and Discussion

4.4.1 Natural Frequencies of Vibration

The natural frequencies of vibration for the stub girder floor system were determined from magnitude spectra as described in Chapter 3. Figure 4.6 shows three representative spectra derived from the experimental data, each of them representing different accelerometer and heel impact locations. The spectra indicate that the stub girder floor system has a complex dynamic response composed of several natural frequencies of vibration. Additional spectra, corresponding to other accelerometer and heel impact locations, are presented in Appendix B.

The natural frequencies of vibration for the stub girder floor obtained from the spectra are summarized in Table 4.1. The values in Table 4.1 represent the spectral peaks below 15 Hz which appeared distinctly throughout the results. Other peaks, representing potential natural frequencies, were evident in some magnitude spectra but were not included because they either appeared infrequently or

had a small relative magnitude.

An examination of the spectra corresponding to a single grid location indicated that the individual modes were excited to varying degrees by impacts at different locations on the floor. However, the floor bay containing line 3 (refer to Fig. 4.5) apparently has dominant natural frequencies of 6.6 and 12.2 Hz regardless of the impact location while the bay corresponding to line 7 has dominant natural frequencies of 6.2 and 11.3 Hz.

The natural frequencies in Table 4.1 have been arranged in ascending order and have been assigned sequential modal numbers. Further reference to those natural frequencies will also be made in terms of the modal designations.

4.4.1.1 Discussion of Natural Frequencies

The dynamic response of the stub girder floor system clearly demonstrates a complicated interaction among its many structural components. The numerous closely spaced natural frequencies of the floor system (see Table 4.1) illustrate this interaction. The stiffness of the stub girder and the cantilever construction appear to be the major factors in the complicated dynamic response.

The effects of the supporting framework were most pronounced in the floor bay containing the link beams (refer to Fig. 4.5) where abrupt changes in the floor stiffness resulted in several closely spaced modes with similar spectral magnitudes (see Fig. 4.6c). Conversely, the

relative uniformity of the structural members within the floor bay containing the cantilever beams was reflected in the overall response of that bay. The spectrum in Fig. 4.6a shows the typical dominance of modes 3 and 7 along line 3 (refer to Fig. 4.5) which centres the bay with the cantilever beams. Spectra corresponding to positions along the stub girder indicate the prominent frequencies of vibration were related to the response of the floor bay in which the heel impact was delivered. As indicated in Fig. 4.6b, the impacts at position 5D excited the prominent frequencies of both floor bays to similar degrees along the stub girder.

The dynamic response of the test area was also influenced by the vibration of the adjacent floor bays. The prominent natural frequencies of those bays may have differed significantly from those of the test area because the pattern of the supporting structure changes considerably (see Fig. 4.2). Therefore, it is possible that some of the spectral peaks which appeared infrequently in the test results were related to the dominant modes of the neighbouring bays. Their inconsistency throughout the data can be explained since they belong to different modal patterns and would thus be evident only at certain locations and for some impact positions.

4.4.2 Mode Shapes

The method described in Sect. 3.8.2 was used to determine the mode shapes of the stub girder floor associated with the seven natural frequencies presented in Table 4.1. Figures 4.7 through 4.15 show plots of the normalized modal patterns along grid lines 3, 5, 7 and D which were included in the experimental program (refer to Fig. 4.5). The individual mode shapes were best defined by the impacts delivered nearest to the point of maximum modal response and therefore, have been presented in this manner.

Figure 4.7 illustrates the relative modal amplitudes of modes 1 and 2 along lines 3, 5, and 7 for an impact at their respective midpoints. The various shapes in mode 1 correspond to a natural frequency of 5.4 Hz while those of mode 2 are associated with a frequency of 6.2 Hz. Line 3 was not included in Fig. 4.7a because the results indicated it was near a nodal line of mode 1 and therefore had a very low amplitude in that mode. Similar information regarding the mode 3 (6.6 Hz) and 4 (7.2 Hz) patterns along the three grid lines has been presented in Fig. 4.8.

Figures 4.7 and 4.8 reveal a typical one-half sine wave shape with a peak amplitude near midspan in modes 1, 2, 3, and 4. The largest response of modes 1, 2, and 4 occurs along line 7, while mode 3 clearly dominates the response along line 3. Line 5, corresponding to the position of the relatively stiff stub girder, exhibits a comparatively small response in all four modes.

Curves representing the relative amplitudes of modes 1 and 2 along line D are shown in Fig. 4.9. The two curves presented for each mode represent the deflected shape associated with impacts at points 5D and 7D. Both modes appear to be accurately defined because of the similarity in the shape of the two curves identifying each mode. At the frequency of the second mode (6.2 Hz), both bays of the test area move entirely in phase although the floor bay containing the link beams experiences much larger amplitudes.

The test results for impacts at 3D were not included for either mode because they were considered unreliable owing to the low modal response at that location in modes 1 and 2. The previously mentioned nodal point near line 3 in mode 1 is clearly visible in Fig. 4.9a.

Figure 4.10 shows the shapes of modes 3 and 4 along line D for impacts at points 3D and 7D. The slight discrepancy in the shapes defined by the solid and broken curves will be explained in the following section on spectral interference effects. Both modes 3 and 4 have a nodal point near line 5, implying that the floor on one side of the stub girder moves out of phase with the floor on the other side. Because of the nodal points near line 5, an impact at point 5D did not excite either mode to a large degree and this information was therefore left out. A comparison of the modal amplitudes along line D in Figs. 4.9 and 4.10, clearly shows the dominance of mode 3 in the floor

bay containing the cantilever beams (refer to Fig. 4.5).

Figure 4.11 presents a three dimensional view of the test area showing the deflected shape associated with mode 2. The modal pattern of the entire test area was derived by relating the information from the individual tests which had a common impact location at the point of maximum modal response. The point of impact is indicated by the large arrow in the figure, while the smaller arrows show the direction of travel of the modal surface along line D.

A similar plot shown in Fig. 4.12 represents the deflected shape of mode 3. Although no discrete data points were included in either figure, they were both drawn to the same scale which implies the modal amplitudes are relative.

Figure 4.13 illustrates the relative modal amplitudes of modes 5 (11.3 Hz) and 6 (11.6 Hz) parallel to the stub girder along lines 3, 5, and 7. The individual curves are associated with the impacts delivered between points B and C on the corresponding lines (refer to Fig. 4.5). Those were the impact positions of the test program which were closest to the point of maximum response along lines 3 and 7 in modes 5 and 6.

The results show modes 5 and 6 have full sine wave shapes along lines 3 and 7 while retaining shapes typical of the first four modes along line 5. The full sine wave shapes support the fact that the frequencies of modes 5 and 6 are higher than those of the previous four modes.

Figure 4.14 shows that the results for mode 7 are similar to those of modes 5 and 6. A comparison of the response along lines 3 and 7 in the three modes indicates that line 7 has the largest response in mode 5, all lines have essentially equal amplitudes in mode 6, and mode 7 is clearly dominant along line 3. The largest response appears to occur at position 3D in mode 7. In all cases, the modal amplitudes along line 5, the location of the relatively stiff stub girder, are comparable to the amplitudes in the first four modes.

The configuration along line D in mode 5, for an impact at position 5D, is illustrated in Fig. 4.15. The modal pattern is consistent with the corresponding mode shapes perpendicular to line D along lines 3, 5, and 7 (see Fig. 4.13a). The nodal points near the midspans of lines 3 and 7 in Fig. 4.13a are quite evident in Fig. 4.15 and the peak modal response along line D, which occurs between grid points 5D and 6D, conforms with the one-half sine wave shape along line 5. A comparison of the modal amplitudes at position 5D in Figs. 4.13a and 4.15 indicates the impact at 5D produced a larger modal response than did the impact between points B and C on line 5.

Although not included in the results, the information in Fig. 4.13b and 4.14 suggests that deformed pattern of line D in modes 6 and 7 would be somewhat similar to that shown for mode 5 in Fig. 4.15.

4.4.2.1 Discussion of Mode Shapes

Although the position of impact was very important in determining the extent to which the various modes of vibration were excited, the overall dynamic response of the stub girder floor was dominated by two distinct modal groups. The first group consists of modes 1, 2, 3 and 4 (see Table 4.1) while modes 5, 6, and 7 comprise the second group. The natural frequencies associated with the four modes of the first group fall within a range of 1.8 Hz while the second group has a range of 0.9 Hz. A frequency range of 4.1 Hz exists between the two modal groups.

The modal pattern associated with the first group was the one-half sine wave shape along lines 3, 5, and 7 shown in Figs. 4.7 and 4.8. In the second group, lines 3 and 7 had full sine wave shapes (see Figs. 4.13 and 4.14) while line 5 retained the shape of the previous group. The two distinct modal patterns which formed along lines 3 and 7 were typical of the first two modes of a simply supported beam.

Other than the variations in amplitude along lines 3, 5, and 7, the major difference in the mode shapes of the first group appears to be the pattern changes along line D (see Figs. 4.9 and 4.10). Therefore, because the modal patterns parallel to the stub girder remain relatively constant, the variations in the modal frequencies can be attributed to changes in the modal patterns perpendicular to the stub girder. The same explanation applies to the second

group since the corresponding mode shapes parallel to the stub girder were also relatively constant (see Figs. 4.13 and 4.14).

The governing effects of the stub girder, the cantilever construction, and the spacing of the cantilever beams were all factors in making the dynamic response of the stub girder floor system quite different than the response of a simple joist floor.

As the major stiffening element of the floor, the stub girder had a considerable influence on the mode shapes of both groups. In particular, the stub girder was responsible for line 5 having nearly the same pattern in both groups, unlike the patterns along lines 3 and 7. By controlling the floor response along its length, the stub girder also became a major factor in the mode shapes parallel to line D (see Fig. 4.5). That influence extended from the core wall to the exterior columns and was very important in the positioning of the nodal points in the various modes. Since the cantilever beams were attached to the stub girder, their response, particularly near the point of attachment, was governed by the response of the stub girder. This was illustrated by the fact that the entire lengths of lines 3 and 7 participated fully in the vibration for impacts delivered anywhere within the test area. Therefore, the stub girder appears to control the effective floor width perpendicular to the beams. The increased stiffness of the floor along the stub girder was illustrated by the modal

amplitudes of line 5 which were in general much lower than the corresponding maximum modal amplitudes within the test area.

The direct effects of the cantilever and link beams on the vibrational patterns of the floor system were less pronounced than those of the stub girder. Of major importance was the extension of the effective vibrating area perpendicular to the stub girders. The mode shapes within the test area were influenced by the modal patterns of the neighbouring floor bays through the cantilever beam system and the continuous floor slab. By extrapolating the mode shapes along line D (see Figs. 4.9, 4.10, and 4.15), some insight can be gained into the mode shapes of the neighbouring bays.

As described previously, the floor bay containing the link beams (line 7) had a significant amplitude in all modes while modes 3 and 7 totally dominated the response of the floor bay containing the cantilever beams (line 3). This result reflects the relative stiffnesses of the cantilever and link beams and the relative continuity of the steel framework within the individual floor bays. Figures 4.9 and 4.10 show the more flexible link beams played a prominent role in the modal patterns perpendicular to the stub girder.

The edge support conditions of the concrete slab influenced all of the modal patterns of the floor system. The interior edge of the concrete slab was solidly attached

to the core wall by reinforcing steel and a supporting steel angle while the outside edge was slightly cantilevered over beams spanning between the exterior columns (refer to Fig. 4.4). The rotational stiffness of the slab-core connection appears to be responsible for the lower modal amplitudes of the interior half of the floor (see Figs. 4.7, 4.8, and 4.14). A further indication of the relative stiffness of the edge supports was the formation of the nodal points in the second modal group closer to the exterior of the slab (see Figs. 4.13 and 4.14).

Modes of a higher order than the full sine wave shape of the second group have been ignored in the results because the two groups considered contributed the most to the floor response. In addition, more accelerometers would have been required to accurately define the mode shapes at higher frequencies.

4.4.2.2 The Effects of Spectral Interference

The phenomenon of "spectral interference" was responsible for the discrepancy in the mode shapes indicated by the solid and broken curves in Fig. 4.10. Spectral interference occurs when two (or more) modes have closely spaced frequencies and is particularly evident when one mode is quite dominant over the other. In general, spectral interference results in an increase in the magnitude of the spectral peaks corresponding to the closely spaced modes. The increase in magnitude is dependent on the spacing, the

associated modal damping ratios, and the unaffected relative amplitude of the spectral peaks.

To illustrate the effects of spectral interference, time traces with a prescribed frequency content were analyzed in the same manner as the transient accelerometer signals recorded at the test site. In the following discussion, the initial time domain amplitude of all components comprising the individual traces is assumed to be equal to one unless otherwise stated. Similarly, the same damping ratio was prescribed for each component.

Figure 4.16a shows the spectrum of a signal composed of a single damped sine wave at a frequency of 20 Hz. A signal composed of two sine waves at frequencies of 20 and 21 Hz, respectively, resulted in the spectrum in Fig. 4.16b. A comparison of the two spectra reveals that spectral interference has resulted in an error of approximately 3% in the spectral magnitudes of the latter signal. Because the increase in amplitude is negligible in structural engineering, it can be concluded that spectral interference is not a problem for two components of equal magnitude and a spacing of at least one Hertz.

When the spacing of the two components is reduced to one-half a Hertz, as illustrated in Fig. 4.16c, the resulting increase in amplitude becomes 14%. The accuracy of the test results was not sufficient for even this amount of error to be overly significant. However, when the two components differ significantly in their initial time domain

amplitudes, the error can increase considerably. For example, two components at 20 and 20.5 Hz with an initial time domain amplitude ratio of two-to-one produce an interference error of 6% and 32% respectively, in the corresponding spectral peaks. This result is shown in the spectrum presented in Fig. 4.16d.

As the relative time domain amplitudes of the two components increases, the spectral interference error of the dominant mode decreases while the error of the less dominant mode increases significantly. For example, the spectral magnitude errors are approximately 0% and 250%, respectively, for the spectral peaks of two components with a five to one amplitude ratio and a frequency spacing of 0.5 Hz.

The information obtained from the analysis of the manufactured signals can be applied to the test results because the separation of the closely spaced modes was similar and the range in modal damping ratios was sufficiently small to be ignored.

In the test results, spectral interference errors were most evident in the patterns of modes 3 and 4 along line D. Both mode shapes were illustrated in Fig. 4.10 for impacts at two locations. The solid curves represent the true mode shapes since the corresponding spectral magnitudes were unaffected by interference errors while those associated with the broken curves were affected to some degree. Had spectral interference not occurred, the amplitude ratio of

the solid and broken curves for each mode would have been uniform along the full length of line D.

Considering mode 3 (Fig. 4.10a), the relative amplitude of the broken to solid curve is approximately 50% and 70% in the floor bays containing lines 3 and 7, respectively. Spectral interference appears to be responsible for the 20% difference between the bays. Since mode 3 dominated the floor response along the entire length of line D for the impacts at position 3D, the 6.6 Hz spike (mode 3) was predominant in the corresponding magnitude spectra and interference errors were negligible for that mode. However, for the impacts delivered at position 7D, the results indicate that mode 3 and mode 2 were predominant in the floor bays containing lines 3 and 7, respectively.

Spectra from positions 3D and 7D for an impact at 7D (see Fig. 4.5) are shown in Fig. 4.17. The dominance of the 6.6 Hz spike in the 3D spectrum (Fig. 4.17a) implies interference errors did not influence the mode 3 magnitudes in that floor bay. However, the 7D spectrum (Fig. 4.17b) indicates the magnitude of the 6.2 Hz (mode 2) component is approximately twice that of the 6.6 Hz (mode 3) component. Therefore, the resulting interference error was sufficient to produce the 20% increase in relative modal amplitude which was evident in that bay.

Similarly, the difference in shape of the solid and broken curves for mode 4 (Fig. 4.10b) can be attributed to spectral interference errors. However, the situation in

this mode was reversed from that of the previous mode since the major interference errors occurred in the 3D impact curve in the floor bay containing line 3. The errors produced an approximate 25% increase in the magnitudes of the corresponding spectral peaks. Therefore, to accurately define the shape of mode 4, the amplitude of the 3D impact curve (broken curve in Fig. 4.10) should be reduced by 25% between positions 2D and 5D.

4.4.3 Modal Damping Values

The modal damping values determined by the one-half power bandwidth method (refer to Sect. 3.8.3) are presented in Table 4.2. Each value in the table represents an average of the results corresponding to the line and impact location indicated. The average values were calculated on the basis of up to five spectra from each accelerometer position along the individual lines. The maximum difference in the values derived from spectra corresponding to the same accelerometer position was 0.5%, while the greatest range in values for an entire line was 0.7%.

The results indicate the majority of the modal damping ratios were in the 2% to 3% range. The exceptions were modes 1 and 6 which had damping ratios of 4.3% and 1.3%, respectively. In contrast to some floor systems, the higher modes of the stub girder floor generally had slightly lower damping ratios than the lower modes of the floor system.

Several modal damping ratios are missing in Table 4.2. Some of the missing values correspond to the modes which were not strongly excited along the particular lines. In general, the low modal response can be attributed to the close proximity of nodal lines associated with those modes. Accordingly, discernable peaks for those modes were not evident in the corresponding magnitude spectra and the one-half power bandwidth method could not be applied. Other values were missing because the closely spaced modes resulted in an overlapping of the spectral peaks and thus poor definition of the individual spikes. Again, the one-half power bandwidth method could not be applied. The latter problem was particularly evident when one mode dominated the others.

The damping ratios obtained from the decay curves of various acceleration-time traces, filtered by the analog system described in Sect. 3.8.4, are presented in Table 4.3. Because the natural frequencies of vibration of the stub girder floor were so closely spaced (see Table 4.1), it was impossible to separate the original signals into individual modal contributions by filtering. Therefore, the values in the table were derived from traces made up of a combination of modes of nearly the same frequency.

Damping values were obtained for two modal combinations. The accelerometer signals were low-pass filtered at 8.5 Hz to acquire the damping ratios associated with a combination of modes 1, 2, 3, and 4. Similar results

for the group of higher order modes were derived by filtering the signals in the range 9.0 to 14.5 Hz. For each value in the table, an average was calculated for five traces from each of the accelerometer positions along the individual lines.

The phenomenon known as "beating" was evident in the majority of the filtered traces. The beating was a result of the closely spaced frequency components of the floor system which produced a "beat" as they moved in and out of phase. Figure 4.18a illustrates the beating phenomenon for a typical trace. To eliminate the effects of the beats in calculating the damping ratios of such curves by the decay method, the peaks of the beat cycles were joined by a smooth curve. As illustrated in Fig. 4.18b, the resulting envelope was subsequently used in determining the amplitude of the trace after a prescribed number of cycles. The resulting damping values represented an average for the modes which were included in the filtered transient signals.

The tabulated results indicate the damping of the floor bay containing the link beams (line 7) was higher than the bay containing the cantilever beams (line 3) for both modal combinations. In what appears to be a contradiction with the values determined by the one-half power bandwidth method, the resultant damping ratios of the second modal group (modes 5, 6, and 7) were generally higher than those of the first modal group along lines 3 and 5. However, a direct comparison is probably not valid since the values

were derived by different methods which commonly yield slightly different results.

In general, the damping values derived by the two methods compare reasonably well and both sets of values were typical of bare concrete floors.

4.4.4 Peak Accelerations

Peak accelerations produced by heel impacts are presented in Table 4.4 for various locations in the test area. The individual values were obtained from filtered traces corresponding to the accelerometer positioned at the point of impact. A typical trace is illustrated in Fig. 4.19.

As mentioned previously, filter limitations prevented the separation of the accelerometer records into individual modal contributions. To obtain the tabulated peak accelerations, the accelerometer signals were filtered in two frequency ranges namely 0.0 to 8.5 Hz and 9.0 to 14.5 Hz. The first filter range included modes one to four while the second included modes five to seven.

The resulting peak accelerations were typically below 2 %g at all locations in both filter ranges. The extremely low values at 3D and 7D for the second filter range provide further evidence that nodal lines occur close to these locations in the higher modes. The relatively small values at the two points on line 5 reflect the substantial stiffness of the stub girder and the single mode

shape which formed along that line.

Because the values in Table 4.4 represent the contributions of several modes rather than a single fundamental mode, a direct application of the annoyance threshold curves of Fig. 2.1 to check the vibrational adequacy of the floor may be disputed. However, separation of the closely spaced modal responses (ie: within the individual groups) may not be appropriate for making an evaluation since the similar patterns of those modes ensure a simultaneous response for most excitations.

Plotting the peak accelerations corresponding to the lower frequency range (see Table 4.4) on the annoyance threshold chart, using the average frequency and damping ratio of the first four modes, indicates that the acceleration levels at the midpoints of lines 3 and 7 fall within the bothersome range. However, the acceleration values in Table 4.4 do not represent the finished state of the building since the tests were conducted when the floor was bare. Upon completion of the building (ie: addition of flooring, partitions, furniture, etc.), the damping levels of the floor system will be increased significantly and the peak acceleration levels substantially reduced resulting in satisfactory vibration characteristics.

The vibration levels of the stub girder floor system were generally considered satisfactory by the experimenters, although in some instances they may have been slightly annoying as suggested by the above evaluation.

4.5 Theoretical Evaluation of the Stub Girder Floor System

This section is devoted to an investigation into the applicability of the theoretical analysis and the floor modelling assumptions presented in Chapter 2 to the stub girder floor system. The evaluation was made by comparing the experimentally observed dynamic parameters with corresponding calculated values.

In Appendix B.1, the fundamental frequency and the peak acceleration of the floor system have been calculated by applying the theory discussed in Chapter 2. At the end of this section, those calculated parameters have been used to simulate a design stage evaluation of the floor system.

4.5.1 Fundamental Frequency

Two possible adaptations of the T-beam analogy (refer to Sect. 2.3.1) to the stub girder floor were considered in calculating the fundamental frequency of the floor system. In each case, the series of beams perpendicular to the stub girders was assumed to form the composite T-sections with the stub girders acting as flexible simple supports for the T-beams.

The first model (see Appendix B.3.1) was an attempt to represent the stub girder floor system as a unit by considering a two span beam with flexible supports at the stub girder positions. This representation allowed the reduced stiffness of the link beam T-sections (refer to Fig 4.2) to be reflected in the calculated frequency. The

frequency of the two span beam was computed using the Rayleigh method.

The second model was a more direct application of the T-beam analogy which considered a single span uniform beam with flexible girder supports. This model focussed on the floor bay containing the main sections of the cantilever beams and ignored the floor bay containing the link beams. The frequency of the assumed T-beam was calculated according to Eqn. 2.1.

To account for flexible supports, the fundamental floor frequency associated with each of the above T-beam models was calculated as a system frequency according to Eqn. 2.2. The stub girders, which comprised the flexible supports, were modelled as composite T-beam sections and Eqn. 2.1 was then used to compute the frequency of the girder supports.

The results of the frequency calculations are summarized in Table 4.5. The fundamental floor frequencies derived for the two span and the single span T-beam models (ie: 5.08 and 5.54 Hz, respectively) are very close to the natural frequency associated with mode 1 (ie: 5.4 Hz) and they are also reasonably close to the more prominent natural frequencies of the first modal group (ie: 6.2 and 6.6 Hz). The single span T-beam model, which corresponds to an application of the current code provisions (17), is perhaps the best for design use since it gives reasonable results and requires fewer computations than the two span model. Although a complex plate analysis might provide a better

indication of the complicated vibration response which was observed, both of the relatively simple models which were considered give results with sufficient accuracy for a design stage evaluation of the stub girder floor system.

4.5.2 Peak Acceleration

The peak acceleration of the stub girder floor resulting from a heel impact has been derived theoretically according to Eqn. 2.17 in Appendix B.4 for three approximations to the effective vibrating panel width. These include the $60t_e$ (where t_e is the effective slab thickness) approximation used in the current code analysis (17), a width computed by the Sokolowski method (see Sect. 2.3.2), and an estimate based on the experimental results. The theoretical floor frequency of 5.54 Hz was used in the calculations with the first two panel width approximations while the frequency of mode 3 (ie: 6.6 Hz) was used in conjunction with the final estimate (see discussion in Appendix B.4).

The results of the calculations are summarized in Table 4.6.

The results clearly show that the effective panel width is substantially underestimated by both the $60t_e$ approximation and the Sokolowski method. Therefore, in each case the calculated peak acceleration is significantly higher than the maximum observed peak acceleration of 1.9 %g (see Table 4.4) indicating that neither method should be

employed when considering a stub girder floor system. The peak acceleration derived using the effective width and natural frequency from the experimental results was quite accurate.

Using the theoretical frequency of 5.54 Hz in conjunction with the observed effective width (13m) also results in an accurate estimate of the measured peak acceleration. In that case the calculated peak acceleration becomes 1.8 %g.

These results suggest that a reasonable estimate of the vibrating panel width for a stub girder floor would be the overall length of the stub girders. The suggested estimate reflects the major control which the stub girder exerts on the vibrational response of the floor system.

4.5.3 Evaluation

The methods recommended in the previous sections to determine the fundamental frequency and the peak acceleration of the stub girder floor system provide reasonably accurate estimates of those parameters. Therefore, a design stage evaluation regarding the vibrational acceptability of the floor system would appear to be feasible using those methods in conjunction with the annoyance threshold chart shown previously in Fig. 2.1.

Plotting the peak acceleration of 1.8 %g at a frequency of 5.54 Hz on the annoyance threshold chart and assuming a critical damping ratio of 3% (ie: bare floor) indicates the

vibration levels of the floor would be slightly annoying. As expected, this conclusion is the same as that drawn previously (see Sect. 4.4.4) with the experimental results.

Table 4.1: Natural Frequencies of the Stub Girder Floor System

Mode	Frequency (Hz)
1	5.4
2	6.2
3	6.6
4	7.2
5	11.3
6	11.6
7	12.2

Table 4.2: Modal Damping Ratios Derived by One-half Power Bandwidth Method

Line #	Impact Location	Modal Damping Ratio (% critical)*						
		1	2	3	Mode 4	5	6	7
3	3D	---	---	2.6	---	---	---	---
	Between 3B & 3C	---	---	2.7	---	2.1	---	1.8
5	5D	---	3.0	3.1	---	2.7	1.3	---
	Between 5B & 5C	---	3.0	2.7	---	2.7	1.2	---
7	7D	4.1	2.8	1.8	1.9	1.8	---	---
	Between 7B & 7C	4.5	2.7	1.7	1.7	1.7	1.3	2.1

* Calculated on the basis of $\xi_n = \Delta f_p / 2f_n$
 (Tabulated values represent the average from all accelerometers on the individual lines)

Table 4.3: Damping Ratios Derived from Decay Curves

Line #	Impact Location	Damping Ratios (% critical)*	
		modes 1,2,3,4 combined †	modes 5,6,7 combined •
3	3D	2.2	2.9
	Between 3B & 3C	2.2	2.7
5	5D	2.1	2.8
	Between 5B & 5C	2.1	2.5
7	7D	3.5	3.4
	Between 7B & 7C	3.4	3.3

* Tabulated values represent the average from all accelerometers on the individual lines

† Acceleration records were lowpass filtered at 8.5 Hz

• Acceleration records were bandpass filtered between 9.0 and 14.5 Hz

Table 4.4: Peak Accelerations of the Stub Girder Floor System

Impact Location	Peak Acceleration (%g)	
	Frequency Range (Hz)	
	0.0 - 8.5	9.0 - 14.5
3D	1.5	0.3
Between 3B & 3C	1.3	1.6
5D	0.6	0.7
Between 5B & 5C	0.4	0.4
7D	1.9	0.3
Between 7D & 7C	1.4	1.1

Table 4.5: Results of Frequency Calculations

Model	Frequency (Hz)
1) Two Span T-beam	
T-beam	7.74
Girder Support	6.73
Floor System	5.08
2) Single Span T-beam	
T-beam	9.37
Girder Support	6.73
Floor System	5.54

Table 4.6: Theoretical Peak Accelerations of the Stub Girder Floor System

Approx. to the Effective Floor Width	Effective Width (m)	Peak Acceleration (%g)
60 X effective slab depth	7.44	3.2
Sokolowski Method	5.10	4.7
Experimental Results	13.00	2.2

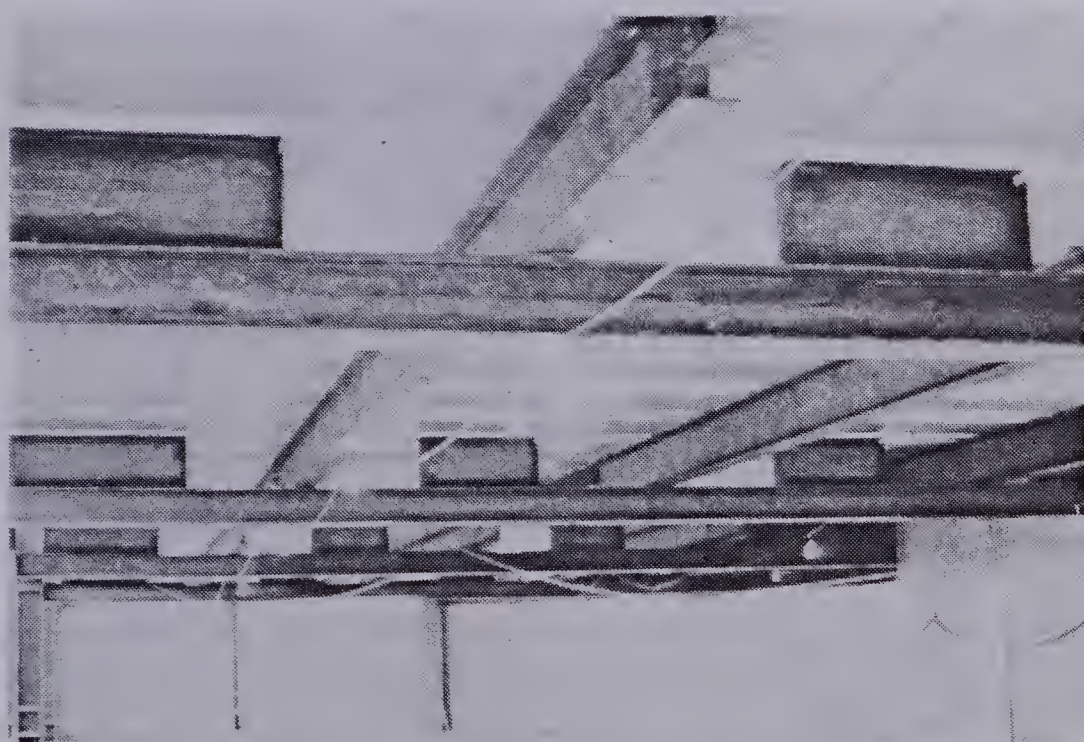
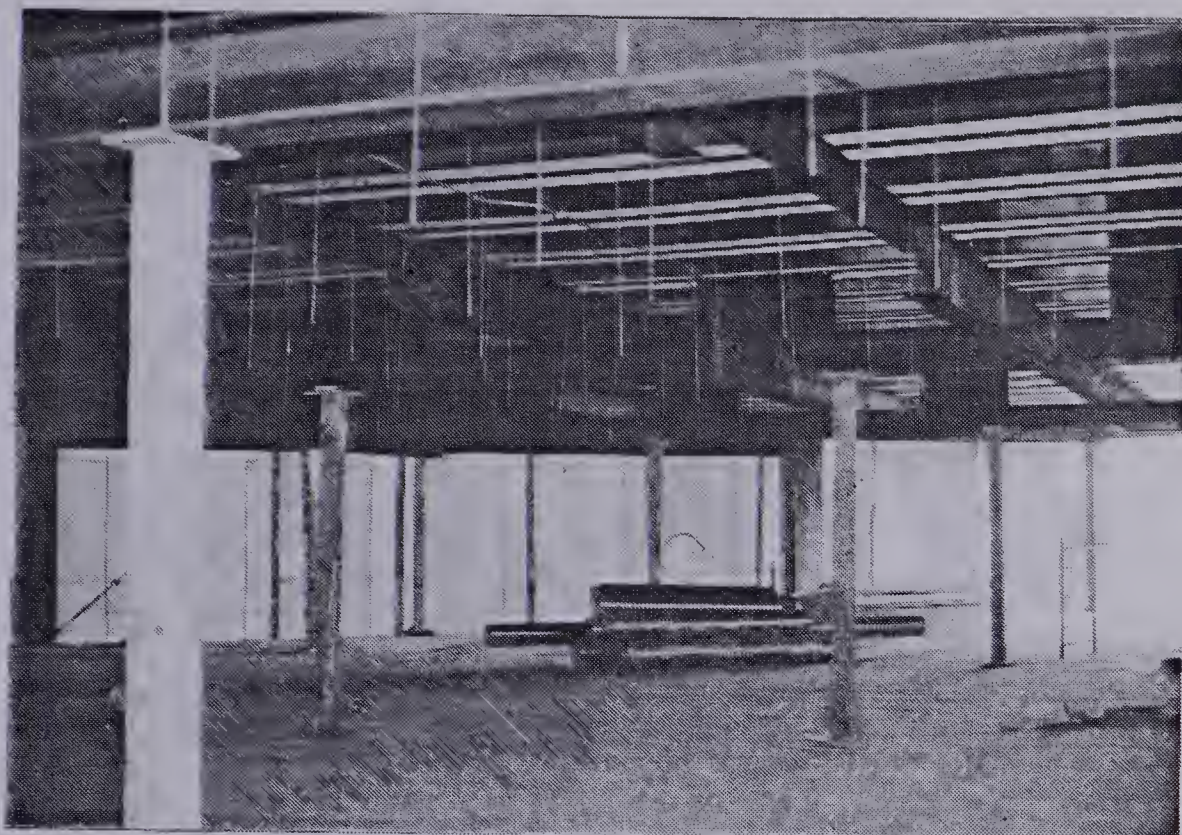


Figure 4.1 Illustration of Stub Girders in the Nova Building

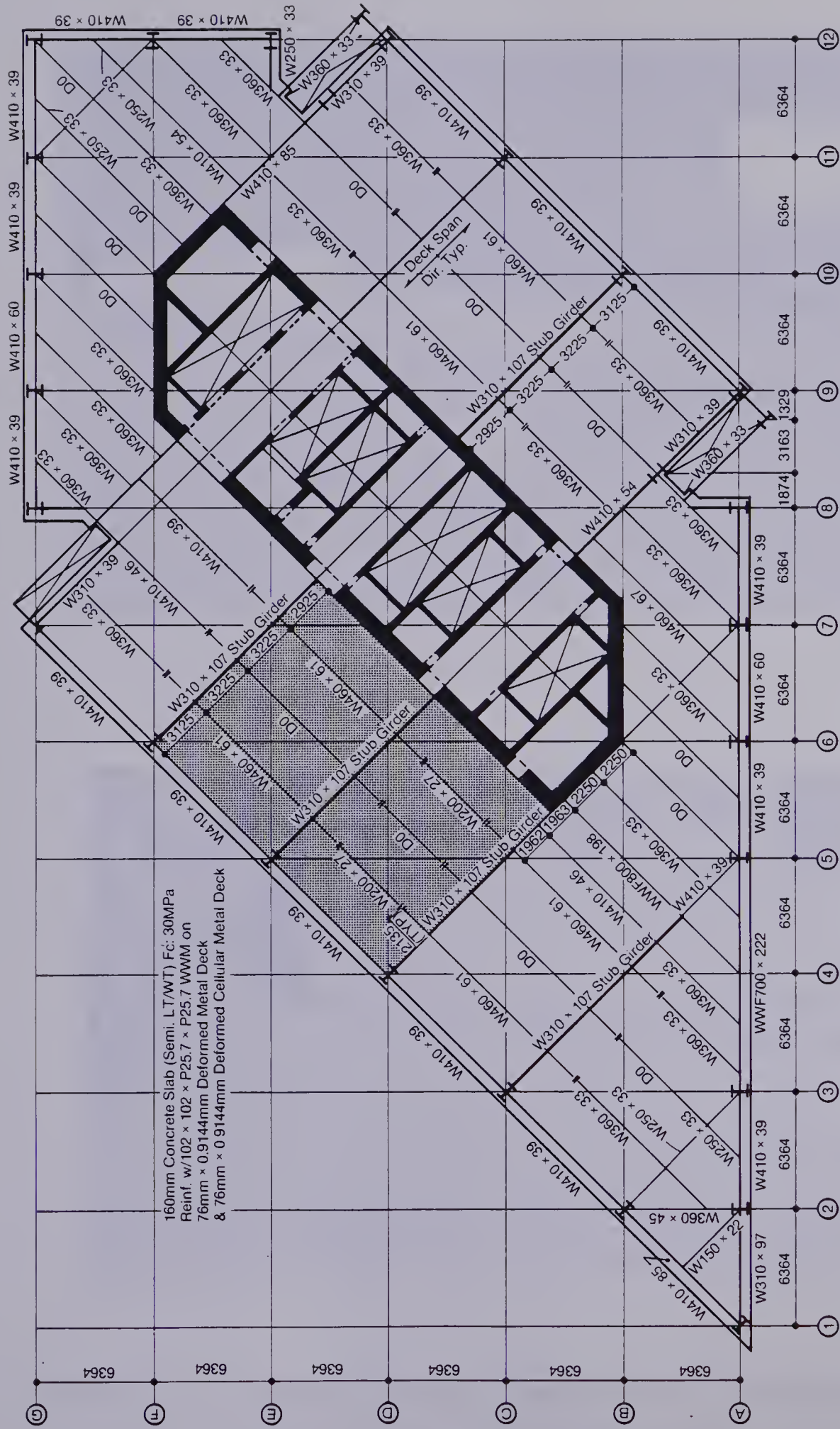


Figure 4.2 General Floor Plan of the Nova Building

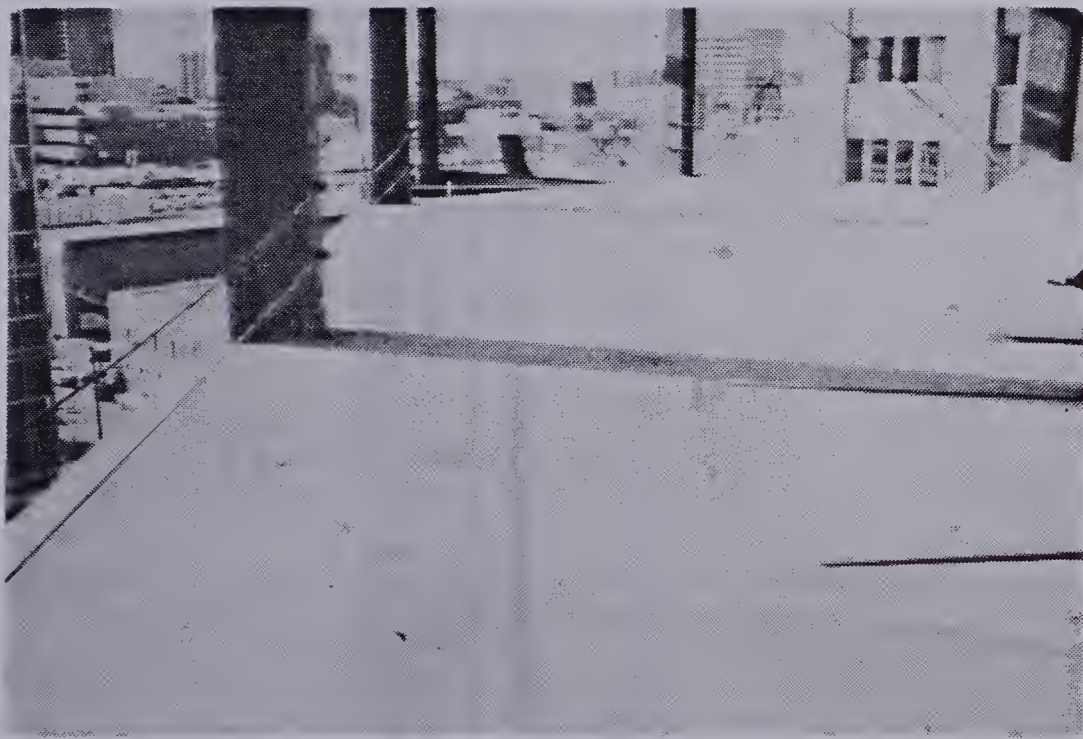
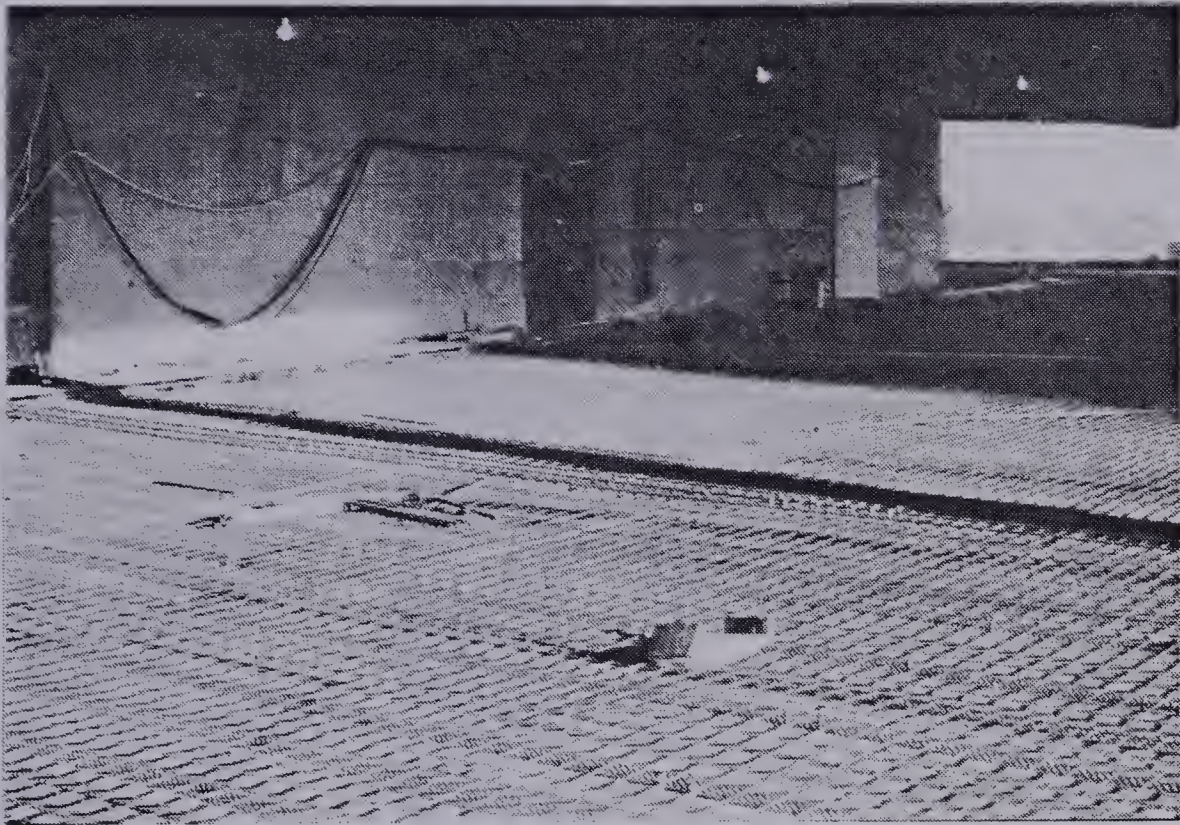


Figure 4.3 Illustrations of Completed and Uncompleted Composite Slab Floor

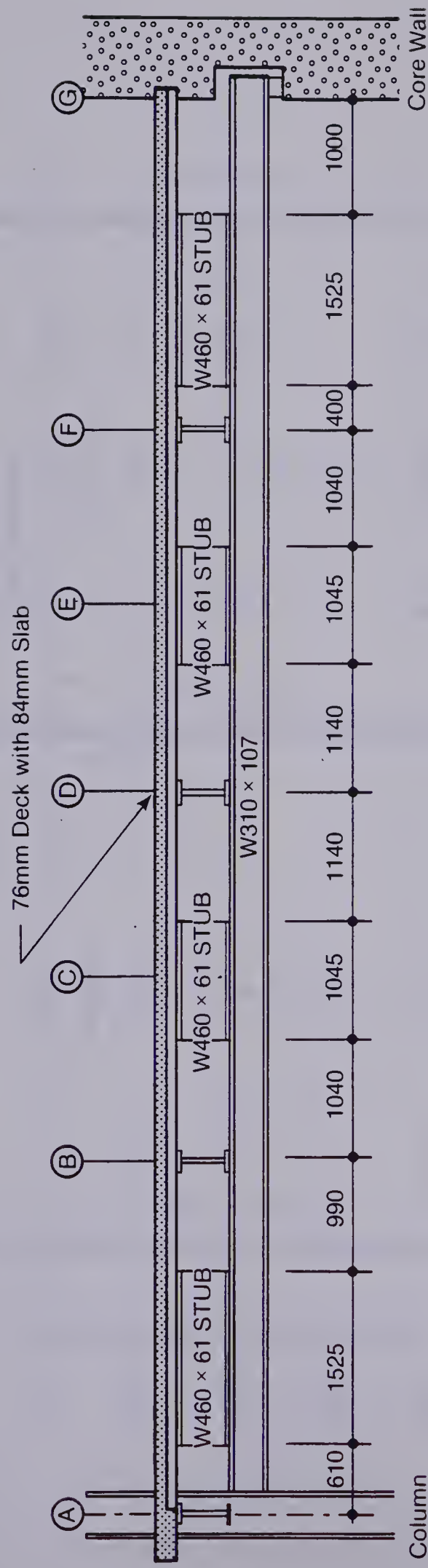


Figure 4.4 Typical Cross-section of Floor at Stub Girder Position

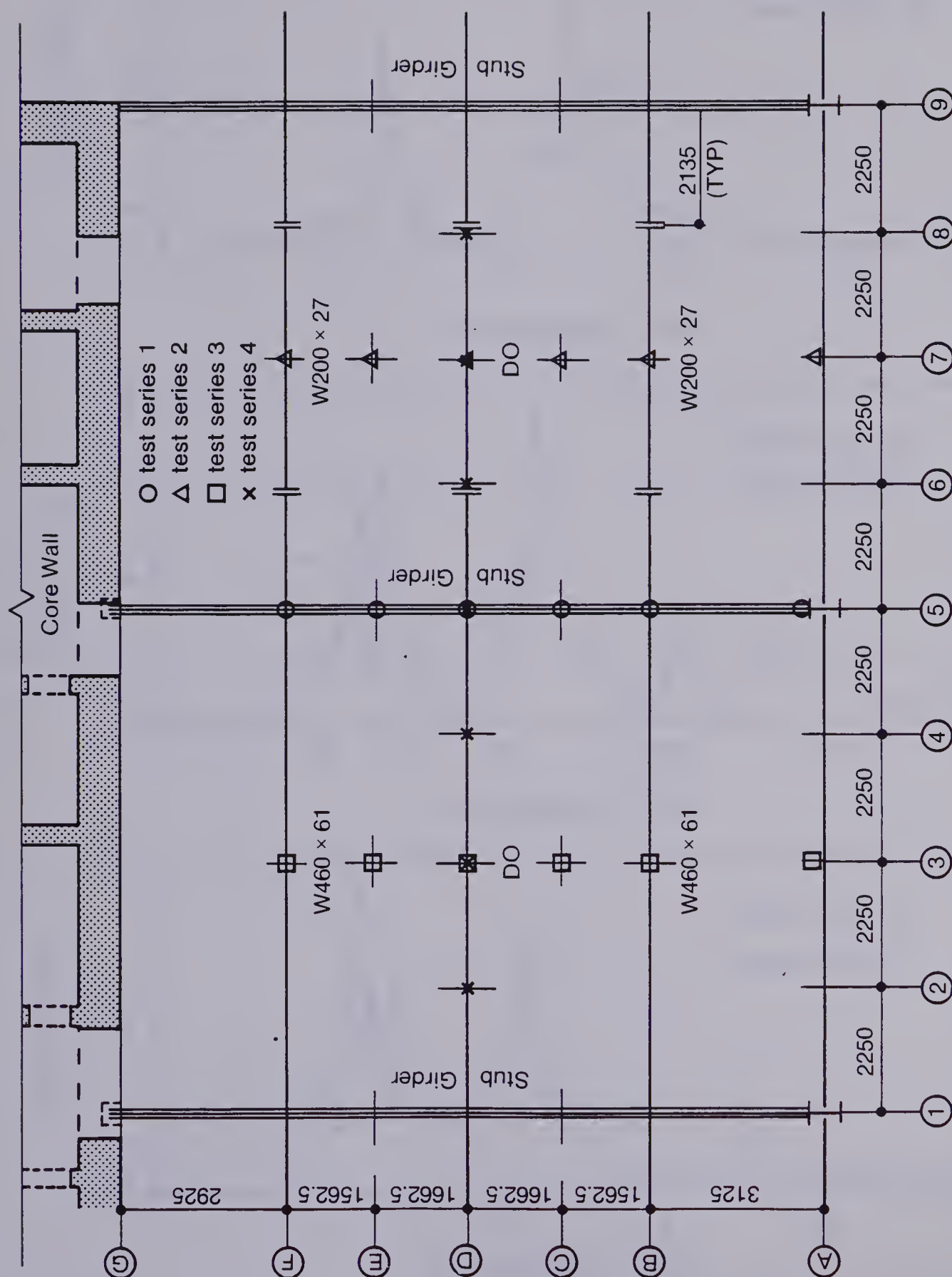


Figure 4.5 Detail of Test Area indicating Accelerometer Positions

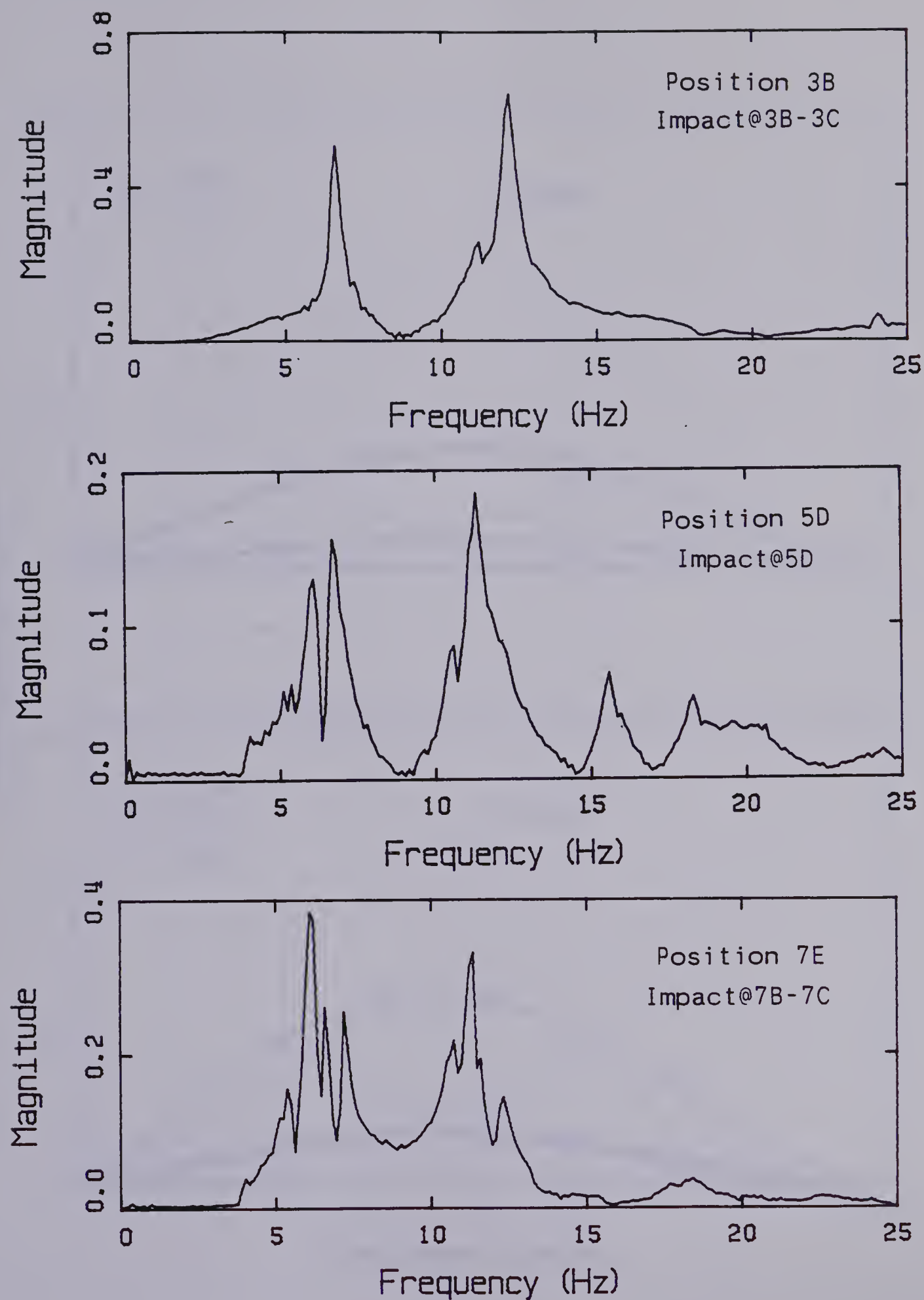


Figure 4.6 Representative Magnitude Spectra

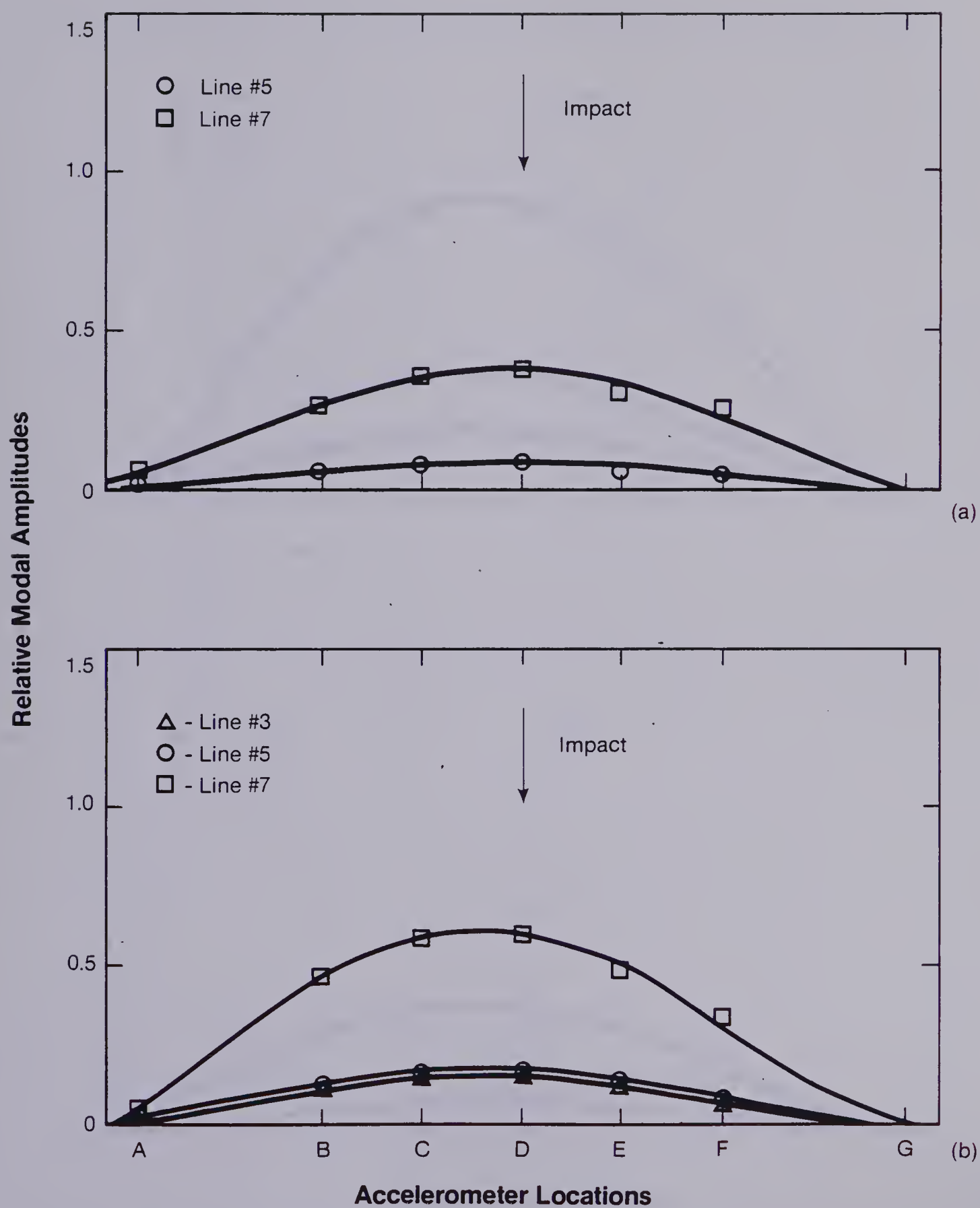


Figure 4.7 Relative Modal Amplitudes along Lines 3, 5, and 7

(a) Mode 1, (b) Mode 2

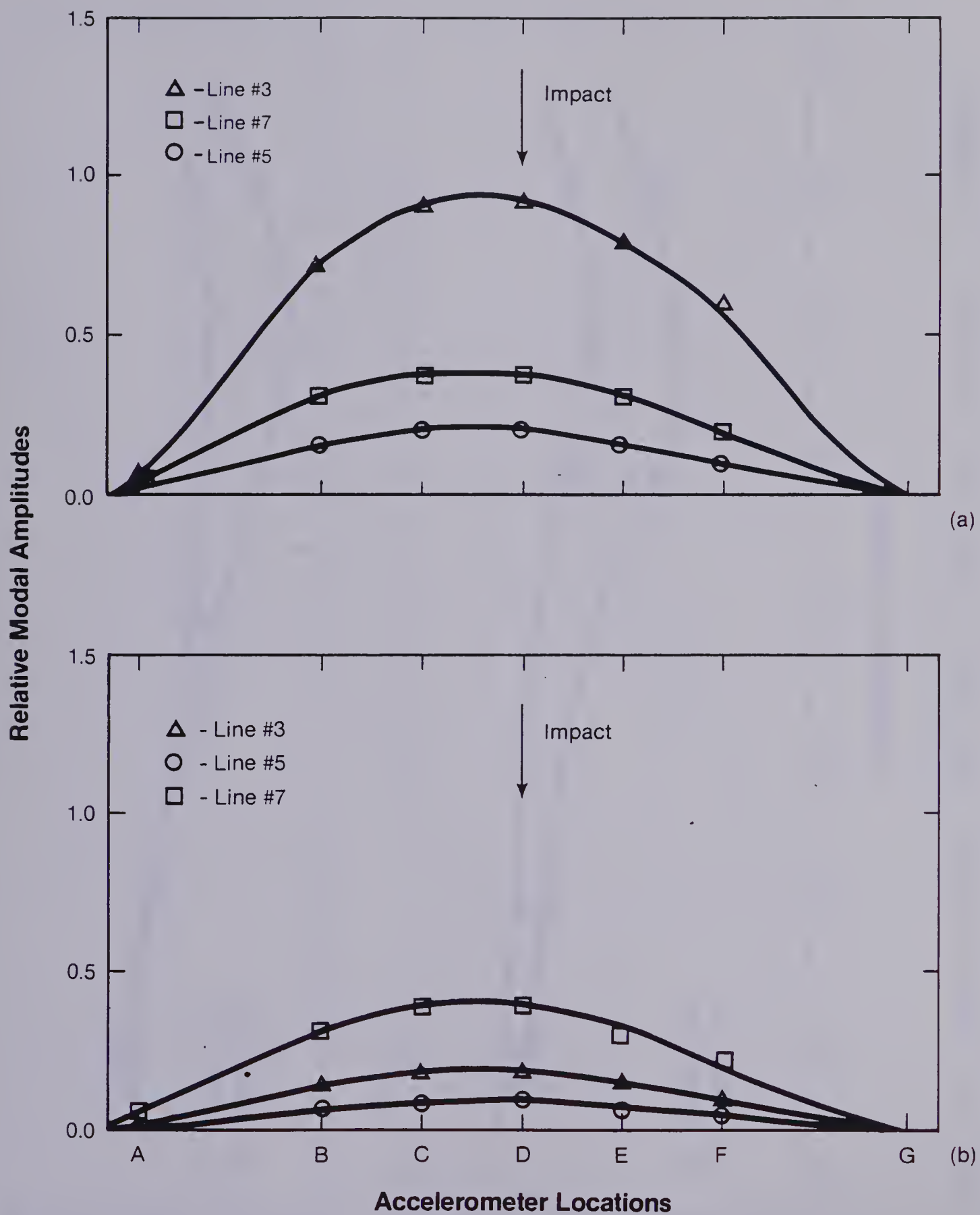


Figure 4.8 Relative Modal Amplitudes along Lines 3, 5, and 7

(a) Mode 3, (b) Mode 4

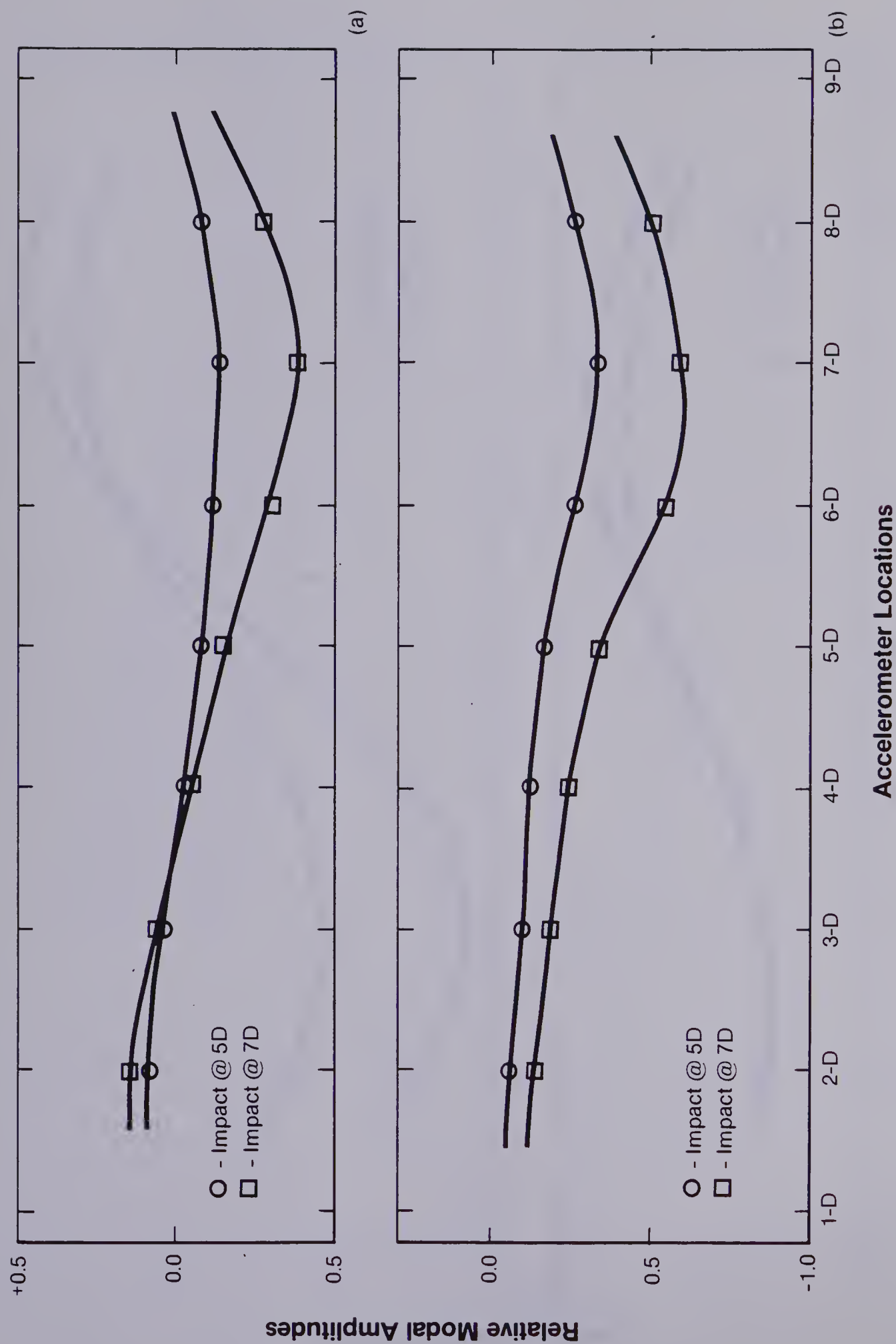


Figure 4.9 Relative Modal Amplitudes along Line D (a) Mode 1, (b) Mode 2

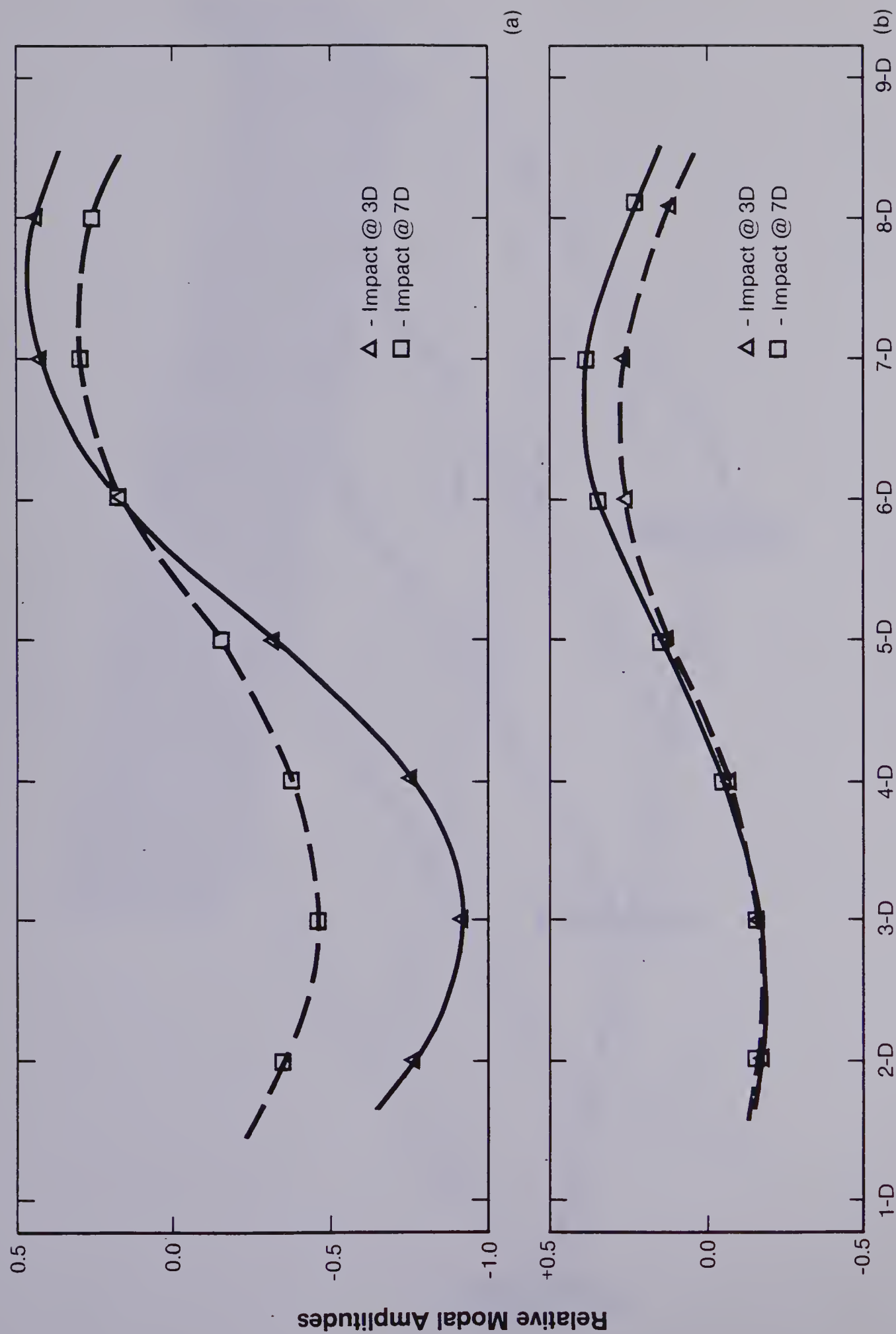


Figure 4.10 Relative Modal Amplitudes along Line D (a) Mode 3, (b) Mode 4

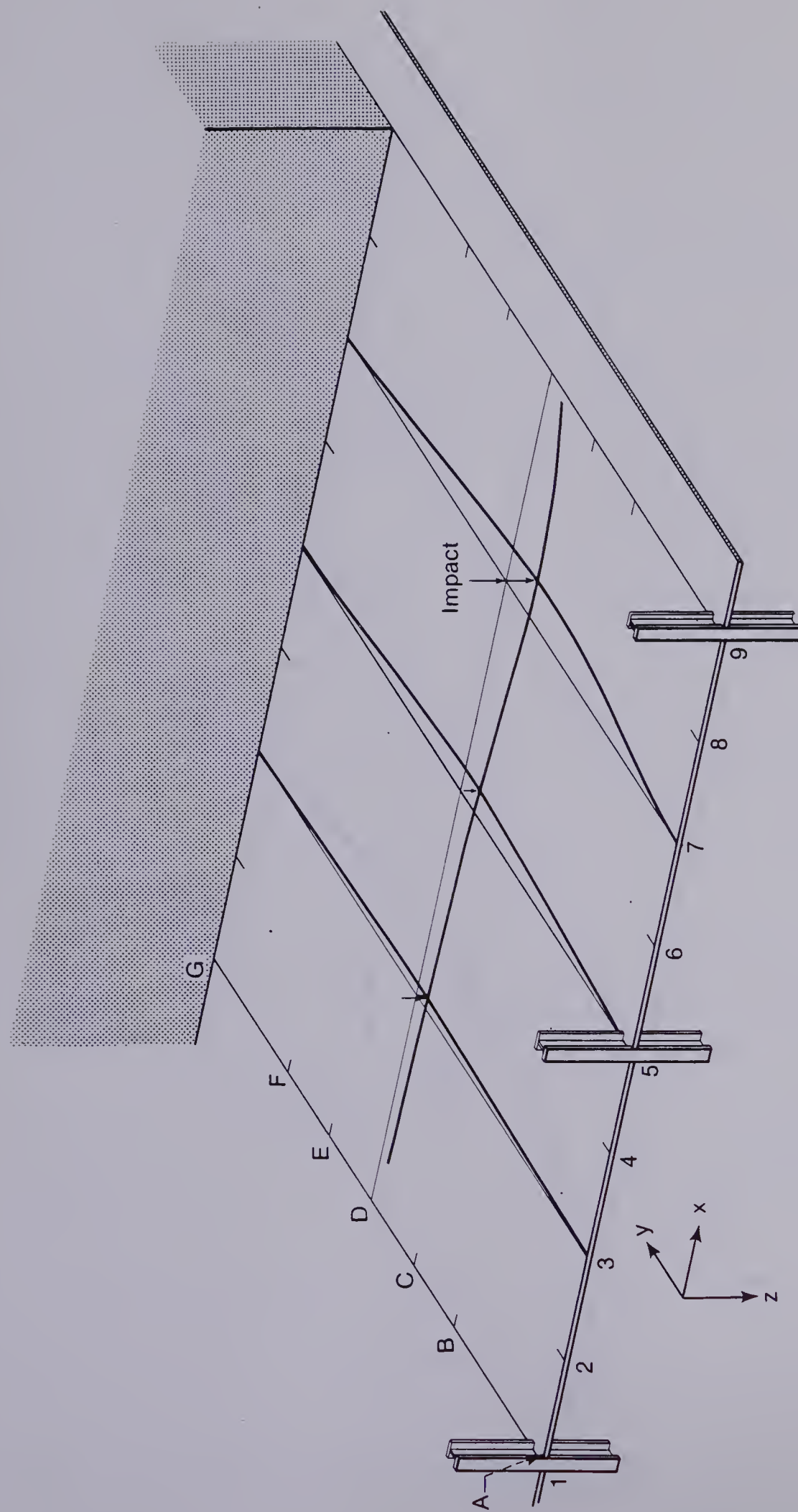


Figure 4.11 Three Dimensional View of Mode 2 over Test Area

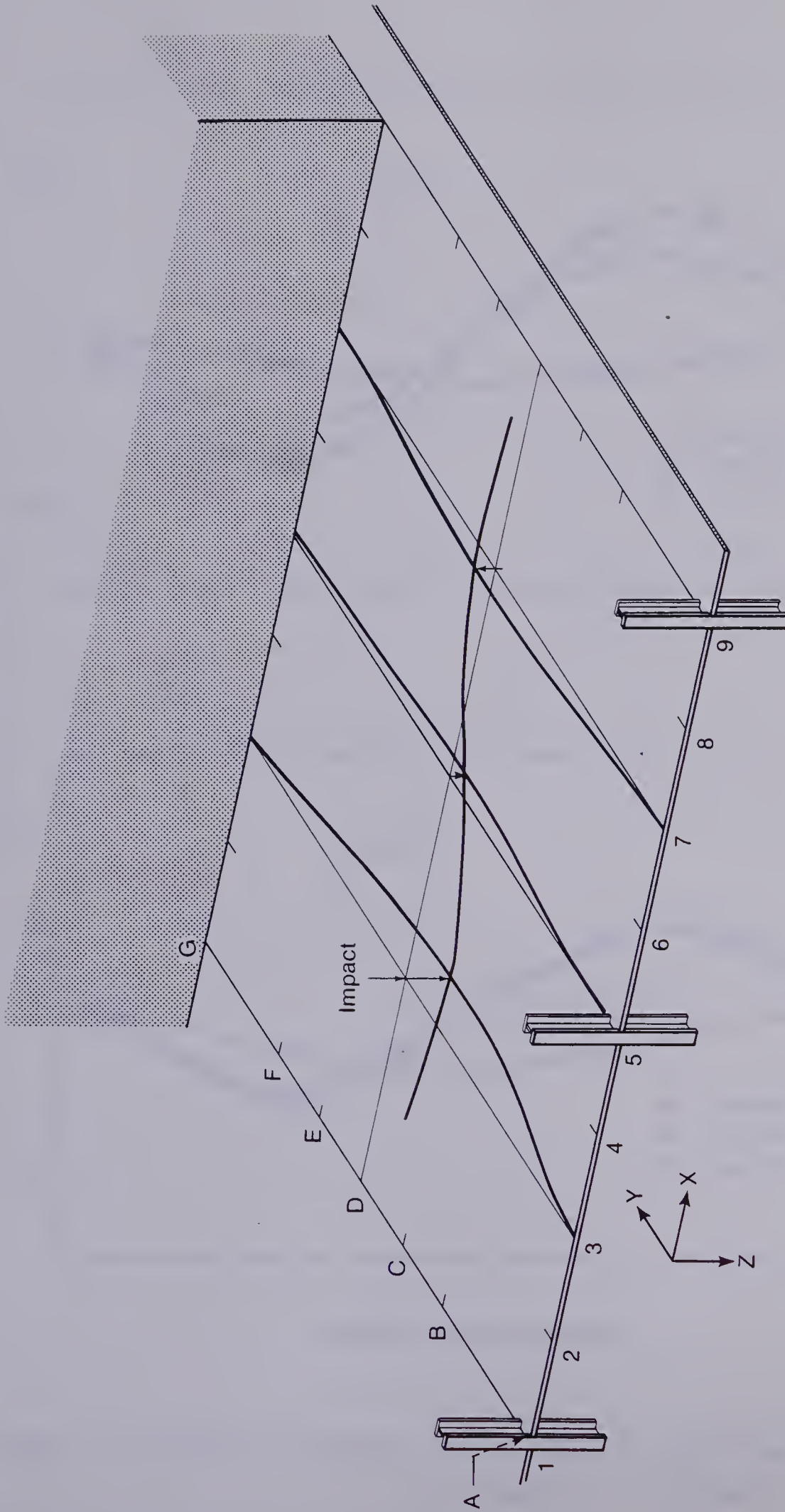


Figure 4.12 Three Dimensional View of Mode 3 over Test Area

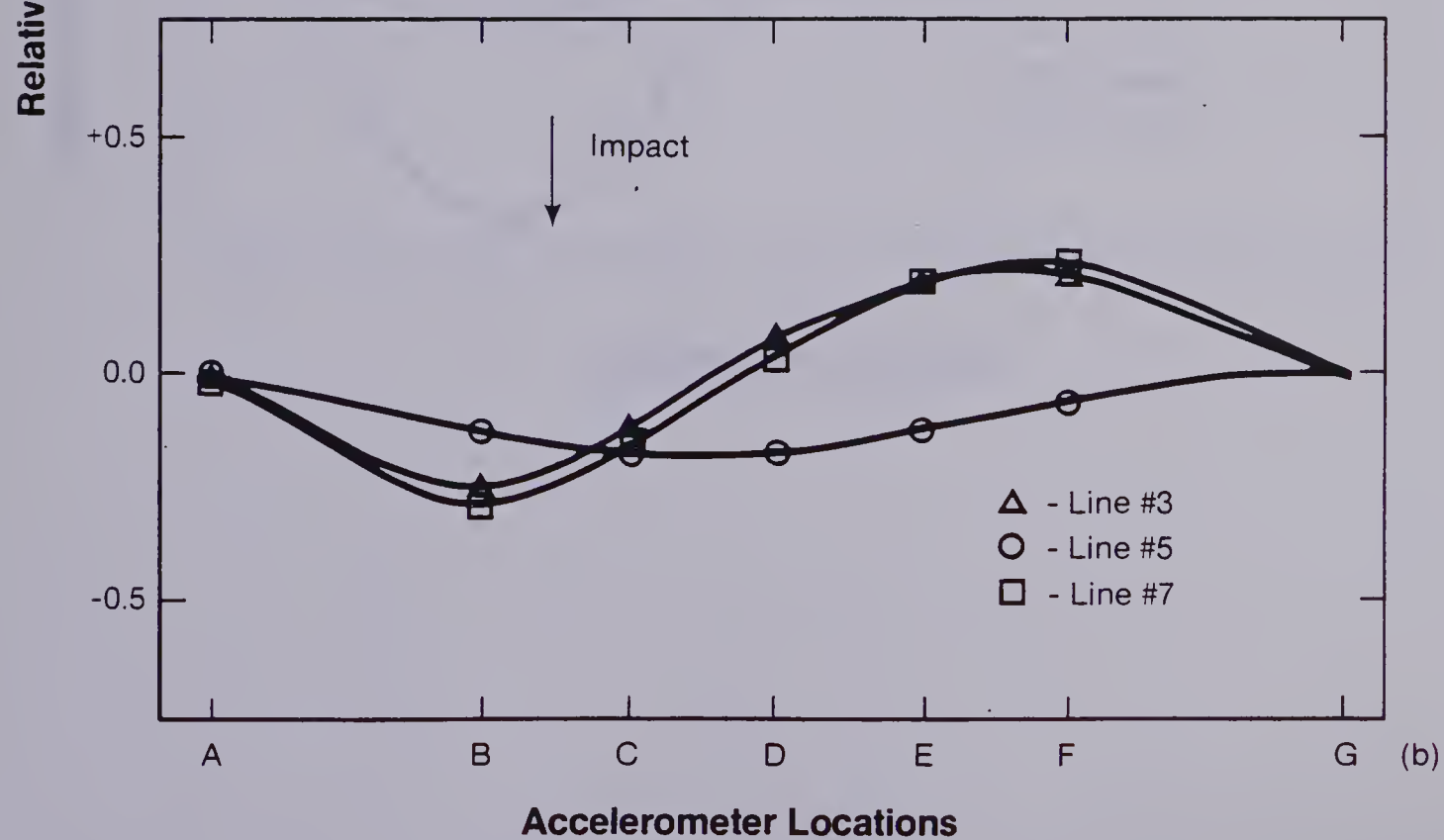
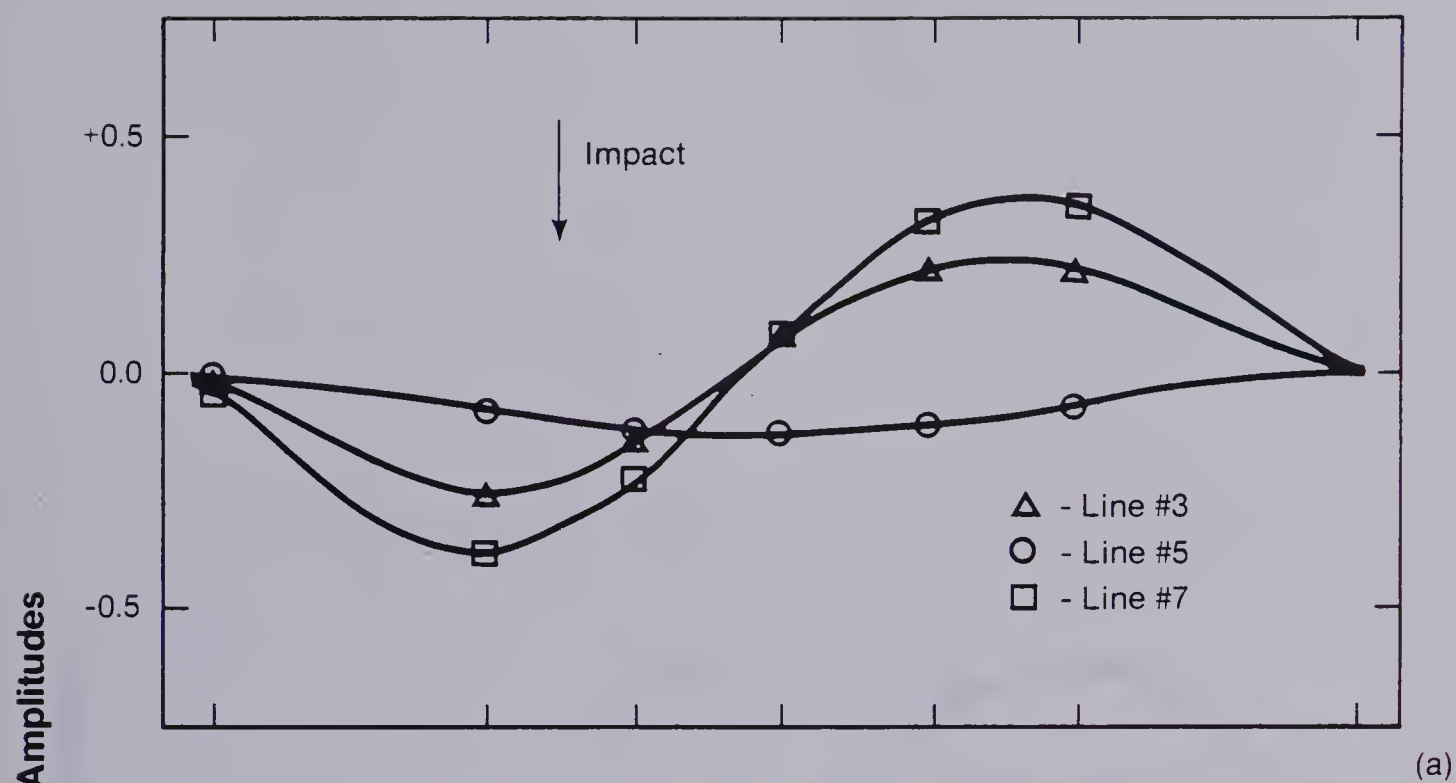


Figure 4.13 Relative Modal Amplitudes along Lines 3, 5, and 7
 (a) Mode 5, (b) Mode 6

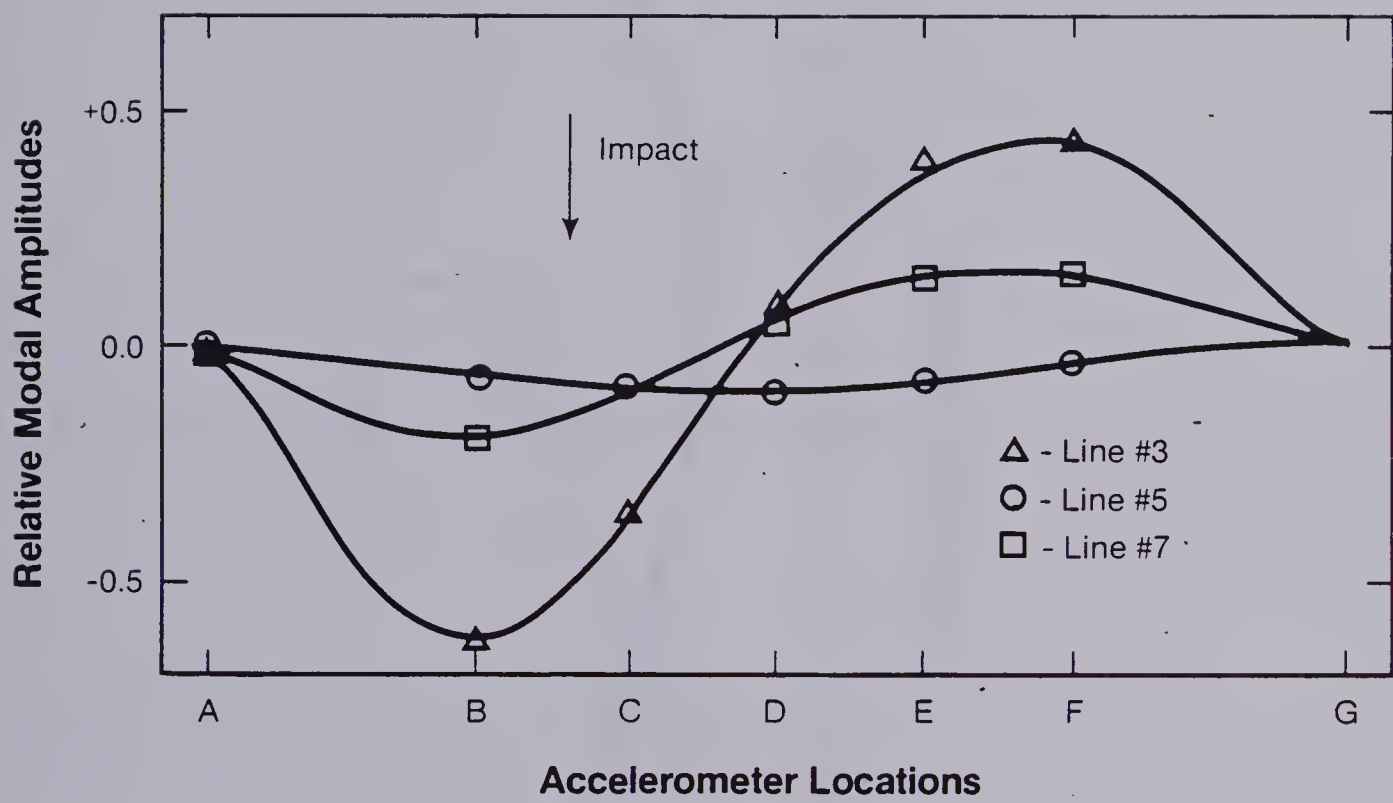


Figure 4.14 Relative Amplitude of Mode 7 along
Lines 3, 5, and 7

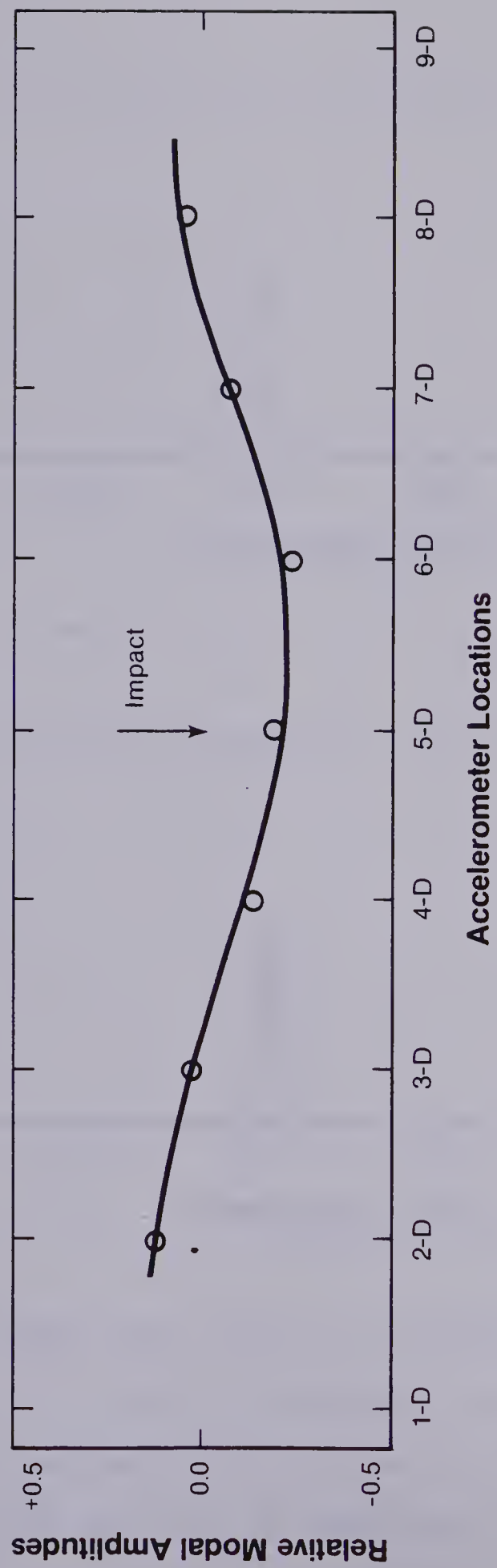


Figure 4.15 Relative Amplitude of Mode 5 along Line D

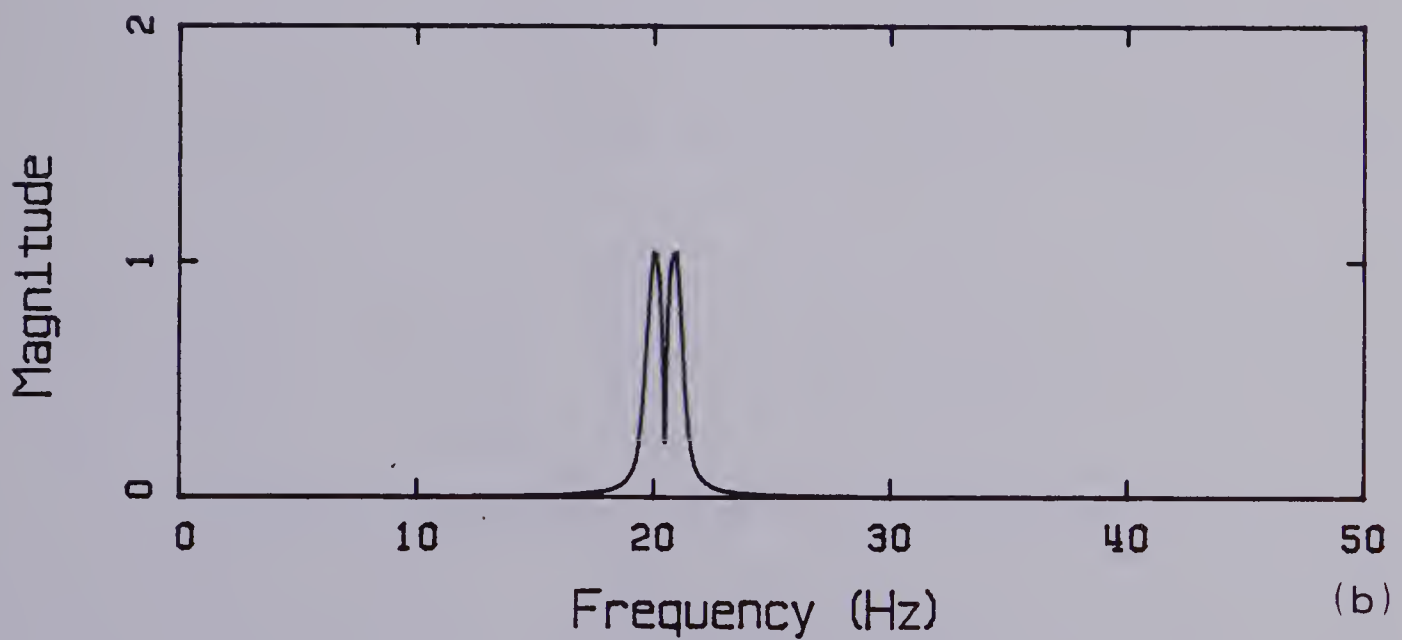
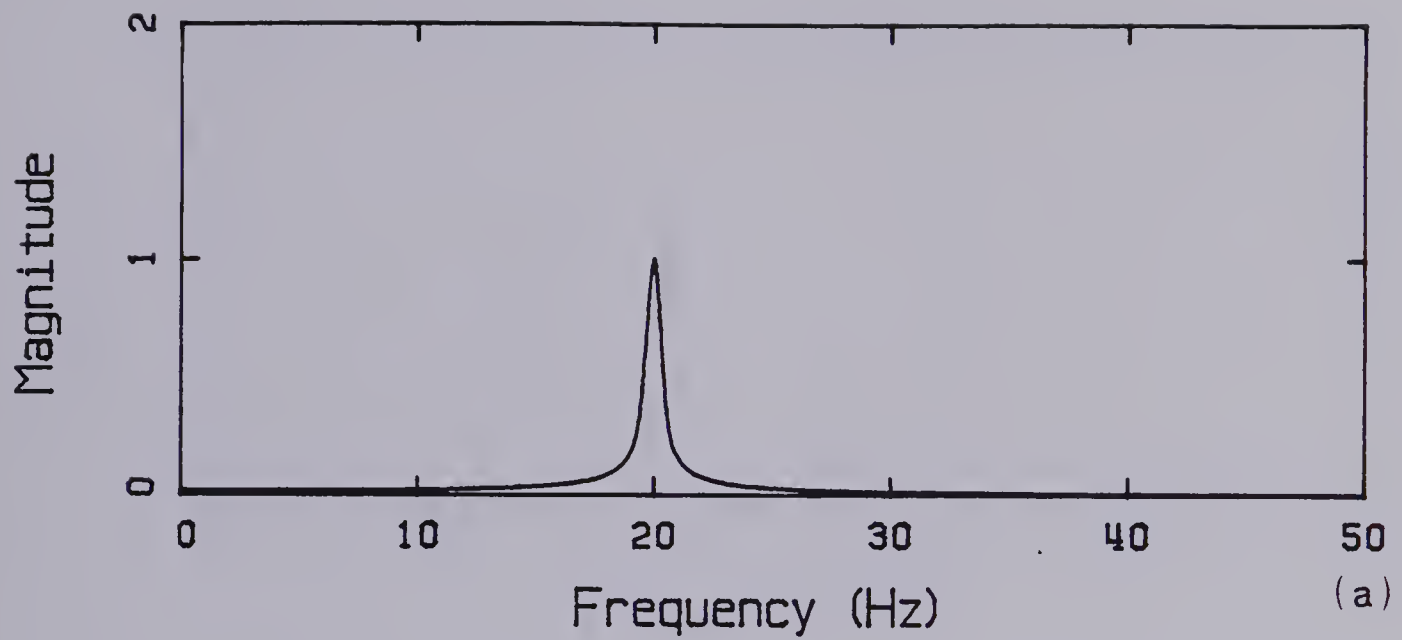


Figure 4.16 Magnitude Spectra From Manufactured Traces

(a) 20 Hz Component, (b) 20 and 21 Hz
Components, (c) 20 and 20.5 Hz Components,
(d) 20 and 20.5 Hz Components with 2:1 Amplitude
Ratio

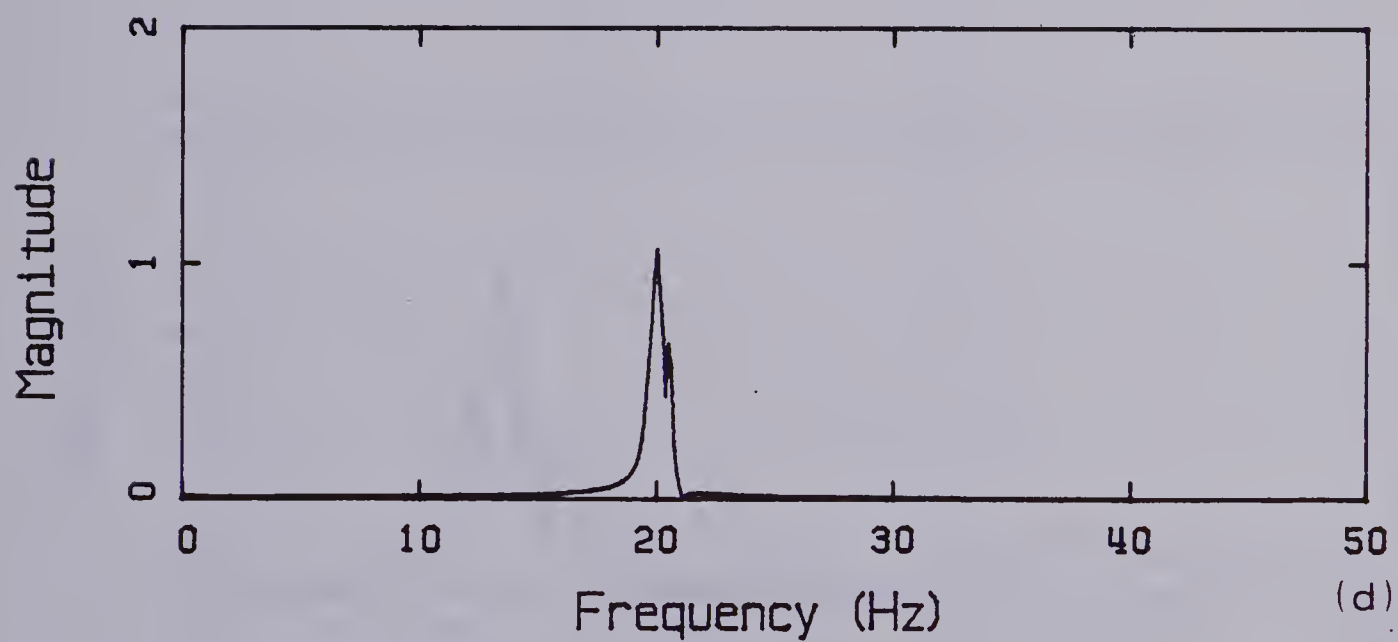
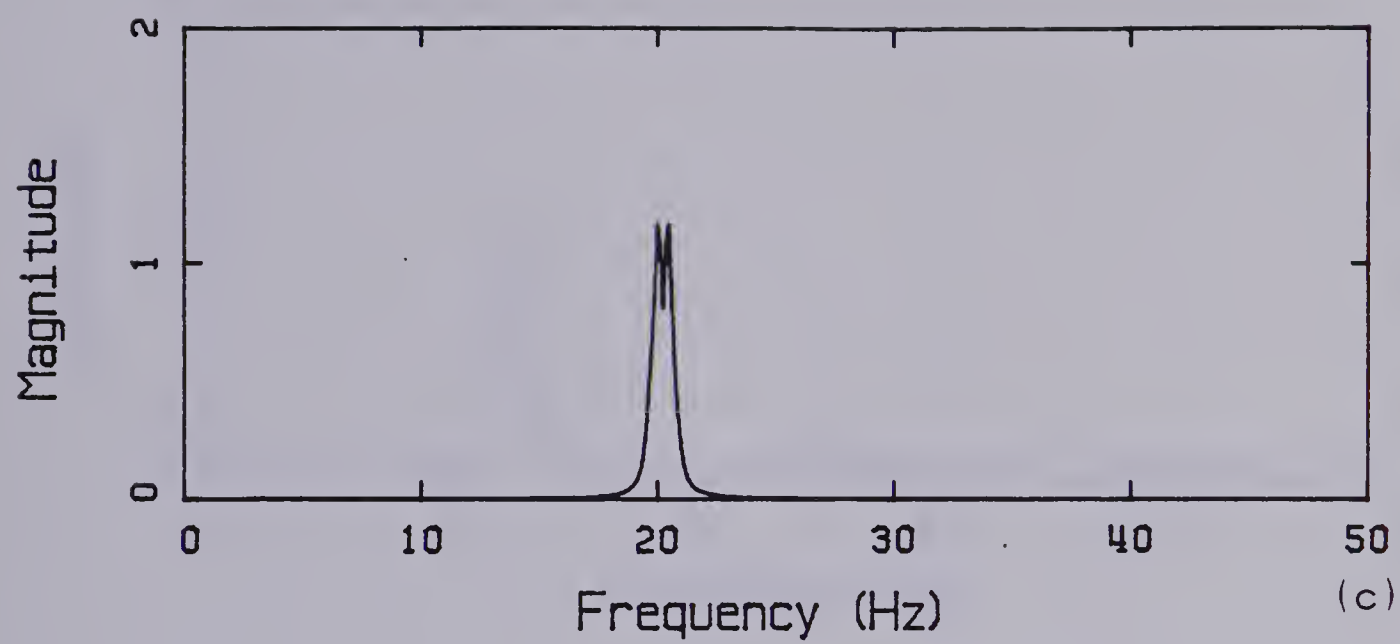


Figure 4.16 Continued

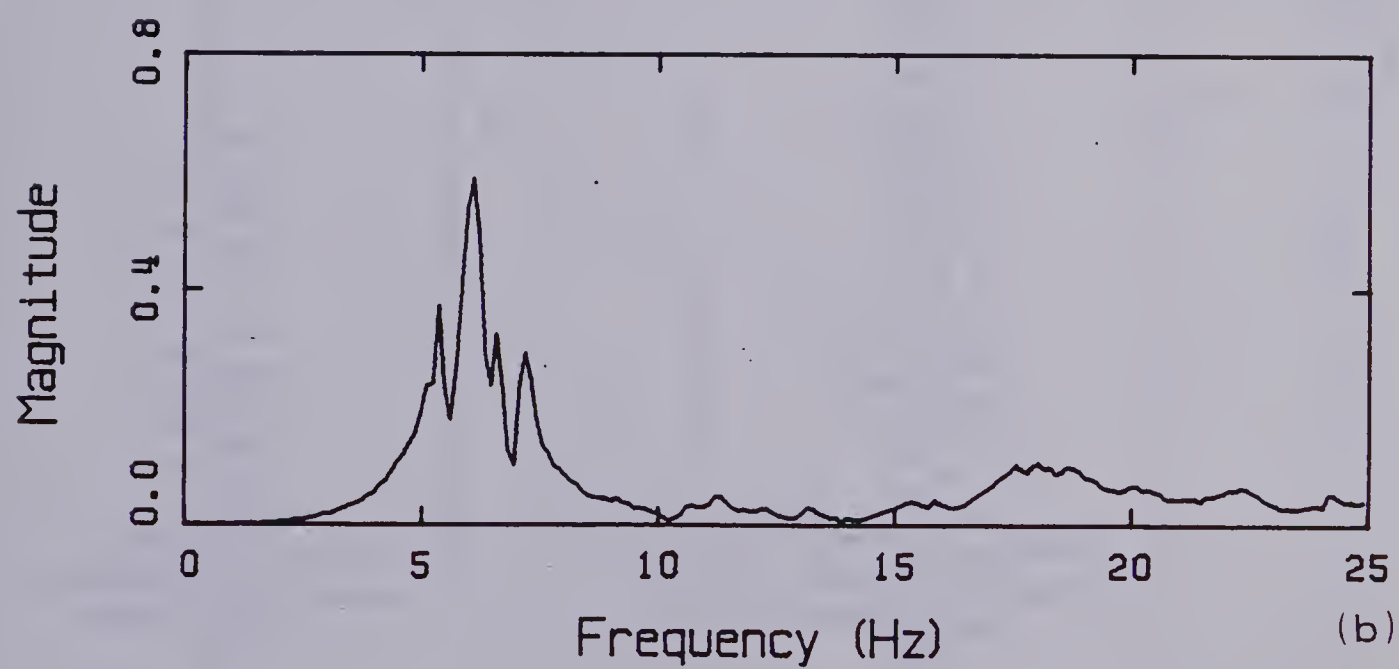
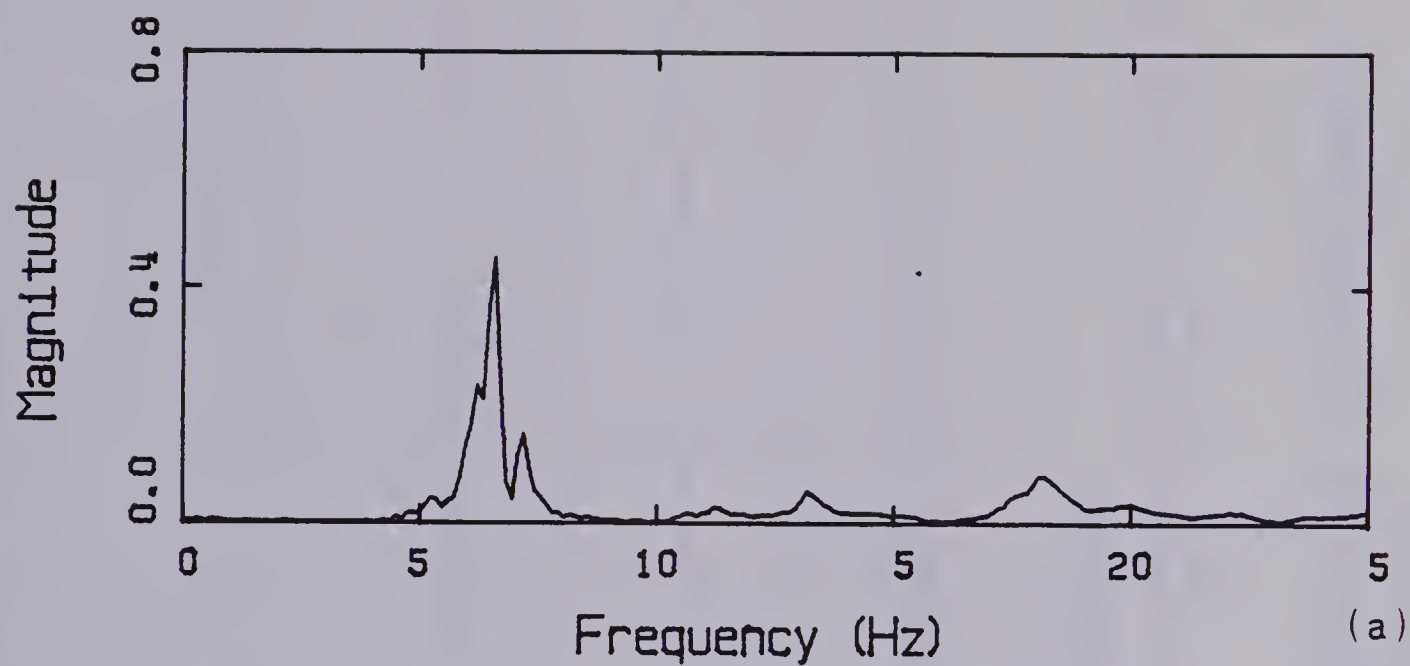


Figure 4.17 Magnitude Spectra from Test Positions
(a) Position 3D, (b) Position 7D

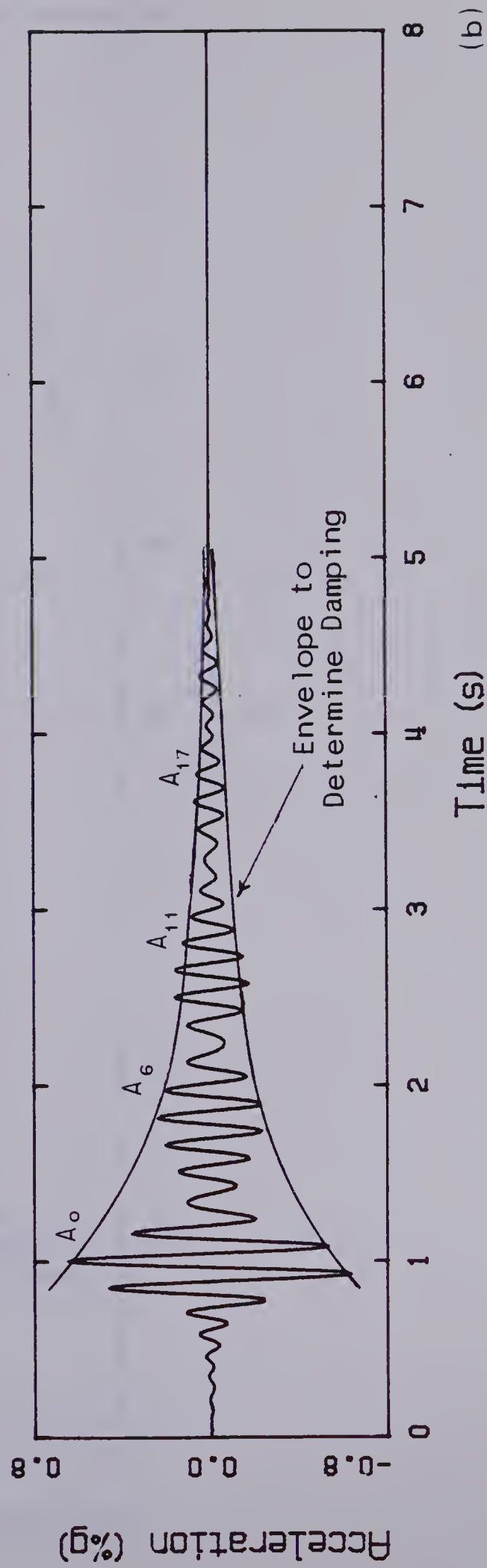
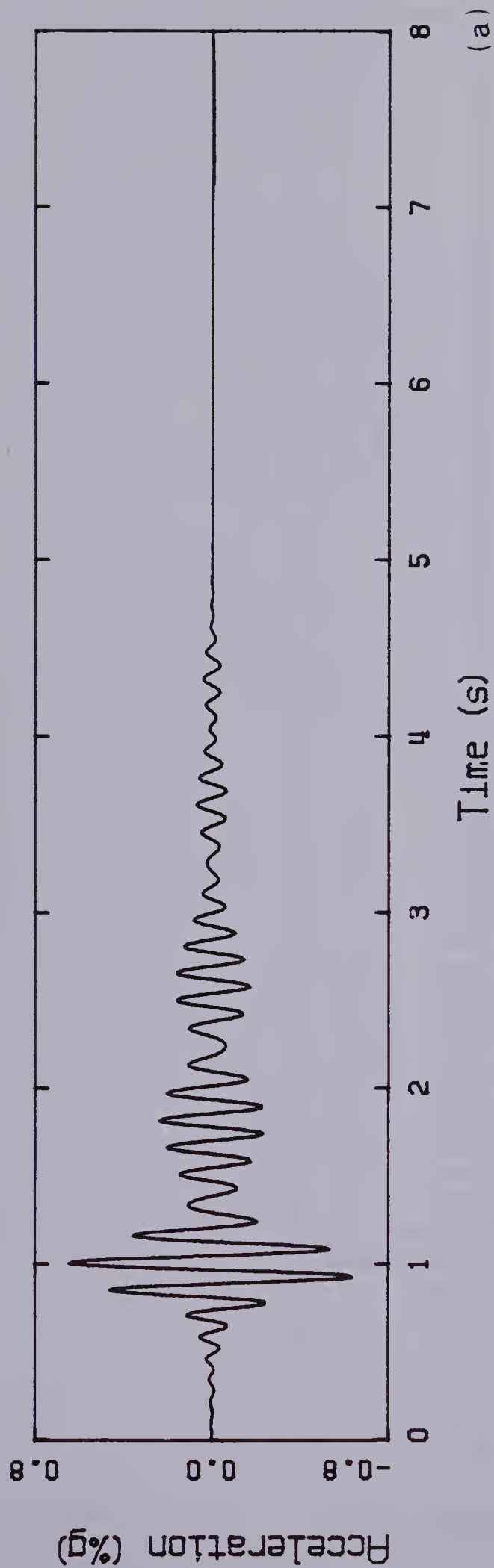


Figure 4.18 (a) Trace Indicating Beating Phenomenon, (b) Envelope used to Determine Damping Ratio

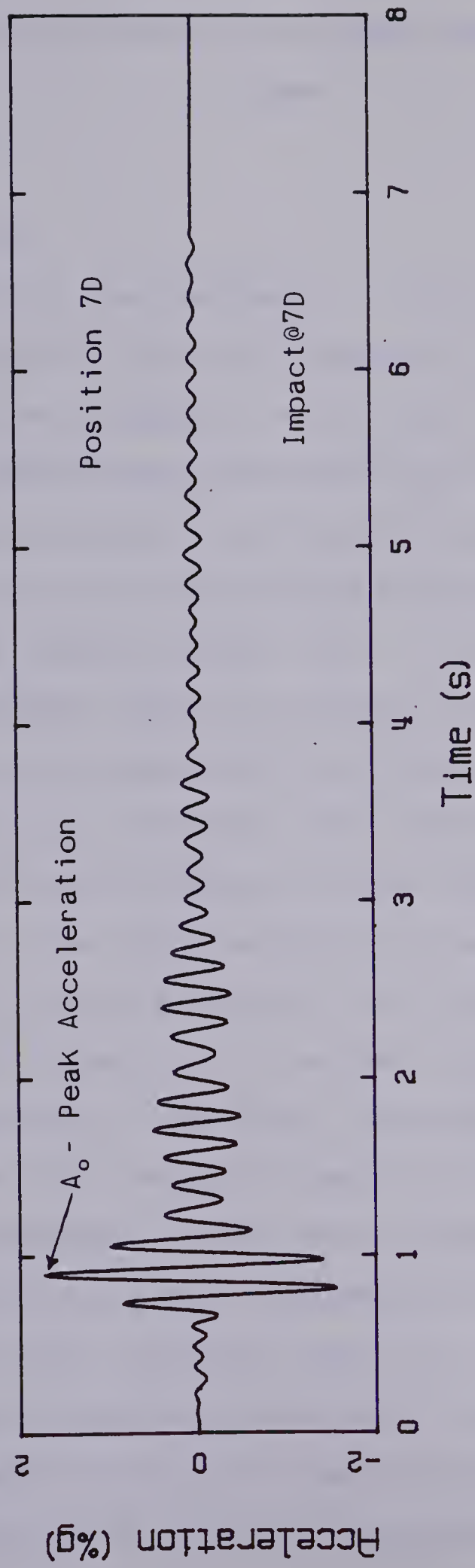


Figure 4.19 Typical Event Indicating Peak Acceleration

5. Dynamic Characteristics of an Open Web Steel Joist Dance Floor

5.1 Introduction

Traditionally, the designers of dance floors have considered primarily structural adequacy, with little regard for the vibrational adequacy of the floor system. As a result, some dance floors have exhibited unsatisfactory vibration characteristics, particularly where a quiet occupancy such as a dining area was affected by the vibration of an adjacent dance floor. To investigate some aspects of a dynamic approach to dance floor design, tests were conducted on an open web steel joist dance floor which displayed bothersome vibration levels during dances.

The experimental study was broken into the determination of the floor response to the standard heel impact test and the evaluation of the floor response during dancing. From the results of the heel impact tests, the natural frequencies of vibration, the peak accelerations, the mode shapes, and the modal damping ratios of the floor system were determined. These results were subsequently used to evaluate the dynamic response of the floor system with regard to quiet occupancy usage (ie: dining).

The dynamic parameters determined in the dance tests included the peak acceleration response generated by the dances and the prominent frequency components of a variety

of dances. These results were used in the derivation of a design proposal pertaining to the vibration serviceability of dance floors.

5.2 Description of Floor System

The dance floor was located on a sunken section of the second floor of a three story dinner and recreation club. The structural system consisted of a non-composite concrete slab supported by open web steel joists (OWSJ) which were in turn simply supported on steel beams. Except for two spans running beneath the sunken floor, the beams were simply supported on steel columns extending the full three story height of the building. The two remaining spans were arranged in a cantilever system supported on columns extending to the second floor level. Figure 5.1 provides a general illustration of the floor system surrounding the dance floor.

The 100 mm thick concrete slab consisted of normal weight concrete cast on 38 mm corrugated steel decking. In the test area, the slab spanned between 600 mm deep open web steel joists, which spanned 12 m and were spaced at 0.94 m. These joists were in turn supported by W610 x 113 link beams (see Fig. 5.1) which spanned 9.3 m. The link beams were simply connected to the cantilevered segments of W610 x 113 girders which extended 1.86 m over column supports ending at the second floor level (circled columns in Fig. 5.1).

Except for one adjacent to the dance floor, these columns are located on or outside the boundary of the dropped area. The 13 m x 18 m sunken floor surface is 400 mm below the general elevation of the second floor.

When the tests took place, the building had been occupied for several months. The finished interior included a 7 m x 9.8 m hardwood dance area with the remainder of the floor surface covered in carpet. The dance floor was surrounded on three sides by an area of tables and chairs used for dining. A low partition divided the tables located on the sunken floor from those on the main level. A stage was included on the remaining side of the recessed area.

The ceiling below the dance floor featured textured drywall hung from the floor joists. Mechanical and electrical ducts were also attached to the joists behind the drywall ceiling.

5.3 Heel Impact Tests

5.3.1 Test procedures

The heel impact study was limited to two series of tests. Each series consisted of a single impact location on the dance floor and one or more accelerometer placements. Five heel drops were delivered in succession in each of the individual tests, with the floor response being allowed to damp out between impacts.

Figure 5.2 presents a planview of the dance floor and surrounding area and shows the number-letter grid established to identify positions on the floor. Lines coinciding with the joist positions within the boundaries of the sunken floor have been numbered sequentially from one to fifteen while lines in the transverse direction have been labelled with the letters A through G. The accelerometer positions and heel impact locations in both test series are also identified in the figure.

The impact position selected for the first test series was the midspan of the floor joist centred on the supporting link beams. This location corresponds to grid position E6 in Fig. 5.2. To determine dynamic characteristics perpendicular to the midspan of the joists, the first test series included the monitoring of accelerations at positions E5 through E11 (see Fig. 5.2).

In the second test series, accelerometers were mounted at positions C6, C7, C9, and C11 (see Fig. 5.2) to determine the vibrational properties of the floor along the supporting beam. The heel drop impacts were delivered at position C6 in this test series.

Accelerometers were also mounted simultaneously at positions C6, D6, and E6 in both test series to measure the floor response along the joists.

5.3.2 Heel Impact Test Results and Discussion

5.3.2.1 Natural Frequencies

Although the scope of the heel impact tests was quite limited, the results were sufficient to identify the natural frequencies of the floor system. Magnitude spectra typical of the response at the midspans of the joists (line E in Fig. 5.2) and along the supporting beams (line C) are presented in Fig. 5.3a and b, respectively. Numerous spikes appearing in the spectra demonstrate that several natural frequencies contributed to the dynamic response of the dance floor. In general, the response was dominated by frequency components below 12 Hz although a group of components between 15 and 20 Hz was also significant in the response along the supporting beam (see Fig. 5.3b) for the impacts delivered at position C6. Additional magnitude spectra for the other test positions are presented in Appendix C.

The fundamental frequency of the floor was approximately 5 Hz as indicated by the predominant frequency component in the magnitude spectra. In addition, components at 9.4 and 9.8 Hz were also prominent in the response at the joist midspans (see Fig. 5.3a) while components at 6.8 and 7.3 Hz were significant in the response along the supporting beam (see Fig. 5.3b), particularly for the impacts over the beam. Possible natural frequencies also occurred at 8.2 and 8.6 Hz although the corresponding spectral peaks were generally lower in magnitude than those

of the five components just mentioned. The prominent natural frequencies of vibration have been tabulated in Table 5.1.

With the exception of the 5.0 Hz component, the prominence of the individual frequency components was specifically related to the impact position. A comparison of two spectra associated with position D6 (see Appendix C), one for an impact at C6 and the other for an impact at E6, confirms the components at 6.8 and 7.3 Hz and those at 9.4 and 9.8 Hz were excited to a larger extent by the former and latter impacts, respectively. The degree of excitation of the individual components can be attributed to the amplitude of the modal response at the impact positions.

Within the boundaries of the sunken floor, the dynamic characteristics are primarily influenced by the presence of two unequal spans of joists and by the beam support which runs below the dance floor (refer to Fig. 5.1). The beam effectively divides the area into two sections, each with a different span and stiffness. Because of the variation in structural properties, each section had distinct dynamic characteristics which combined to produce the observed response of the sunken floor. Unfortunately, the study did not include measurements on the floor area over the 300 mm deep joists and related contributions of that portion of the floor to the overall system response are uncertain.

5.3.2.2 Mode Shapes

The results of the heel impact tests were used to determine the mode shape corresponding to the fundamental frequency (ie: 5.0 Hz) of the floor system. Although an attempt was also made to identify the mode shapes associated with the other prominent natural frequencies, the experimental results were insufficient to reliably determine those modal patterns. Therefore, shapes associated with modes 2, 3, 4, and 5 have not been included in the results. The limited scope of the heel impact tests and the close spacing of the natural frequencies were responsible for the uncertainty of those modes.

The normalized shape of mode 1 along the supporting beam (line C in Fig. 5.2), perpendicular to the midspan of the joists (line E), and in the transverse direction along joist line 6, has been presented in Fig. 5.4a, b, and c, respectively. In each case, the curves identifying the mode shape have been extrapolated to the boundaries of the sunken floor area (broken portion of curves). The pattern along the supporting beam (Fig. 5.4a) corresponds to an impact at 6C while the pattern shown for the joist centreline (Fig. 5.4b) is associated with an impact at 6E. Two curves are included in Fig. 5.4c, one for both of the above impact positions. Although the shape of the two curves differs slightly, the mode appears to be reasonably well defined.

Figures 5.4a, b, and c reveal a typical one-half sine wave configuration along grid lines C, E and 6 in the

fundamental mode of vibration. The maximum modal response occurred at the impact position along lines C and E, and near the 6E impact position in the transverse direction along line 6. These results demonstrate that the largest modal response will always occur near position 6E since mode shapes remain unchanged regardless of the impact position.

With the exception of the mode shape along the beam (line C) near position C13, the nodal points appear to occur near the boundaries of the sunken floor. The apparent node by C13 (Fig. 5.4c) can be attributed to the column support at that location.

The mode shapes, both parallel and perpendicular to the floor joists, suggest that the entire sunken floor area participates as the vibrating panel in the fundamental mode, with nodal lines of vibration occurring near the boundaries of the sunken area. The architectural layout supports that type of response since a 0.4 m drop and a low partition isolate the sunken floor. Structurally, the continuity of the non-composite concrete slab throughout the sunken area facilitates the observed response.

5.3.2.3 Modal Damping Ratios

The damping ratios associated with the five prominent natural frequencies in Table 5.1 were determined by the one-half power bandwidth method and are presented in Table 5.2. Also included are the critical damping ratios for the first mode, determined from the decay curves of

several appropriate acceleration-time records.

The accelerometer records were lowpass filtered at 6.0 Hz to obtain the traces used in calculating the exponential decay corresponding to the fundamental mode. The resulting filtered traces were not affected by the beating phenomenon described in the previous chapter since the first mode was very distinct (ie: pure modal response). Since the pure transient response associated with modes 2, 3, 4, and 5 could not be obtained because of filter limitations (see Appendix A), the decay method was not employed for those modes.

The modal damping ratios derived from spectra or decay curves associated with the test positions along line C and along line E, respectively, were averaged to obtain the values presented in Table 5.2 for the supporting beam and the joist midspans. The maximum range in the individual modal values was 0.7% for a single location and 1.0% over an entire line.

The results indicated the fundamental mode was the most highly damped with a ratio of approximately 5.0% critical while the other modes generally had values in the 2.5 to 3.0% range. The 5.0% damping of the fundamental mode compares favorably to the damping of other completed open web steel joist floor systems with some furnishings in place.

5.3.2.4 Peak Acceleration

Filtered acceleration-time records corresponding to impact positions C6 and E6 were examined to determine the peak acceleration of the floor system caused by a heel drop impact (refer to Sect. 2.2). A peak acceleration of 1.0 %g was observed for the impact over the supporting beam (C6) while the impact at the midspan of the joists (E6) produced a peak acceleration of 1.4 %g. A typical filtered trace from position E6 is shown in Fig. 5.5.

The experimental results show that the peak acceleration at position E6 was maximum with respect to the other accelerometer positions in all of the tests. This result in conjunction with the fundamental mode shape of the floor (see Fig. 5.4), suggests the maximum peak acceleration (produced by a heel impact) of the entire sunken floor would be approximately 1.4 %g.

Since the peak accelerations were derived from filtered traces representing the pure modal response of the floor, they may be directly applied to the annoyance threshold chart of Fig. 2.1. This figure reveals that the the floor system is more than adequate for walking vibrations in a quiet occupancy. Consequently, one would certainly expect that the floor would be adequate for similar usage (ie: dining) in the dance hall environment where larger vibration levels are to be expected and tolerated.

5.4 Theoretical Evaluation of the Floor System

In Appendix C, the fundamental natural frequency and the peak acceleration of the dance floor have been derived theoretically in accordance with the appropriate equations in Chapter 2. The contributions of the drywall ceiling, the flooring material, and the ductwork to the mass of the floor system were considered in the calculations. The theoretical frequency and peak acceleration values are subsequently used to simulate a design stage evaluation of the floor system with respect to vibrational acceptability.

5.4.1 Fundamental Frequency

The detailed calculations to determine the fundamental frequency of the dance floor have been presented in Appendix C.2. Because the joists were supported on flexible link beams (refer to Fig. 5.2), the fundamental floor frequency was calculated according to Eqn. 2.2 as a system frequency. The results of the calculations were as follows:

frequency of joists (f_j).....6.7 Hz

frequency of supporting beams(f_g)....5.2 Hz

fundamental floor frequency (f_f).....4.1 Hz

The calculated fundamental floor frequency of 4.1 Hz is 18% lower than the 5.0 Hz value derived experimentally. Since the mass estimates were probably quite accurate, the difference can likely be attributed to a significant (ie: approximately 40%) underestimate of the actual floor stiffness. A possible explanation lies in the calculation

for the frequency of the supporting beam where only the steel beam was assumed to contribute to the stiffness. The assumption of even partial composite action would be sufficient to raise the theoretical floor frequency to the measured value. However, inaccuracies of 20% are quite common in the frequency calculations and the theoretically derived value (4.1 Hz) would be sufficiently accurate to use in an evaluation of the floor at the design stage.

5.4.2 Peak Acceleration

In Appendix C.3, the peak acceleration of the dance floor was calculated theoretically according to Eqn. 2.16 for three approximations to the effective vibrating panel width. The results of those calculations have been summarized in Table 5.5. The first two values in Table 5.5 represent totally theoretical estimates while the last value was derived using experimental observations.

The measured peak acceleration of 1.4 %g was significantly overestimated by the current code practice (60t_e approximation). This can be attributed to the large difference in the actual vibrating panel width (see Fig. 5.4b) from the code value. By using the more detailed Sokolowski method (see Sect. 2.3.2) to estimate the vibrating panel width, the accuracy of the theoretically derived peak acceleration was significantly improved. As expected, the value calculated using the experimental results was also reasonably accurate.

5.4.3 Evaluation

To simulate a design stage evaluation of the floor system, the theoretical peak acceleration of 1.49 %g was plotted on the annoyance threshold chart (see Fig. 2.1) at a frequency of 4.1 Hz. With an estimated damping ratio of 6% critical (suggested design value for finished floor without partitions), the floor system would be considered adequate for walking vibrations in a quiet occupancy. Note that this conclusion would also have been reached with the peak acceleration of 2.5 %g obtained with the code provision. Therefore, the theoretical evaluation provided a realistic appraisal regarding the dynamic characteristics of the floor system.

5.5 Dance Vibration Study

5.5.1 Test Procedures

The dance vibration study was undertaken to determine the floor response under the dynamic loads generated during dances. The floor response during a typical evening of dancing was monitored at the position perceived by patrons to exhibit the worst vibration levels.

Two accelerometers were mounted near the edge of the dance floor between grid lines E and F corresponding to the one-third points of the joists along lines 5 and 6. These positions are denoted by "DVS" (dance vibration study) in

Fig. 5.2. The floor response was then monitored over an evening of dancing, with the vibrations resulting from waltzes, polkas, and modern rock and roll dances being included. General remarks regarding the number of couples on the dance floor were also recorded.

5.5.2 Dance Test Results and Discussion

5.5.2.1 Results

The results of the dance tests were particularly enlightening with regard to the bothersome vibration levels perceived by patrons seated in the dining area adjacent to the dance floor. Typical magnitude spectra corresponding to a waltz, a polka, and a fast rock and roll dance are presented in Fig. 5.6a, b and c, respectively. In general, the spectra derived from the numerous dance records show components at or near the fundamental floor frequency (5.0 Hz) to be much lower in magnitude than the predominant dance frequency component. In some cases, the second harmonic of the dance component was also more pronounced than the fundamental floor frequency (see Fig. 5.6b). These spectra show that the floor responded primarily at the prominent dance frequencies and not the natural frequencies of the floor system. These results clearly demonstrate that the floor response was not a resonant excitation but rather one of forced vibrations at well below the fundamental frequency of the floor.

The floor response to several dances has been summarized in Table 5.3. The tabulated results include the prominent dance frequencies, the relative spectral magnitudes of the various frequency components, the average peak accelerations of the floor during the individual dances, the maximum peak accelerations observed during each dance, and comments regarding the perceived vibration levels.

The test results reveal a range in prominent dance frequencies from 1.9 Hz for a waltz to 3.3 Hz for a fast rock and roll dance. The principal frequencies of the floor response to each dance appear to be directly related to the musical beat and dance step and to be unaffected by the number of people participating. Since the majority of the people dancing kept time with the music, this result was not surprising. Considering the broad range of dances observed, a dance frequency of greater than 4.0 Hz appears unlikely although the harmonics may reach 8.0 Hz.

The relative spectral magnitudes are given to provide an indication of the relative floor response attributed to the dominant frequency components of each dance. To determine the values in Table 5.3, the spectral magnitudes of the components were normalized to the overall maximum spectral magnitude obtained in the results. This accounts for the one rock and roll component having a value of 1.0. These results confirm that in every dance, except the extremely low response waltzes, the 5.0 Hz component had a

spectral magnitude which was significantly lower than that of the prominent dance frequency component. The spectral magnitudes of the components within each dance category (for example, fast rock and roll) appear to be affected by the number of people dancing.

The recorded dance records were filtered at 6.5 Hz and 25.0 Hz in deriving the average and maximum peak acceleration values presented in Table 5.3. The peak amplitudes of the time domain response for each dance were averaged over a thirty second period to obtain the average peak accelerations. The average and maximum peak acceleration levels of a typical dance record are shown in Fig. 5.7.

A comparison of the two average peak acceleration values presented for each dance indicates that components above the fundamental frequency of the floor contributed little to the total response. These results also indicate that the acceleration levels of the floor system were related to the type of dance activity and, to a lesser degree, the number of people dancing.

The maximum peak accelerations of each dance record were included in Table 5.3 to provide an indication of the peak response which occurred over short periods of time. The maximum accelerations were, in general, much higher than the average accelerations and therefore they may have influenced the levels of annoyance perceived by patrons seated near the dance floor. Comments, made by patrons

seated within two meters of the accelerometers, regarding the perceived level of annoyance during each dance, have been reflected in the vibration evaluation remarks included in Table 5.3. Patrons seated outside of the sunken floor area did not appear to be bothered by the vibration levels during any of the dances.

Magnitude spectra and filtered acceleration-time records for several of the dances discussed in this section are presented in Appendix C.

Since the dining areas surrounding the dance floor constitute quiet occupancies, the annoyance threshold chart of Fig. 2.1 was used to evaluate the floor response associated with the various dances. The same annoyance level classifications as those obtained at the site were found by plotting the average peak accelerations (for the records filtered at 6.5 Hz) on the chart. The average peak acceleration values which exceed the threshold of definite perception criteria (0.5 %g curve in Fig. 2.1) are underlined in Table 5.3.

5.5.2.2 Discussion

The results of the dance tests show that the dynamic characteristics of the open web steel joist floor were unacceptable for a combined dining-dancing occupancy. In responding to the dynamic loads generated by couples dancing, the floor exhibited amplitudes of vibration which were annoying to patrons seated within the sunken area (see

Fig. 5.2). This unacceptable dynamic response was attributed to an inadequate floor stiffness.

The floor system possesses sufficient structural capacity because it was designed to satisfy the standard, span-related, deflection criteria associated with live loading. However, that criteria was not adequate with regard to the dynamic response of the floor system since patrons perceive the actual vibratory amplitudes and not the span related values.

Although the floor will continue to vibrate during dances, the vibrational characteristics could be significantly improved by substantially increasing the stiffness of the floor. Several of the methods mentioned in Sect. 2.4 could be employed in this respect. Under the present conditions, a slight improvement in the floor response could be achieved by moving the dance area closer to the stage where the vibration levels are lower. Another alternative would be to remove the dining area on the sunken floor since the majority of complaints were made by patrons seated in that area. However, some additional stiffness would likely be necessary even in that event, because the dance floor vibrations at full capacity have apparently caused some concern among the people dancing as well.

In Appendix G of the CSA S16.1-M78 standard, a lower limit of 10 Hz has been recommended for the fundamental frequency of dance floors. However, it may not be possible to economically meet this criteria. Because the dance

frequencies were always less than 4 Hz, the results of this study suggest a fundamental frequency of 8.0 Hz would be sufficient to prevent the predominant frequency or the associated harmonics of any dance from creating a harmful resonant response condition. In addition, the stiffness required to achieve a fundamental frequency of 8.0 Hz would likely result in acceptable dynamic characteristics for most dance floors.

5.6 Design Proposal for Dance Floors

5.6.1 Introduction

The following design proposal for simple beam or open web steel joist dance floors pertains to vibration serviceability and is meant to be considered in addition to current strength requirements at the design stage. The method can be used to determine the vibrational acceptability of seating or dining areas located adjacent to and on the same span as the dance floor.

The results of the dance tests described in this chapter have been used in deriving preliminary estimates of design loads and acceptable peak acceleration levels. Further tests are required to confirm the reliability of those estimates.

5.6.2 Analytical Development

5.6.2.1 Model of Floor System

The floor system is divided into a series of T-beams with a top flange width equal to the spacing of the joists or beams. The concrete slab is assumed to act compositely with the joists or beams whether or not shear connection has been provided. The T-beams are assumed to be simply supported and to have uniform flexural rigidity ($E_s I_t$) and mass (\bar{m}) along their lengths (L). The dynamic load generated by people dancing is simulated by a harmonic load (P_0) acting over the portion of the T-beam which supports the dance floor. The dance floor model is illustrated in Fig. 5.8.

5.6.2.2 Theoretical Derivation

With the above floor model, the dance floor design proposal was developed by deriving the acceleration response of the assumed T-beams to the harmonic load. The derivation of the T-beam response is presented in the remainder of this section while the necessary design parameters are discussed in the following section.

The mode shapes ($\phi_n(x)$) of the T-beam model are given by (29)

$$\phi_n(x) = \sin \frac{n\pi x}{L} \quad (5.1)$$

in which $n = 1, 2, 3, \dots$

The displacement response of the T-beam is defined as

$$v(x,t) = \sum_{n=1}^{\infty} \phi_n(x) Y_n(t) \quad (5.2)$$

in which $Y_n(t)$ is the generalized displacement in the n^{th} mode. The uncoupled equation of motion (damped case) for the T-beam is

$$M_n \ddot{Y}_n(t) + 2m_n \xi_n \omega_n \dot{Y}_n(t) + M_n \omega_n^2 Y_n(t) = P_n(t) \quad (5.3)$$

in which ξ_n = is the damping ratio of the n^{th} mode
 ω_n = the natural frequencies of the T-beam in radians/second
 $(\dot{})$ = denotes a differentiation with respect to time

and

$$M_n = \int_0^L \phi_n^2(x) m(x) dx = \frac{\bar{m}L}{2} \quad (5.4)$$

is the generalized mass for mode shape $\phi_1(x)$ and

$$P_n(t) = \int_0^L \phi_n(x) p(x,t) dx = \frac{P_o L}{n\pi} \sin \bar{\omega} t \left(\cos \frac{n\pi d}{L} - \cos \frac{n\pi c}{L} \right) \quad (5.5)$$

is the generalized loading which is constant for all modes in this case.

The harmonic response of the T-beam (solution to Eqn. 5.3) is given by

$$Y_n(t) = \frac{P_o L}{n\pi M_n \omega_n^2} \left(\cos \frac{n\pi d}{L} - \cos \frac{n\pi c}{L} \right) [(1 - \beta_n^2)^2 + (2\xi_n \beta_n)^2]^{-\frac{1}{2}} \sin(\bar{\omega} t - \theta) \quad (5.6)$$

in which

$$\beta_n = \bar{\omega}/\omega \quad (5.7)$$

is the frequency ratio in the n^{th} mode and

$$\theta_n = \tan^{-1} \left(\frac{2\xi_n\beta_n}{1 - \beta_n^2} \right) \quad (5.8)$$

is the phase angle by which the response lags the applied load ($0 \leq \theta \leq 180^\circ$). To obtain the acceleration response of the T-beam, Eqn. 5.6 was differentiated twice and then substituted into Eqn. 5.2 resulting in

$$\ddot{v}(x,t) = \sum_{n=1}^{\infty} \frac{2P_o\beta_n^2 D_n}{n\bar{m}\pi} \sin \frac{n\pi x}{L} \left(\cos \frac{n\pi c}{L} - \cos \frac{n\pi d}{L} \right) \sin (\bar{\omega}t - \theta) \quad (5.9)$$

in which

$$D_n = [(1 - \beta_n^2)^2 + (2\xi_n\beta_n)^2]^{-1/2} \quad (5.10)$$

is the dynamic magnification factor for the n^{th} mode.

The T-beam response in the first mode is assumed to approximate the acceleration response of the dance floor. Therefore, the maximum response in the first mode becomes the peak acceleration (A_o) of the dance floor. This response is given by

$$A_o = \frac{2P_o\beta_1^2 D_1}{\pi\bar{m}} \sin \frac{\pi x}{L} \left(\cos \frac{\pi c}{L} - \cos \frac{\pi d}{L} \right) \quad (5.11)$$

5.6.2.3 Design Parameters

The experimental results presented in Sect. 5.5.2.1 have been used to derive an effective dance load (P_o) and

peak acceleration limits for evaluating the dynamic response of dance floors. The prominent excitation frequencies (ie: dance frequencies) were also considered in the proposal.

By substituting the maximum peak accelerations (for the records filtered at 6.5 Hz) determined in the dance tests (see Table 5.3) in Eqn. 5.11 and by considering the loading conditions during the tests, a proposed effective dance load of 0.212 KN/m was obtained. The derived value reflects the loading conditions which would be expected under a capacity crowd and a vigorous dance activity.

With the 0.212 KN/m effective dance load substituted in Eqn. 5.11, the expression for the peak acceleration response of the T-beams (in units of %g) becomes

$$A_o = \frac{1376\beta_1^2 D_1}{\bar{m}} \sin \frac{\pi x}{L} \left(\cos \frac{\pi c}{L} - \cos \frac{\pi d}{L} \right) \quad (5.12)$$

Equation 5.12 is the proposed design equation to check the vibration serviceability of dance floors.

To make use of Eqn. 5.12 in assessing the vibration serviceability of a dance floor, a knowledge of acceptable acceleration levels is required. The proposed values are presented in Table 5.4. The values were established from the maximum peak accelerations (for the records filtered at 6.5 Hz) derived in the dance tests. The evaluations apply to the acceleration levels of seating areas located on the same span as the dance floor. If no seating areas are located on the same span as the dance floor, significantly

higher levels of acceleration may be tolerable.

The prominent dance frequencies obtained in the test results (see Table 5.3) suggest a forcing frequency ($\bar{\omega}$) of 3.5 Hz would be sufficient in calculating the frequency ratio (β) for use in Eqn. 5.12.

5.6.2.4 Summary of Recommended Design Procedures

- 1) Calculate the uniform mass (\bar{m}) and natural frequency (f_j) of the assumed T-beam. If the joists are supported on flexible beams use the system frequency of the floor (refer to Eqns. 2.1 and 2.2).
- 2) With the natural frequency determined in (1), calculate a frequency ratio from the expression

$$\beta = 3.5/f_j \quad (5.13)$$

The dynamic magnification factor (D) can then be obtained from the expression

$$D = [(1 - \beta^2)^2 + (2\xi\beta)^2]^{-1/2} \quad (5.14)$$

The critical damping ratio for use with Eqn. 5.15 can be estimated from the values suggested in Appendix G of the CSA 16.1-M78 standard, with due consideration of the floor finish.

- 3) Evaluate the peak acceleration of the dance floor according to the expression

$$A_o(\%g) = \frac{1376\beta^2 D}{\bar{m}} \sin \frac{\pi x}{L} \left(\cos \frac{\pi c}{L} - \cos \frac{\pi d}{L} \right) \quad (5.15)$$

in which \bar{m} = mass per unit length of the

assumed T-beam (kg/m)

L = length of the T-beam

c & d = position of the dance floor on the
T-beam (see Fig. 5.8)

x = position where peak acceleration
is to be determined

The peak acceleration should be determined at the position (x) where the seating area is closest to the dance floor. The calculated value is then compared with the recommended acceleration limits in Table 5.4. If the calculated value exceeds the vibration level considered acceptable, the floor system should be redesigned. In the majority of cases, the new floor design should include an increase in the floor stiffness or a reduction in the span of the joists.

5.6.2.5 Design Example

Consider the dance floor studied in this chapter. The dynamic parameters for the floor were as follows:

floor frequency.....5.0 Hz

frequency ratio.....0.7

dynamic magnification factor.....1.94

mass.....238.0 kg/m

Since the seating area of the floor in question begins at approximately $5/6 L$ (refer to Fig. 5.1), the peak acceleration will be evaluated at that location. The dance floor will be assumed to be fully loaded (ie: up to $2/3 L$). By substituting the above values into Eqn. 5.15, a peak acceleration of 4.1 %g is obtained. Since 4.1 %g exceeds the maximum allowable level of 1.75 %g (see Table 5.4), the floor design is unsatisfactory as was concluded experimentally.

Assuming the floor is redesigned to have a frequency of 8.0 Hz by increasing the stiffness, the parameters become

floor frequency.....8.0 Hz

frequency ratio.....0.4375

dynamic magnification factor.....1.24

A peak acceleration of 1.03 %g results when these values are substituted in Eqn. 5.15. Since a peak acceleration of 1.03 %g is less than the allowable 1.25 %g, the dynamic response of the floor would be acceptable.

Table 5.1: Natural Frequencies of the OWSJ Floor System

Mode	Frequency (Hz)
1	5.0
2	6.8
3	7.3
4	9.4
5	9.8

Table 5.2: Modal Damping Ratios of the OWSJ Dance Floor

Test Positions and Impact Location	Modal Damping Ratio (% critical)* Determined by the One-half Power Bandwidth Method† Mode					By Decay Method• Mode 1
	1	2	3	4	5	
Joist Midspans (E5 - E13) Impact - E6	5.9	2.3	---	2.5	2.9	5.0
Beam Support (C6, C7, C9, C11) Impact - B6	5.4	3.0	3.4	---	2.7	4.9

* Tabulated values represent the average from all accelerometers on the individual lines

† Calculated on the basis of $\xi_n = \Delta f_p / 2f_n$

• Calculated on the basis of $\xi = \frac{1}{2\pi m} \ln \frac{A_o}{A_m}$

Table 5.3: Summary of Dance Test Results

Type of Dance	Prominent Dance Freq.	Relative Dance Component	Spectral Magnitudes*		Average Continuous Components Below 25 Hz		Accel. (%g) Components Below 6.5Hz
			Floor Freq. (5Hz)	Fundamental			
Fast Rock & Roll	3.3	1.00	0.34	0.15	2.0	1.6	1.6
	6.6	0.22					
Fast Rock & Roll	2.9	0.80	0.15	0.14	1.8	1.6	1.6
	5.8	0.45					
Moderate Rock&Roll	2.8	0.57	0.14	0.04	1.5	1.3	1.3
	5.6	0.21					
Polka	2.2	0.36	0.04	0.07	0.9	0.7	0.7
	4.4	0.22					
Modern	3.1	0.29	0.11	0.01	1.0	0.7	0.7
	4.7	0.18					
Modern	2.6	0.26	0.11	0.01	0.6	0.5	0.5
	5.2	0.18					
Waltz	1.9	0.02	0.04	0.01	0.2	0.1	0.1
	3.8	0.03					
	5.4	0.03					
Waltz	none	----	0.04	0.01	0.3	0.2	0.2

* Provides an indication of the the relative floor response associated with the dominant components of the individual dances. The spectral magnitude of each component was normalized to the overall maximum spectral magnitude of the components (ie: one rock and roll component has a value of 1.0).

Table 5.3: Continued

Type of Dance Activity	Maximum Peak Acceleration Components Below 25 Hz	Acceleration (%g) Components Below 6.5 Hz	Approx. Number of Couples Dancing	Remarks
Fast Rock & Roll	4.4	3.0	30 - 35	vb
Fast Rock & Roll	3.4	2.7	25 - 30	vb
Moderate Rock & Roll	2.3	2.1	25	vb
Polka	1.6	1.3	20 - 25	b
Modern	1.8	1.4	25 - 30	b
Modern	1.0	0.8	30 - 35	a
Waltz	0.3	0.2	20	a
Waltz	0.4	0.3	25	a

vb - very bothersome, b - bothersome to some, a - acceptable

Table 5.4: Proposed Dance Floor Acceleration Level Evaluations

Peak Acceleration (%g)	Evaluation
0.00 -- 1.25	acceptable
1.25 -- 1.75	marginal
over 1.75	unacceptable

Table 5.5: Theoretical Peak Accelerations of the OWSJ Dance Floor

Approx. to the Effective Floor Width	Effective Width (m)	Peak Acceleration (%g)
60 X effective slab depth	5.16	2.5
Sokolowski Method	8.73	1.5
Experimental Results	13.00	1.2

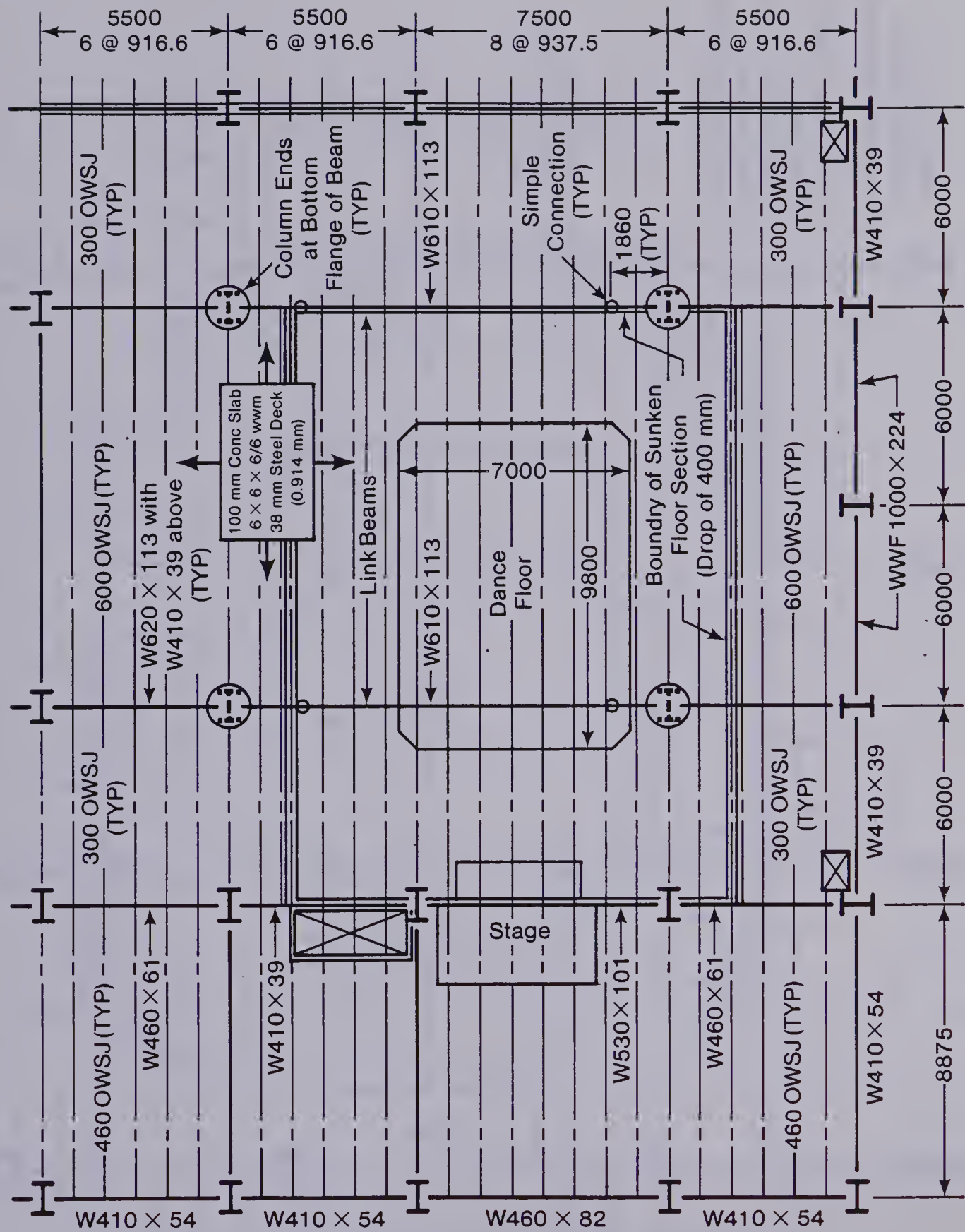


Figure 5.1 Structural Layout of Dance Floor and Surrounding Area

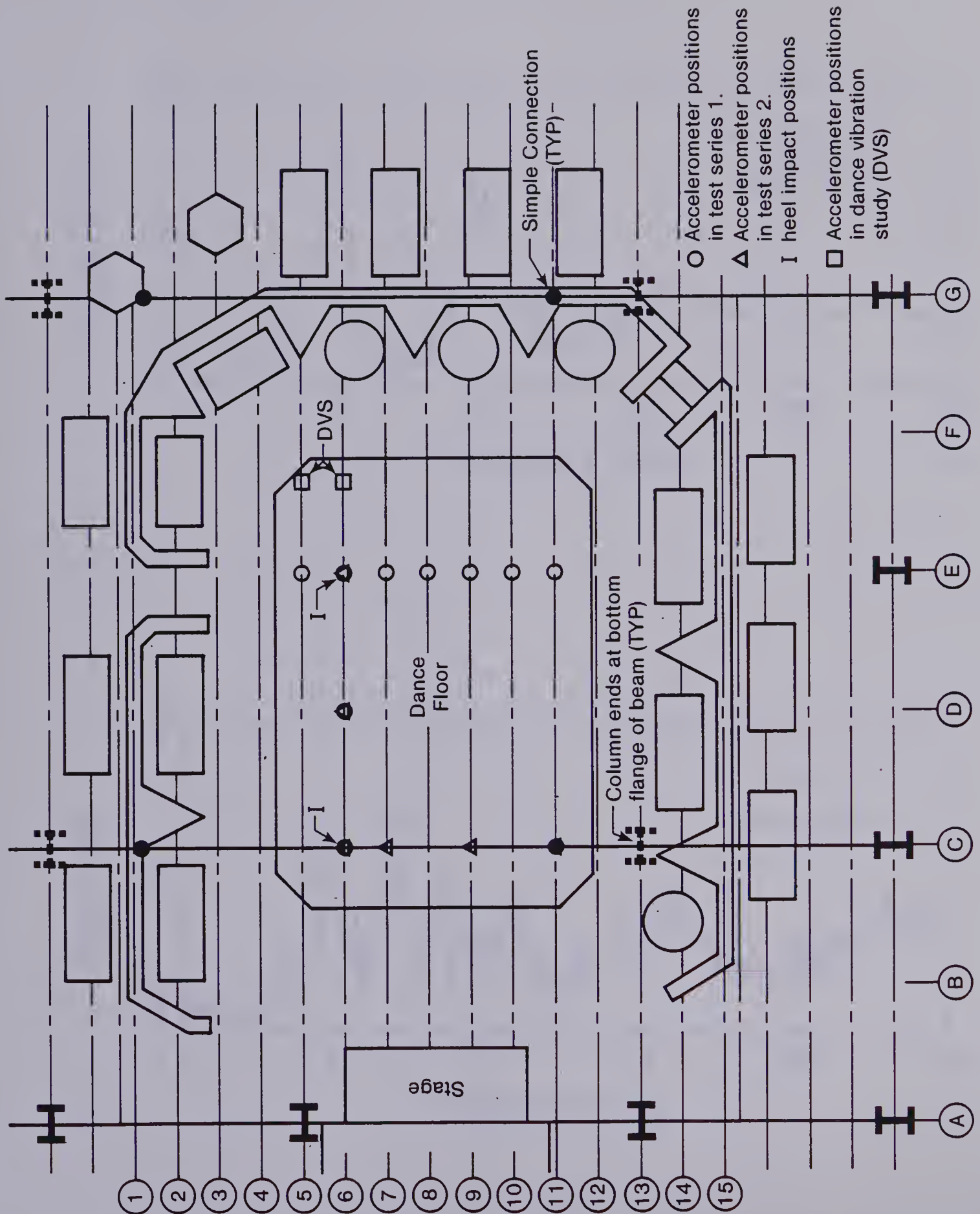


Figure 5.2 Detail Planview of Sunken Dance Floor Area

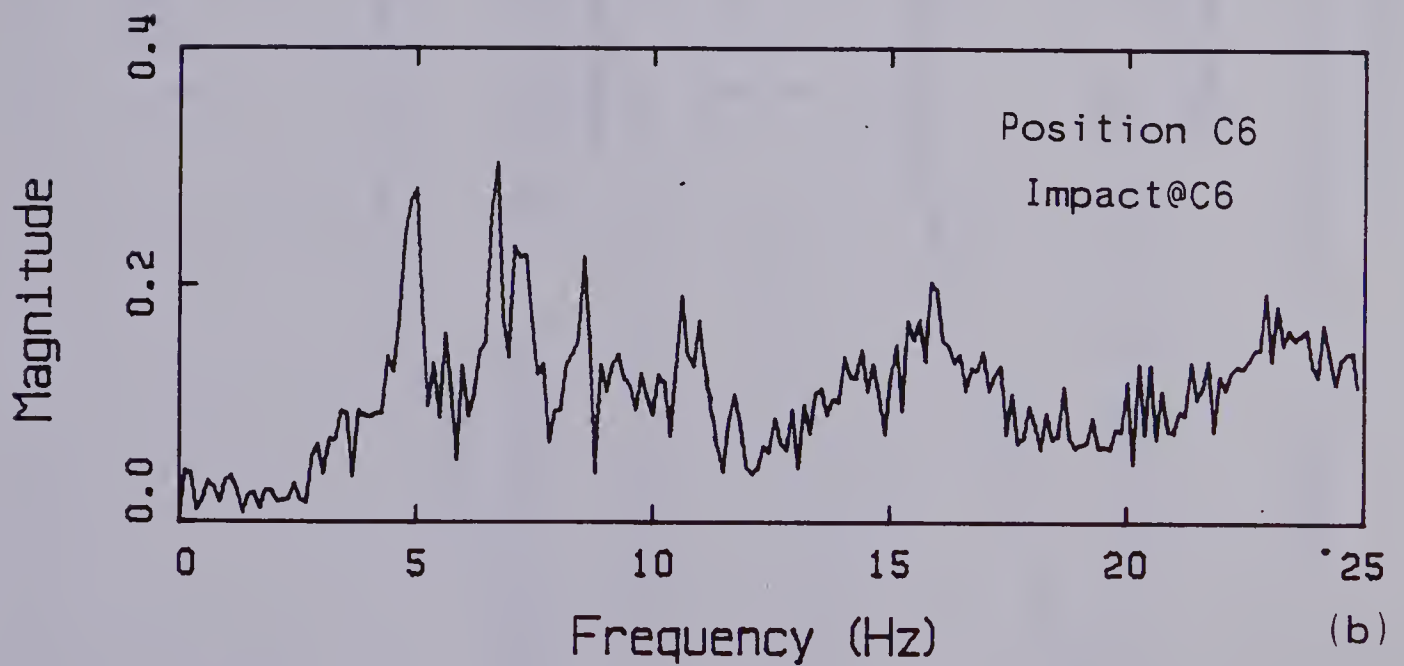
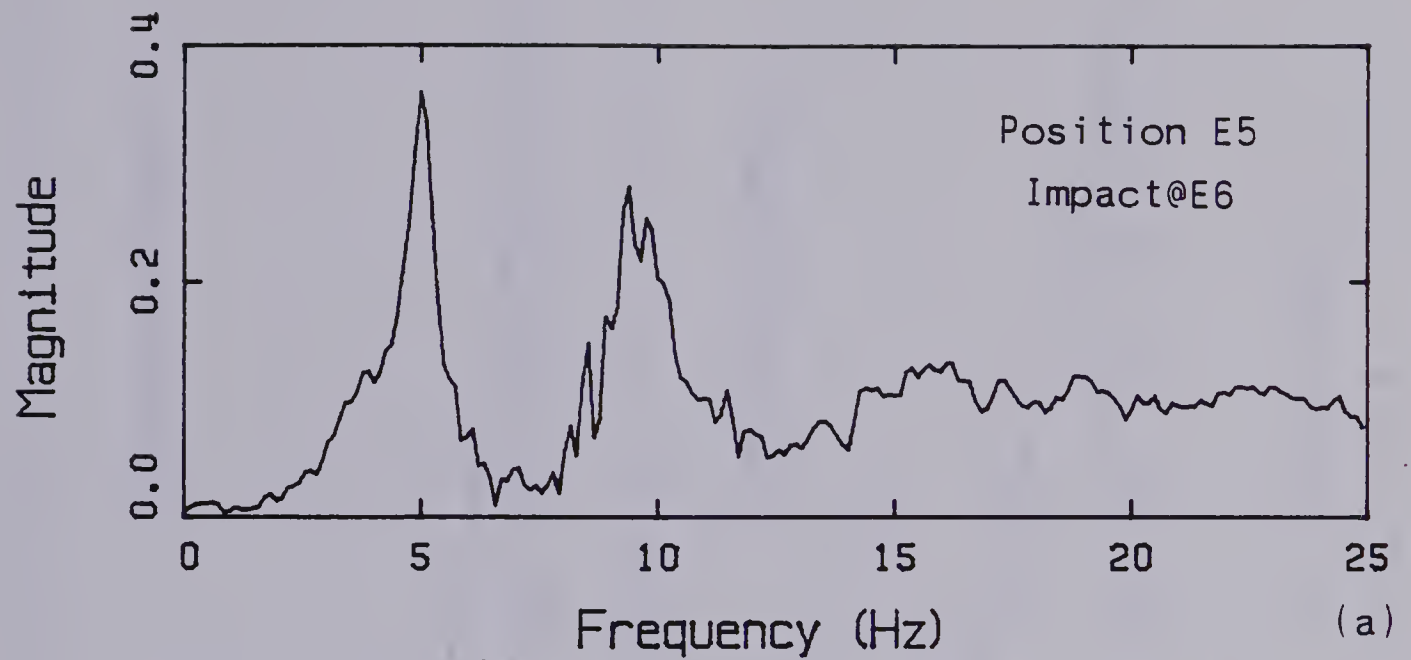


Figure 5.3 Typical Magnitude Spectra (a) Response at Midspan of Joists, (b) Response Over Supporting Beam

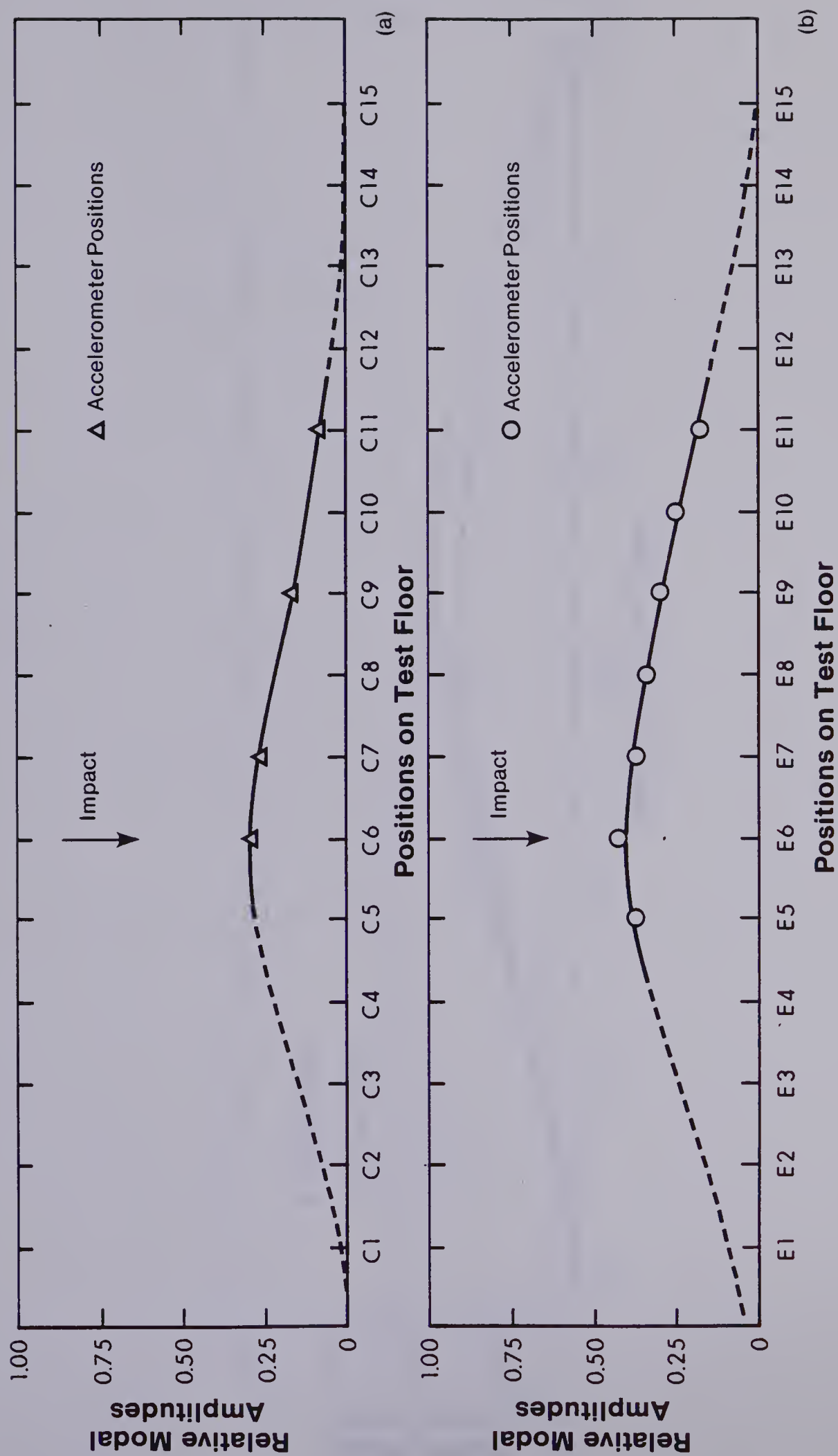


Figure 5.4 Vibration Patterns of Mode 1 (a) Along Line C,

(b) Along Line E, (c) Along Line 6

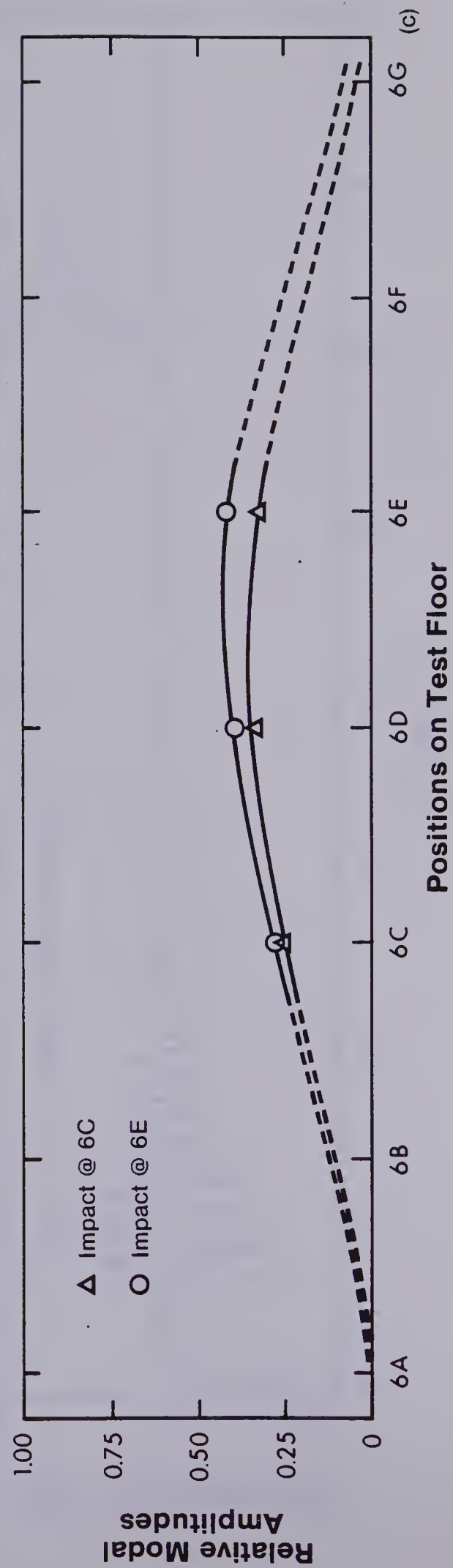


Figure 5.4 Continued

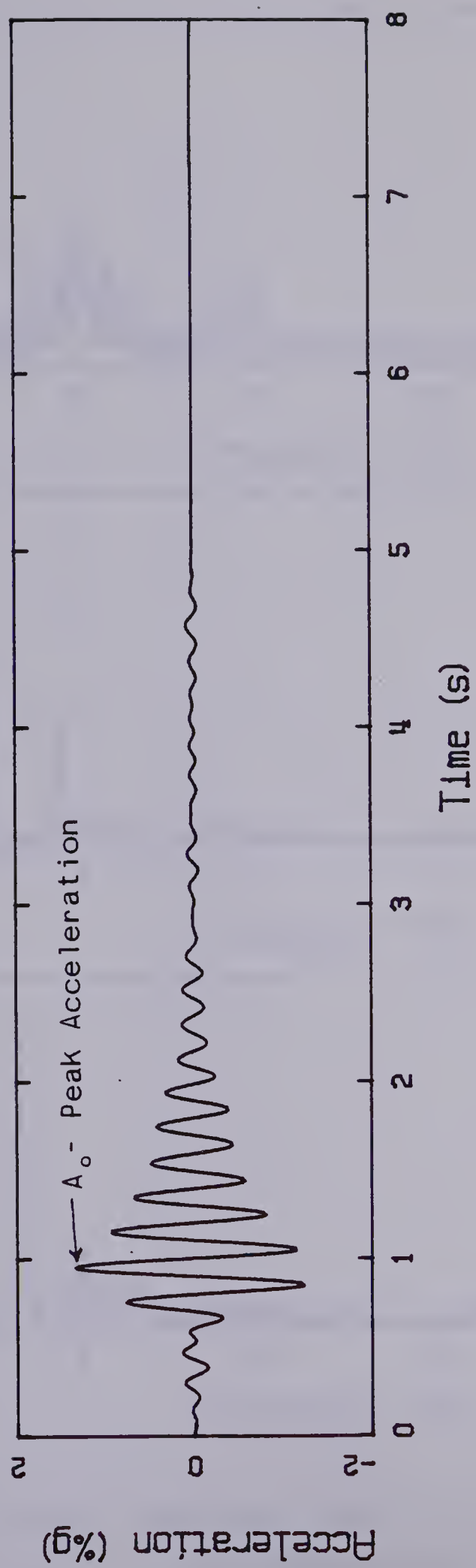


Figure 5.5 Peak Acceleration at Position E6

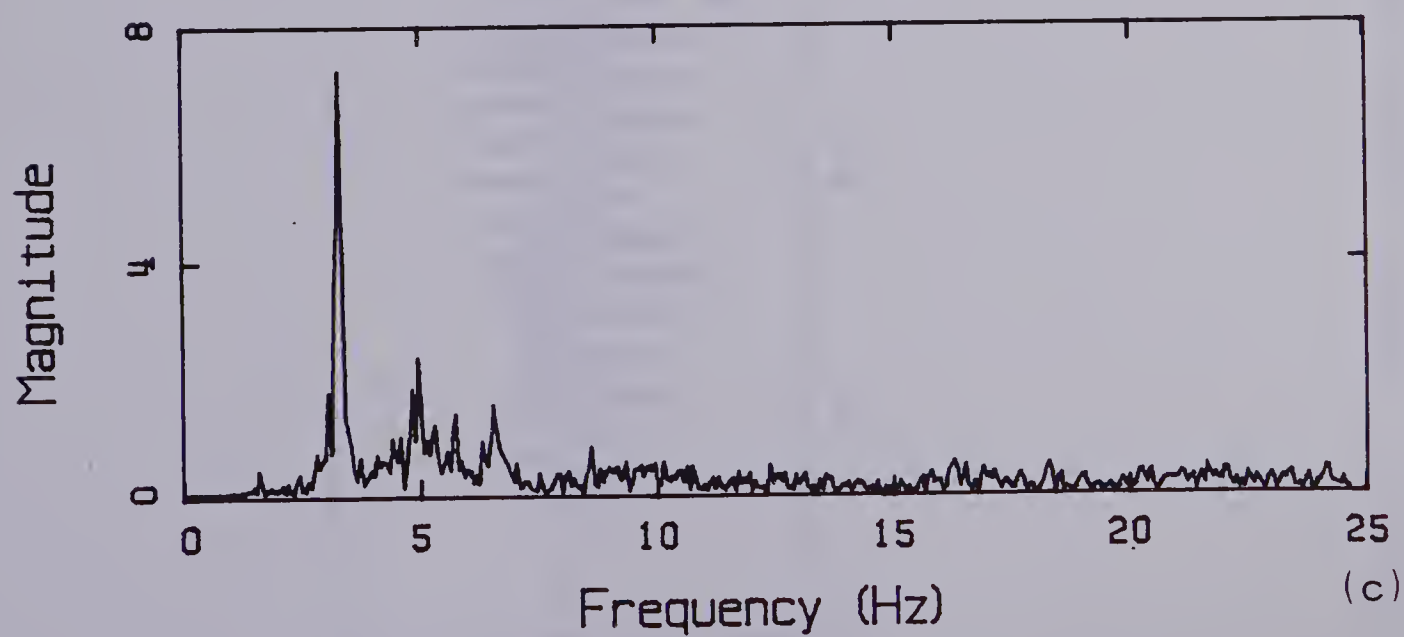
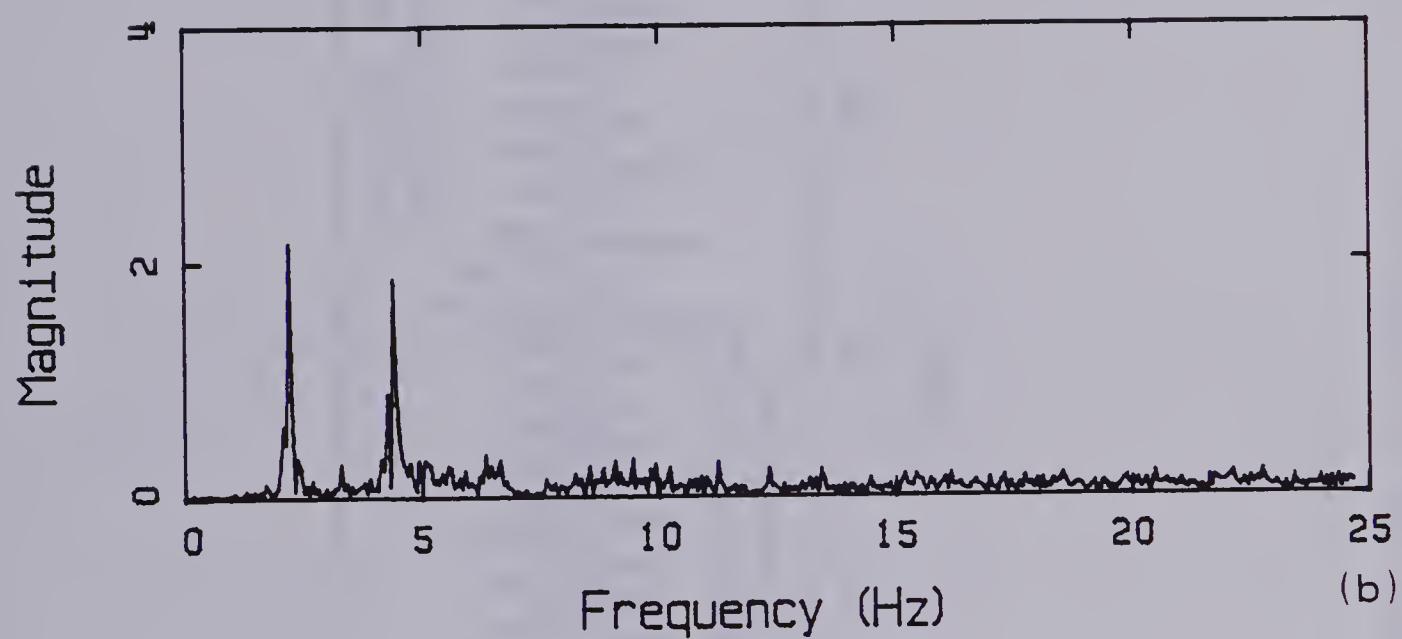
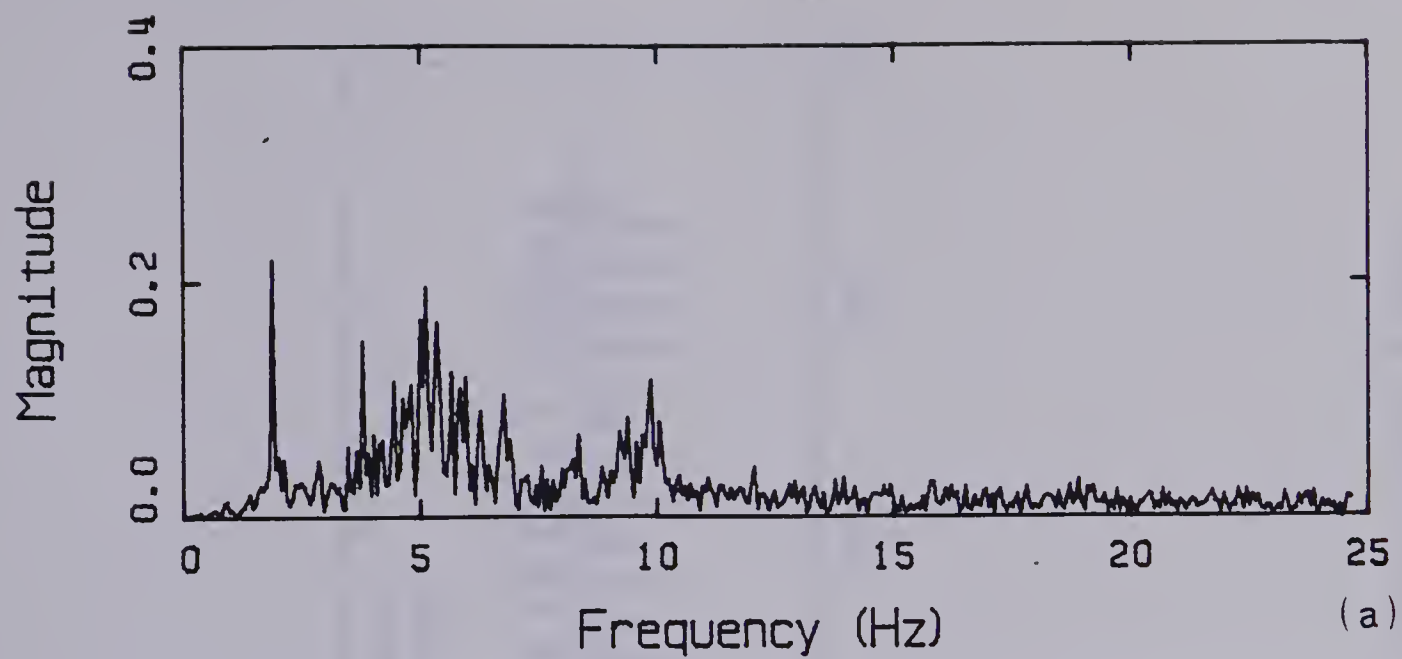


Figure 5.6 Typical Magnitude Spectra (a) Waltz, (b) Polka, (c) Rock and Roll

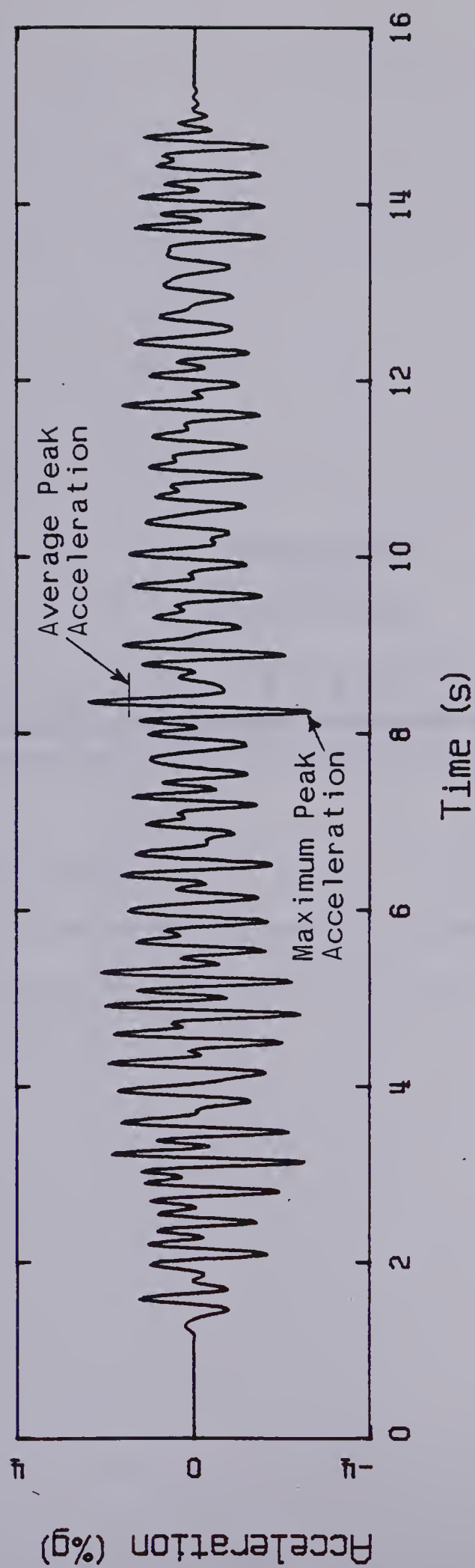


Figure 5.7 Average and Maximum Peak Acceleration of a Typical Dance Record

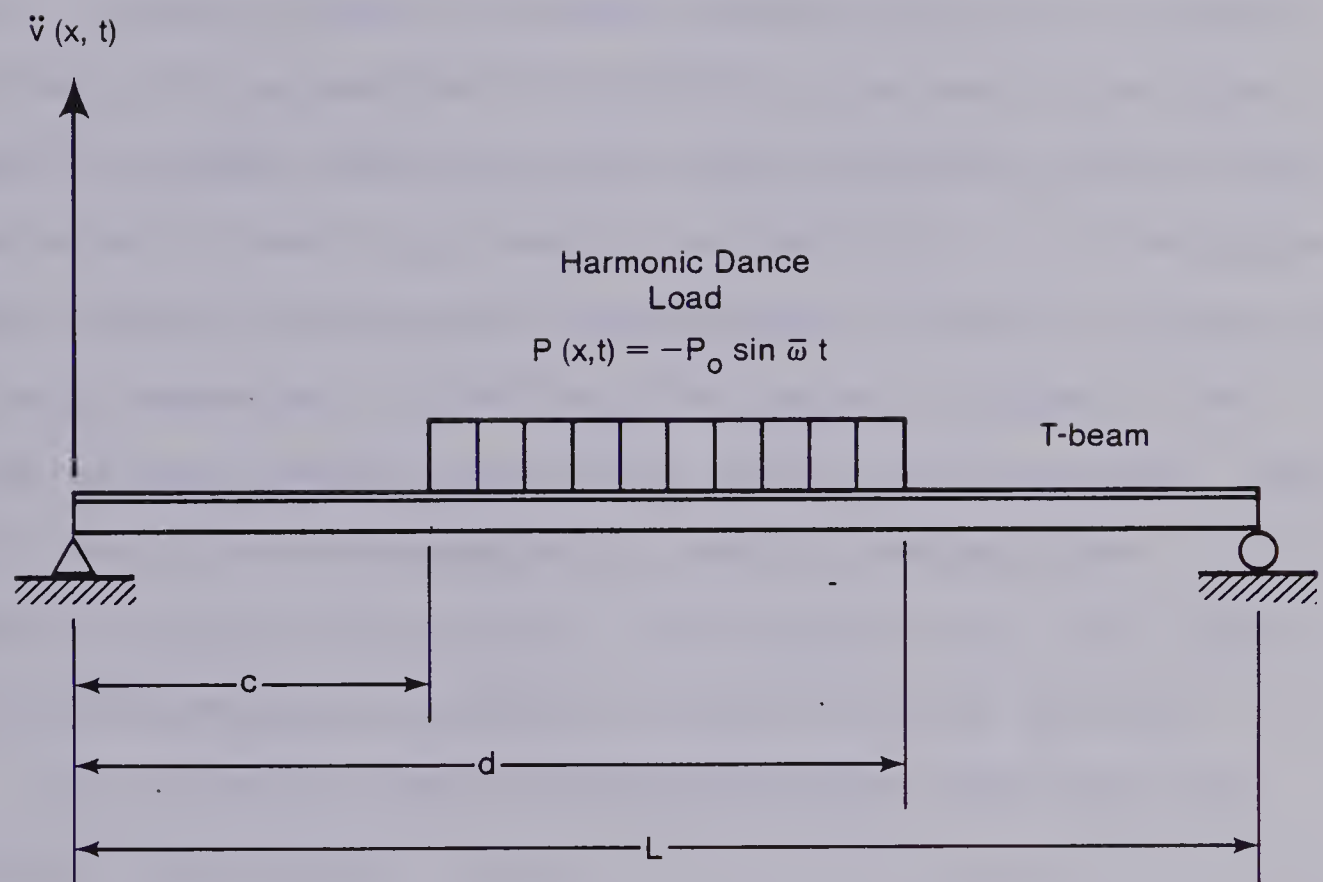


Figure 5.8 Model of Dance Floor for Design Proposal

6. Summary and Conclusions

The dynamic characteristics of a stub girder floor system and a steel joist-concrete slab dance floor were determined through comprehensive experimental investigations. The dynamic parameters derived for each floor system through a frequency domain analysis included the natural frequencies of vibration, the associated mode shapes and modal damping ratios, and the peak accelerations generated by heel drop impacts on the floors. In the dance floor study, the prominent frequencies of several dances and various parameters reflecting the forced response of the floor system during those dances were also determined. The test results were subsequently used to evaluate the applicability of the current CSA Standard S16.1-M78 floor vibration annoyance criteria to the two floor systems.

The following conclusions were drawn from the stub girder floor study:

- 1) The stub girder floor system had a very complex dynamic response which was characterized by several natural frequencies of vibration. Although some frequency components were evident above 15 Hz, the floor response was dominated by prominent frequency components at 5.4, 6.2, 6.6, 7.2, 11.3, 11.6, and 12.2 Hz.
- 2) The mode shapes associated with the seven prominent natural frequencies of vibration fell into two distinct categories. The modes for the first

category were characterized by a one-half sine wave shape parallel to the stub girder in both floor bays of the test area and along the stub girder.

Modes 1, 2, 3 and 4 were in this category.

Modes 5, 6, and 7, on the otherhand, fell into the second category since they had full sine wave shapes parallel to the stub girder in both floor bays while retaining the one-half sine wave shape along the stub girder. Differences in the modal patterns perpendicular to the stub girder appear to be responsible for the variation in modal frequencies within the two individual groups.

- 3) Of the structural members, the stub girder was the most influential on the dynamic characteristics of the floor system. However, the cantilever construction in the transverse direction had a considerable effect on the mode shapes which formed in that direction.
- 4) Since the dynamic tests were conducted when the floor was bare, the low vibration levels which were observed suggest that the floor system is more than satisfactory for quiet occupancy usage and could be considered as an alternative for floors where dynamic considerations are very important.
- 5) The theoretical calculations show that the standard T-beam analogy can be used to reasonably predict the prominent lower frequency of a stub girder

floor. However, neither the $60t_e$ approximation or the Sokolowski method should be employed to estimate the effective vibrating panel width when deriving a peak acceleration for the floor. The test results indicate the overall length of the stub girder is a good approximation to the effective panel width of a stub girder floor.

By using the calculated natural frequency and peak acceleration values in conjunction with the common annoyance threshold chart (see Fig. 2.1), a realistic design stage evaluation can be made of the serviceability of the stub girder floor system under the dynamic loads generated by human occupancy.

The following conclusions were drawn from the open web steel joist dance floor study:

- 1) The open web steel joist dance floor has five prominent natural frequencies of vibration, namely, 5.0, 6.8, 7.2, 9.4, and 9.8 Hz. The fundamental floor frequency of 5.0 Hz was the most pronounced at all test positions on the dance floor.
- 2) The test results indicate that the entire sunken floor area participates as the vibrating panel in the fundamental mode of vibration (ie: 5.0 Hz). The architectural and structural layouts of the floor system caused the floor to respond in this manner.

- 3) An evaluation of the floor response to heel drop impacts indicated that the floor system would be satisfactory for use as quiet occupancy (ie: dining). However, the vibrations which occurred during dancing were bothersome to patrons seated in the dining areas adjacent to the dance floor. Therefore, the floor system was inadequate for the combined dining-dancing occupancy.
- 4) The annoying vibrations which occurred during dances were not the result of a resonant response but rather the result of a forced response at well below the fundamental frequency of the floor. An inadequate floor stiffness appears to be responsible for the annoying vibrations of the combined dining-dancing occupancy.
- 5) With the exception of the $60t_e$ approximation to the effective vibrating panel width, the current CSA floor vibration criteria gave a reasonable appraisal of the dance floor's performance for quiet occupancy usage. The Sokolowski method provided a much better estimate of the effective floor width and is recommended for all simple beam and joist floors.
- 6) Although specified for quiet occupancies, the annoyance threshold chart in the above criteria appears to be indirectly applicable to a combined dining-dancing occupancy if the threshold of

definite perception is considered as an acceptable acceleration limit (0.5 %g curve in Fig. 2.1). The experimental results indicate that the vibration levels during each of the dances which created average peak accelerations (filtered signals) greater than the prescribed limit were annoying to patrons seated around the dance floor.

- 7) A proposal for the dynamic design of dance floors is contained herein. The procedure provides a realistic design stage appraisal of the dynamic response of steel beam or joist floors to people dancing. Additional studies on other dance floors are recommended to verify the approach.

REFERENCES

1. Lenzen, K.H. and Keller, J.E., *Vibrations of Steel Joist-Concrete Slab Floor Systems -- Part I*, The University of Kansas Centre for Research in Engineering Science, Lawrence, Kansas, Sept. 1960.
2. Rieher, H. and Meister, F.J., *The Effect of Vibration on People*, (in German), *Forschung auf dem Gebiete des Ingenieurwesens*, Vol. 2, No. 11, 1931.
(Translation: Report No. F-TS-616-RE, H.Q. Air Material Command, Wright Field, Ohio, 1946)
3. Lenzen, K.H. and Keller, J.E., *Vibrations of Steel Joist-Concrete Slab Floor Systems -- Part II*, The University of Kansas Centre for Research in Engineering Science, Lawrence, Kansas, May 1960.
4. Keller, J.E., *Damping Considerations in Vibration Response of Humans*, The University of Kansas Centre for Research in Engineering Science, Lawrence, Kansas, May 1960.
5. Wiley, J.A. and Lenzen, K.H., *A Study of Rectangular Anisotropic Plates by the Ritz Method*, The University of Kansas Centre for Research in Engineering Science, Lawrence, Kansas, 1960.
6. Barr, G.W., *Vibration Damping of Anisotropic Plates*, M.Sc. Thesis, University of Kansas, May 1961.
7. Lyons, W.C., *A Study of Various Devices for Controlling Vibrating Floor Systems*, M.Sc. Thesis, University of Kansas, May 1962.
8. Lenzen, K.H., *Vibrations of Steel Joist-Concrete Slab Floor Systems -- Final Report*, The University of Kansas Centre for Research in Engineering Science, Lawrence, Kansas, Aug. 1962.
9. Meyer, L.D. and Lenzen, K.H., *Vibrations in Floor Systems of Steel Framed Buildings*, The University of Kansas Centre for Research in Engineering Science, Lawrence, Kansas, 1976.

10. Ohmart, R.D., *An Approximate Method for the Response of Stiffened Plates to Aperiodic Excitation*, The University of Kansas Centre for Research in Engineering Science, Lawrence, Kansas, April 1968.
11. Lenzen, K.H. and Murray, T.M., *Vibrations of Steel Beam-Concrete Slab Floor Systems*, The University of Kansas Centre for Research in Engineering Science, Lawrence, Kansas, Feb. 1969.
12. Lenzen, K.H. and Dorsett, L.P., *Effect of the Variation of Structural Parameters on the Vibrational Characteristics of Steel Joist-Concrete Slab Floor Systems and Suggested Designs*, The University of Kansas Centre for Research in Engineering Science, Lawrence, Kansas, April 1969.
13. Sokolowski, M., Lenzen, K.H., and Dorsett, L.P., *The Variation of the Vibrational Characteristics of Steel Joist-Concrete Slab Floor Systems with Changes in the Structural Parameters*, Engineering Archives of the Polish Academy of Sciences, Vol. XVIIIA, March 1971.
14. Moderow, R.R., *Vibration Characteristics of Steel Joist-Concrete Slab Floor Systems*, M.Sc. Thesis, University of Kansas, May 1971.
15. Galambos, T.V., *Vibration of Steel Joist-Concrete Slab Floors*, Steel Joist Institute, Arlington, VA, Technical Digest #5, 1973.
16. Allen, D.E. and Rainer, J.H., *Vibration Criteria for Longspan Floors*, Division of Building Research, National Research Council of Canada, Vol. 3, No. 2, CJCCE, June 1976.
17. *Steel Structures for Buildings - Limit States Design*, CSA Standard S16.1-M78, Canadian Standards Association, Dec. 1978.
18. Wilson, J. and Heidebrecht, A., *Vibration Characteristics of Long Span Floors Systems*, Report for the Canadian Steel Industries Council, McMaster University, Hamilton, Ontario, 1976.

19. Rainer, J.H., *Dynamic Tests on a Steel Joist-Concrete Slab Floor*, Noise and Vibration Division of Building Research, National Research Council of Canada, Vol. 7, No. 2, CJCE, June 1980.
20. Heins, C.P., Jr. and Yoo, C.H., *Dynamic Response of a Building Floor System*, Building Science, Vol. 10, Pergamon Press, Great Britain, 1975.
21. Fahy, F.J. and Wescott, M.E., *Measurement of Floor Mobility at Low Frequencies in some Buildings with Long Floor Spans*, Journal of Sound and Vibration, Vol. 57, 1978.
22. Allen, D.L., *Vibrational Behavior of Longspan Floor Slabs*, Canadian Structural Engineering Conference, 1974.
23. Chadha, J. and Allen, D.L., *Natural Frequency Determination of Long Span Floor Slabs*, Transactions of the ASME Journal of Eng., Vol. 94, Series B, No. 2, May 1972.
24. Goldman, D.E., *A Review of Subjective Responses to Vibratory Motion of the Human Body in the Frequency Range 1 to 70 cps*, Naval Medical Research Institute, Report NM-004-001, Washington, 1948.
25. Wright, D.T. and Green, R., *Human Sensitivity to Vibrations*, Report No. 7, Ontario Joint Highway Research Programme, Feb. 1969.
26. Wiss, J.F. and Parmalee, R.A., *Human Perception of Transient Vibrations*, Journal of the Structural Division, ASCE, April 1974.
27. Timoshenko, S., Young, D.H., and Weaver, W., Jr., Vibration Problems in Engineering - Fourth Edition, John Wiley and Sons Inc., New York, N.Y., 1974.
28. Collacott, R.A., Vibration Monitoring and Diagnosis, John Wiley and Sons Inc., New York, N.Y., 1979.

29. Clough, R.W. and Penzien, J., Dynamics of Structures, McGraw-Hill Inc., New York, N.Y., 1975.
30. *The Evaluation of Damping Characteristics of Floor Systems of Steel-Framed Buildings*, Unpublished Report by the American Iron and Steel Institute, Oct. 1975.
31. *Piezoelectric Accelerometers and Vibration Preamplifiers*, Theory and Application Handbook, Bruel and Kjaer Publication, Naerum, Denmark, 1976.
32. *Making Sense of Vibration Measurements*, Application Note 17, Nicolet Scientific Corporation, July 1981.
33. Randall, R.B., Frequency Analysis, Bruel and Kjaer Publication, Naerum, Denmark, Sept. 1977.
34. Nelson, H.D. and Walter, P.L., *Limitations and Corrections in Measuring Structural Dynamics*, Experimental Mechanics, Vol. 19, No. 9, Sept. 1979.
35. Schwartz, M. and Shaw, L., Signal Processing: Discrete Spectral Analysis, Detection, and Estimation, McGraw-Hill Company Inc., New York, N.Y., 1975.
36. Benjamin, R.R. and Cornell, C.A., Probability, Statistics, and Decision for Civil Engineers, McGraw-Hill Inc., New York, N.Y., 1970.
37. Maurice, R.D., Convolution and Fourier Transforms for Communication Engineers, John Wiley and Sons Inc., New York, N.Y., 1976.
38. Churchill, R.V. and Brown, J.W., Fourier Series and Boundary Value Problems - Third Edition, McGraw-Hill Inc., New York, N.Y., 1978.
39. Harris, F.J., *Trigonometric Transforms - A Unique Introduction to the FFT*, Spectral Dynamics Corporation, Technical Publication DSP-005, Oct. 1977.

40. Stanley, W.D., Digital Signal Processing, Reston Publishing Company Inc., Reston, Virginia, 1975.
41. Stearns, S.D., Digital Signal Analysis, Hayden Book Company Inc., Rochelle Park, New Jersey, 1975.
42. Colaco, J.P., *A Stub-Girder System for High Rise Buildings*, Engineering Journal, AISC, July 1972.
43. Murray, T.M. and Hendrick, W.E., *Floor Vibration and Cantilevered Construction*, AISC Engineering Journal, Third Quarter, 1977.

APPENDIX A

A. Some Aspects of Filtering

A.1 Introduction

The data reduction process described in Chapter 3 included the separation of the acceleration-time records into various modal contributions by filtering. This appendix is devoted to a discussion of the analog and digital filters which were employed in the filtering process. Particular attention is given to the finite impulse response (FIR) digital filter which was designed specifically for this study.

In the following sections several categories of filters are defined, the characteristics of the analog and digital filters used in this study are examined, and the mathematical formulation and implementation procedures of the FIR filter are presented. In addition, the limitations, the advantages, and the disadvantages of the two filter types are discussed in relation to the floor vibration data.

A.2 Filter Categories

A filter, defined in the context of this study, is a device or algorithm which separates the components of a signal on the basis of frequency. Complying with this definition, both analog and digital filters are commonly classified according to their frequency response

characteristics.

A lowpass filter eliminates the frequency components from a signal which are above a specified cutoff frequency, while allowing the components below the cutoff to pass. In contrast, a highpass filter eliminates the frequency components below the specified cutoff and passes those above. A bandpass filter can be thought of as a lowpass and a highpass filter operating in sequence, thus allowing only those frequencies within a specified range to pass while excluding all others. Filter bandwidth or passband are the terms normally used to describe the frequency range associated with a particular bandpass filter setting.

The idealized frequency domain amplitude functions associated with the three filter categories are shown in Fig. A.1. In each case, the shaded areas indicate the frequency components which are allowed to pass through the filter. Practical filters have response characteristics which approximate, to varying degrees, the ideal response behavior indicated in the figure.

In this study, lowpass filters were used to obtain filtered signals corresponding to the first dominant mode of vibration, while bandpass filters of various bandwidths were used to acquire the filtered signals representing the contributions of higher order modes.

A.3 Analog Filter

The analog filter used in this study was a Krohn-Hite model 3342, two channel, multi-purpose filter. The filter characteristics approximate those of a Butterworth maximum flat filter of the eighth order (35) with a nominal attenuation slope of 48 dB/octave when used in either the single channel lowpass or highpass modes. The 48 dB/octave attenuation implies that the amplitudes of frequency components at two, three, and four times the specified cutoff frequency are reduced by 48, 96, and 144 dB, respectively. The filter also functioned as a single channel bandpass filter by using the two channels in sequence, the first channel in the lowpass mode and then the second in the highpass mode.

Figure A.2 shows the frequency domain attenuation characteristics of the filter in the various operational modes. In contrast to the idealized behavior shown in Fig. A.1, the attenuation curves of the practical filter are sloped rather than vertical at the cutoff frequencies. This is typical of filters in general, although the attenuation rates may vary. When using the filter in the bandpass mode with relatively small bandwidths, the cutoff characteristics lead to an overall amplitude loss (see Fig. A.2c) which influences the results obtained. Because of this, the analog filter cannot be used to separate the frequency components of closely spaced modes.

The normalized attenuation and phase characteristics of the Krohn-Hite filter are illustrated in Fig. A.3.

Figure A.3a shows the 48 dB/octave/channel attenuation of the filter and the 3 dB amplitude loss which occurs at the cutoff frequency. Signal components with frequencies up to 90% of the cutoff frequency are passed at full amplitude. The nonlinear phase response of the filter shown in Fig. A.3b implies that the frequency components transmitted through the filter are time-shifted relative to each other, resulting in a distorted version of the true filtered signal. In the case of transients, this distortion could cause severe errors in the amplitude of the filtered record although the amount of error would depend on the magnitude of the individual frequency components.

The major advantages of using the analog filter system in the study was the ability to process large quantities of vibration data directly, quickly, and inexpensively. The major disadvantages included the non-linear phase response and the amplitude loss in the bandpass mode which were discussed previously.

A.4 Digital Filter

A.4.1 Design of Finite Impulse Response Filter

A finite impulse response (FIR) filter was designed specifically for this study to enable the filtering of the digitized accelerometer records on the digital computer. A

FIR filter is a digital filter composed of a finite number of terms which form a discrete transfer function or "impulse response" in the time domain. The actual design of the FIR filter involved the determination of an unknown impulse response $h(t)$ in the time domain which corresponded to a bandpass filter in the frequency domain. The following is a presentation of the mathematical concepts and design procedures of the FIR filter. The use of the filter is described in the following section.

The Fourier series method (40) was used to approximate the desired frequency domain amplitude response $A_d(f)$ of the FIR bandpass filter. The amplitude response corresponding to the unknown impulse response $h(t)$ was assumed to be a periodic function of frequency which could therefore be expanded in a Fourier series in the frequency domain. Figure A.4 illustrates the desired frequency domain amplitude response. Considering a cosine series and letting $A(f)$ represent the approximation to $A_d(f)$ which results from terminating the infinite series after M terms, the response is given by

$$A(f) = \frac{\alpha_0}{2} + \sum_{m=1}^M \alpha_m \cos 2\pi mf\Delta t \quad (A.1)$$

in which

$$\alpha_m = \frac{4}{f_s} \int_0^{f_s/2} A_d(f) \cos 2\pi mf\Delta t df \quad (A.2)$$

where

M = any integer including zero

f_s = period of the transfer function in the

frequency domain

$\Delta t = 1/f_s =$ is the time between discrete samples of the transfer function

In this case $A_d(f)$ is assumed to be equal to one within the bandwidth defined by the frequency limits f_1 and f_2 and equal to zero otherwise. Therefore, α_m applies only in the range f_1 to f_2 resulting in

$$\begin{aligned}\alpha_m &= \frac{4}{f_s} \int_{f_1}^{f_2} (1.0) \cos 2\pi m f \Delta t \, df \\ &= \frac{2}{\pi m} (\sin 2\pi m \Delta t f_2 - \sin 2\pi m \Delta t f_1)\end{aligned}\quad (A.3)$$

Expressing Eqn. A.1 in exponential form gives

$$A(f) = \sum_{m=-M}^M C_m e^{j2\pi m \Delta t f} \quad (A.4)$$

in which

$$C_m = C_{-m} = \frac{\alpha_m}{2} \quad (A.5)$$

Equation A.4 can be considered as the evaluation of the unknown discrete transfer function ($h(t)$) on the unit circle in the z -plane. Replacing $e^{j2\pi \Delta t f}$ by z , and denoting the initial series by $H_1(z)$, leads to the expression (40)

$$H_1(z) = \sum_{m=-M}^M C_m z^m \quad (A.6)$$

which represents a FIR transfer function. However, in this form with positive powers of z , the filter would produce an output advanced in time with respect to the input, which is impossible. Therefore, the final transfer function $H(z)$

must be delayed for an appropriate length of time. The final amplitude response or transfer function, including the delay, is defined by

$$H(z) = z^{-m} H_1(z) = z^{-m} \sum_{m=-M}^{-M} C_m z^m \quad (A.7)$$

which can be expressed in the form

$$H(z) = \sum_{n=0}^{2M} h_n z^{-n} \quad (A.8)$$

in which

$$h_n = C_{m-n} \quad (A.9)$$

One final problem remains because the coefficients of the impulse response $h(t)$ were derived by terminating the Fourier series expansion of the desired amplitude response $A_d(f)$ with a finite number of terms (ie: $2M$ terms). The abrupt termination may lead to poor convergence of the resulting series which implies the actual frequency domain response $H(z)$ could differ significantly from the desired frequency response $A_d(f)$. This difficulty is alleviated by smoothing the impulse response $h(t)$ with a time domain window (40). The coefficients of the Hamming window function which was employed in this study are given by

$$w(t) = 0.54 + 0.46 \cos \frac{2\pi t}{\tau} \quad (A.10)$$

for

$$|t| \leq \frac{\tau}{2}$$

and

$$w(t) = 0$$

elsewhere. Making the appropriate substitutions of Eqn. A.3 into Eqn. A.9 and applying the Hamming window function with the proper time delay results in the final expression for the time domain impulse response which is

$$h(t_n) = \frac{1}{\pi(M-n)} [\sin 2\pi(M-n)\Delta t f_2 - \sin 2\pi(M-n)\Delta t f_1] \times \left[0.54 + 0.46 \cos \frac{\pi(M-n)}{M} \right] \quad (\text{A.11})$$

in which f_1 & f_2 = limits of filter bandwidth

$2M$ = number of terms used to form the impulse response

n = any positive interger including zero.

The frequency domain amplitude functions corresponding to three impulse responses comprised of M equal to 100, 300, and 500 terms respectively, are shown in Fig. A.5. In each case, the upper and lower frequency limits (ie: f_1 and f_2) were set at 10 Hz and 20 Hz implying a 10 Hz bandwidth. A comparison of the three amplitude functions clearly shows that the frequency response characteristics of the FIR filter are controlled by the number of terms (M) used to form the impulse response in the time domain. As more terms are used, the frequency response becomes a better approximation to the ideal behavior shown previously in Fig. A.4.

A.4.2 Use of FIR filter

The FIR filter was implemented through a "convolution" of the impulse response ($h(t)$) with selected discrete acceleration signals ($g(t)$). The convolution of two discrete time functions is denoted as $g(t) * h(t)$ and is defined mathematically as (40)

$$g(t_n) * h(t_n) = \sum_{m=0}^{N-1} g(m) h(n-m) \quad (A.12)$$

in which m = any positive integer including zero

N = total number of discrete points in time domain sequences.

Because an excessive number of computations would be required to evaluate Eqn. A.12 for the relatively long acceleration-time signals of this study, the Fast Fourier Transform (FFT) algorithm was used to perform the convolution indirectly. This was possible through the Convolution Theorem (40) which states that a Fourier transform converts a convolution in the time domain into a multiplication in the frequency domain. The following steps describe the process in detail:

- 1) An impulse response, $h(t)$, with the desired frequency domain response is calculated according to Eqn. A.11.
- 2) The forward Fourier transform (Eqn. 3.1) of the impulse response is calculated using the FFT algorithm resulting in

$$h(t) \rightarrow H(f)$$

- 3) Similarly, the selected acceleration-time record, $g(t)$, undergoes a forward transform resulting in

$$g(t) \rightarrow G(f)$$

- 4) A complex multiplication of the discrete frequency components from (2) and (3) is performed with the result

$$R(f) = G(f) \times H(f)$$

- 5) The inverse Fourier transform (Eqn. 3.2) of $R(f)$ is calculated using the FFT algorithm resulting in the filtered acceleration-time signal $r(t)$ as

$$R(f) \rightarrow r(t) = g(t) * h(t)$$

Figure A.6 provides a schematic illustration of the above process. By multiplying the amplitude response of the FIR filter ($H(f)$) and the frequency domain representation of the accelerometer signals, the frequency components of the signals which are outside the filter bandwidth are eliminated. The filtered signal is obtained by returning to the time domain since only the desired frequency components remain to contribute to the response.

One of the requirements for the convolution process is that both the impulse response and the acceleration-time record contain an equivalent number of terms. Since M was normally set equal to 400 terms in the study, it was necessary to add a significant number of zeroes to the end

of the impulse response sequences. However, the large number of zeroes were necessary to obtain a "linear convolution" thus preventing the associated error, known as wrap around error (40), in the filtered signals. Other important aspects of convolving discrete time signals are discussed in related textbooks.

A.4.3 Advantages and Disadvantages of FIR Filter

The major advantage of the FIR filter is that it possesses a linear phase response regardless of the selected filter bandwidth or the number of terms used to form the impulse response. Therefore, unlike the analog filter, the frequency components of the filtered signal are not time-shifted relative to each other thus preventing the accompanying distortion. Another advantage was the desired amplitude response characteristics could be closely approximated for any filter bandwidth by using the appropriate number of terms to form the impulse response. Very steep attenuation slopes could thus be obtained and the amplitude loss associated with the bandpass mode of the Krohn-Hite filter was not a problem. The FIR filter was also very easy to use and it could be implemented to sequentially filter any number of signals.

The disadvantages of the FIR filter include a linear phase shift which increases as the number of terms in the impulse response is increased and an economical limitation imposed on the lengths of the signals which could be

filtered (ie: computer costs). Because the FIR filter inherently has a linear phase shift, filtered signals are time-shifted relative to the corresponding unfiltered signals. Since the unfiltered signals are periodic and of finite duration, the phase shift must be limited to prevent the misrepresentation of the true filtered signal. Therefore, the number of terms used to form the FIR filter must be limited appropriately.

A.5 Filter Limitations

The concept of filter "rise-time" becomes important when considering the filtering of the transient accelerometer signals. Rise-time can be thought of as the time it takes for a particular filter to pass at full amplitude, a sine wave within the filter bandwidth. The rise-time phenomenon is illustrated in Fig. A.7.

The rise time effect becomes particularly important when filtering transient signals to obtain the peak modal response since the initial peak amplitude can be severely truncated.

Rise-time is inversely proportional to the filter bandwidth and can therefore present problems when using extremely narrow passbands to separate the frequency components associated with closely spaced modes which contribute to a transient event. Therefore, because of the rise-time effect, both the analog and digital (FIR) filters were limited on the minimum bandwidth which could be used in

filtering the transient events. Tests conducted with the FIR filter indicated that a minimum bandwidth of four hertz was possible without affecting the results. Similar tests were not conducted with the analog filter, although passbands of less than five hertz were not used with that filtering system.

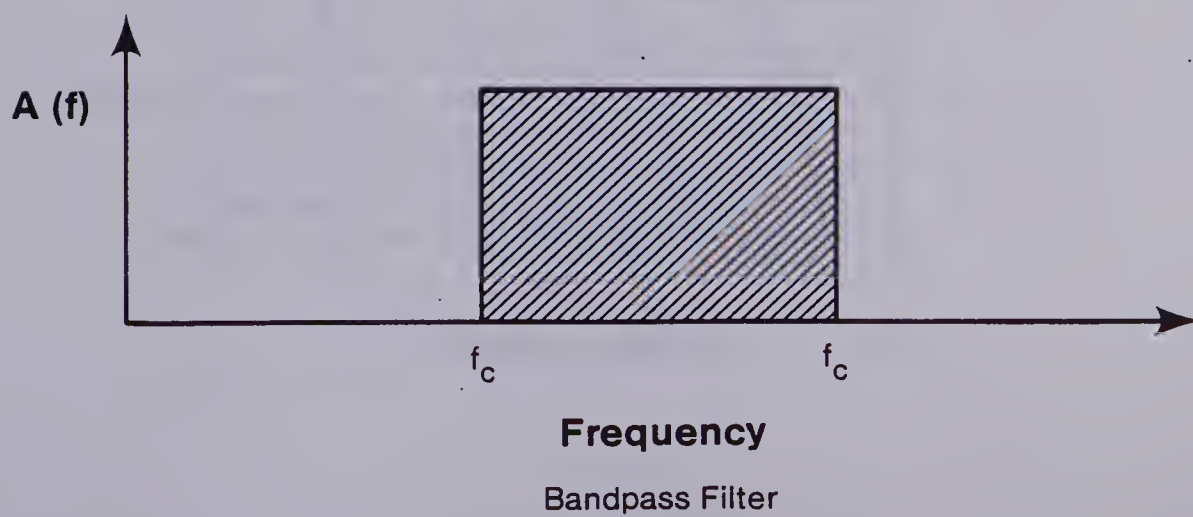
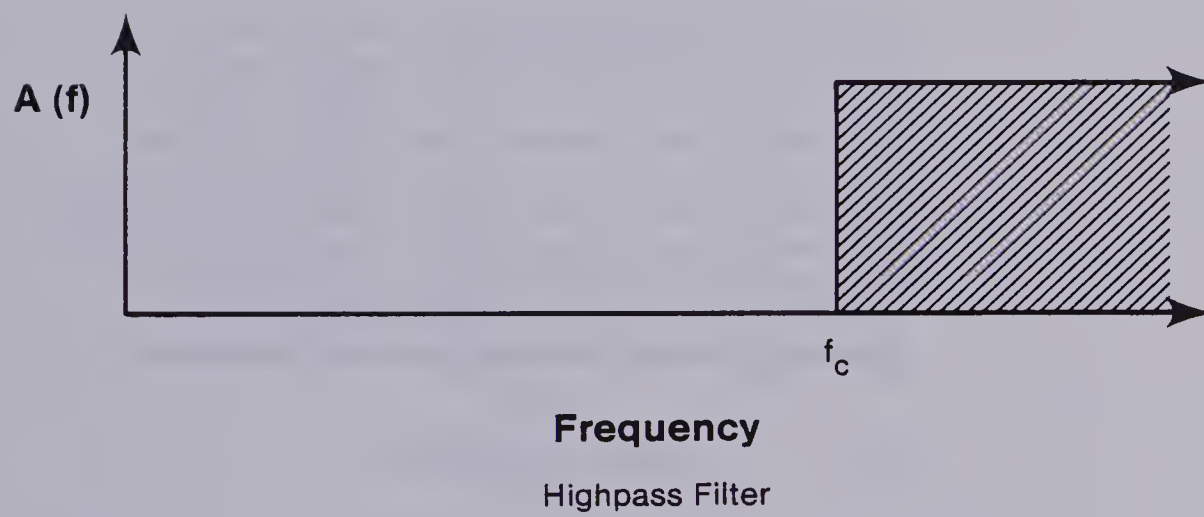
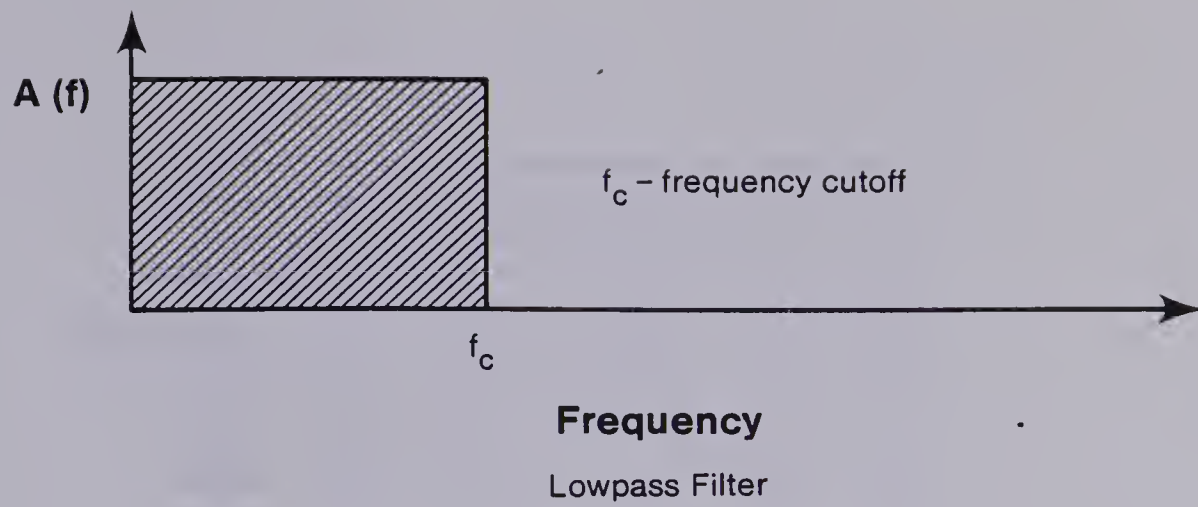
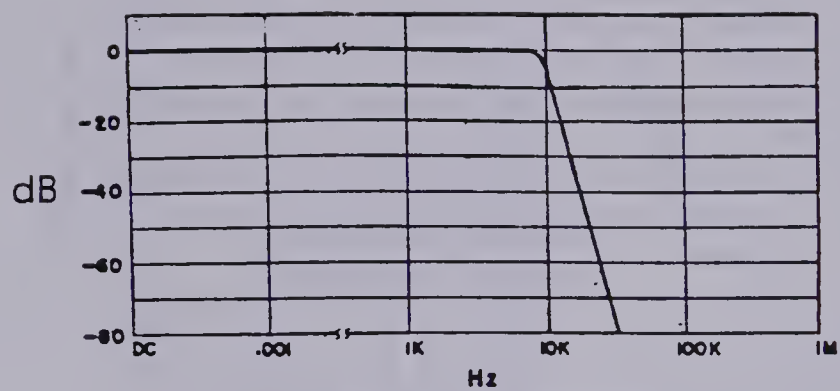
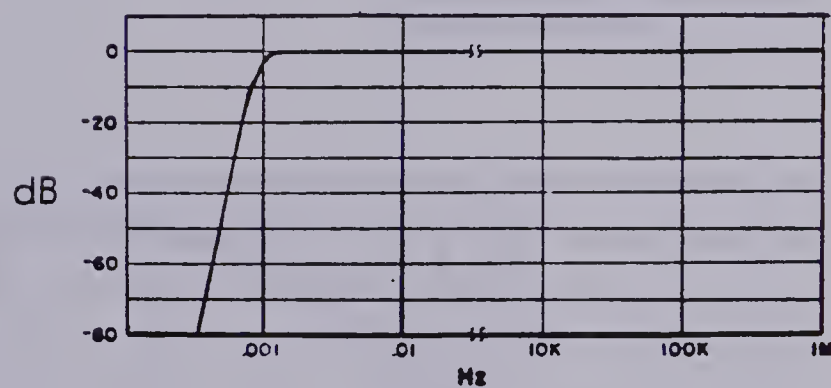


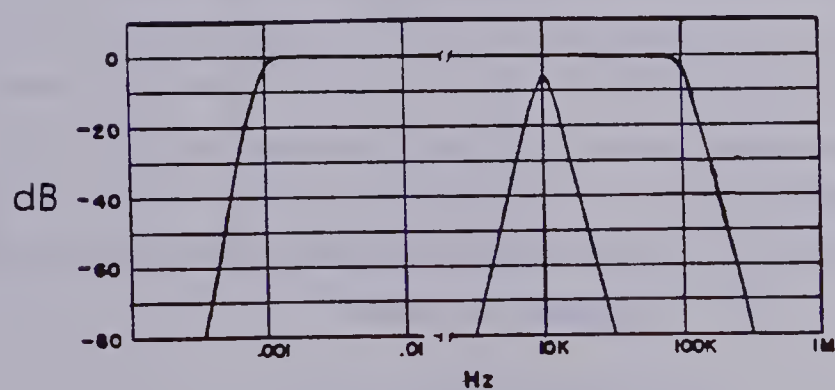
Figure A.1 Frequency Characteristics for Three Filter Categories



Lowpass Mode (a)

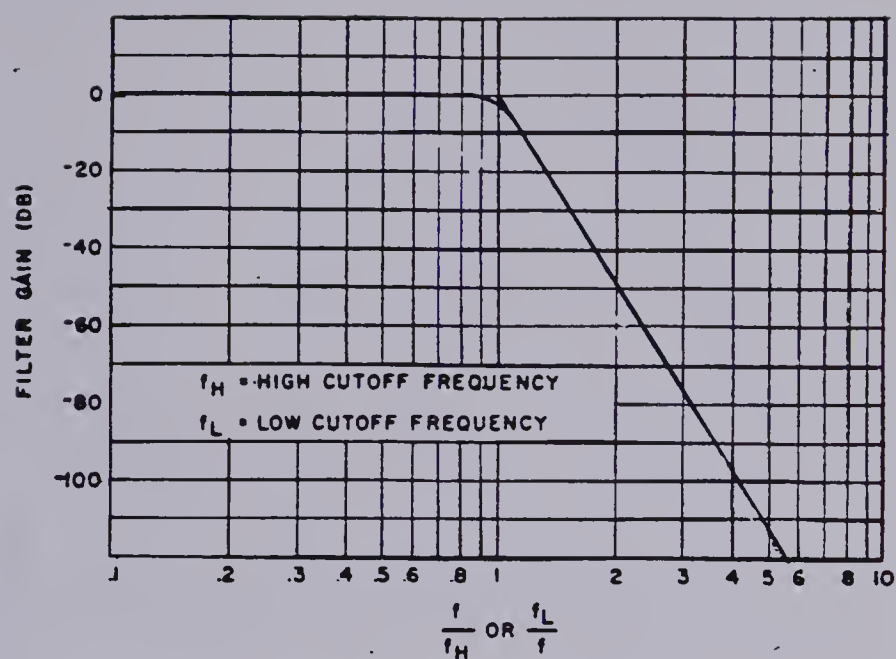


Highpass Mode (b)



Bandpass Mode (c)

Figure A.2 Attenuation Characteristics of Krohn-Hite Filter



Normalized Attenuation
Characteristics

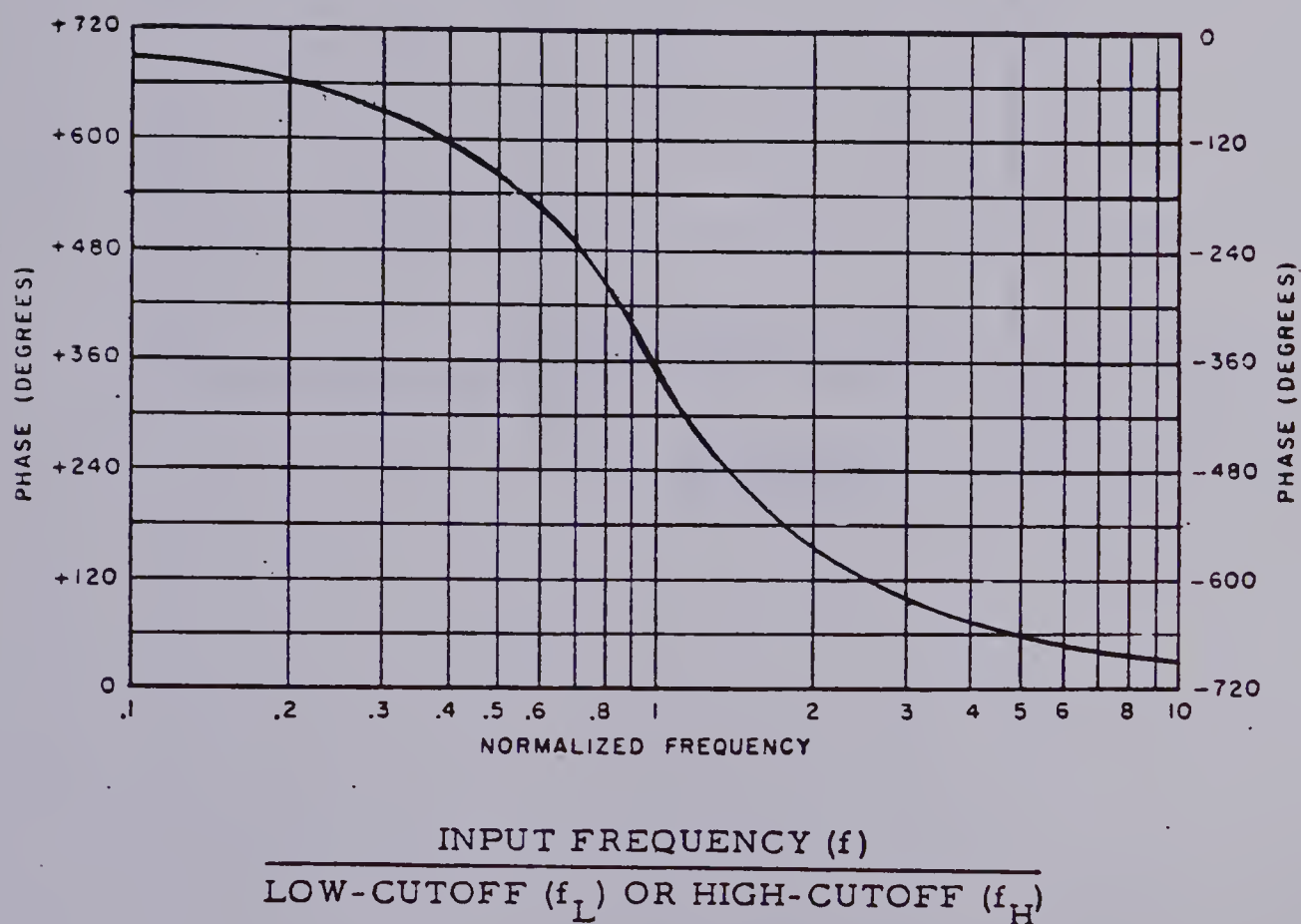


Figure A.3 Normalized Attenuation and Phase Characteristics
of Krohn-Hite Filter

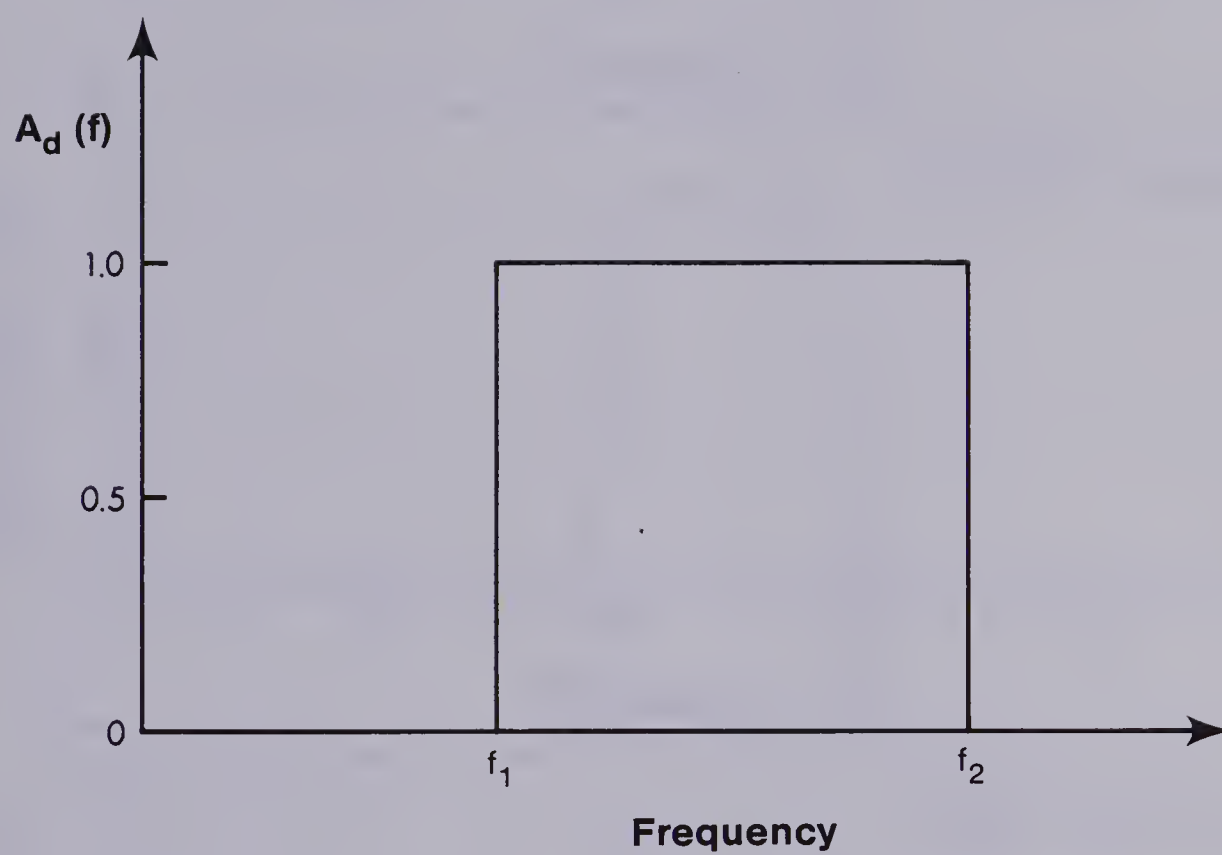


Figure A.4 Desired Frequency Domain Characteristics of FIR Filter

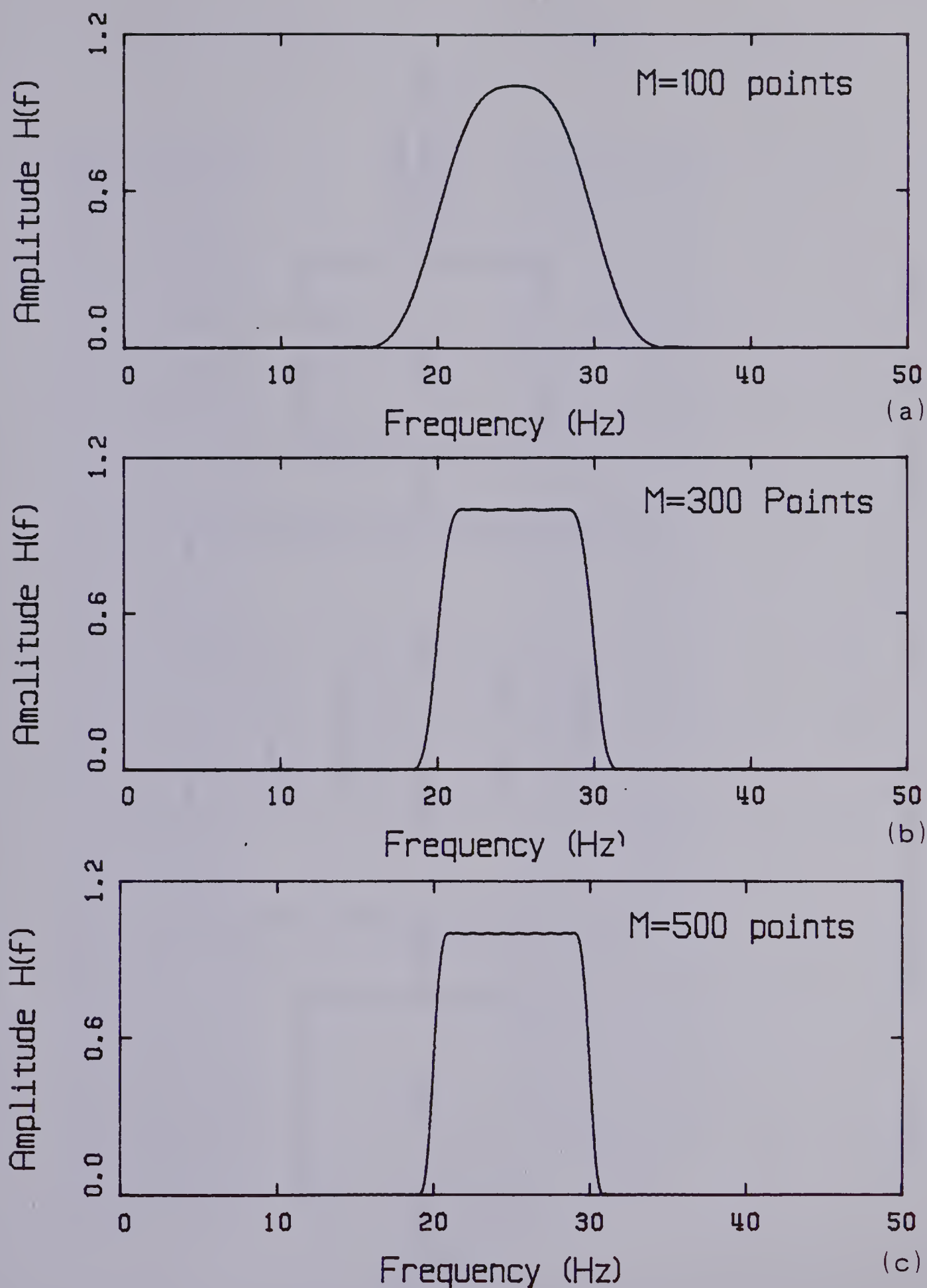


Figure A.5 Frequency Domain Response of Three FIR Filters

(a) 100 Terms, (b) 300 Terms, (c) 500Terms

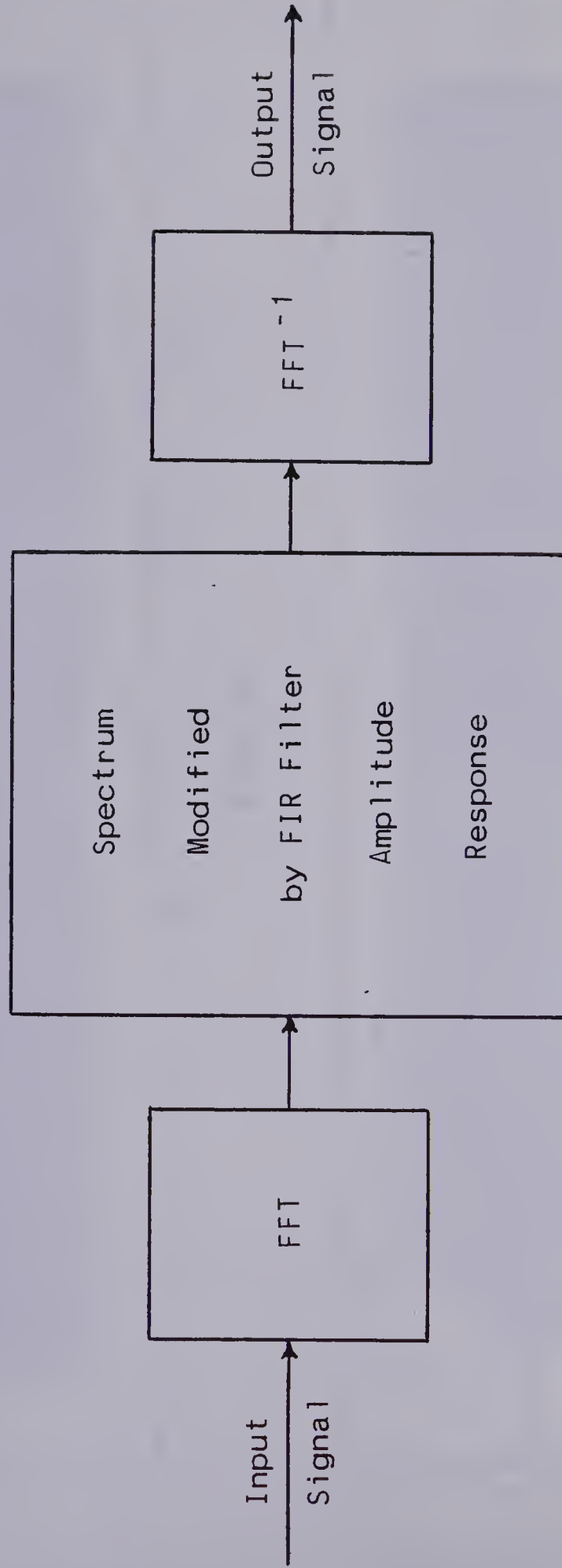


Figure A.6 Schematic Describing Convolution with FIR Filter

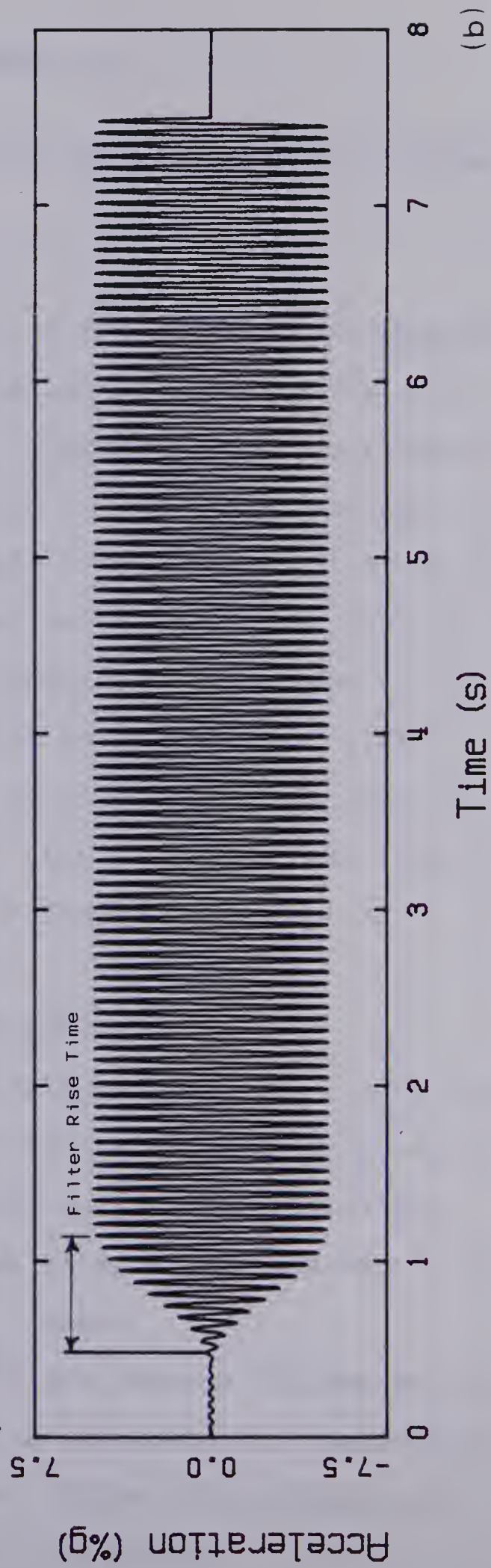
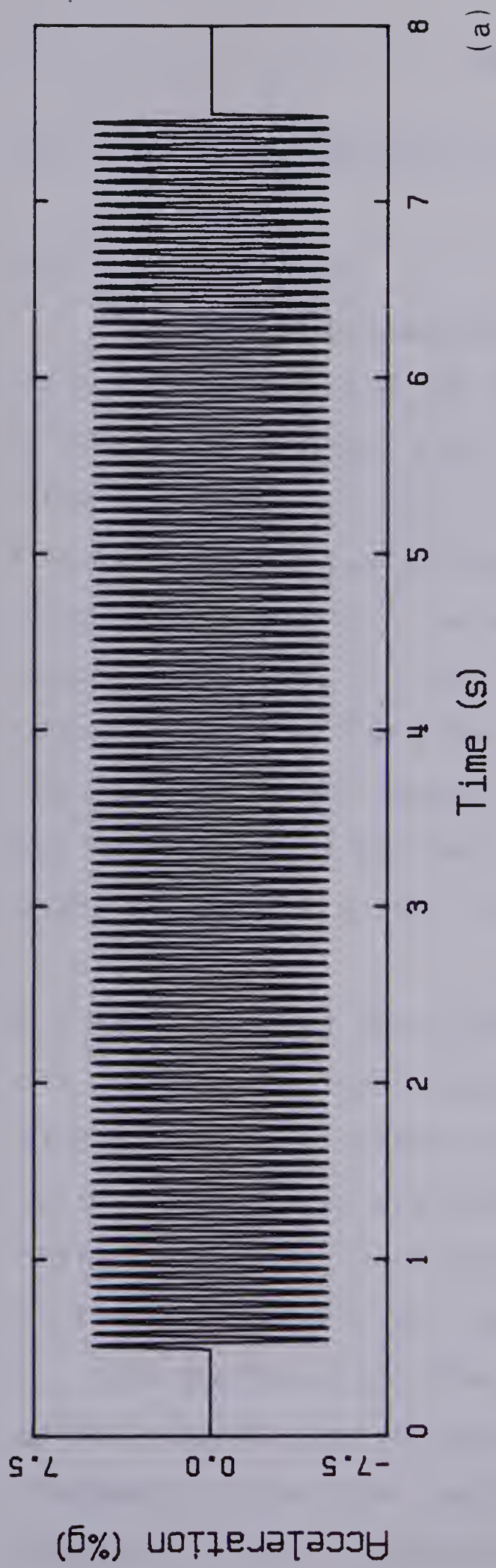


Figure A.7 Filter Rise-time Concept (a) Input Sine Wave, (b) Filter Output

APPENDIX B

B. Theoretical Analysis of the Stub Girder Floor System

B.1 Introduction

The theoretical analyses to determine the fundamental natural frequency and the peak acceleration of the stub girder floor system (refer to Chapter 4) are described in this appendix. The application of the T-beam analogy to the floor system and the subsequent frequency calculations are discussed in detail. The peak acceleration response of the stub girder floor to a heel impact is derived for various approximations to the effective vibrating panel width. The last section of the appendix contains magnitude spectra derived from the experimental results of the heel impact tests on the stub girder floor system.

B.2 Application of the T-beam Analogy

In applying the T-beam analogy (see Sect. 2.3.1) to the stub girder floor system, the series of beams perpendicular to the stub girders was assumed to form the T-sections (refer to Fig. 4.1). The stub girders were assumed to act as flexible supports for the T-beams.

The section properties of the assumed T-beams and the girder supports were required to evaluate the fundamental frequency of the floor system. Those calculations are presented in the remainder of this section. In the

following section, calculations for the fundamental frequencies of the T-beams, the stub girder supports, and the overall floor system are presented. The information necessary to evaluate the section properties of the T-beams and the girder supports is presented in Table B.1.

B.2.1 Section Property Calculations

B.2.1.1 Effective Thickness of Concrete Slab

The effective thickness of the concrete slab (t_e) was calculated as the average weight of concrete in and above the ribs of the metal deck, including the weight of the deck (43). The average weight (W_a) for a one meter width between the stub girders was calculated as follows (note: there are six sheets of each type of metal deck between the stub girders):

$$\begin{aligned}
 W_a &= (1/9.0) \left[(225 + \underbrace{10.3}_{\text{type-1 deck}}) (.812) (6) + \right. \\
 &\quad \left. (220 + \underbrace{14.4}_{\text{type-2 deck}}) (.688) (6) \right] \\
 &= 234.9 \text{ kg/m}^2
 \end{aligned}$$

The effective depth of the concrete slab becomes

$$t_e = \frac{234.9 \text{ kg/m}^2}{1900.0 \text{ kg/m}^3} = 0.124 \text{ m} \quad \text{or} \quad 124 \text{ mm}$$

B.2.1.2 Mass and Moment of Inertia of T-beam Sections

To reflect the uncracked state of the floor when the testing took place, the concrete area below the neutral axis of the T-beams has been included in the moment of inertia calculations. An effective width of concrete slab equal to the average spacing of the transverse beams was considered to act compositely with the steel sections. Cross-sections of the assumed T-beams are shown in Fig. B.1. The section properties determined for the composite T-beam sections were as follows:

1) Cantilever Beam Section

$$\bar{y} = 115.9 \text{ mm}$$

$$I_t = 9.83 \times 10^8 \text{ mm}^4$$

$$\bar{m} = 841.1 \text{ kg/m}$$

2) Link Beam Section

$$\bar{y} = 78.21 \text{ mm}$$

$$I_t = 2.02 \times 10^8 \text{ mm}^4$$

$$\bar{m} = 806.8 \text{ kg/m}$$

B.2.1.3 Mass and Moment of Inertia of Girder Supports

The mass and moment of inertia of the stub girder supports were determined in a manner similar to that used for the T-beams. However, because the stub girders consisted of two cross-sections (ie: with and without the stubs), the two corresponding moments of inertia were averaged to obtain the value used in the subsequent frequency calculations. A typical cross-section of the stub girder T-section is presented in Fig. B.1. Since the stub girders were designed compositely, the effective width of the concrete slab was determined from the specifications in

Sect. 17.3.2.1 of the CSA S16.1-M78 code. The effective width was taken to be 2750 mm. The section properties determined for the two stub girder T-sections were as follows:

1) Cross-section including stub

$$\bar{y} = 279.7 \text{ mm}$$

$$I_t = 5.46 \times 10^9 \text{ mm}^4$$

2) Cross-section excluding stub

$$\bar{y} = 262.6 \text{ mm}$$

$$I_t = 5.10 \times 10^9 \text{ mm}^4$$

The weighted-average of the moment of inertia over the length of the stub girder was calculated as

$$I_t = \frac{(5.71) (5.46 \times 10^9)}{(12.5)} + \frac{(6.79) (5.10 \times 10^9)}{(12.5)}$$

$$= 5.26 \times 10^9 \text{ mm}^4$$

Although the moment of inertia was derived for an "effective width" of concrete slab, a width equal to the centre to centre spacing of the stub girders has been considered in calculating the mass of the girder supports. The mass contributions of the transverse beams were averaged over the length of the girders as follows

$$\bar{m} = \left[\underbrace{(234.9) (9.0)}_{\text{slab \& deck}} + \underbrace{(106.9)}_{\text{W310X107}} + \underbrace{\frac{(5.14) (60.9)}{(12.5)}}_{\text{stubs}} + \right.$$

$$\left. \underbrace{\frac{(2.135) (6) (60.9)}{(12.5)}}_{\text{cantilever beams}} + \underbrace{\frac{(2.635) (6) (26.6)}{(12.5)}}_{\text{link beams}} \right] = 2342.1 \text{ kg/m}$$

B.3 Frequency Calculations

B.3.1 Two Span Beam by Rayleigh Method

To model the stub girder floor system as a unit, a two span T-beam with flexible simple supports was considered. This allowed the reduced stiffness of the link beam sections to be reflected in the frequency calculations. The Rayleigh method (29) has been used to evaluate the fundamental frequency of the two span beam. Because the mass per unit length of the cantilever and link beam T-sections was nearly the same, the T-beam was assumed to have a constant mass along its length, which also simplified the frequency calculations. The T-beam model and the assumed deflected shape are illustrated in Fig. B.2. The assumed shape function ($\psi(x)$) of the T-beam is defined by

$$\psi_{(x)} = \sin \frac{2\pi x}{L} \quad (B.1)$$

the displacement (v) by

$$v(x,t) = \psi_{(x)} Z_o \sin \omega t \quad (B.2)$$

and the velocity (\dot{v}) by

$$\dot{v}(x,t) = \omega \psi_{(x)} Z_o \cos \omega t \quad (B.3)$$

The frequency of the T-beam was obtained by equating the maximum potential energy (V_{max}) of the beam to the maximum kinetic energy (K_{max}). The potential energy of the flexural system is given by

$$V = \frac{1}{2} \int_0^L EI_{(x)} \left(\frac{\partial^2 v}{\partial x^2} \right)^2 dx \quad (B.4)$$

and the kinetic energy by

$$K = \frac{1}{2} \int_0^L m(x) (\dot{v})^2 dx \quad (B.5)$$

After substituting Eqns. B.2 and B.3 in Eqns. B.4 and B.5 and differentiating, the maximum potential energy became

$$V_{\max} = \frac{16\pi^4}{L^4} \frac{Z_o^2}{2} \int_0^L EI_{(x)} \left(\sin \frac{2\pi x}{L} \right)^2 dx \quad (B.6)$$

and the maximum kinetic energy became

$$K_{\max} = \bar{m}\omega^2 \frac{Z_o^2}{2} \int_0^L \left(\sin \frac{2\pi x}{L} \right)^2 dx \quad (B.7)$$

By setting V_{\max} equal to K_{\max} the fundamental frequency (ω) of the beam in radians per second was obtained, with the variation in the stiffness of the beam accounted for by integrating over the appropriate limits. The resulting frequency expression was

$$\omega^2 = \frac{16\pi^4}{\bar{m}L^4} (0.59 EI_{\textcircled{1}} + 0.409 EI_{\textcircled{2}}) \quad (B.8)$$

which upon substitution of the values derived in the preceding section and converting to cycles per second (Hz) gave the final T-beam frequency (f_j) which was 7.74 Hz.

To obtain the frequency of the floor system, the frequency of the supporting girders (spring supports in Fig. B.3) was required. Since the girders were assumed to be of uniform mass and stiffness and to be simply supported, the frequency expression Eqn. 2.1 of Sect. 2.3.1 could be

applied as follows

$$f_g = 1570 \sqrt{\frac{(200000) (5.26 \times 10^9)}{(2342.1) (12500)^4}}$$

$$= 6.73 \text{ Hz}$$

The system frequency of the stub girder floor was calculated as the system frequency of the two span beam according to Eqn. 2.2 as follows

$$f_f = \sqrt{\frac{1}{\frac{1}{7.74^2} + \frac{1}{6.73^2}}}$$

$$= 5.08 \text{ Hz}$$

B.3.2 Single Span Beam by Standard Procedure

To investigate a direct application of the current CSA code provisions to the stub girder floor system, a single span T-beam of uniform mass and stiffness was considered. The T-beam was assumed to represent the floor bay containing the main section of the cantilever beams (refer to Fig. 4.1) and, as in the previous case, the stub girders were assumed to act as flexible supports. The frequency of the T-beam was calculated according to Eqn. 2.1 as follows

$$f_j = 1570 \sqrt{\frac{(200000) (9.83 \times 10^8)}{(841.1) (9000)^4}}$$

$$= 9.37 \text{ Hz}$$

Since the frequency of the girder supports was the same as that derived in the previous section, the fundamental frequency of the floor system was determined as follows

$$f_f = \sqrt{\frac{1}{\frac{1}{9.37^2} + \frac{1}{6.73^2}}}$$

$$= 5.54 \text{ Hz}$$

B.4 Peak Acceleration Calculations

In this section, the peak acceleration of the stub girder floor associated with a heel impact has been estimated theoretically according to Eqn. 2.16 in Sect. 2.3.2. Three approximations to effective width of the vibrating panel were considered. These include the $60t_e$ (where t_e is the effective slab thickness) approximation incorporated in the current CSA standard (17), an effective width derived by the Sokolowski et al method described in Sect. 2.3.2, and an estimate of the vibrating panel width based on the experimental results.

To obtain a totally theoretical evaluation of the peak acceleration, the fundamental frequency of 5.54 Hz

determined in the last section has been used in the calculations with the first two of the above effective width estimates. The natural frequency of mode 3 (ie: refer to Table 4.1) of 6.6 Hz has been used in the final peak acceleration calculation which considers the experimentally observed vibrating panel width. Because the shapes of modes 1 through 4, perpendicular to the midspans of the transverse beams, were quite similar (refer to Figs. 4.7 and 4.8), the effective panel width was essentially the same for those modes (ie: full width from the core wall to the exterior edge of the slab). Therefore, mode 3 was selected for the calculations on the basis that it was the most prominent of the lower modes and because the corresponding modal pattern perpendicular to the stub girder substantiates the assumed length of the vibrating panel as the distance between the stub girder supports. The peak acceleration calculations associated with the above discussion are as follows:

- 1) Effective width determined by $60t_e$ approximation:

approximate mass of floor...250.0 kg/m
 effective depth of slab.....0.124 m
 effective width.....7.44 m

$$A_o = \frac{9655 (5.54)}{(9.0) (7.44) (250.0)}$$

$$= 3.2 \%g$$

- 2) Effective width determined by Sokolowski method
(see Sect. 2.3.2):

$$D_x = 15888.5 \text{ E}$$

$$D_y = 3.15 \times 10^8 \text{ E}$$

$$\epsilon = .267$$

$$\text{effective panel width} = 5.10 \text{ m}$$

$$A_o = \frac{9655 (5.54)}{(9.0) (5.10) (250.0)}$$

$$= 4.7 \%g$$

- 3) Effective width from experimental results:

Referring to Fig. 4.8 the effective panel width of mode 3 along lines 3 and 7 is approximately 13.0 m.

$$A_o = \frac{9655 (6.6)}{(9.0) (13.0) (250.0)}$$

$$= 2.2 \%g$$

Table B.1 Section Properties of Structural Components

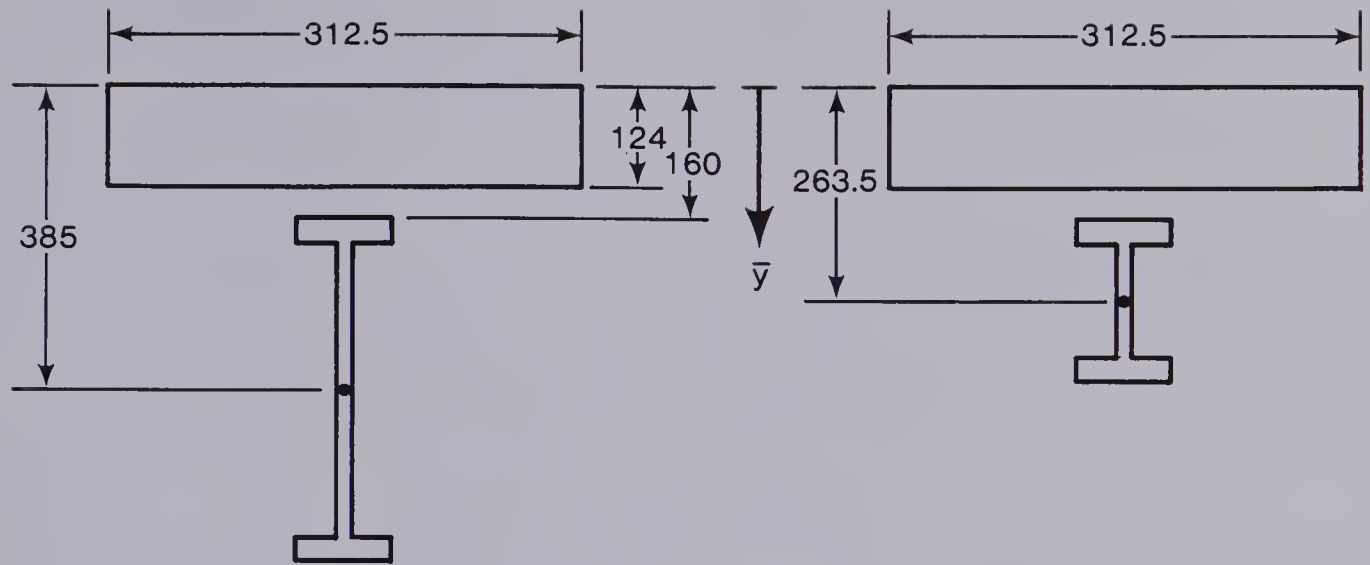
Concrete Slab		Metal Deck	
total thickness...	160 mm	type 1	type 2
mass density.....	1900 kg/m	width	812 688 mm
strength.....	30 MPa	mass	10.3 4.4 kg/m
modular ratio.....	10	concrete mass:	
		160 mm slab	225 220 kg/m

Steel Members

Stub Girders	Cantilever Beams
main section....W310X107	section.....W460X61
stubs.....W460X61	ave. spacing.....3.125 m
spacing.....9.0 m	total length.....13.27 m
length.....12.5 m	length of overhangs..2.135 m

Link Beams

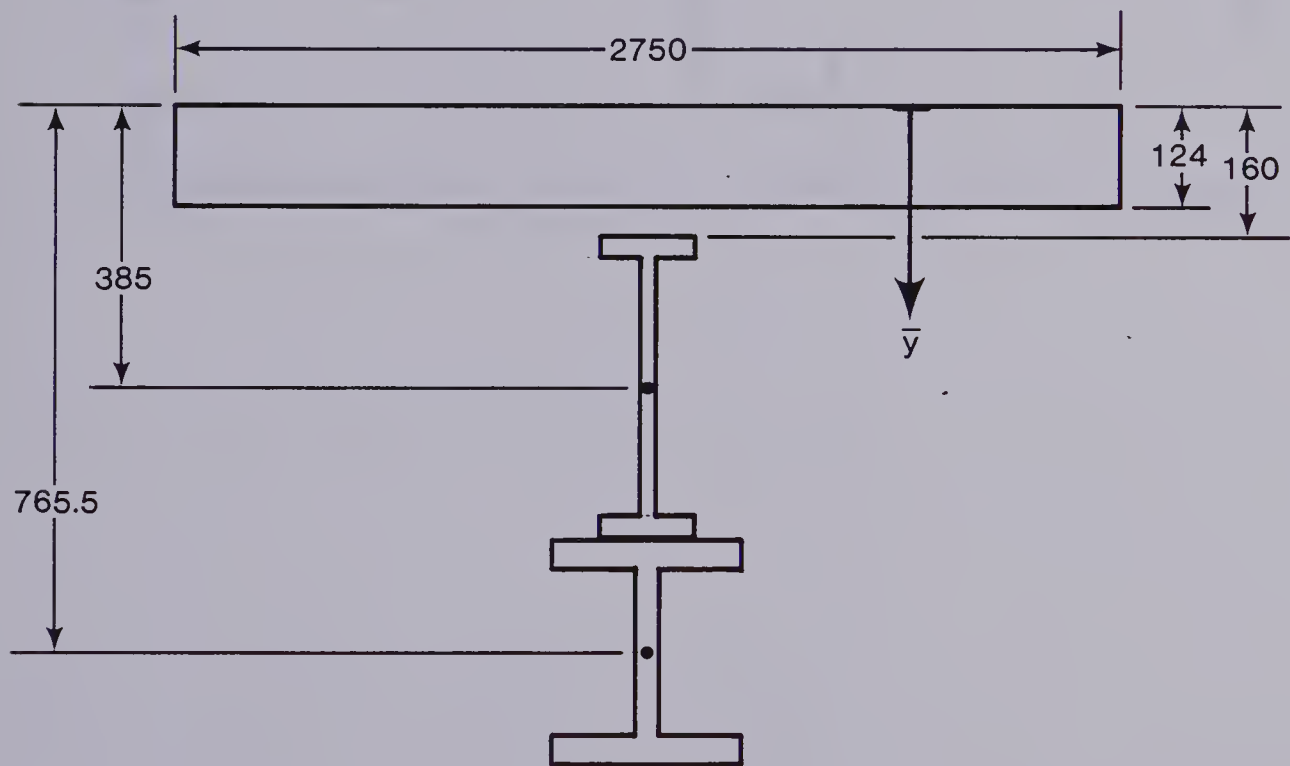
section.....	W200X27
ave. spacing.....	3.125 m
length.....	4.37 m



(a) Cantilever Beam Section

(b) Link Beam Section

(a)



(b)

Figure B.1 Typical T-beam Cross-sections (a) Transverse Beams
(b) Girder Supports

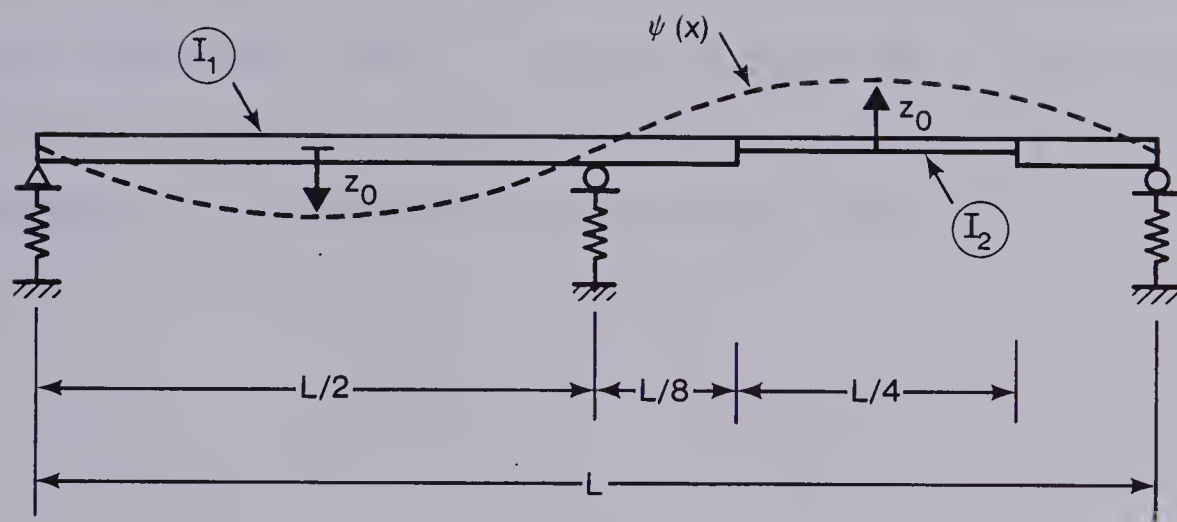


Figure B.2 Assumed Vibration Pattern of T-beam Model

B.5 Magnitude Spectra from the Stub Girder Floor Tests

Included in this section are magnitude spectra from the heel impact tests on the stub girder floor system. The accelerometer position and the impact location given in each of the spectra corresponds to the grid shown in Fig. 4.5.

Figures B.3 through B.8 are arranged to allow a comparison of the response at similar positions along lines 3, 5, and 7, for impacts at similar positions on each of the respective lines. Figures B.9 and B.10 show spectra associated with the response at three positions along line D for impacts at various positions along line D.

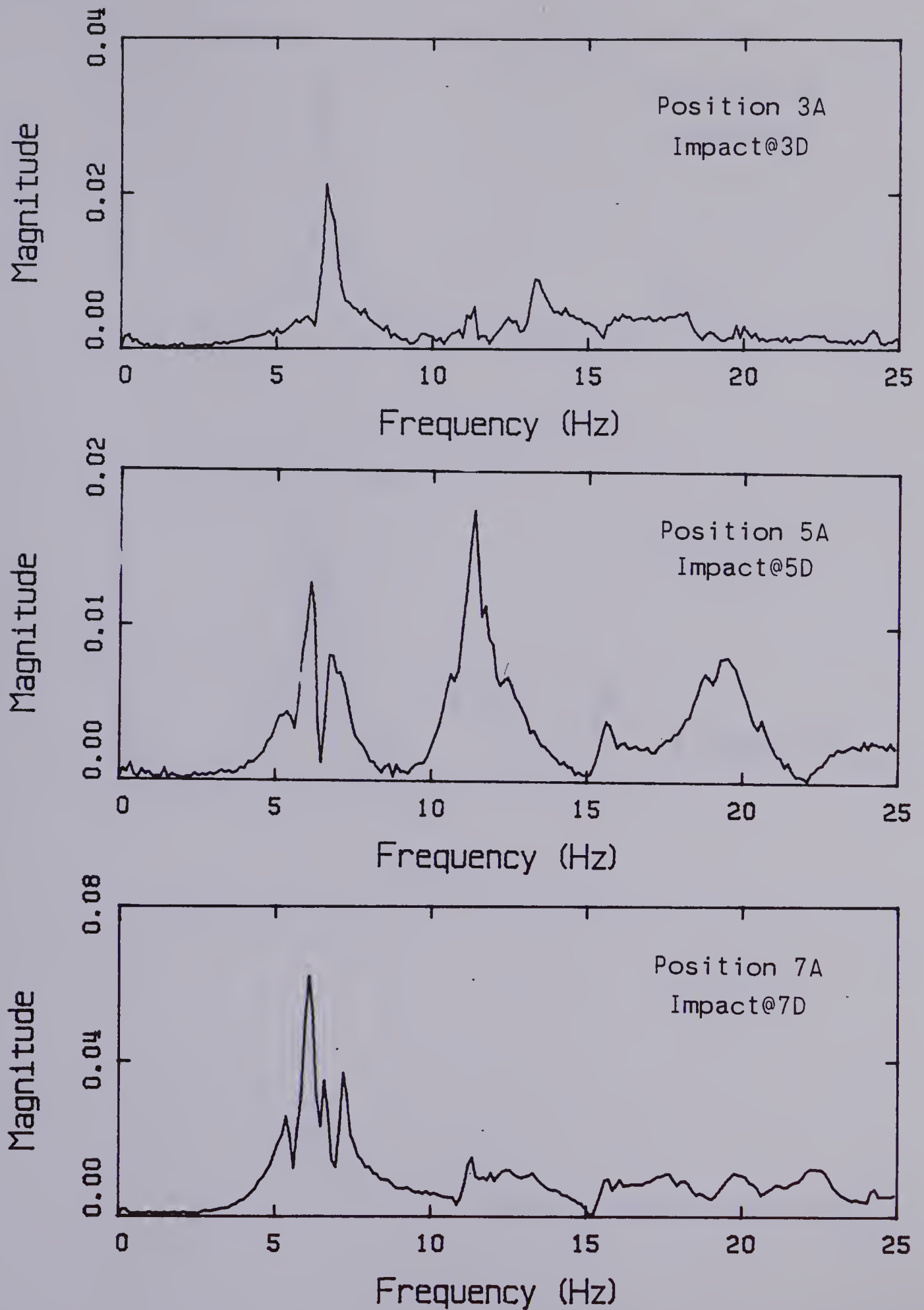


Figure B.3 Magnitude Spectra for Positions 3A, 5A, and 7A
for Midline Impacts

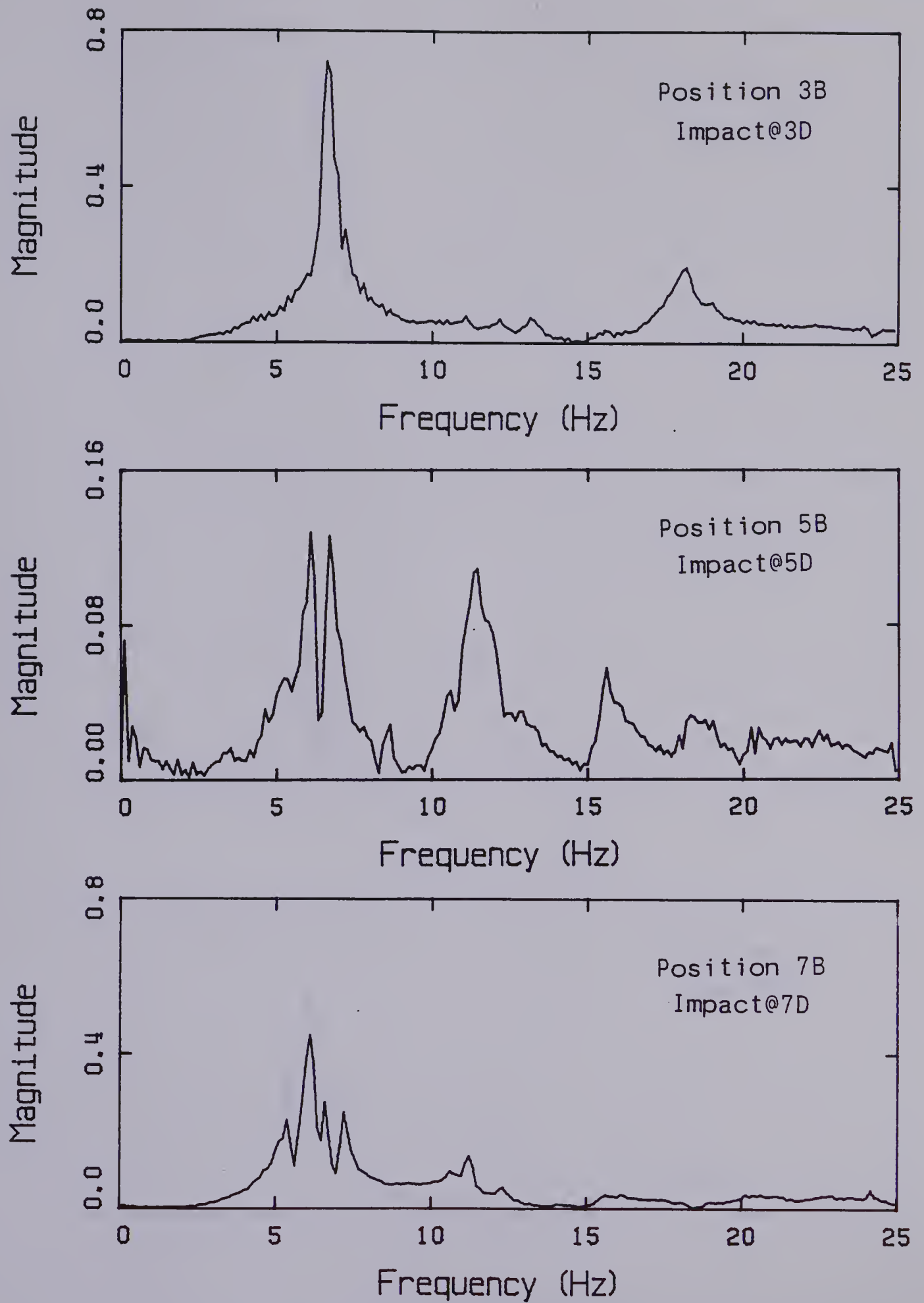


Figure B.4 Magnitude Spectra for Positions 3B, 5B, and 7B for Midline Impacts

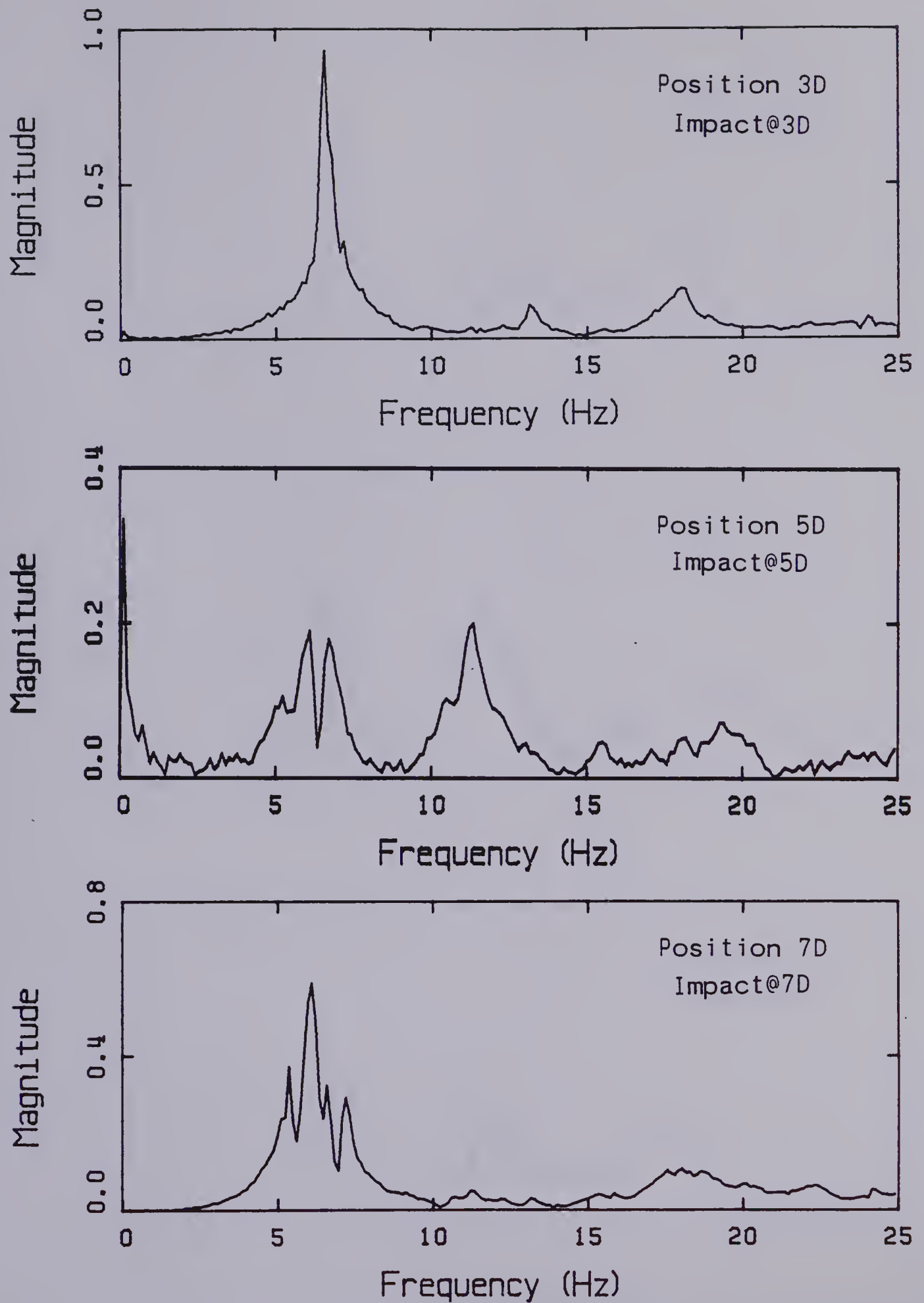


Figure B.5 Magnitude Spectra for Positions 3D, 5D, and 7D for Midline Impacts

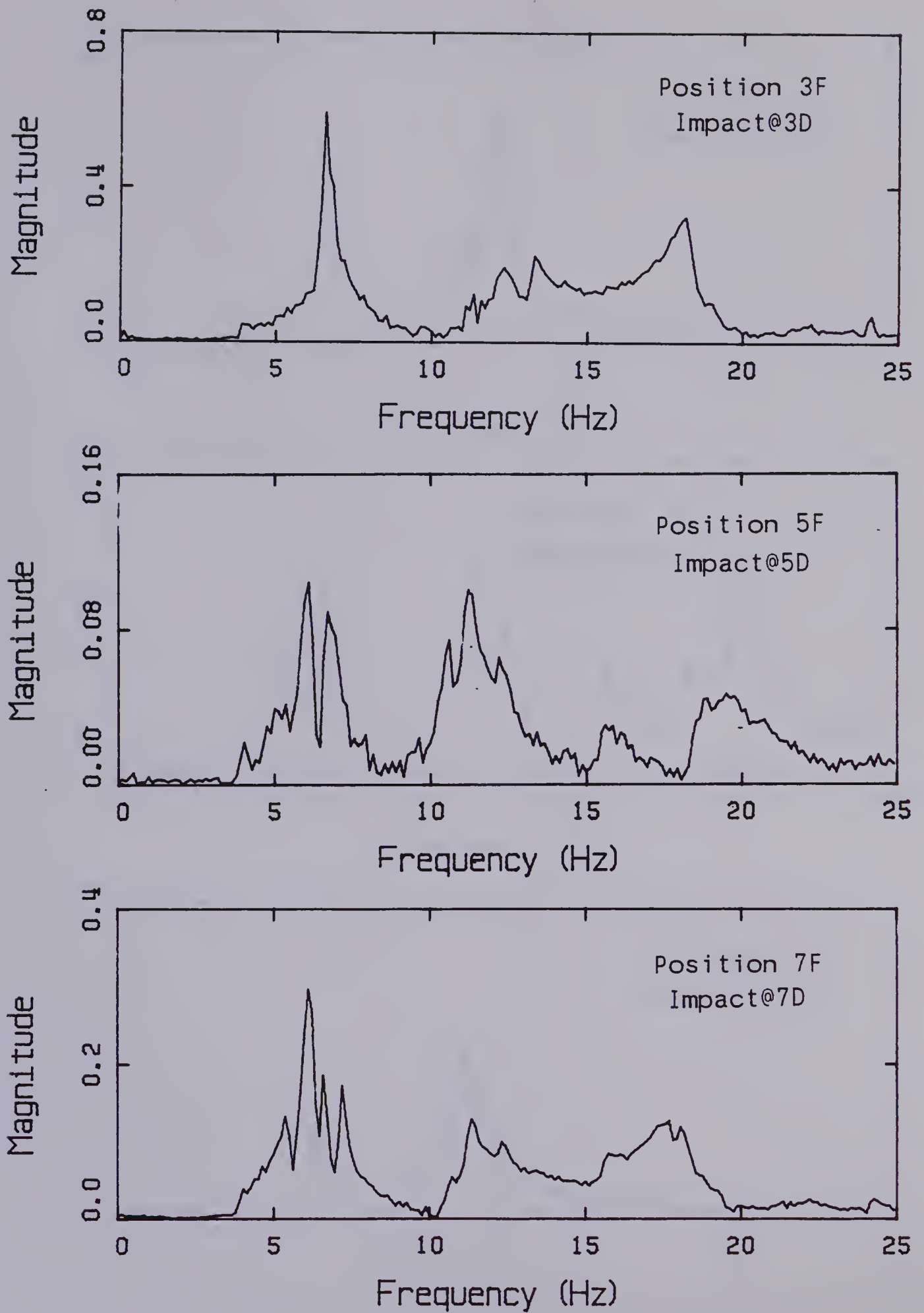


Figure B.6 Magnitude Spectra for Positions 3F, 5F, and 7F for Midline Impacts

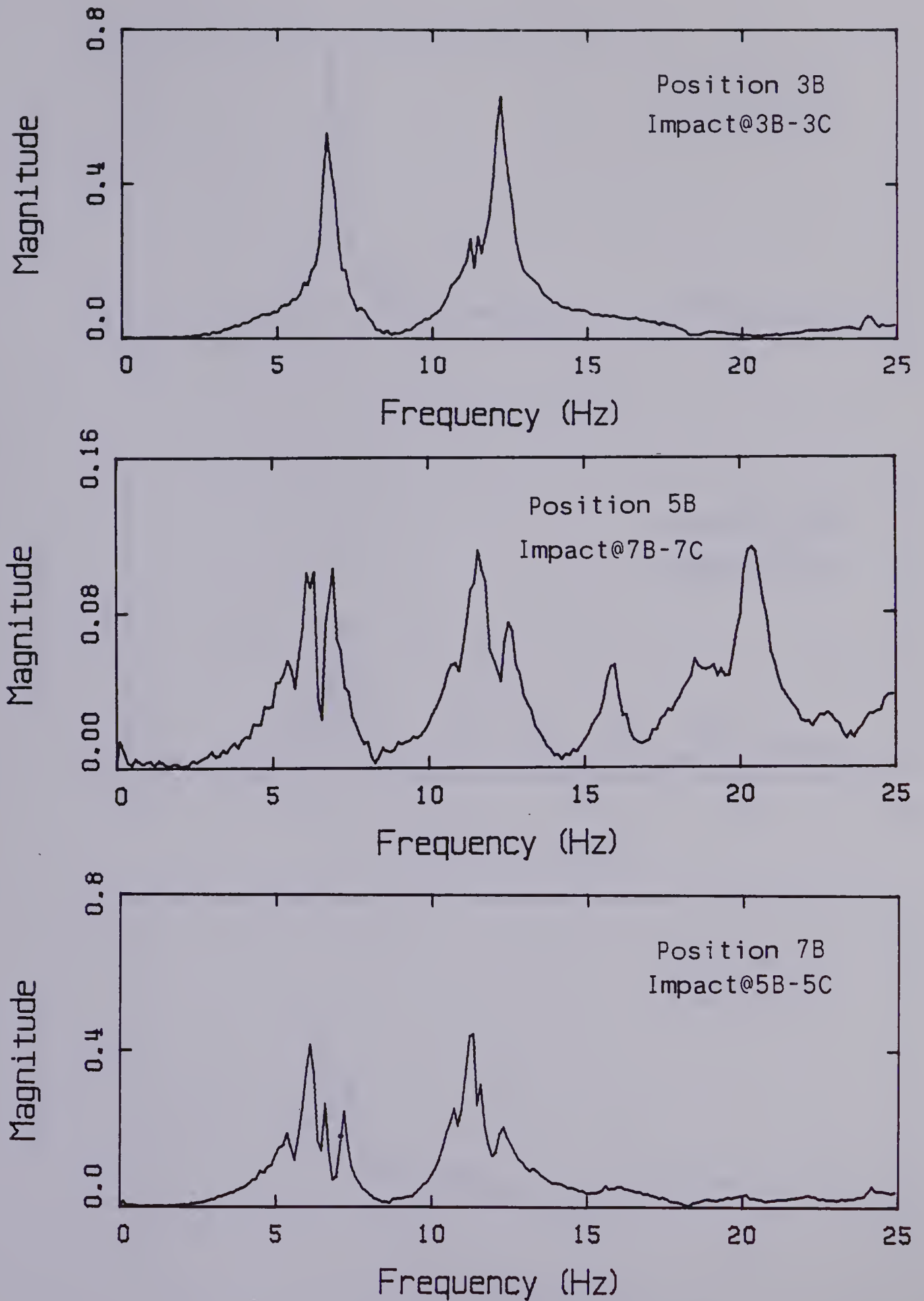


Figure B.7 Magnitude Spectra for Positions 3B, 5B, and 7B for One-third Point Impacts

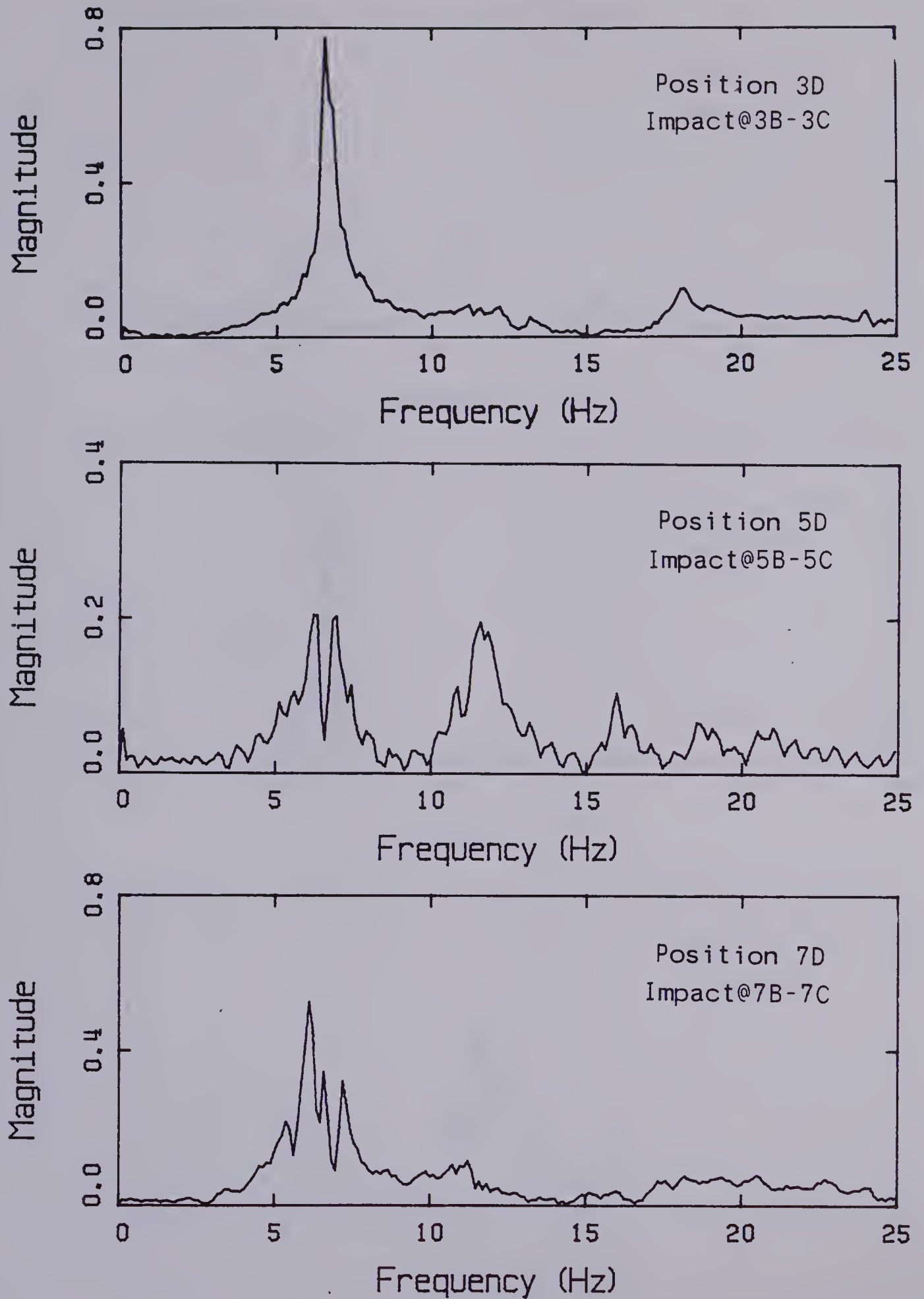


Figure B.8 Magnitude Spectra for Positions 3D, 5D, and 7D for One-third Point Impacts

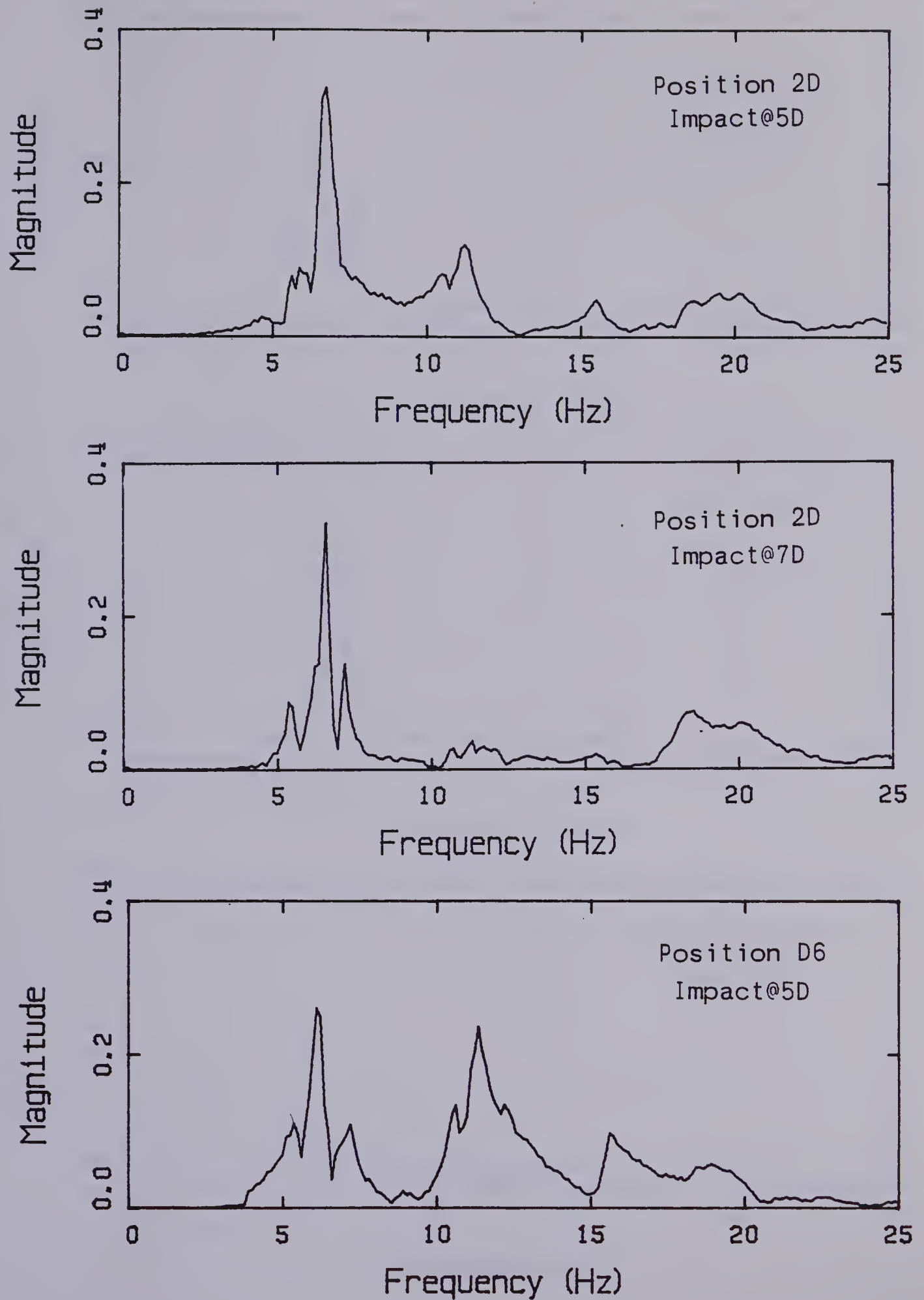


Figure B.9 Magnitude Spectra for Positions along Line D

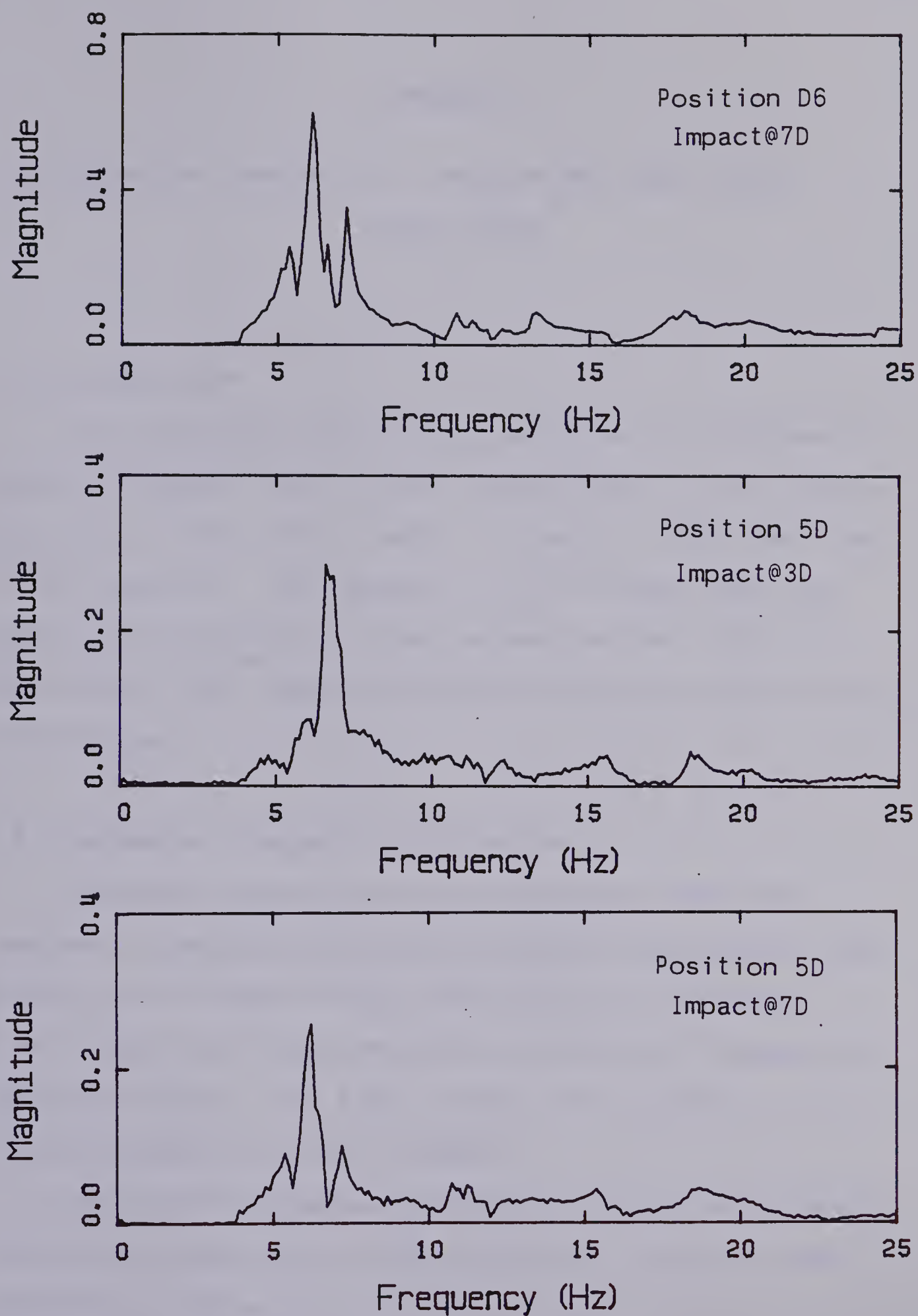


Figure B.10 Magnitude Spectra for Positions along Line D

APPENDIX C

C. Theoretical Analysis of the Open Web Steel Joist Dance Floor

C.1 Introduction

The theoretical analyses to determine the fundamental natural frequency and the peak acceleration of the open web steel joist dance floor (refer to Chapter 5) are described in this appendix. The appendix also includes magnitude spectra and acceleration-time records derived from the experimental heel impact and dance vibration studies of the floor system.

C.2 Fundamental Frequency Calculations

Since the framing system of the dance floor was composed of open web steel joists simply-supported on steel girders, the T-beam analogy (see Sect.2.3.1) could be directly applied to determine the fundamental frequency of the floor system. The steel girders were assumed to act as flexible supports for the T-beams.

The structural member information used in calculating the section properties of the composite T-beams has been presented in Table C.1.

In the remainder of this section, the fundamental frequencies of the T-beams, the girder supports, and the

overall floor system are calculated.

To determine the effective thickness (t_e) of the concrete slab, the mass of concrete and steel deck in a one square meter area was first calculated as follows

$$12.2 + 2400 [0.062 + (0.5) (0.038)] = 206.6 \text{ kg/m}^2$$

The effective slab thickness was then determined by dividing the above mass/unit area by the mass density of concrete (ie: 2400 kg/m^3). The resulting effective slab thickness was 86.0 mm.

The mass per meter of the assumed T-beam (refer to Sect. 2.3.1) was calculated as follows

$$\bar{m} = \underbrace{23.36}_{\text{joist}} + 0.9375 (\underbrace{206.6}_{\text{concrete \& deck}} + \underbrace{12.7}_{\text{ceiling}} + \underbrace{10.0}_{\text{flooring \& ducts}}) = 238.3 \text{ kg/m}$$

A cross-section of a typical T-beam is illustrated in Fig C.1. The areas and dimensions used in calculating the moment of inertia of the composite T-beam are included in the figure. The resulting moment of inertia was $450 \times 10^6 \text{ mm}^4$.

By substituting the values derived above into Eqn. 2.1, the fundamental frequency of the T-beam was determined as follows

$$f_j = 1570 \sqrt{\frac{(200000) (4.5 \times 10^8)}{(238.3) (12000)^4}}$$

$$= 6.7 \text{ Hz}$$

Because the open web steel joists were supported on flexible beams, the fundamental frequency of the floor was calculated as a system frequency using Eqn. 2.2. The non-composite concrete slab was assumed not to contribute to the stiffness in calculating the frequency of the supporting beam (f_g).

The mass per meter of the supporting beam becomes

$$\bar{m} = \underbrace{113.4}_{\text{steel section}} + 9.0(\underbrace{206.6}_{\text{concrete \& deck}} + \underbrace{12.7}_{\text{ceiling}} + \underbrace{10.0}_{\text{flooring \& ducts}}) = 2177 \text{ kg/m}$$

The fundamental frequency of the supporting beam was determined by substituting the appropriate values into Eqn. 2.1 as follows

$$f_g = 1570 \sqrt{\frac{(200000) (8.75 \times 10^8)}{(2177) (9280)^4}}$$

$$= 5.2 \text{ Hz}$$

The fundamental frequency of the floor system was then determined using Eqn. 2.2 as follows

$$f_f = \sqrt{\frac{1}{\frac{1}{6.7^2} + \frac{1}{5.2^2}}}$$

$$= 4.1 \text{ Hz}$$

C.3 Peak Acceleration Calculations

In the following peak acceleration calculations, three approximations to the effective width of the vibrating panel are considered. These include the $60t_e$ approximation described in Sect. 2.3.2, an estimate derived according to the method presented by Sokolowski, and finally an estimate based on the experimental results. In all cases, the peak accelerations are evaluated using Eqn. 2.17.

- 1) determine peak acceleration using $60t_e$ approximation:

$$A_o = \frac{9655 (4.1)}{(60) (0.086) (12) (254.2)}$$

$$= 2.51 \%g$$

- 2) determine peak acceleration using effective width derived by the Sokolowski method:

effective width.....8.73 m

$$A_o = \frac{9655 (4.1)}{(8.73) (12) (254.2)}$$

$$= 1.49 \%g$$

- 3) determine the peak acceleration using the effective width and fundamental frequency derived experimentally:

effective width.....13.0 m (see Fig. 5.4b)

floor frequency..... 5.0 Hz

$$A_o = \frac{9655 (5.0)}{(13.0) (12) (254.2)}$$

$$= 1.22 \%g$$

Table C.1 Relative Section Properties and Information

Concrete Slab:	600 mm owsj:
total thickness.....100 mm	type: Dominion Bridge
deck thickness.....38 mm	M-series
deck mass.....12.2 kg/m	spacing.....937.5 mm
mod. of elast.....25000 MPa	length.....12000.0 mm
mass density.....2400 kg/m	mass.....23.26 kg/m
modular ratio.....8.0	

Beam Supports

steel section.....W610 x 113
link beam length..... 9280 mm
overhang length..... 1860 mm
distance between
column supports.....13000 mm

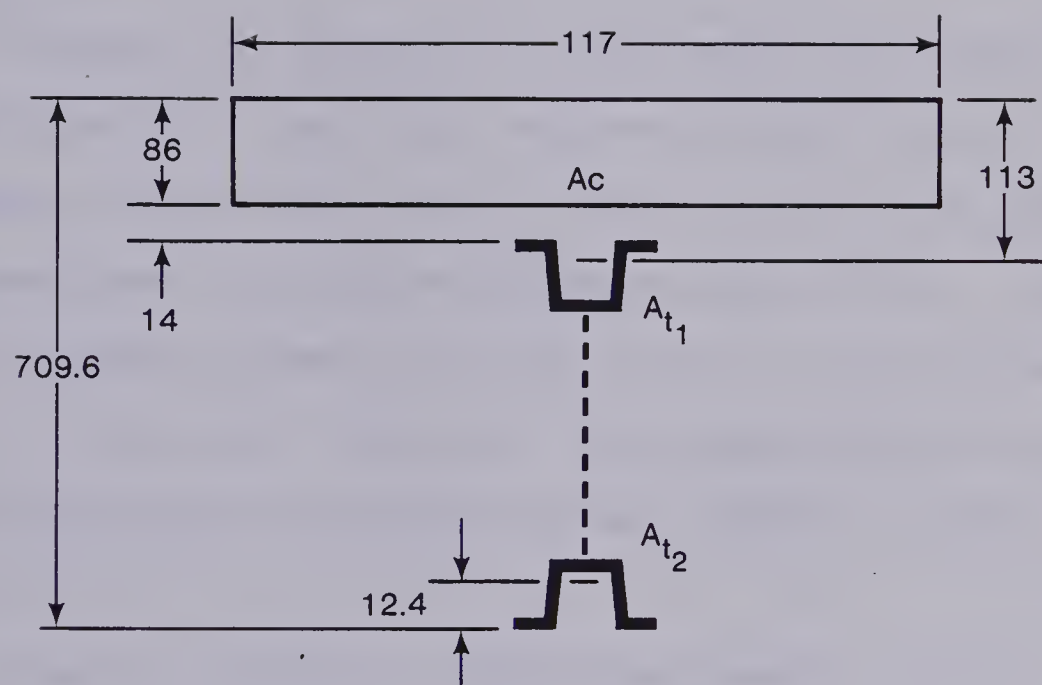


Figure C.1 Typical T-beam Cross-section

C.4 Magnitude Spectra and Acceleration-time Records from the Dynamic Study of the OWSJ Dance Floor

This section contains magnitude spectra derived from the results of the heel impact and dance vibration studies on the open web steel joist dance floor. Acceleration-time records of the floor response during various dances are also included.

Figures C.2 through C.5 show magnitude spectra associated with the floor response along line E at the midspan of the floor joists (refer to Fig. 5.2) and the response over the supporting beam along line C. Spectra are also included for position D6, which is the one-quarter point of the joist centred on the supporting beams. The various spectra correspond to heel impacts at positions E6 or C6.

Figure C.6 presents magnitude spectra typical of the floor response during a modern dance and a moderate rock and roll dance.

Figures C.7 through C.11 show typical unfiltered and filtered acceleration-time records associated with the floor response during a variety of dances including rock and roll, polkas, and waltzes.

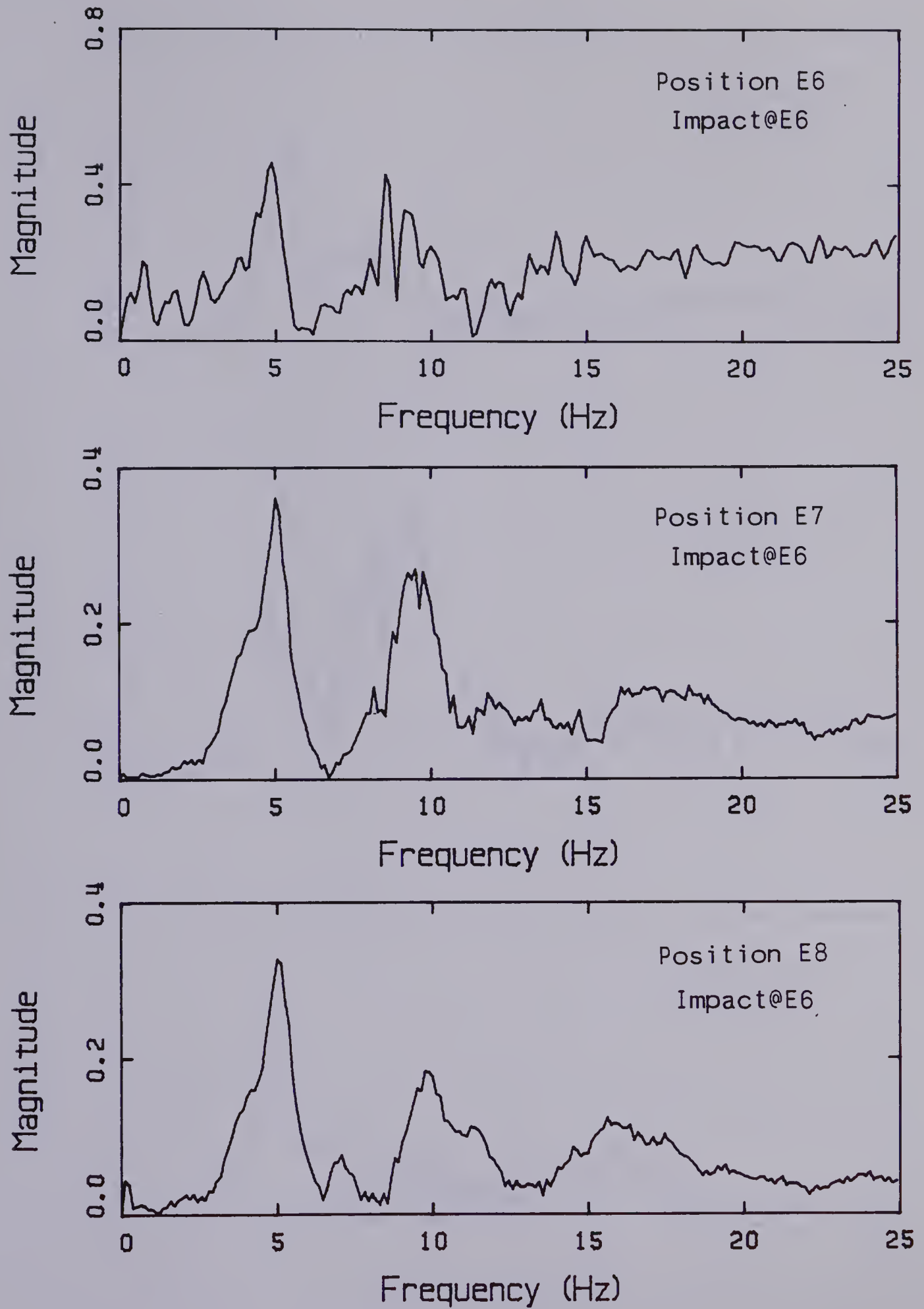


Figure C.2 Magnitude Spectra for Positions E6, E7, and E8
for Impacts at E6

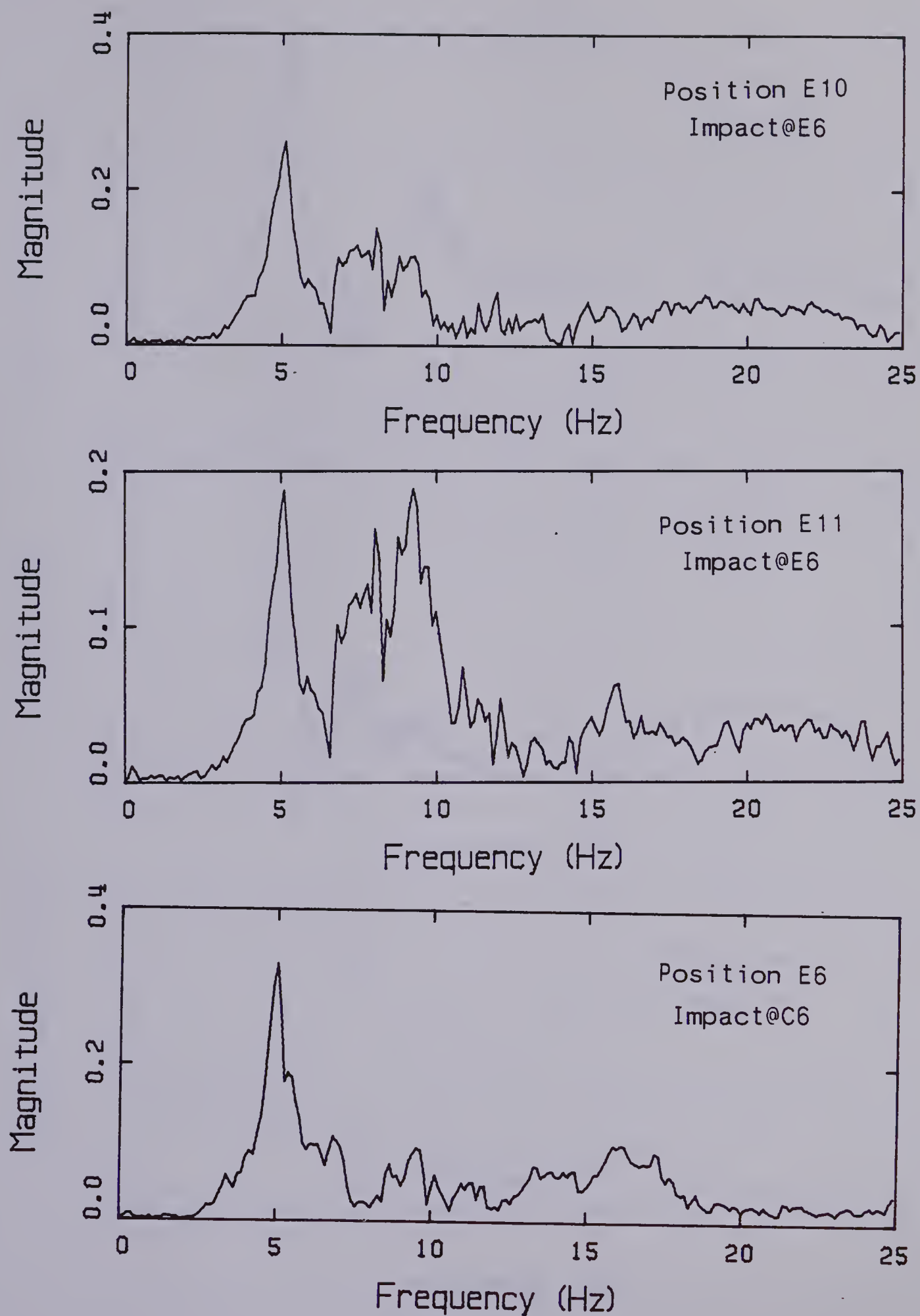


Figure C.3 Magnitude Spectra for Positions E10, E11, and E6
for Impacts at E6 or C6

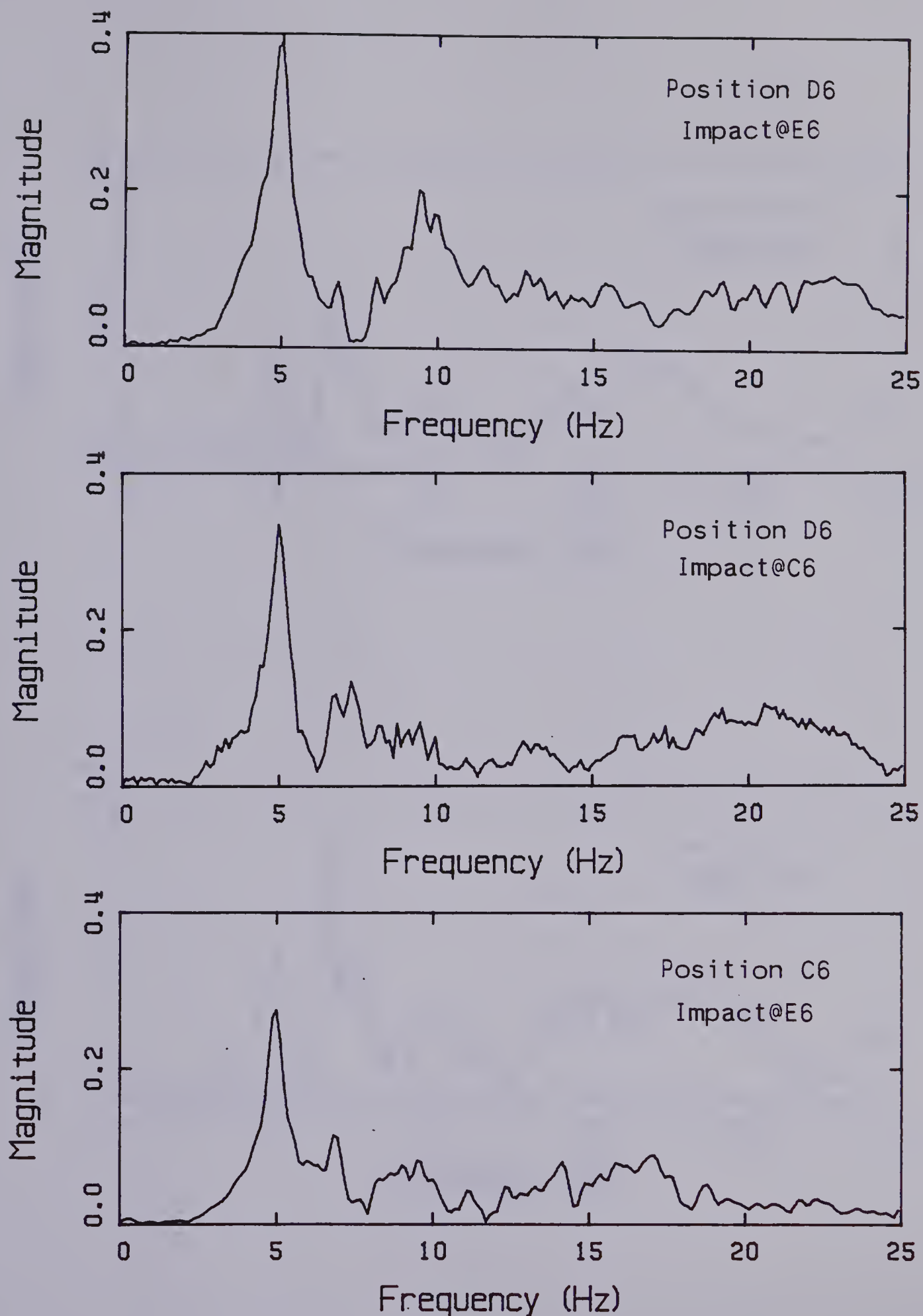


Figure C.4 Magnitude Spectra for Positions D6 and C6
for Impacts at C6 or E6

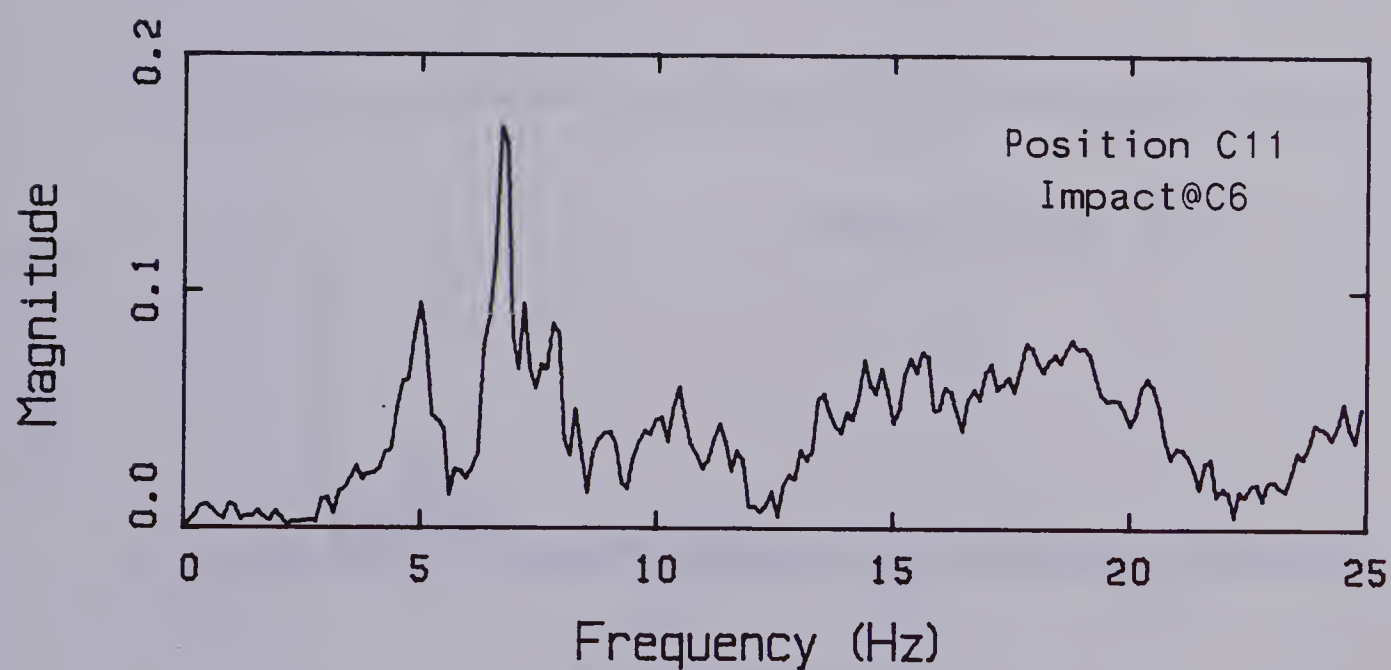
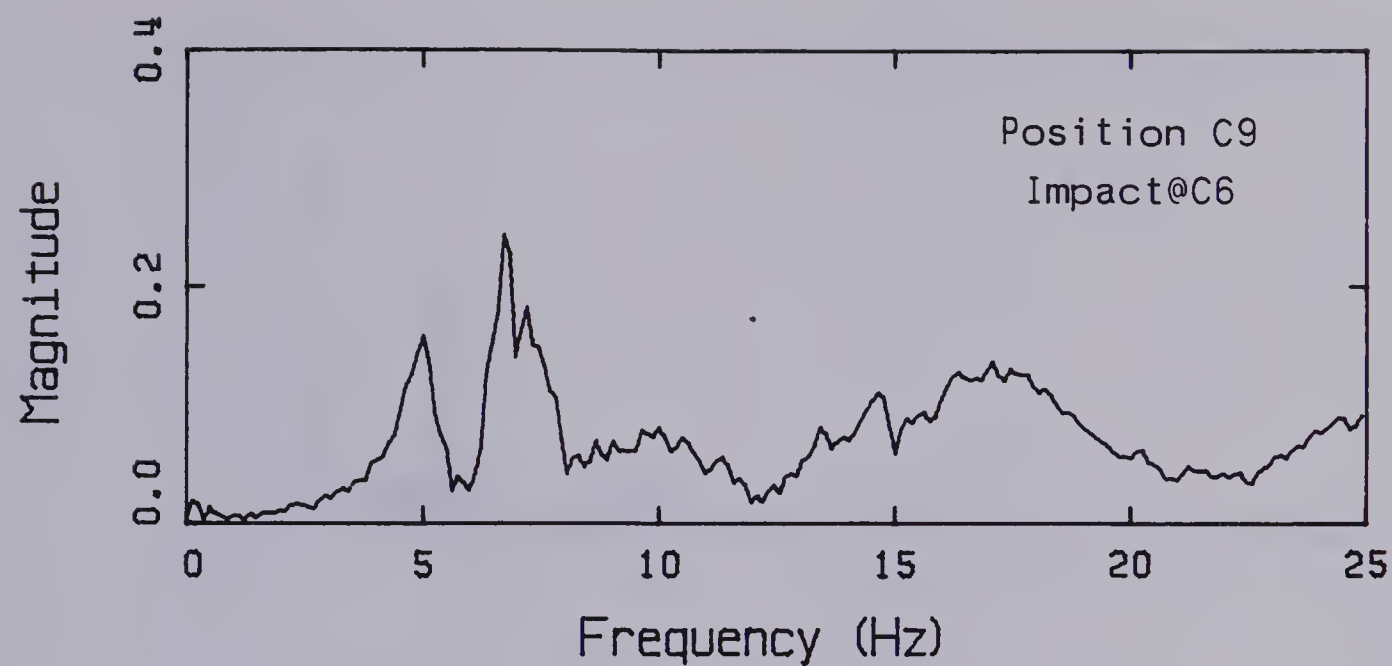


Figure C.5 Magnitude Spectra for Positions C9 and C11
for Impacts at C6

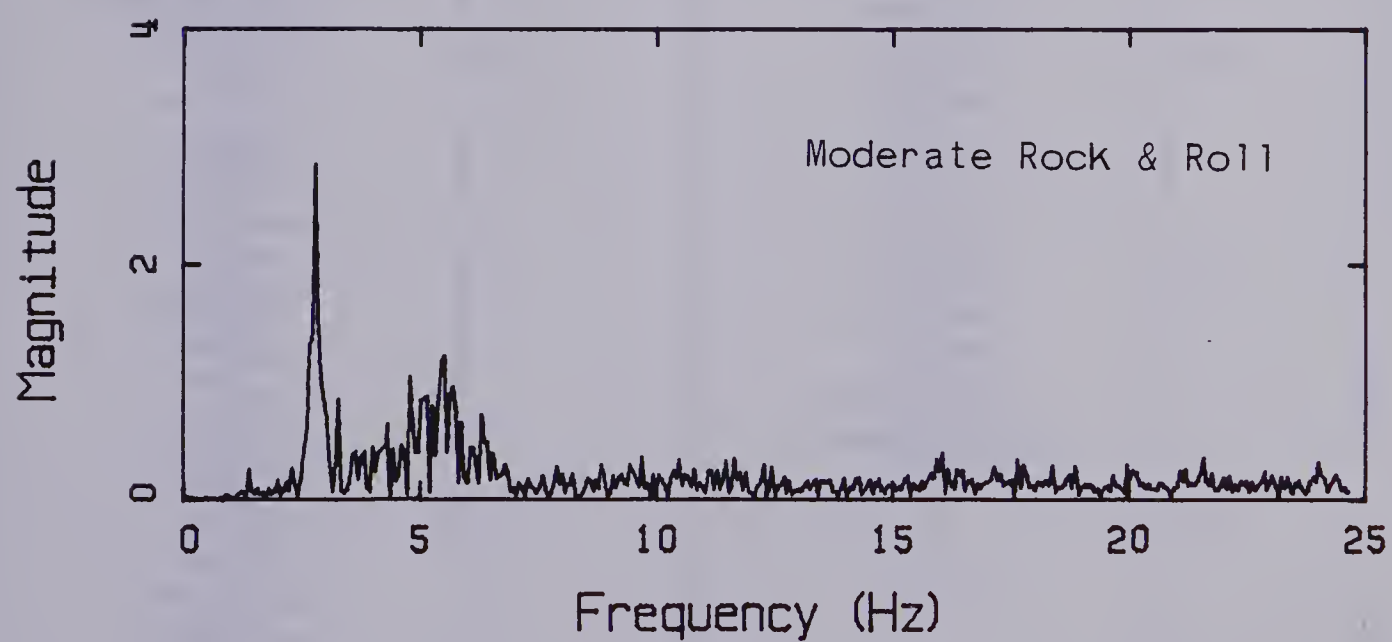
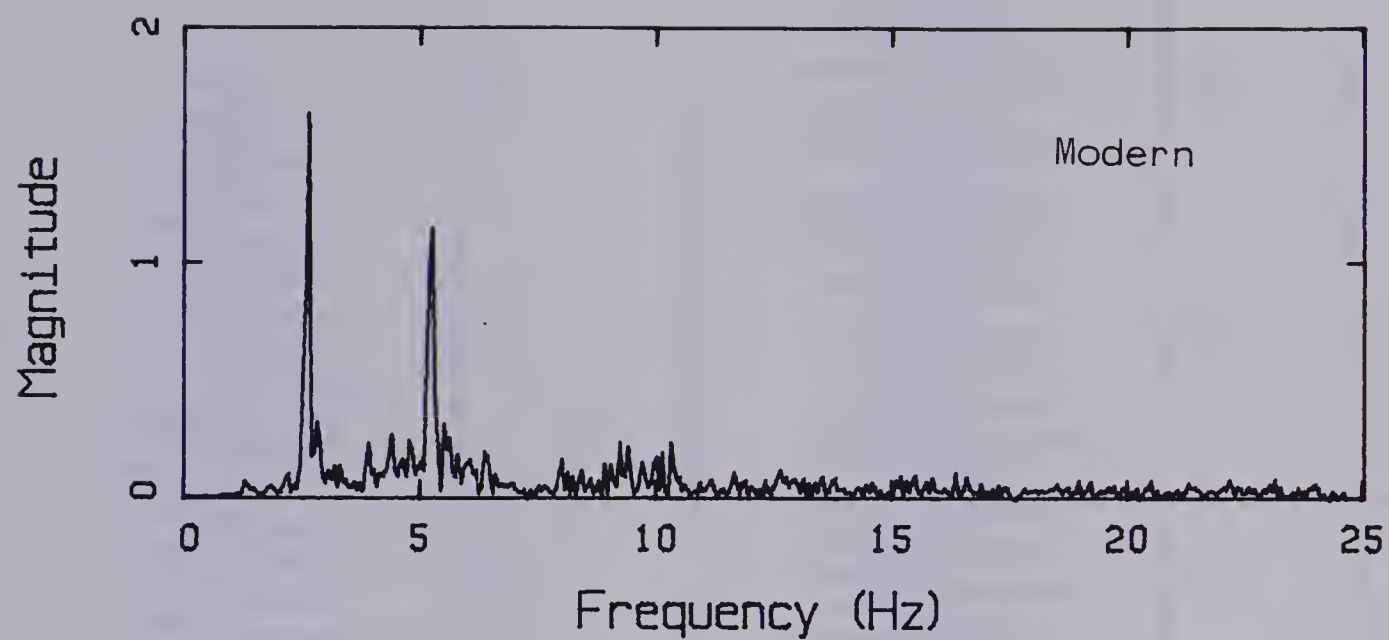


Figure C.6 Magnitude Spectra for a Modern Dance and a Moderate Rock & Roll Dance

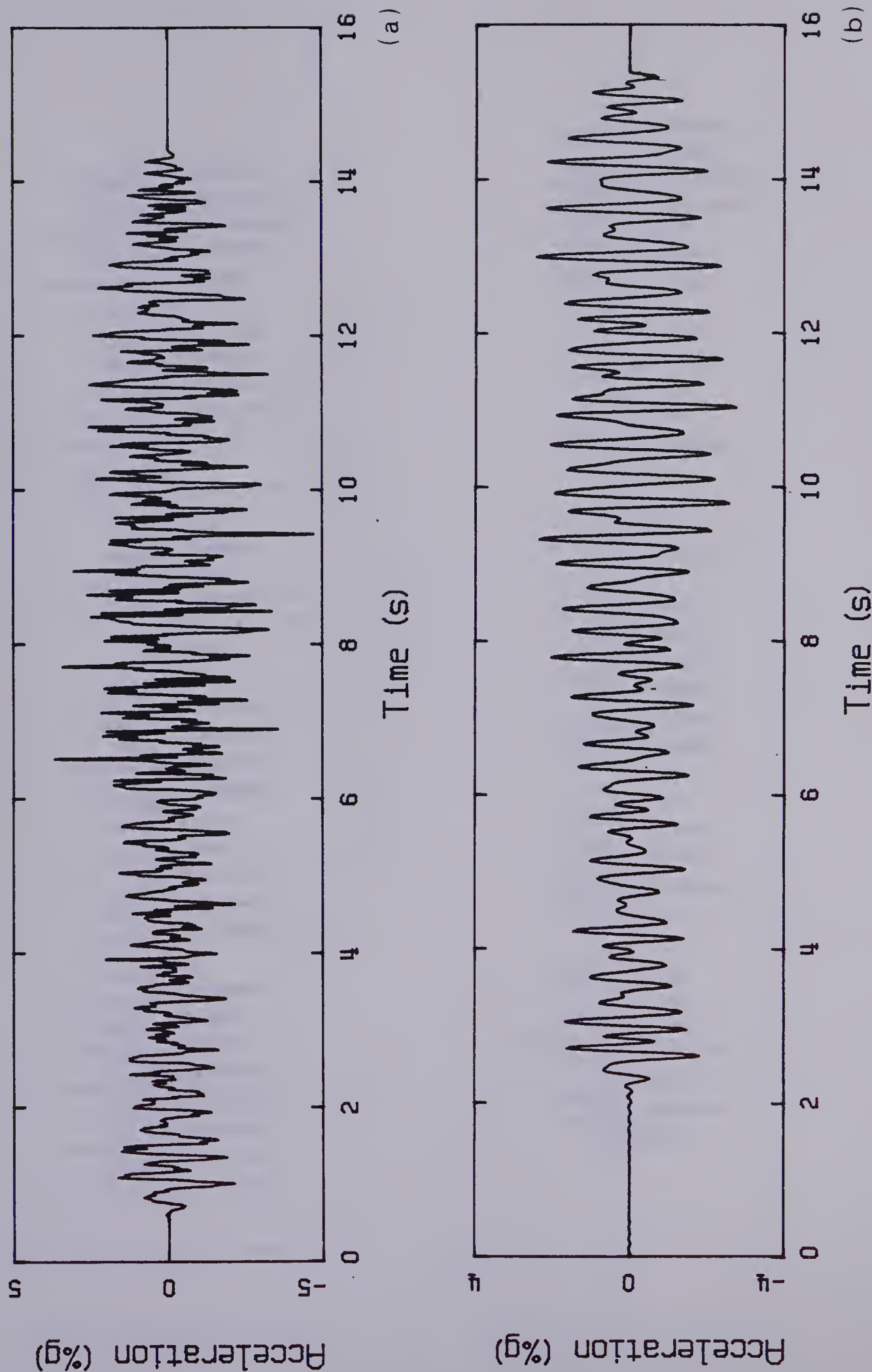


Figure C.7 Typical Acceleration-time Record for a Fast Rock & Roll Dance
(a) Unfiltered, (b) Filtered @ 6.5 Hz

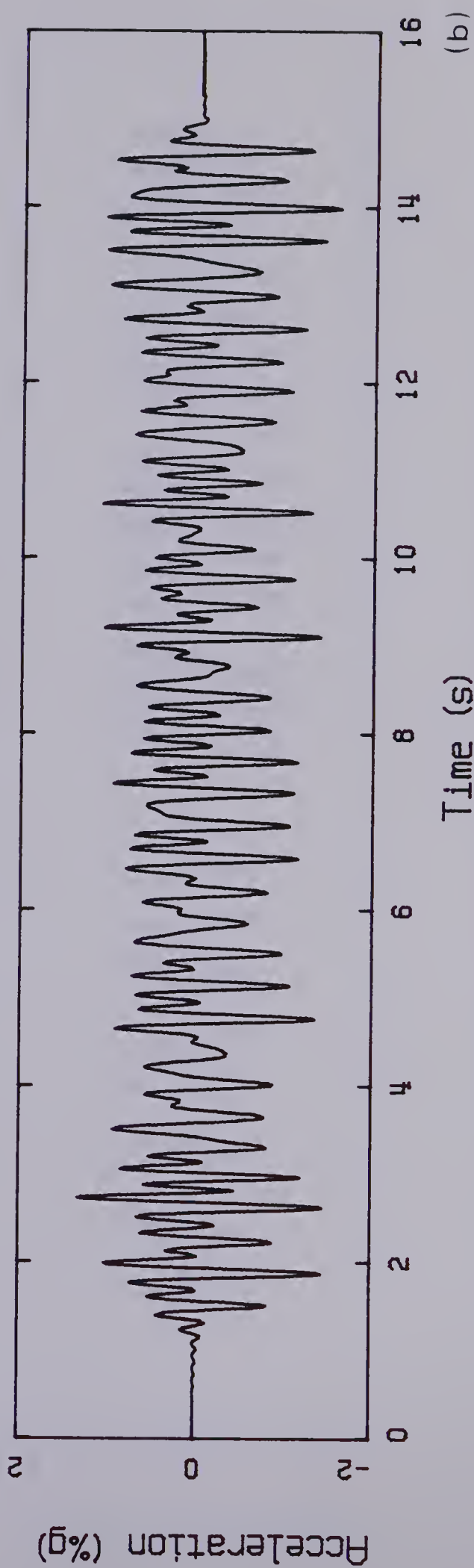
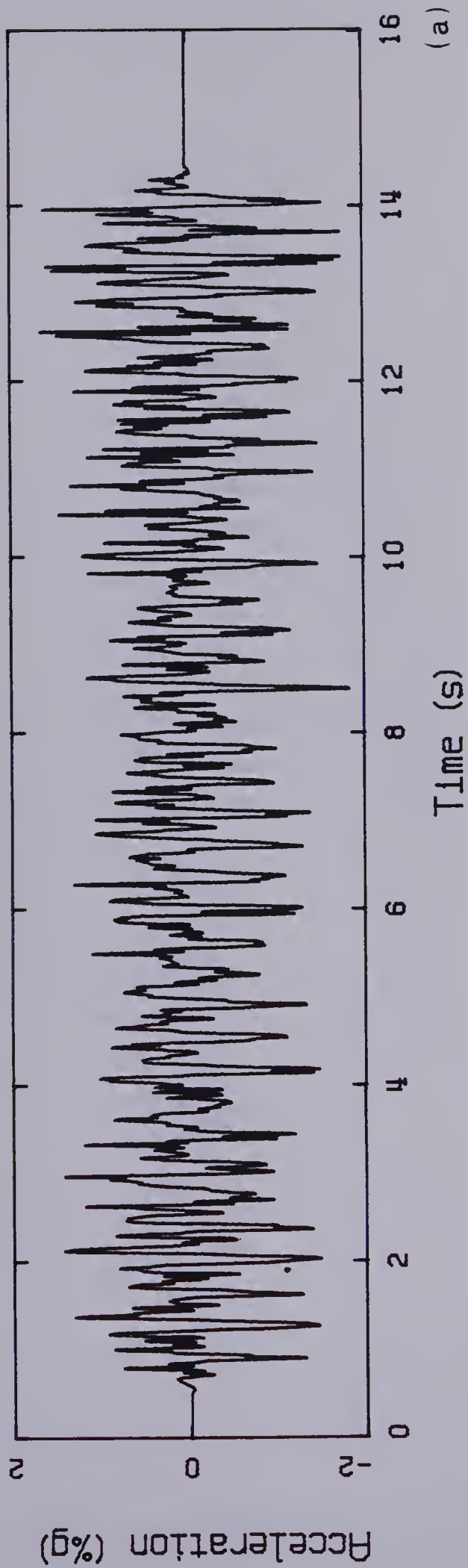


Figure C.8 Typical Acceleration-time Record for a Moderate Rock & Roll Dance
(a) Unfiltered, (b) Filtered @ 6.5 Hz

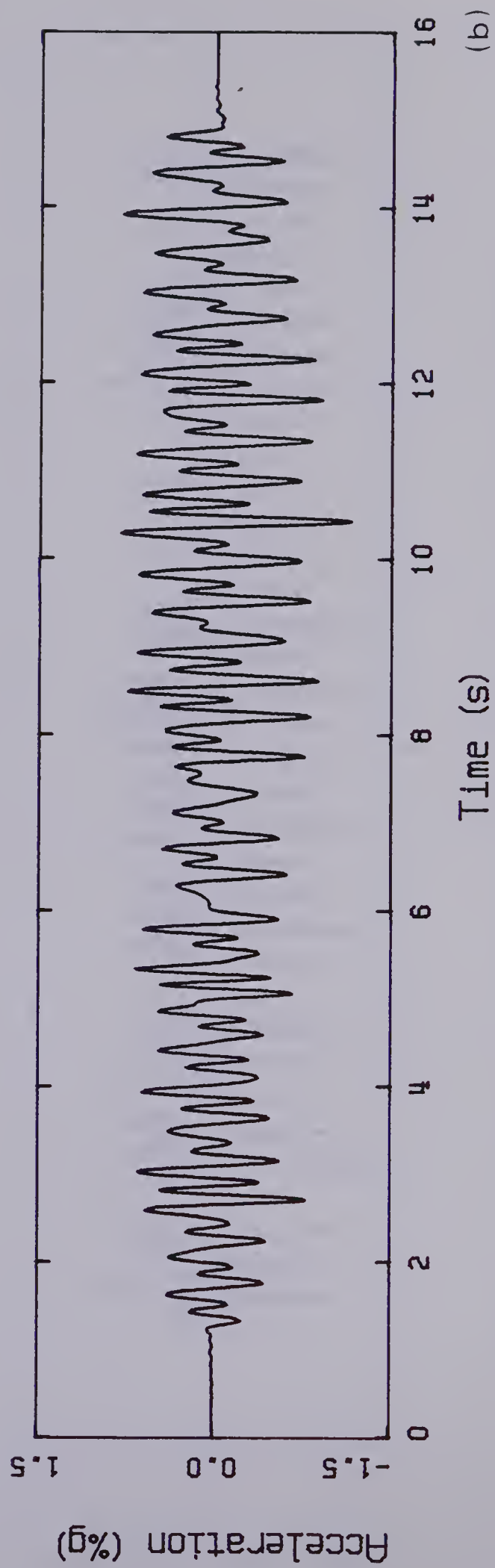
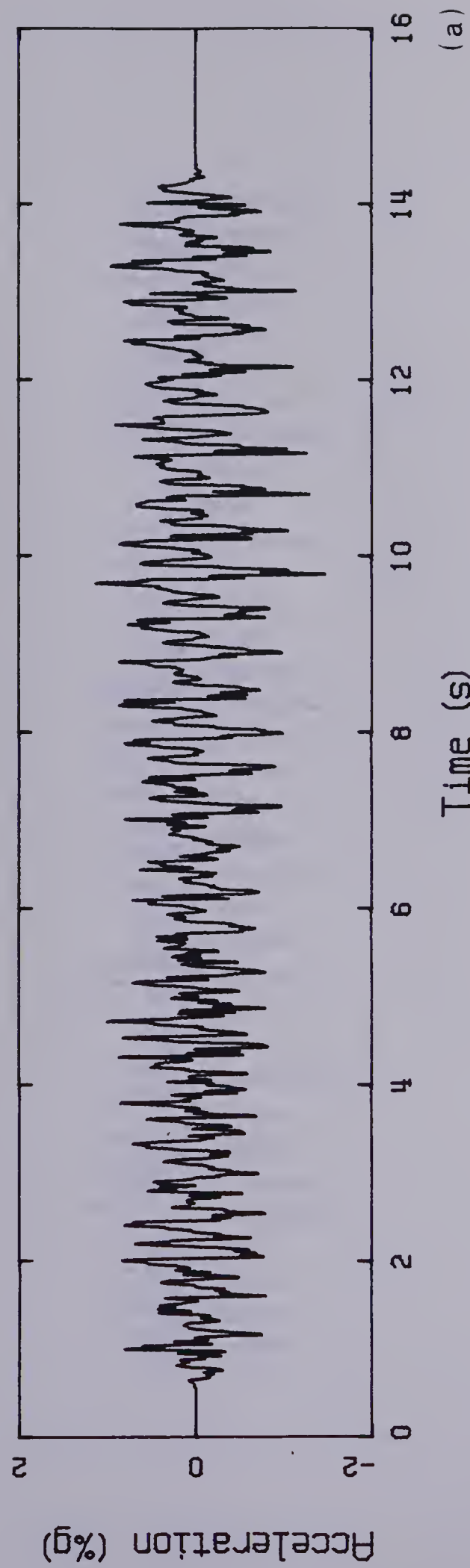


Figure C.9 Typical Acceleration-time Record for a Polka
(a) Unfiltered, (b) Filtered @ 6.5 Hz

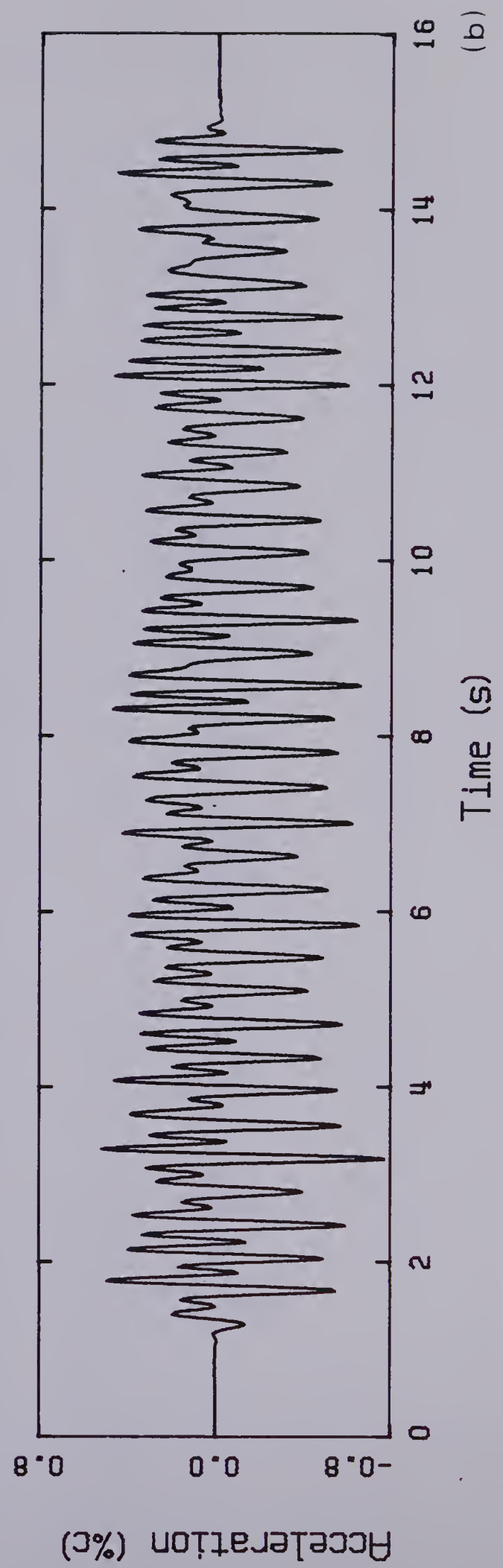
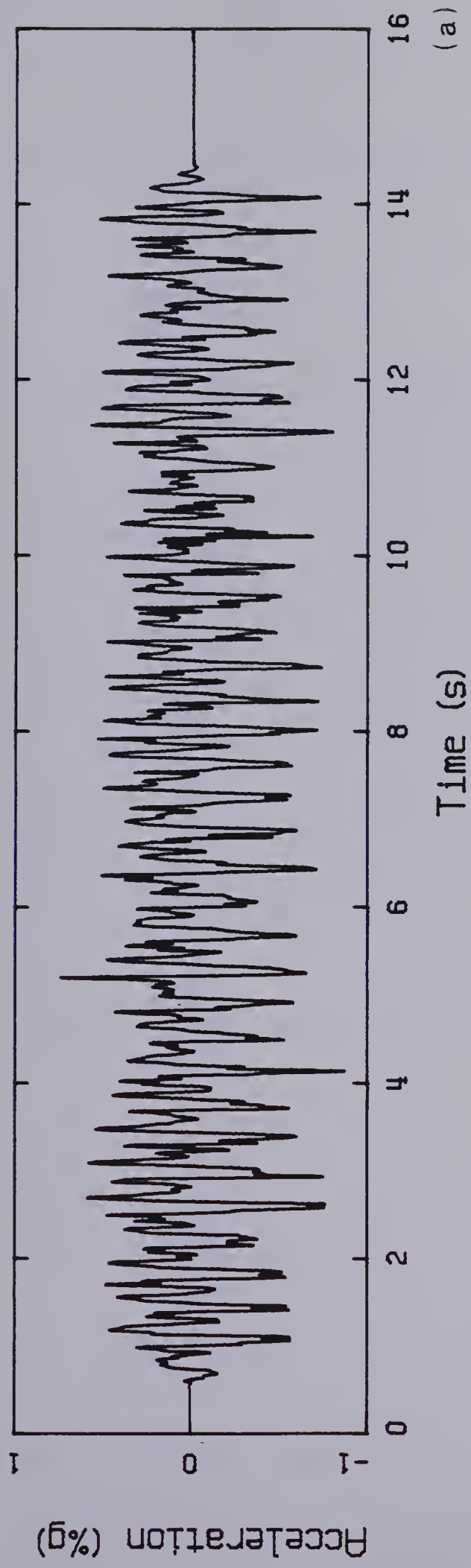


Figure C.10 Typical Acceleration-time Record for a Modern Dance
(a) Unfiltered, (b) Filtered @ 6.5 Hz

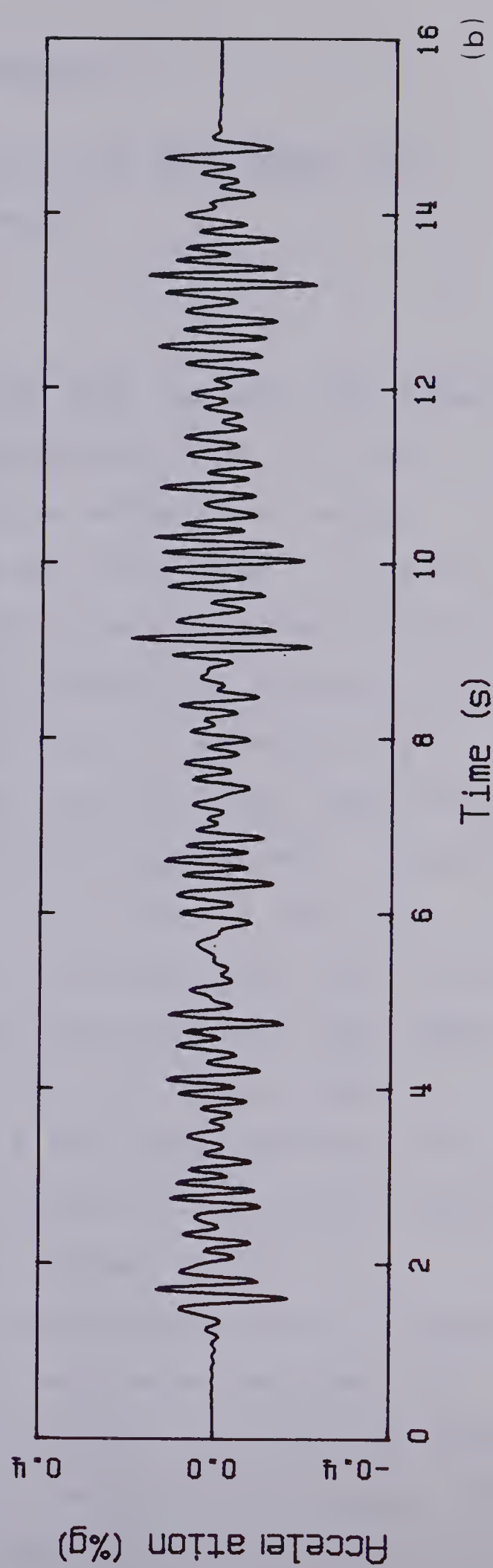
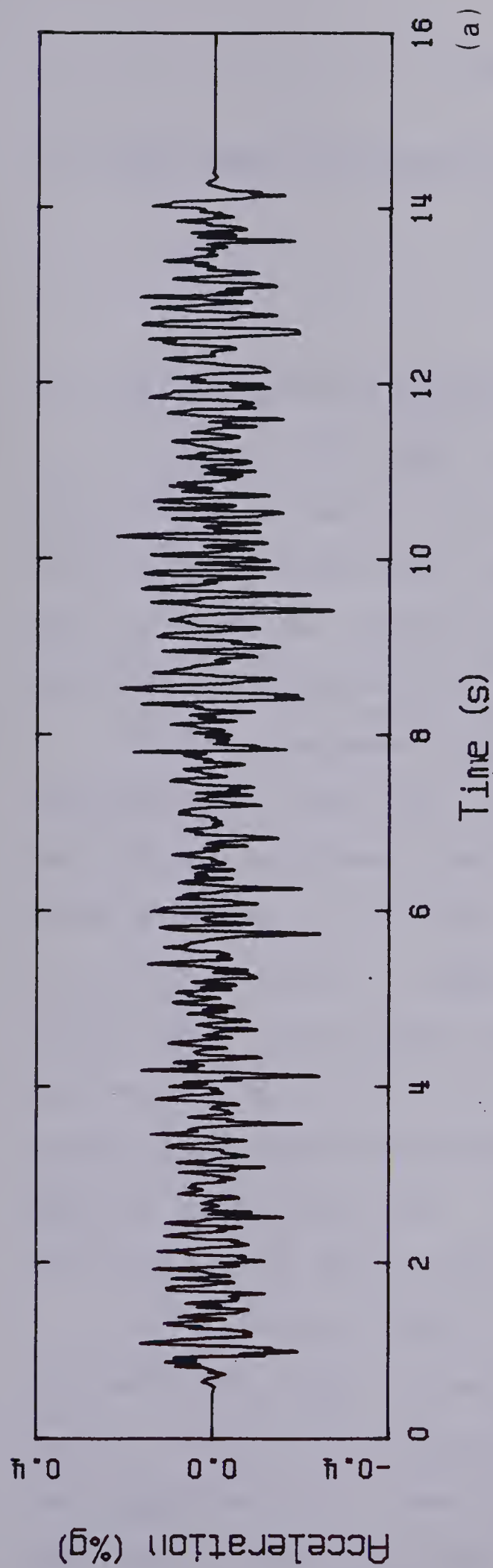


Figure C.11 Typical Acceleration-time Record for a Waltz
(a) Unfiltered, (b) Filtered @ 6.5 Hz

APPENDIX D

D. Heel Impact Loading Function and Mass Damper Test Results

D.1 Loading Function Associated with the Heel Drop Impact

The plate-like beam illustrated in Fig. D.2 was constructed to measure the force versus time loading function associated with the heel drop impact. This was done to check the validity of the corresponding function obtained by researchers at the University of Kansas (10).

The test equipment consisted of a Universal one thousand pound load cell, an electronic signal amplifier, and a Bruel and Kjaer type 7003 FM tape recorder. The test setup acted as an electronic scale with the load cell providing an electric signal which was proportional to the force input. The signals resulting from heel drop impacts delivered directly over the load cell support were subsequently plotted against a time scale to provide the desired loading function. A typical force versus time curve obtained in the above manner is shown in Fig. D.1.

To investigate some of the variables which influence the heel drop impact, several tests were conducted with various subjects of different weights (ie: above and below the suggested 77 kg) wearing a variety of shoe types. The test results indicated that regardless of shoe type, the

loading function is relatively constant for a single individual. However, the weight of the person delivering the impacts significantly affects the magnitude of the peak force response. For all subjects, the peak value of the measured force was always significantly below that obtained at the University of Kansas. In general, the enclosed area of the loading function was also approximately 15-20% less. The impact curve in Fig. D.1 corresponds to an individual weighing 78 kg.

D.2 Plywood Mass Damping Unit Test Results

The results of dynamic tests conducted with several plywood mass dampers are presented in this section. The test results include the natural frequencies and the acceleration-time records of the damping units.

Each damping unit was constructed of several sheets of plywood (with a width of 660 mm) bolted together at the centre of the long span. Layers of concrete blocks were placed over the top sheet of plywood. Each end of the damping unit was simply supported on a wooden dowel. Figure D.3 provides an illustration of the plywood damper.

The natural frequency of the unit was altered by varying the number of layers of plywood or concrete blocks and by changing the span length between the supports. Table D.1 provides a summary of the natural frequencies obtained for several different setups with a span of 2.4 m and again for a span of 1.88 m. For the 2.4 m span, each

layer of blocks weighed approximately 85 kg while for the 1.88 m span the corresponding value was approximately 70 kg. Figure D.4 shows a typical magnitude spectrum and acceleration-time record derived from the test results. The acceleration-time record clearly shows the frictional damping of the plywood mass damper unit.

In some instances, the plywood dampers can be used to increase the damping of a floor system exhibiting bothersome vibrations in response to normal human activities. The increase in damping is achieved by attaching plywood dampers, with a natural frequency approximately 0.5 Hz below the fundamental floor frequency, to the bottom chords of the floor joists. By moving out of phase with the joists, the dampers also reduce the vibratory amplitudes of the floor system.

Table D.1 Summary of Plywood Damper Test Results

Span (m)	Layers of Plywood	Layers of* Blocks	Frequency (Hz)
2.40	6	1	4.15
2.40	6	2	3.50
2.40	4	2	3.00
2.40	4	1	3.75
1.88	4	1	6.20
1.88	4	2	4.85
1.88	4	3	4.25

* Each layer of blocks weighs approximately 85 kg for the 2.4 m span and 70 kg for the 1.88 m span.

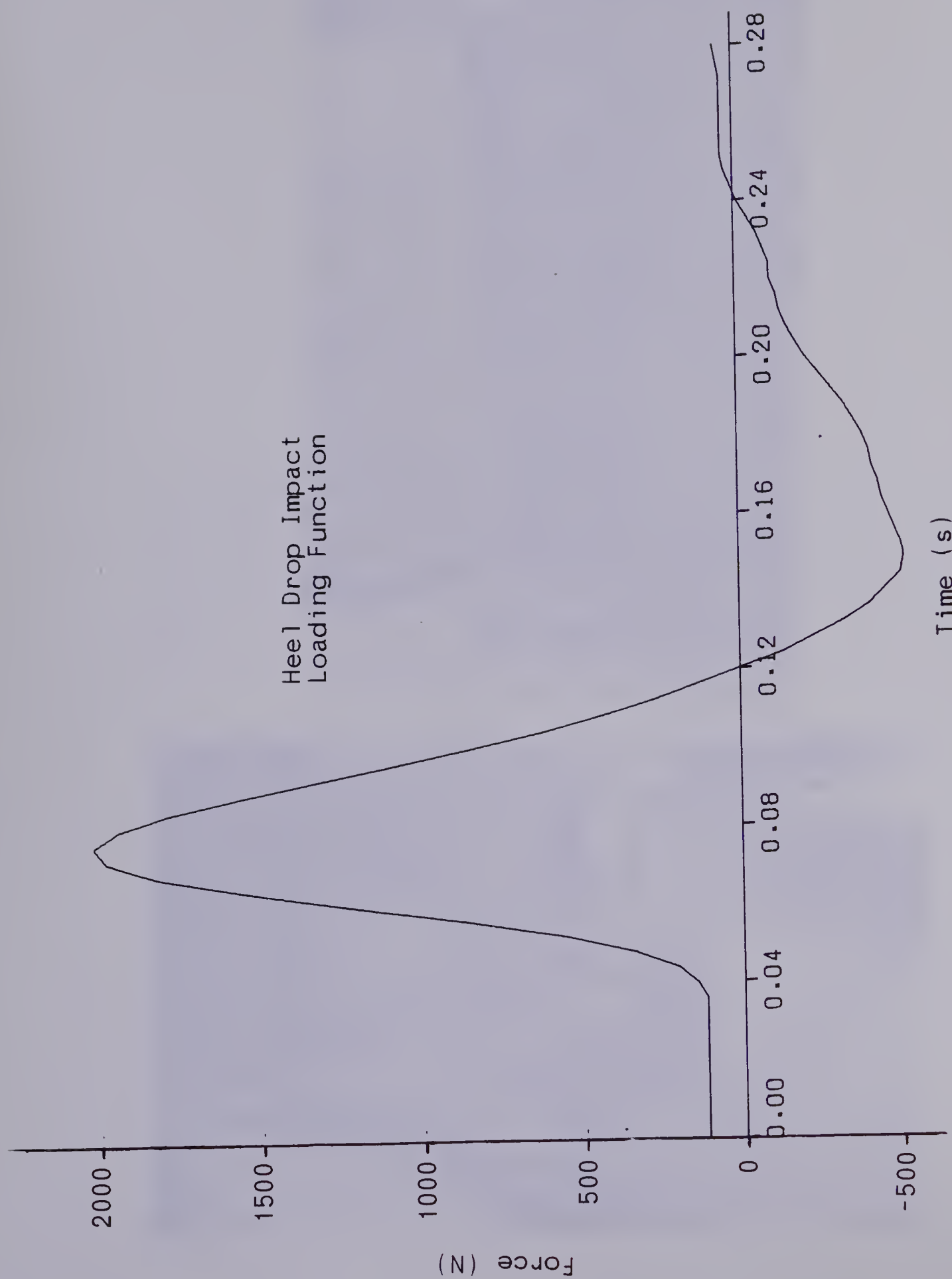


Figure D.1 Measured Heel Drop Impact Force vs. Time Curve

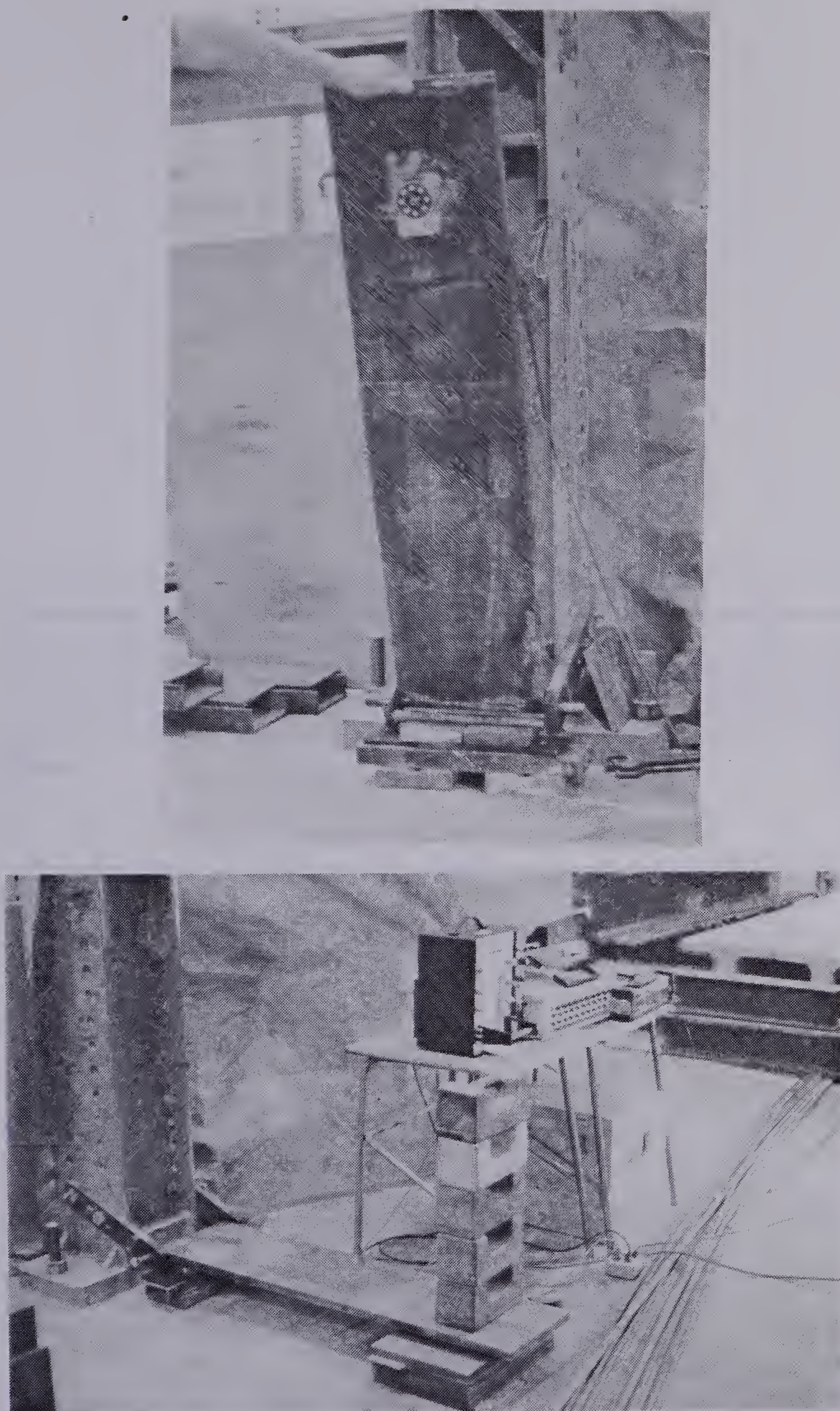


Figure D.2 Illustration of Beam Fitted with Load Cell

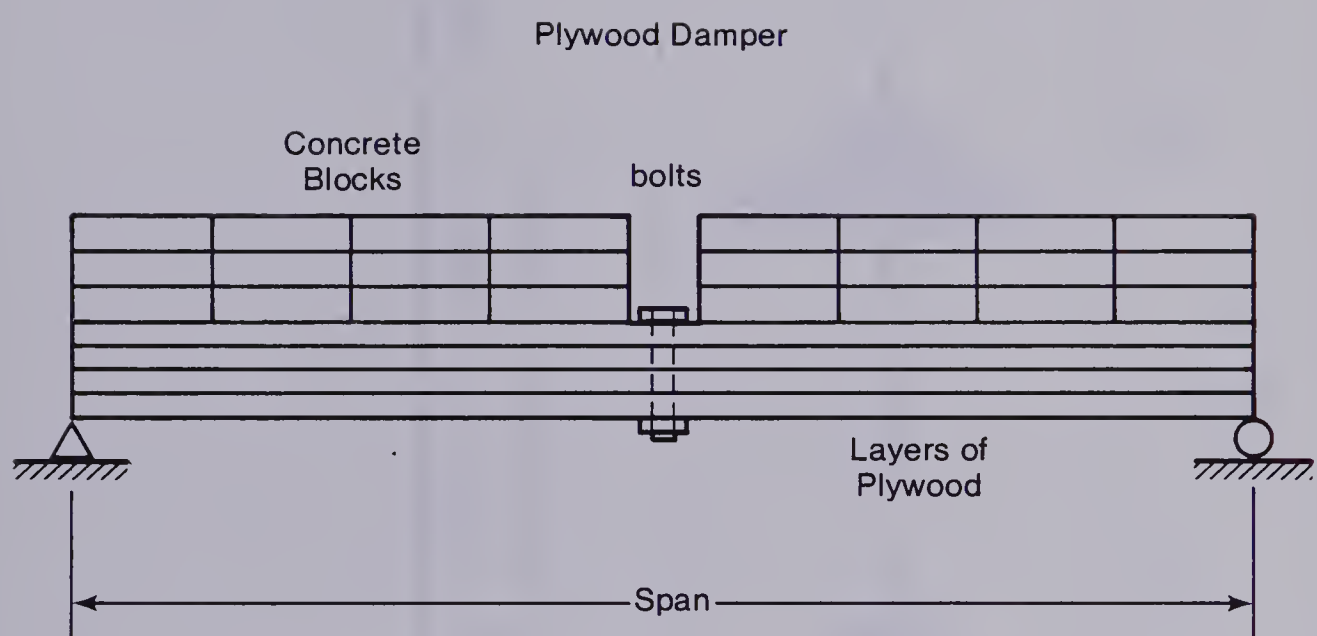


Figure D.3 Illustration of Plywood Damper Unit

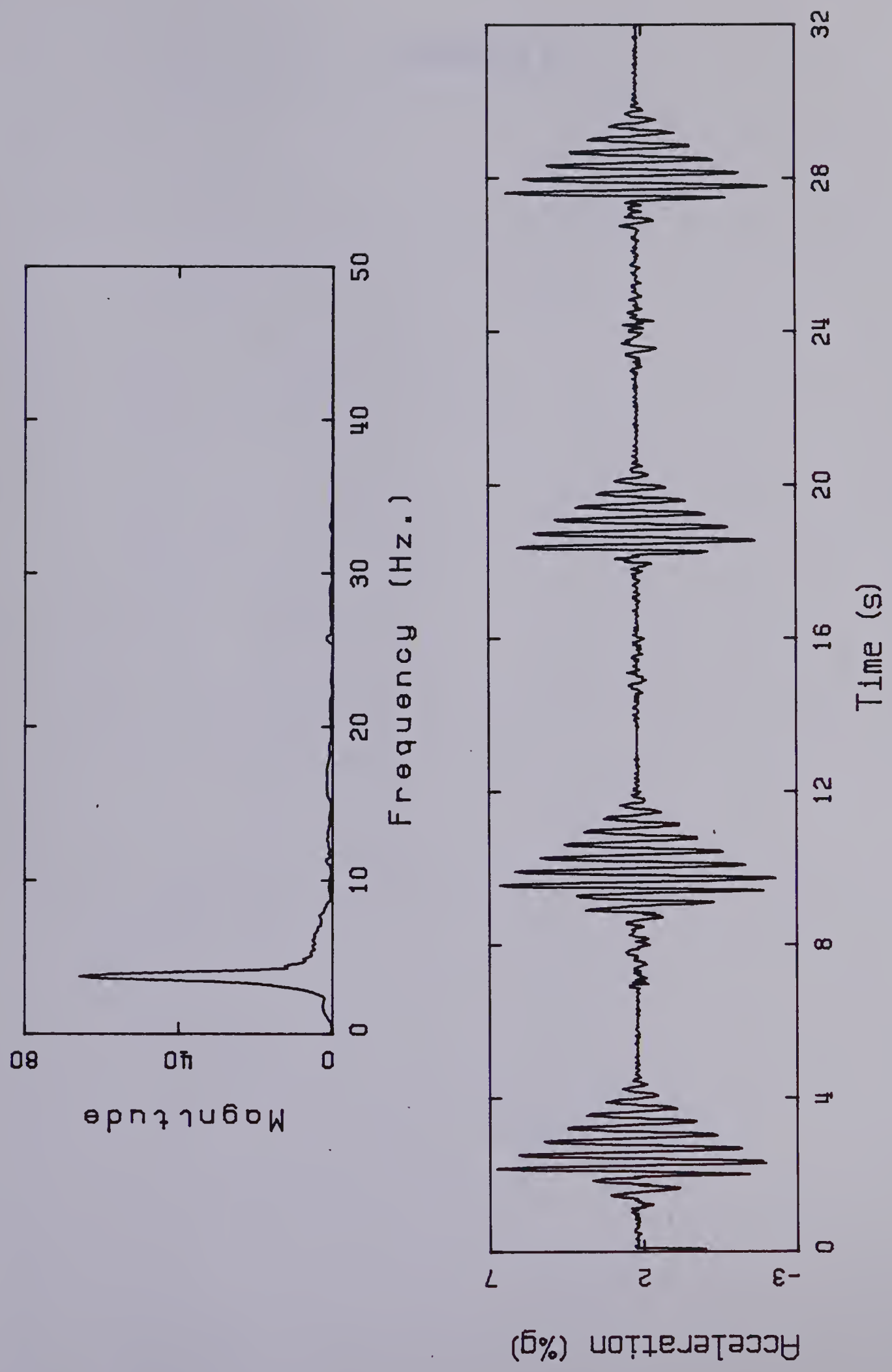


Figure D.4 Typical Magnitude Spectrum and Acceleration-Time Record for Plywood Damper

APPENDIX E


```

1 C      This program reads the discrete (digitized) accelerometer
2 C      records from a tape and prepares them for further processing.
3 C      Since the records are stored in binary form, a conversion
4 C      process is necessary to convert the discrete values to
5 C      voltages. After the conversion process, the program
6 C      multiplies each discrete value by a specified scaling factor
7 C      to convert to acceleration records with units of %gravity.
8 C      The program then outputs the discrete acceleration values
9 C      along with a discrete time vector for further signal processing.
10
11
12 C      THE FOLLOWING IS THE PROCEDURE ON HOW TO RUN THIS PROGRAM.
13 C      1. MOUNT THE TAPE..... $SOURCE CAM1
14 C      2. POSITION THE TAPE..... $CONTROL =T* POSN=FILENUMBER=
15 C      3. RUN THE PROGRAM.....
16 C      $RUN LOOK=PLTLIB 4=T* 6=DATA 6=OUTPUT 7=SUMMARY 9=-PDF
17 C      4. VIEW THE PLOT (OPTIONAL).....$RUN *PLOTSEE PAR=-PDF
18 C      6. TO GET A HARD COPY OF THE PLOTS.....
19 C      $RUN NEW:CALCOMPQ PAR=FILE=- PEN=3BLK RETURN=CIVE
20 C      6. TO DO ANOTHER FILE REPEAT STEPS 2 TO 5
21 C      7. RELEASE THE TAPE..... $RELEASE *T=
22 C      *****
23 C      *****
24 C      NOTES ON THE DATA FILE TO BE USED WITH THIS PROGRAM:
25
26 C      THE DATA FILE SHOULD CONTAIN 3 LINES
27 C      LINE 1.... NCHAN,NSTEP,NFREQ,
28 C      LINE 2.... ICODE,FACT(1),...,FACT(NCHAN),TB,TA,
29 C      LINE 3.... BLKN01,BYTE1,BLKN02,BYTE2,
30 C      COMMON /BLK1/ TVOL(50000,4),XV(50000)
31 C      REAL=4 FACT(4), YMAX(8) VALMAX(4)
32 C      &,PAGSIZ(6),LMAR,TITLE(5,4)
33 C      INTEGER=4 BLKN01, BLKN02, BLKM1, LSTBLK, BYTE1, BYTE2, FREAD
34 C      &,LENT(2)
35 C      INTEGER=2 REG(1024), N01, NCOMP, NC, INDEX(4), NUM, ICODE,
36 C      1 NVAL
37 C      LOGICAL=1 READSW /F/
38 C      DATA XC, YC /7.0, 2.5/, PERMAX
39 C      1 /0.5/, INDEX /4=0/,ABSMAX/10.0/,PAGSIZ/11.0,8.5,1.0,1.0,
40 C      2 1.5,1.0/,HEI/0.15/,LENT/18,16/,
41 C      3TITLE/'ACCE','LERA','TION','(%G')','DISP','LACE',
42 C      4'MENT','(MM)',',',10='/'
43 C      EQUIVALENCE (INDEX,NVAL), (PAGSIZ(1),XSIZE), (PAGSIZ(2),YSIZE)
44 C      1, (PAGSIZ(3),RMAR), (PAGSIZ(4),LMAR), (PAGSIZ(5),TMAR)
45 C      1, (PAGSIZ(6),BMAR)
46 C      ABSMAX = Absolute maximum voltage allowed, values above
47 C      this are set to zero.
48 C      BLKM1 = Block number 1 minus 1
49 C      BLKN01 = Block No. 1, the block number in the file to start
50 C      plotting with.
51 C      BLKN02 = Block No. 1, the last block number to plot.
52 C      BYTE1 = BYTE 1, 2*BYTE1 is the record number to start
53 C      plotting with in BLKN01.
54 C      BYTE2 = BYTE 2, 2*BYTE2 is the last record number to plot.
55 C      FACT = Conversion factor for changing voltages to deflections
56 C      or accelerations. FACT(i) is the factor for
57 C      channel i.
58 C      I = Integer variable used in looping (e.g. 00 10 I=).
59 C      ICODE = Integer CODE => to plot accelerations
60 C      => to plot deflections
61 C      II = Integer variable used in looping (e.g. 00 10 II=).
62 C      INDEX(i) is the number of values in TVOL after
63 C      choosing every NSTEP values, for channel i.
64 C      J = Integer variable used in looping (e.g. 00 10 J=).
65 C      K = Integer variable used in looping (e.g. 00 10 K=).
66 C      LSTBLK = Last Block, used for deciding how many blocks must
67 C      be skipped to reach BLKN01.
68 C      N = Number of the last record for the current block
69 C      being processed. Really only affects BLKN02.
70 C      NC = Used for converting digitized values to voltages.
71 C      NCHAN = Number of channels on the tape.
72 C      NCOMP = Used for converting digitized values to voltages.
73 C      N01 = Used for converting digitized values to voltages.
74 C      NFREQ = Digitizing frequency (points/second)
75 C      NP = NP(i), Number of points to be plotted for channel i
76 C      NPA = Number of points to look ahead from a major event.
77 C      This is calculated as TA*NSTEP/NFREQ+1.
78 C      NSKIP = Number of records to SKIP for the current block
79 C      being processed. Really only affects BLKN01.
80 C      NSKIPK = is equal to the channel number being processed *2.
81 C      Is used for finding the first record of a block
82 C      of tapes that have more than 1 channel.
83 C      NSTEP = Number of steps to take when processing data, or
84 C      simply, every NSTEP values are processed.
85 C      NUM = Number of bytes for a record.
86 C      PERMAX = Percentage of the maximum value for channel i. Used
87 C      for deciding if a major event has occurred.
88 C      READSW = Read switch, logical switch used when reading tape.
89 C      REG = Region binary data is stored while converting to voltages
90 C      TA = Time after a major event (in seconds) to plot.
91 C      TB = Time before a major event (in seconds) to plot.
92 C      TEMP = a variable to temporarily store values.
93 C      TVOL = Array to store readings. TVOL(i,j) is reading i
94 C      channel j.
95 C      VALMAX = MAXimum VALUE encountered for channel being processed.
96 C      XA = Value at the origin for the x-axis.
97 C      XB = Units/inch (scale) for the x-axis.
98 C      XC = Length of the x-axis in inches.
99 C      YA = Value at the origin for the y-axis.
100 C      YB = Units/inch (scale) for the y-axis.
101 C      YC = Length of the y-axis in inches.
102 C      XV = X plotting Vector, contains the time.
103 C      YMAX = Maximum and minimum values for a given channel.
104 C      XMAX(i) => maximum value for channel i
105 C      XMAX(i+NCHAN) => minimum value for channel i
106 C      CALL FREAD(-2, 'ENDLINE', 0)
107 C      CALL FREAD(-2, 'ENOFIL', 1)
108 C      READ IN LENGTH OF EACH BLOCK
109 C      II IS THE NUMBER VALUES READ (E.G. MAXIMUM NUMBER OF BLOCKS)
110 C      CALL FREAD(S, '31=4:', NCHAN, NSTEP, NFREQ)
111 C      CALL FREAD(5, 'I=2,R=4 V,2R=4:', ICODE, FACT, NCHAN, TB, TA)
112 C      CALL SETOSR(4, 1600, 1600)
113 C      00 S II=1,NCHAN

```



```

114     YMAX(II)=-1.OE80
115     YMAX(II+NCHAN)=1.OE80
116 5    CONTINUE
117     YC=YSIZE-TMAR-BMAR
118     YC=YC/NCHAN
119     YGAP=0.1*YC
120     YC=YC-YGAP
121     IF(NCHAN.GT.1) YC=YC+YGAP/FLOAT(NCHAN-1)
122     IF(YC.LT.1.0) YC=1.0
123     XC=XSIZE-RMAR-LMAR-0.3-HEI
124     IF(XC.LT.1.0) XC=1.0
125  C    CONVERSION FACTORS TO CHANGE DIGITIZED VALUES TO VOLTAGES
126     NO1 = 15 * 16 ** 3
127     NC = 7 * 16 ** 2 + 15 * 16 + 15
128     NCOMP = 15 * 16 ** 2 + 15 * 16 + 15
129  C    CALCULATE THE NUMBER OF BLOCKS TO SKIP ON TAPE
130     LSTBLK = 1
131     10 CALL FREAD(5, '4I=4:', BLKN01, BYTE1, BLKN02, 8YTE2, 8190)
132  C    MAKE SURE BLOCK NUMBERS ARE WITHIN ALLOWABLE RANGES
133     IF (BLKN01 .LT. 1) BLKN01 = 1
134     IF (BLKN02 .LT. 1) BLKN02 = 1
135     IF (BLKN01 .EQ. LSTBLK) GO TO 20
136     BLKM1 = BLKN01 - 1
137     IF (LSTBLK .GT. 1) LSTBLK = LSTBLK + 1
138     IF (LSTBLK .GT. BLKM1) GO TO 20
139  C    SKIP THE REQUIRED BLOCKS HERE
140     CALL SKIP(0, BLKM1 - LSTBLK + 1, 4, 8180)
141  C
142  CCCCCCCCCCCCCCCCCCCCCCCCCCCCCCCCCCCCCCCCCCCCCCCCCCCCCCCCCCCCCC
143  C
144  C    READ IN DATA OFF OF TAPE FROM BLKN01 TO BLKN02.
145  C    NUM = LENGTH OF BLOCK (IN BYTES)
146  C
147     20 DO 70 I = BLKN01, BLKN02
148         IF (I .EQ. LSTBLK .AND. READSW) GO TO 30
149  C    READ NUMBERS INTO REG
150     CALL READ(REG, NUM, 0, II, 4, 8180)
151     READSW = .TRUE.
152     NSKIP = 1
153  C    N = NUMBER OF 'NUMBERS' ON THE LINE, EVERY NUMBER IS 2 BYTES LONG
154     N = NUM / 2
155  C    CALCULATE STARTING VECTOR ELEMENT NUMBER
156     IF (I .EQ. BLKN01) NSKIP = BYTE1 / 2 + 1
157     IF (NSKIP .LT. 1) NSKIP = 1
158  C    CALCULATE ENDING VECTOR ELEMENT NUMBER
159     IF (I .EQ. BLKN02) N = BYTE2 / 2 + 1
160     IF (N .GT. NUM/2) N = NUM / 2
161  C
162  C    THE FOLLOWING LOOP CONVERTS THE DIGITIZED NUMBER SOMEHOW
163  C
164     30 CONTINUE
165     DO 40 J = NSKIP, N
166         REG(J) = REG(J) - NO1
167         IF (REG(J) .GT. NC) REG(J) = REG(J) - NCOMP
168     40 CONTINUE
169     DO 60 K = 1, NCHAN
170         NSKIPK = NSKIP + K - 1
171         II = NCHAN * NSTEP
172         DO 50 J = NSKIPK, N, II
173             INDEX(K) = INDEX(K) + 1
174  C    CONVERT DIGITIZED VALUES TO VOLTAGES
175             TEMP = REG(J) / 204.8
176             IF (ABS(TEMP) .GT. ABSMAX) TEMP = 0.0
177  C    CONVERT VOLTAGES TO READINGS
178             TEMP = TEMP * FACT(K)
179  C    FIND MAXIMUM AND MINIMUM VALUES
180             IF (YMAX(K) .LT. TEMP) YMAX(K) = TEMP
181             IF (YMAX(K + NCHAN) .GT. TEMP) YMAX(K + NCHAN) = TEMP
182             TVOL(INDEX(K),K) = TEMP
183     50 CONTINUE
184     60 CONTINUE
185     70 CONTINUE
186     WRITE(6,210) (I,YMAX(I),YMAX(I + NCHAN),I=1,NCHAN)
187  C    VALMAX = VALUES ABOVE THIS ARE A MAJOR EVENT
188     DO 80 K = 1, NCHAN
189     80 VALMAX(K) = PERMAX = AMAX1(YMAX(K),ABS(YMAX(K + NCHAN)))
190  C    NP(K) = NUMBER OF POINTS FOR CHANNEL K
191     NP = 0
192     LAST1 = 1
193     I = 0
194     90 I = I + 1
195     IF (I .GT. NVAL) GO TO 160
196     DO 100 K = 1, NCHAN
197         IF (ABS(TVOL(I,K)) .GE. VALMAX(K)) GO TO 110
198     100 CONTINUE
199     GO TO 90
200     110 CONTINUE
201     NP = NP + 1
202     NPA = NFREQ * TB / NSTEP + 1
203     J = I - NPA
204     IF (J .LT. LAST1) J = LAST1
205     NPA=I-J
206     WRITE(6,111) K,I,NPA,NP,J
207 111    FORMAT('0',TS,'Major event on channel',I2,' record',IS,'.'/
208     &T10,'Moving',I4,' records to location',IS,' from',I6,'.')
209     WRITE(7,112) K,(II,II=1,NCHAN)
210 112    FORMAT(' MAJOR EVENT OCCURING ON CHANNEL',I3/
211     &'0',20(8X,I2,8X))
212     DO 121 II=1,NPA
213     121 CONTINUE
214     WRITE(7,161) (TVOL(J+II-1,JJ),JJ=1,NCHAN)
215     NPA = NPA - 4
216     DO 120 II = 1, NCHAN
217     120 CONTINUE
218     NP = NP + NPA / 4 - 1
219     I = I - 1
220     130 NPA = NFREQ * TA / NSTEP + 1
221     140 I = I + 1
222     IF (I .GT. NVAL) GO TO 159
223     IF (NPA .LE. 0) GO TO 155
224     NPA = NPA - 1
225     NP = NP + 1
226

```



```

227      DO 150 II = 1, NCHAN
228          TVOL(NP,II) = TVOL(I,II)
229
230      150 CONTINUE
231      WRITE(7,151) (TVOL(I,II),II=1,NCHAN)
232      151 FORMAT(' ',20E20.8)
233      IF (ABS(TVOL(I,K)) .GE. VALMAX(K)) GO TO 130
234      GO TO 140
235      155 CONTINUE
236      LAST1=I
237      I=I-1
238      WRITE(6,156) LAST1
239      156 FORMAT(T10,'Event ended at record',I5,'.')
240      GO TO 90
241      159 CONTINUE
242      I=I-1
243      WRITE(6,156) I
244      160 CONTINUE
245      CALL PLOTS
246      XV(1) = 0.0
247      DO 170 I = 2, NP
248          XV(I) = XV(I - 1) + FLOAT(NSTEP) / FLOAT(NFREQ)
249      170 CONTINUE
250      CALL SCALE(YMAX, YC, 2=NCHAN, 1)
251      YA = YMAX(2=NCHAN + 1)
252      YB = YMAX(2=NCHAN + 2)
253      CALL SCALE(XV, XC, NP, 1)
254      XA = XV(NP + 1)
255      XB = XV(NP + 2)
256      CALL PLOT(0.0,0.0,3)
257      CALL PLOT(XSIZE,0.0,2)
258      CALL PLOT(XSIZE,YSIZE,2)
259      CALL PLOT(0.0,YSIZE,2)
260      CALL PLOT(RMAR+0.3*HEI,BMAR,-3)
261      YSIZE=YSIZE-BMAR-TMAR
262      YSIZE=(YSIZE-LENT(ICODE)*HEI)/2.0+0.25
263      CALL SYMBOL(-0.3,YSIZE,HEI,TITLE(1,ICODE),90.0,LENT(ICODE))
264      LENT(1)=10
265      YSIZE=(XC-LENT(1)*HEI)/2.0
266      CALL SYMBOL(YSIZE,1.5*HEI,HEI,'TIME (SEC)',0.0,LENT(1))
267      DO 171 K=1,NCHAN
268          CALL AXIS2(0.0,0.0,' ',1,YC,90.0,YA,YB,1.0)
269          CALL AXIS2(0.0,-YA/YB,' ',-1,XC,0.0,XA,XB,1.0)
270          TVOL(NP+1,K)=YA
271          TVOL(NP+2,K)=YB
272          CALL LINE(XV,TVOL(1,K),NP,1,0,' ')
273          CALL PLOT(0.0,YC+YGAP,-3)
274      171 CONTINUE
275      C SEE IF ANOTHER FILE IS TO BE PROCESSED
276      GO TO 10
277      180 WRITE (6,220)
278      STOP 16
279      190 CONTINUE
280      CALL PLOT(0.0, 0.0, 999)
281      STOP
282      210 FORMAT ('0', T5, 'Channel:', I3, ' Maximum reading:', F8.4, ' Mini
283      mum reading:', F8.4)
284      220 FORMAT ('-',T5,'Error unexpected end-of-file on tape!!')
285      END

```

End of file


```

1      C      This program calculates the mean value of the acceleration-time
2      C      signals prepared by the previous program from data stored
3      C      on magnetic tape. An array is created and filled with
4      C      zeroes prior to the reading of the acceleration or
5      C      displacement values. The array has a number of points
6      C      which is equal to an integer power of two. The values of
7      C      time record are set into the array leaving zeroes at each
8      C      end of the record to satisfy the requirements of the
9      C      Fourier frequency analysis. The program also includes the
10     C      option of applying a window function to the discrete values
11     C      of the time trace. The window function corresponds to an
12     C      inverse cosine curve ( flattened s shape) and is implemented
13     C      by setting the option variable to a number other than one.
14     C      Note a data file is required in which the following
15     C      variables are given: (NCHAN,NFREQ,OPT,LVEC,PATH,PATH1)
16     C
17     C      NOTE: further options... can have the program output the
18     C      individual acceleration or displacement vectors along
19     C      with a time vector for plotting.
20     C      (compiled version in CMEAN)
21     C
22     C      Option 1: Set PATH1 equal to 99 and PATH unequal
23     C      to 9 to have the program only output
24     C      the array for Fourier analysis.
25     C      Option 2: Set PATH equal to 9 and PATH1 unequal
26     C      to 99 to have the program only output
27     C      the vectors for plotting the time
28     C      records.
29     C      Option 3: Set PATH equal to 9 and PATH1 equal
30     C      to 99 to have the program output both
31     C      the array and the vectors.
32     C
33     C      IMPLICIT REAL*4 (A-H,O-Z,S)
34     C      REAL*4 VEC(6192,4)/32768=0.0/
35     C      INTEGER N,NCHAN,NFREQ,LVEC,OPT,PATH,PATH1
36     C      DIMENSION RMEAN(4),TIME(6192)
37     C      READ (4,10) NCHAN,NFREQ,OPT,LVEC,PATH,PATH1
38     C      10 FORMAT (6I10)
39     C      READ (5,12) N
40     C      12 FORMAT (I10)
41     C      T=0.0
42     C      TS=1/FLOAT(NFREQ)
43     C      NS=NFREQ/2
44     C      NS1=NS+1
45     C      NS2=NS+NFREQ/4
46     C      NS3=NS2+1
47     C      NS4=NS+NFREQ/2
48     C      NN=N+NFREQ/2
49     C     >NN=(NFREQ/2)+1
50     C     >NN1>NN=(NFREQ/4)
51     C     >NN2>NN1+1
52     C      DO 15 I=NS1,NN
53     C      READ (5,20) (VEC(I,J),J=1,NCHAN)
54     C      20 FORMAT (1X,4E20.7)
55     C      15 CONTINUE
56     C      DO 30 J=1,NCHAN
57     C      SUM=0
58     C      DO 40 I=NS1,NN
59     C      SUM=SUM+VEC(I,J)
60     C      40 CONTINUE
61     C      RMEAN(J)=SUM/FLOAT(N)
62     C      WRITE(6,50) J,RMEAN(J)
63     C      50 FORMAT('THE MEAN VALUE OF CHANNEL ',I3,' 15',G15.7)
64     C      30 CONTINUE
65     C      DO 60 J=1,NCHAN
66     C      DO 70 I=NS1,NN
67     C      VEC(I,J)=VEC(I,J)-RMEAN(J)
68     C      70 CONTINUE
69     C      60 CONTINUE
70     C      IF (OPT.EQ.1) GO TO 200
71     C      PI=ACOS(-1.0)
72     C      CONVP=PI/160.0
73     C      DANG=(60.0/(FLOAT(NFREQ)/4.0))*CONVP
74     C      DO 300 J=1,NCHAN
75     C      ANG=0.0
76     C      DO 310 I=NS1,NS2
77     C      GAIN=1.0-COS(ANG)
78     C      VEC(I,J)=VEC(I,J)*GAIN
79     C      ANG=ANG+DANG
80     C      310 CONTINUE
81     C      ANG=(CONVP*60.0)-DANG
82     C      DO 320 I=NS3,NS4
83     C      GAIN=COS(ANG)
84     C      VEC(I,J)=VEC(I,J)*GAIN
85     C      ANG=ANG-DANG
86     C      320 CONTINUE
87     C      ANG=0.0
88     C      DO 330 I>NN1,>NN2
89     C      DECR=COS(ANG)
90     C      VEC(I,J)=VEC(I,J)*DECR
91     C      ANG=ANG+DANG
92     C      330 CONTINUE
93     C      ANG=(CONVP*60.0)-DANG
94     C      DO 340 I>NN2,>NN
95     C      DECR=1.0-COS(ANG)
96     C      VEC(I,J)=VEC(I,J)*DECR
97     C      ANG=ANG-DANG
98     C      340 CONTINUE
99     C      300 CONTINUE
100    C      200 CONTINUE
101    C      This optional loop outputs each acceleration or displacement
102    C      vector individually along with a time vector so they can be
103    C      plotted.
104    C      IF (PATH.NE.9) GO TO 107
105    C      TIME(1)=0.0
106    C      DO 111 I=2,LVEC
107    C      TIME(I)=T+TS
108    C      T=T+TS
109    C      111 CONTINUE
110    C      DO 113 J=1,NCHAN
111    C      JJ=J+10
112    C      LVEC1=LVEC-(NFREQ/2)
113    C      LVEC1=4000
114    C      WRITE (JJ,115) LVEC1

```



```

114      115 FORMAT('0.0,1.0,8.0,','2.0, '/14, ',4, ')
115      DO 117 I=1,LVEC1
116      WRITE (JJ,118) TIME(I),VEC(I,J)
117      118 FORMAT (2E20.8)
118      117 CONTINUE
119      113 CONTINUE
120      107 CONTINUE
121      IF (PATH1.NE.99) GO TO 109
122      C      WRITE (6,80) LVEC,NCHAN
123      C      80 FORMAT (2I8, ',1, ')
124      DO 90 I=1,LVEC
125      WRITE(6,100) (VEC(I,J),J=1,NCHAN)
126      100 FORMAT(' ',4E20.8)
127      90 CONTINUE
128      108 CONTINUE
129      STOP
130      END
End of file

```



```

1  C      This program reads an array (which consists of a number
2  C      of real valued discrete time signals) and then performs
3  C      specific operations on them according to the path code.
4  C      If path #1 is specified the program will calculate the
5  C      forward transform (ie. transform with the aid of the
6  C      IMSLLIB subroutine 'FFTRC' from the time domain to the
7  C      frequency domain) of each vector in turn and then perform
8  C      a complex multiplication with the Fourier coefficients
9  C      of a finite impulse response filter. Following this the
10 C      inverse transform (ie. transform with the aid of the
11 C      IMSLLIB subroutine 'FFTCC' from the frequency domain to
12 C      the time domain) is calculated resulting in an output
13 C      vector which is the filtered time trace. Path #2 per-
14 C      forms only the forward transform with the resulting
15 C      output array consisting of complex Fourier coefficients.
16 C      The program reads in the following variables.
17 C
18 C      N      ... number of data points in one
19 C              vector of the array 'VEC'
20 C      NCHAN... the number of channels or time
21 C              vectors in array 'VEC'
22 C      NPATH... specify either '1' or '2' which
23 C              implies output as described above
24 C      NFREQ... the digitizing frequency
25 C              (points/sec)
26 C      ICODE... determines titles for time plots
27 C              1... acceleration
28 C              2... displacement
29 C      OPT... provides the option of having the
30 C              program output the 'X' and 'Y'
31 C              values for the filtered time traces
32 C              1... output given
33 C      HANS... determines whether or not a non-
34 C              linear correction factor is applied
35 C              to the fourier coefficients
36 C              99... implies correction
37 C      NTAPE... designates which FM tape the data
38 C              is coming from. Used to determine
39 C              which channels are corrected
40 C      NSPEC... specifies either the magnitude or
41 C              phase spectrum values to be output
42 C              86... phase spectrum
43 C
44 C      NOTE: THIS PROGRAM WORKS WITH SINGLE PRECISION VARIABLES
45 C
46 C      TO RUN THIS PROGRAM:      R =FORTG1EST SCAROS=FFTSS
47 C                                R =LOAD#**IMSLLIB 5=DATAFILE 6=-OUT
48 C
49 C
50 C
51 C      IMPLICIT REAL*4(A - H,O - Z,$)
52 C      COMMON /BLK1/ VEC(33000,4), XV(33000)
53 C      DIMENSION A(33000), WK(33000), PHASE(300,4), RPHASE(300,6)
54 C      DATA NWKSIZ /33000/
55 C      COMPLEX X(17000), FIL(17000)
56 C      INTEGER N, NCHAN, NPATH, ICODE, OPT, NN, NO, HANS, NTAPE, NSPEC
57 C      CALL FTNCMD('EQUATE 96=SERCOM:')
58 C      READ (4,10) N, NCHAN, NPATH, NFREQ, ICODE, OPT, HANS, NTAPE, NSPEC
59 C      10 FORMAT (9I8)
60 C      IF (ISIZE(N,-1) .GT. NWKSIZ) GO TO 220
61 C      CN = N
62 C      NO2 = N / 2 + 1
63 C      DO 30 I = 1, N
64 C      READ (5,40) (VEC(I,J),J=1,NCHAN)
65 C      40 FORMAT (1X, 5E20 8)
66 C      30 CONTINUE
67 C      DO 180 J = 1, NCHAN
68 C      DO 50 I = 1, N
69 C      A(I) = VEC(I,J)
70 C      50 CONTINUE
71 C      CALL FFTRC(A, N, X, WK, WK)
72 C      DO 60 I = 1, NO2
73 C      Y(I) = CONJG(X(I))/CN
74 C      60 CONTINUE
75 C      The next section applies a non-linear correction factor to
76 C      the Fourier Coefficients. This applies only to the data
77 C      digitized at 500 points/second. Since the correction curve
78 C      has very high multipliers at low frequencies, only values
79 C      above 4 Hz. will be altered. For the traces digitized at
80 C      500 points/sec. this corresponds to point #33
81 C      IF(HANS.NE.99) GO TO 12
82 C      Since certain channels don't require a correction they may
83 C      be skipped by altering the next line or lines. Note that
84 C      this depends on the tape under consideration.
85 C      IF(NTAPE.NE.1) GO TO 77
86 C      IF(J.NE.1) GO TO 77
87 C      GO TO 79
88 C      IF(NTAPE.EQ.2) NSKIP=3
89 C      IF(J.EQ.NSKIP) GO TO 12
90 C      79 CONTINUE
91 C      FACT=0.0
92 C      FREQ=0.0
93 C      OFREQ=FLOAT(NFREQ)/FLOAT(N)
94 C      DO 14 I=33,NO2
95 C      FREQ=I*OFREQ
96 C      FACT=11.4*FREQ**(-0.72)
97 C      X(I)=X(I)*FACT
98 C      14 CONTINUE
99 C      12 CONTINUE
100 C
101 C      IF (NPATH .EQ. 1) GO TO 70
102 C      IF (NPATH .EQ. 2) GO TO 150
103 C
104 C      *****
105 C      *****
106 C      70 CONTINUE
107 C      REAL*4 PAGESIZ(6), TITLE(5,4), YMAX(10), LMAR
108 C      INTEGER*4 LENT(2)
109 C      INTEGER*2 INOEX(4)
110 C      DATA XC, YC /7.0, 2.5/, INOEX /4*0/, PAGESIZ /11.0, 8.5, 1.0, 1.0,
111 C      11.5, 1.0/, HELL /0.15/, LENT /18, 16/, TITLE /'ACCE', 'LERA', 'TION
112 C      2', ' (%G', ' )', 'DISP', 'LACE', 'MENT', '(MM)', ' ', 10* ' /
113 C      EQUIVALENCE (PAGESIZ(1),XSIZE), (PAGESIZ(2),YSIZE), (PAGESIZ(3),RMAR)

```



```

114      1, (PAGSIZ(4),LMAR), (PAGSIZ(5),TMAR), (PAGSIZ(6),BMAR)
115      C      I      = Integer variable used in looping (e.g. 00 10 I=)
116      C      ICODE = Integer CODE => to plot accelerations
117      C              => to plot deflections
118      C      II     = Integer variable used in looping (e.g. 00 10 II=)
119      C      J      = Integer variable used in looping (e.g. 00 10 J=)
120      C      K      = Integer variable used in looping (e.g. 00 10 K=)
121      C      NCHAN  = Number of CHANNELS on the tape.
122      C      NP     = NP(I), Number of Points to be plotted for channel i
123      C      NSTEP  = Number of STEPS to take when processing data, or
124      C                  simply, every NSTEP values are processed
125      C                  for deciding if a major event has occurred
126      C      VEC    = Array to store readings VEC(I,J) is reading i
127      C                  channel j.
128      C      XA     = Value at the origin for the x-axis
129      C      XB     = Units/inch (scale) for the x-axis.
130      C      XC     = Length of the x-axis in inches
131      C      YA     = Value at the origin for the y-axis.
132      C      YB     = Units/inch (scale) for the y-axis.
133      C      YC     = Length of the y-axis in inches
134      C      XV     = X plotting Vector, contains the time.
135      C      YMAX    = Maximum and minimum values for a given channel.
136      C                  XMAX(i) => maximum value for channel i
137      C                  XMAX(i+NCHAN) => minimum value for channel i
138      IF (J.NE. 1) GO TO 90
139      READ (3,80) (FIL(K),K=1,N02)
140      80 FORMAT (1X, 2E20.8)
141      90 CONTINUE
142      DO 100 I = 1, N02
143      X(I) = X(I) + FIL(I)
144      100 CONTINUE
145      DO 110 I = 1, N02
146      X(N + 2 - I) = CONJG(X(I))
147      110 CONTINUE
148      CALL FFTCC(X, N, WK, WK)
149      DO 120 I = 1, N
150      VEC(I,J) = REAL(X(I)*DN)
151      120 CONTINUE
152      IF (J.NE. NCHAN) GO TO 180
153      C *****
154      C *****
155      DO 20 JJ = 1, NCHAN
156      YMAX(JJ) = -1.0E60
157      YMAX(JJ + NCHAN) = 1.0E60
158      20 CONTINUE
159      DO 107 JJ=1,NCHAN
160      DO 109 I=1,N
161      IF (YMAX(JJ) .LT. VEC(I,JJ)) YMAX(JJ)=VEC(I,JJ)
162      IF (YMAX(JJ + NCHAN) .GT. VEC(I,JJ)) YMAX(JJ + NCHAN)=VEC(I,JJ)
163      109 CONTINUE
164      107 CONTINUE
165      YC = YSIZE - TMAR - BMAR
166      YC = YC / NCHAN
167      YGAP = 0.1 * YC
168      YC = YC - YGAP
169      IF (NCHAN .GT. 1) YC = YC + YGAP / FLOAT(NCHAN - 1)
170      IF (YC .LT. 0) YC = 1.0
171      XC = XSIZE - RMAR - LMAR - 0.3 - HEI
172      IF (XC .LT. 1.0) XC = 1.0
173      C THE FOLLOWING VALUE IS USED FOR NP (NUMBER OF POINTS OUT
174      C OF ARRAY TO PLOT) SINCE THE LAST TWO SECONDS OF THE TRACES
175      C ARE USUALLY ZERO. NOTE THIS ONLY APPLIES TO DATA DIGITIZED
176      C AT 500 POINTS/SECOND
177      C note the value of NP =N-1000 but I changed for crane test
178      NP = N
179      IF (NFREQ EQ. 250) NP=N-250
180      CALL PLOTS
181      XV(1) = 0.0
182      DO 130 I = 2, NP
183      XV(I) = XV(I - 1) + 1.0 / FLOAT(NFREQ)
184      130 CONTINUE
185      C *****
186      C *****
187      C The following section will output two vectors namely the 'x'
188      C and 'y' coordinates of the filtered time trace to be plotted
189      C with a commercial plotting routine.
190      IF (DPT NE 1) GO TO 701
191      DO 705 J=1,NCHAN
192      JJ=10+J
193      IF (NFREQ EQ. 500) NP=N-1000
194      WRITE (JJ,703) NP
195      703 FORMAT ('8','/'2,'/14','4,')
196      DO 705 I=1,NP
197      WRITE (JJ,707) XV(I),VEC(I,J)
198      707 FORMAT (2E20.8)
199      705 CONTINUE
200      GO TO 180
201      C *****
202      C *****
203      701 CONTINUE
204      CALL SCALE(YMAX, YC, 2*NCHAN, 1)
205      YA = YMAX(2*NCHAN + 1)
206      YB = YMAX(2*NCHAN + 2)
207      CALL SCALE(XV, XC, NP, 1)
208      XA = XV(NP + 1)
209      XB = XV(NP + 2)
210      CALL PLOT(0.0, 0.0, 3)
211      CALL PLOT(XSIZE, 0.0, 2)
212      CALL PLOT(XSIZE, YSIZE, 2)
213      CALL PLOT(0.0, YSIZE, 2)
214      CALL PLOT(0.0, 0.0, 2)
215      CALL PLOT(RMAR + 0.3 + HEI, BMAR, -3)
216      YSIZE = YSIZE - BMAR - TMAR
217      YSIZE = (YSIZE - LENT(ICODE)*HEI) / 2.0 + 0.25
218      CALL SYMBOL(-0.3, YSIZE, HEI, TITLE(1,ICODE), 90.0, LENT(ICODE))
219      LENT(1) = 10
220      YSIZE = (XC - LENT(1)*HEI) / 2.0
221      CALL SYMBOL(YSIZE, 1.5*HEI, HEI, 'TIME (SEC)', 0.0, LENT(1))
222      DO 237 JJ=1,NCHAN
223      CALL AXIS2(0.0, 0.0, ' ', 1, YC, 90.0, YA, YB, 1.0)
224      CALL AXIS2(0.0, -YA/YB, ' ', -1, XC, 0.0, XA, XB, 1.0)
225      VEC(NP + 1,JJ) = YA
226      VEC(NP + 2,JJ) = YB
227      CALL LINE(XV, VEC(1,JJ), NP, 1, 0.0)

```



```

227 CALL PLOT(0.0, YC + YGAP, -3)
228 237 CONTINUE
229 CALL PLOT(0.0, 0.0, 999)
230 GO TO 180
231 C *****
232 C *****
233 C 150 CONTINUE
234 C IF (J.NE.1) GO TO 160
235 C COMPLEX CVEC(4500,4)
236 C 160 CONTINUE
237 C DO 170 I = 1, N02
238 C CVEC(I,J) = X(I)
239 C 170 CONTINUE
240 C
241 C 150 CONTINUE
242 C *****
243 C *****
244 C This portion of the program calculates the magnitude
245 C of the Fourier coefficients to be plotted along a
246 C frequency axis. The magnitudes are determined by taking
247 C the Squareroot of the sum of the squares of the two
248 C parts of the complex numbers in (X(I))
249 C IF (J.NE.1) GO TO 87
250 C IF (NFREQ.EQ.250) NPO=800
251 C For nfreq=500 NPO was equal to 205
252 C IF (NFREQ.EQ.2000) NPO=8100
253 C IF (NFREQ.EQ.1000) NPO=4000
254 C IF (NFREQ.EQ.500) NPO=1700
255 C DIMENSION FMAG(8200,2)
256 C FRHZ=0.0
257 C TP=FLOAT(N)/FLOAT(NFREQ)
258 C OFREQ=FLOAT(NFREQ)/FLOAT(N)
259 C PI=ARCOS(-1.0)
260 C NOTE: "XMAG" IS USED TO ALTER THE VALUES OF THE FOURIER
261 C COEFFICIENTS PARTICULARLY FOR THE FIR FILTER
262 C XMAG=1.0
263 C FMAG(1,1)=0.0
264 C DO 300 I=2,NPO
265 C FRHZ=FRHZ+OFREQ
266 C FMAG(I,1)=FRHZ
267 C 300 CONTINUE
268 C 87 CONTINUE
269 C IF (NSPEC.EQ.88) GO TO 133
270 C JJ=10+J
271 C DO 340 I=1,NPO
272 C FMAG(I,2)=(XMAG*TP*CABS(X(I)))
273 C IF (I.NE.1) GO TO 39
274 C WRITE (JJ,360) NPO
275 C 360 FORMAT ('0.0,30.0,8,'/'2,'/14,'/4,')
276 C 33 CONTINUE
277 C WRITE (JJ,380) FMAG(I,1),FMAG(I,2)
278 C 380 FORMAT (2E20.8)
279 C 340 CONTINUE
280 C
281 C Alternatively the phase spectrum may be determined for
282 C future plotting. The same arrays are used as for the
283 C magnitude spectrum. The phase spectrum is calculated
284 C as... phase=arctan(B/A) ... where A is the real
285 C part and B the imaginary part of the complex fourier
286 C coefficient. The phase angles are calculated in radians
287 C and then converted to degrees. Note that the function
288 C used gives angles in the range -180" and +180"
289 C 133 CONTINUE
290 C IF (NSPEC.NE.88) GO TO 180
291 C CONV=180/PI
292 C DO 157 I=1,NPO
293 C IF (REAL(X(I)) EQ.0.0.AND.AIMAG(X(I)) EQ.0.0) GO TO 261
294 C PHASE(I,J)=ATAN2(AIMAG(X(I)),REAL(X(I)))*CONV
295 C GO TO 263
296 C 261 PHASE(I,J)=0.0
297 C 263 CONTINUE
298 C 157 CONTINUE
299 C This next section corrects the phase angles of all
300 C the accelerometers for the input/output lag associated
301 C with the filters used in conjunction with the digitization
302 C of the data
303 C IF (J.EQ.3.OR.J.EQ.4) GO TO 251
304 C DO 253 I=1,NPO
305 C FREQ=I*OFREQ
306 C FILCOR=7.4098*(FREQ**0.913)
307 C PHASE(I,J)=PHASE(I,J)+FILCOR
308 C IF (PHASE(I,J).GT.180.0) PHASE(I,J)=PHASE(I,J)-360.0
309 C 253 CONTINUE
310 C GO TO 255
311 C 251 CONTINUE
312 C DO 257 I=1,NPO
313 C FREQ=I*OFREQ
314 C IF (FREQ.GT.15.0) FREQ=15.0+I*OFREQ-0.132
315 C FILCOR=25.8835*(EXP(0.14532*FREQ))
316 C PHASE(I,J)=PHASE(I,J)+FILCOR
317 C IF (PHASE(I,J).GT.180.0) PHASE(I,J)=PHASE(I,J)-360.0
318 C 257 CONTINUE
319 C 255 CONTINUE
320 C This optional loop performs a non-linear correction to
321 C the phase angles of certain accelerometers.
322 C IF (HANS.NE.99) GO TO 241
323 C IF (NTAPE.NE.1) GO TO 243
324 C IF (J.NE.NTAPE) GO TO 241
325 C GO TO 245
326 C 243 IF (NTAPE.EQ.2) NSKIP=3
327 C IF (J.EQ.NSKIP) GO TO 241
328 C 245 CONTINUE
329 C COR=0.0
330 C FREQ=0.0
331 C DO 247 I=1,NPO
332 C FREQ=I*OFREQ
333 C COR=220.83*(FREQ**0.1136)
334 C PHASE(I,J)=PHASE(I,J)-COR
335 C IF (PHASE(I,J).LT.-180) PHASE(I,J)=PHASE(I,J)+360.0
336 C 247 CONTINUE
337 C 241 CONTINUE
338 C IF (J.NE.NCHAN) GO TO 180
339 C DO 211 I=1,NPO

```



```

340      RPHASE(I,1)=PHASE(I,1)-PHASE(I,2)
341      IF (RPHASE(I,1).GT.180.0) RPHASE(I,1)=360-RPHASE(I,1)
342      IF (RPHASE(I,1).LT.-180.0) RPHASE(I,1)=360+RPHASE(I,1)
343      RPHASE(I,2)=PHASE(I,1)-PHASE(I,3)
344      IF (RPHASE(I,2).GT.180) RPHASE(I,2)=360-RPHASE(I,2)
345      IF (RPHASE(I,2).LT.-180) RPHASE(I,2)=360+RPHASE(I,2)
346      RPHASE(I,3)=PHASE(I,1)-PHASE(I,4)
347      IF (RPHASE(I,3).GT.180) RPHASE(I,3)=360-RPHASE(I,3)
348      IF (RPHASE(I,3).LT.-180) RPHASE(I,3)=360+RPHASE(I,3)
349      RPHASE(I,4)=PHASE(I,2)-PHASE(I,3)
350      IF (RPHASE(I,4).GT.180) RPHASE(I,4)=360-RPHASE(I,4)
351      IF (RPHASE(I,4).LT.-180) RPHASE(I,4)=360+RPHASE(I,4)
352      RPHASE(I,5)=PHASE(I,2)-PHASE(I,4)
353      IF (RPHASE(I,5).GT.180.0) RPHASE(I,5)=360-RPHASE(I,5)
354      IF (RPHASE(I,5).LT.-180.0) RPHASE(I,5)=360+RPHASE(I,5)
355      RPHASE(I,6)=PHASE(I,3)-PHASE(I,4)
356      IF (RPHASE(I,6).GT.180) RPHASE(I,6)=360-RPHASE(I,6)
357      IF (RPHASE(I,6).LT.-180) RPHASE(I,6)=360+RPHASE(I,6)
358
359      211 CONTINUE
360      NCHAN=NCHAN+2
361      DO 215 NN=1,NCHAN
362          JJ=10+NN
363          DO 213 I=1,NPD
364              IF (I.NE.1) GO TO 112
365              WRITE (JJ,159) NPD
366          159 FORMAT ('5','/2','/14','4','')
367          112 CONTINUE
368              WRITE (JJ,161) FMAG(I,1),RPHASE(I,NN)
369          161 FORMAT (2E20.8)
370      213 CONTINUE
371      215 CONTINUE
372      180 CONTINUE
373      STOP
374      220 CONTINUE
375      WRITE (96,230)
376      230 FORMAT (T5, '***ERROR*** Work array WK not large enough(')
377      N = ISIZE(N,96)
378      STOP 999
379      END
380
381      C *****
382      C *****
383      C *****
384      C *****
385      C *****
386      C *****
387      C *****
388      C *****
389      C *****
390      C *****
391      C *****
392      C *****
393      C *****
394      C *****
395      C *****
396      C *****
397      C *****
398      C *****
399      C *****
400      C *****
401      C *****
402      C *****
403      C *****
404      C *****
405      C *****
406      C *****
407      C *****
408      C *****
409      C *****
410      C *****
411      C *****
412      C *****
413      C *****
414      C *****
415      C *****
416      C *****
417      C *****
418      C *****
419      C *****
420      C *****
421      C *****
422      C *****
423      C *****
424      C *****
425      C *****
426      C *****
427      C *****
428      C *****
429      C *****
430      C *****
431      C *****
432      C *****
433      C *****
434      C *****
435      C *****
436      C *****
437      C *****
438      C *****
439      C *****
440      C *****
441      C *****
442      C *****
443      C *****
444      C *****
445      C *****
446      C *****
447      C *****
448      C *****
449      C *****
450      C *****
451      C *****
452      C *****

```



```

453      JK = JK + 1
454      C      Increase the number of squared terms
455      KT = KT + 1
456      C      Set switch to say "last term found was a squared term"
457      SWT = TRUE
458      GO TO 90
459      80 CONTINUE
460      C      Increase the number of terms found by 1
461      N = N + 1
462      C      Remember what this term is for later, is also the possibly
463      C      the maximun term to date (could be the same)
464      NOLD = I
465      C      Set switch to say "last term found was a NOT squared term"
466      SWT = .FALSE.
467      90 CONTINUE
468      C      Factor out term just found
469      K = K / I
470      C      Change starting term to start dividing with All other
471      C      factors must be at least as large as the term just found
472      J = I
473      C      Check for next factor
474      GO TO 10
475      END
End of file

```


B30350